Cyclopentadienyldiphosphine Complexes of Zirconium and Hafnium

by

Paul Bernard Duval

B.Sc. (Hons.), Dalhousie University, 1993

A thesis submitted in partial fulfillment of

the requirements for the degree of

Doctor of Philosophy in

THE FACULTY OF GRADUATE STUDIES

(Department of Chemistry)

We accept this thesis as conforming

to the required standard

THE UNIVERSITY OF BRITISH COLUMBIA

August 1998

© Paul Bernard Duval, 1998

ABSTRACT

The preparation of zirconium and hafnium complexes coordinated by a cyclopentadienyldiphosphine ligand are reported. Metal chloride complexes [P$_2$Cp]MCl$_3$ (P$_2$Cp = η^5-C$_5$H$_3$-1,3-(SiMe$_2$CH$_2$PPr$^i_2$)$_2$, M = Zr, Hf) are six-coordinate with an apical cyclopentadienyl donor tethered by two pendant chelating phosphines. Alkylating reactions give [P$_2$Cp]MCl$_x$R$_{3-x}$ (R = Me, CH$_2$Ph, CH$_2$CMe$_3$, CH$_2$SiMe$_3$, x = 0, 2). The monoalkyl derivatives exhibit fluxional coordination of the side-arm phosphines, which generates an equilibrium mixture of isomers. A similar solution behaviour is noted for the trimethyl species [P$_2$Cp]M(CH$_3$)$_3$. In comparison, in the bulkier trialkyl complexes the side-arms remain dangling with no observation of phosphine coordination. The dialkyl complexes [P$_2$Cp]MClR$_2$ are not isolable, but instead yield a thermally sensitive equilibrium mixture of alkyl complexes, which upon thermolysis generates in high yield the first structurally characterized alkylidene complexes [P$_2$Cp]M=CH(R)Cl (R = CH$_2$Ph, CH$_2$CMe$_3$, CH$_2$SiMe$_3$). Kinetic studies indicate a composite reaction mechanism of α-abstraction from the dialkyl complex.

Reaction of [P$_2$Cp]Zr=CH(R)Cl with ethylene yields an ethylene adduct [P$_2$Cp]Zr(η^2-CH$_2$=CH$_2$)Cl. Kinetic studies show this reaction to be first order in both alkylidene and ethylene. Insertion reactions of alkylidenes with carbon monoxide generates ketene complexes [P$_2$Cp]M(η^2-C(O))=CH(R)Cl, while a reaction with tert-butyl isocyanide produces an analogous ketenimine. Reaction of the ketene complexes with ethylene gives metallacyclic complexes resulting from insertion of one ethylene unit. These species in turn react with carbon monoxide to produce acyl-ylide zwitterionic complexes.

Methyl substituted phosphines give the zirconium chloride ^{Me}[P$_2$Cp]MCl$_3$ (^{Me}[P$_2$Cp]MCl$_3$ = η^5-C$_5$H$_3$-1,3-(SiMe$_2$CH$_2$PMe$_2$)$_2$). Alkylation reactions yield ^{Me}[P$_2$Cp]ZrCl(CH$_2$Ph)$_2$. Thermolysis of this complex produces a toluyne complex

^{Me}[P$_2$Cp]ZrCl(η^2-C$_6$H$_3$Me) instead of the anticipated alkylidene complex. Photolysis of the dibenzyl species generates a metal complex resulting from activation of a benzyl ligand.

The ethylene complexes [η^5-C$_5$H$_3$-1,3-(SiMe$_2$CH$_2$PR$_2$)$_2$]Zr(η^2-CH$_2$=CH$_2$)Br (R = Me, Pr^i) can be prepared from the reaction of the starting trichloride with two equivalents of EtMgBr. Both of these ethylene derivatives react with carbon monoxide to give carbonyl complexes, and with dihydrogen to produce asymmetric dinuclear hydride complexes. Reaction of ethylene complexes with 1,2-diphenylacetylene eliminates the ethylene ligand to give an alkyne complex. Alkylating reagents permit the formation of the alkyl-ethylene complexes [η^5-C$_5$H$_3$-1,3-(SiMe$_2$CH$_2$PPr^i)$_2$]Zr(η^2-CH$_2$=CH$_2$)(R) (R = Me, Cp).

TABLE OF CONTENTS

List of Figures

List of Tables

GLOSSARY OF TERMS

The following abbreviations, most of which are commonly found in the literature, are used in this thesis.

Å	angström (10^{-10} m)
Anal.	analysis
atm	atmosphere
B_{eq}	equivalent isotropic thermal parameter
br	broad
Bu^t	tertiary butyl group, $-C(CH_3)_3$
Bz	benzyl group, $-CH_2Ph$
$^{13}C\{^1H\}$	observe carbon-13 while decoupling proton
°C	degrees Celcius
cal	calories
calc	calculated
Chem 3D	molecular modelling program for the Macintosh computer
cm^{-1}	wave number
COSY	COrrelated SpectroscopY
Cp	cyclopentadienyl group, $\{C_5H_5\}^-$
Cp*	pentamethylcyclopentadienyl group, $\{C_5(CH_3)_5\}^-$
d	doublet
D	deuterium
dd	doublet of doublets
d_n	n deuterated
d of sept	doublet of septets
deg	degrees
DME	1,2-dimethoxyethane

E_a	activation energy
equiv	equivalent(s)
ESR	Electron Spin Resonance
Et	ethyl group, $-CH_2CH_3$
g	gram
$\Delta G°$	Gibb's standard free energy of reaction
$\Delta G^{\ddagger}$	Gibb's energy of activation
GC-MS	Gas Chromatography/Mass Spectrometry
h	hour
^1H	proton
$\Delta H°$	enthalpy of reaction
$\Delta H^{\ddagger}$	enthalpy of activation
HOMO	Highest Occupied Molecular Orbital
Hz	Hertz, $second^{-1}$
I	spin
IR	infrared
$^nJ_{A-B}$	n-bond scalar coupling constant between nuclei A and B
K	degrees Kelvin, or equilibrium constant
k_1	forward rate constant
k_{-1}	reverse rate constant
k_{obs}	observed rate constant
kcal	kilocalories
kHz	kiloHertz
$^6Li\{^1H\}$	observe lithium-6 while decoupling proton
$^7Li\{^1H\}$	observe lithium-7 while decoupling proton
ln	natural log
Ln	n number of ligands

LUMO	Lowest Unoccupied Molecular Orbital
m	multiplet, or medium for infrared data
m	meta
M	molar, or central metal atom
Me	methyl group, $-CH_3$
mg	milligram
MHz	megaHertz
mL	millilitre
mmol	millimole
MO	Molecular Orbital
mol	mole
ms	millisecond
MS	Mass Spectrometry
NOESY	Nuclear Overhauser Enhancement SpectroscopY
NMR	Nuclear Magnetic Resonance
o	ortho
$^{31}P\{^{1}H\}$	observe phosphorus-31 while decoupling proton
p	para
Ph	phenyl group, $-C_6H_5$
ppm	parts per million
n-Pr	propyl group, $-CH_2CH_2CH_3$
Pr^i	isopropyl group, $-CH(CH_3)_2$
q	quartet
R	hydrocarbyl substituent
r	correlation
s	singlet, or seconds, or strong for infrared data
$\Delta S°$	entropy of reaction

$\Delta S^{\ddagger}$	entropy of activation
sext	sextet
S_N2	substitution, nucleophilic, 2nd order
t	triplet
T	temperature
THF	tetrahydrofuran
THT	tetrahydrothiophene
VT	Variable Temperature
X	chloride or alkyl group
α	on a carbon that is directly bonded to a metal
β	on a carbon that is two bonds away from a metal
δ	chemical shift
Δ	heat
$\Delta_{1/2}$	peak width at half height
η^n	n-hapto
μ-X	X-bridging ligand
ν_{x-x}	vibrational band for bond x-x

ACKNOWLEDGEMENTS

To Vasiliky

who made this all possible

Chapter 1

Introduction to Cyclopentadienyl

Complexes of Zirconium and Hafnium

1.1   Introduction

The chemistry of transition metal organometallic complexes is a field of study that has grown immensely in recent years, and currently is a focal point for both industrial applications and fundamental research.[1] The versatility of this chemistry originates from the degree of covalency in the metal-carbon bond that typically defines an organometallic complex. This feature is generally lacking in classical Werner complexes, which have significant ionic character in the bonding owing to the coordination of metal ions by either hard anionic ligands (i.e. Cl^-, NO_3^-, OH^-), or by neutral donors (i.e. H_2O, NH_3) in dative interactions. The covalent nature of the bonding in organometallic complexes is demonstrated by the pronounced stability of derivatives that obey the "18-electron rule", an accounting system of electrons for transition metal organometallic species that is an expanded version of the octet rule for covalent compounds of the p-block elements. The bridge between inorganic and organic chemistry is also exemplified by the coordination of organic molecules such as ethylene to a transition metal. The donation of electrons from the ligand to the metal in the formation of a σ-bond is often complemented by π-backbonding from the metal (Figure 1.1). This synergistic bonding potentially modifies the reactivity of both the metal centre and the bound ligand, a synthetically useful feature that is generally absent in classical inorganic coordination compounds. Thus,

references begin on page 17

much of the rich chemistry available to transition metal organometallic complexes can be traced to these two main facets: 1) the reactivity of the polar M–C bond, and 2) the synergistic bonding between the metal and organic fragment. Indeed, the combination of both of these properties adds a new dimension that has been extended to a number of catalytic organic transformations that are mediated at the coordination sphere of a metal centre.
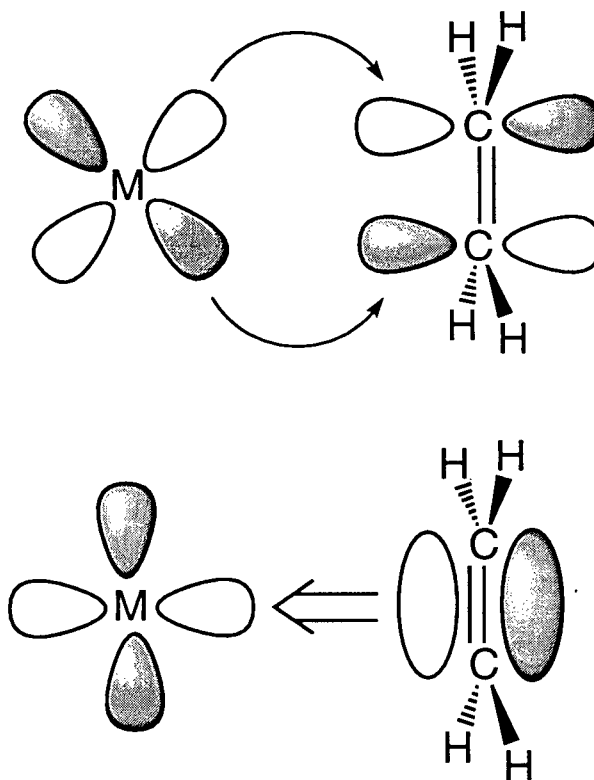
Figure 1.1   Schematic diagram of the bonding of ethylene to a transition metal

1.2   Cyclopentadienyl Complexes

The explosive growth in the field of organometallic chemistry since the early 1950's is largely rooted in the discovery of ferrocene, $Fe(C_5H_5)_2$, in 1951.[2,3] The elucidation of the structure[4] and bonding of this sandwich complex introduced inorganic chemists to the potential of the ancillary cyclopentadienyl (Cp) ligand, which has since spawned a wealth of

organometallic compounds. An examination of the molecular orbital scheme for the cyclopentadienyl anion illustrates how this planar aromatic five-membered ring coordinates to a metal as a ligand.[5] The diagram is shown below in Figure 1.2; each ring carbon contributes a p orbital to give five molecular orbitals.
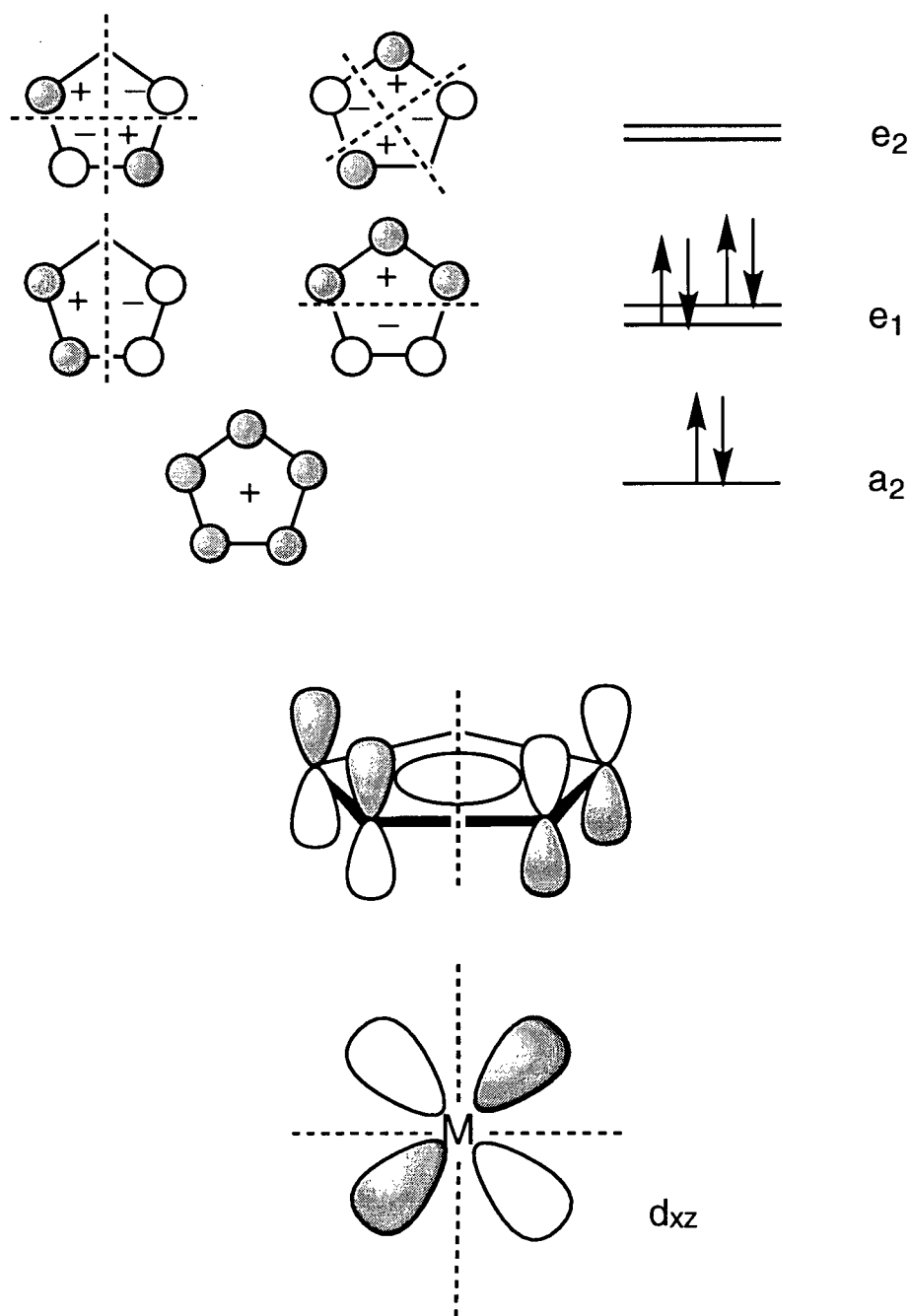
Figure 1.2 The molecular orbital scheme for the cyclopentadienyl anion.

These are built up in increasing energy, beginning with the low energy symmetric a_1 orbital, followed by two sets of doubly degenerate orbitals, with one (e_1) and two (e_2) nodal planes, respectively. These molecular orbitals may then interact with metal valence orbitals of appropriate symmetry; the filled symmetric a_1 orbital overlaps with a metal s orbital to form a σ-bond, while the occupied e_1 orbitals act as π-donors into the metal d_{xz} and d_{yz} orbitals. The interaction of one of the degenerate e_1 orbitals with the metal d_{yz} orbital is illustrated as an example in Figure 1.2. The empty e_2 orbitals are of appropriate symmetry to interact with a filled metal d_{xy} orbital, but the δ-overlap is negligible for bonding.

Based on the molecular orbital depiction shown above, the cyclopentadienyl anion can be characterized as a good σ- and π-donor and a poor π-acceptor, a combination that stabilizes a metal by increasing its electron density, that is especially useful for early metals in high oxidation states. Coordination simultaneously confers resistance to the Cp ligand with respect to both electrophilic and nucleophilic attack. These combined qualities are ideal for a spectator or ancillary ligand, which is specified to moderate the chemistry elsewhere in the coordination sphere of the metal while not participating directly in any of the reactions. An added benefit is the steric and electronic saturation provided by the η^5-hapticity of the planar ring, thereby offering stereochemical control to the reactivity at the metal centre. Perhaps the most advantageous feature of this ligand is that these steric and electronic factors can be modified by introducing alkyl substituents to the ring. A simple example is the permethylated analogue C_5Me_5 (Cp*), which is bulkier, more electron releasing as a donor, and forms complexes that are generally more soluble in organic solvents and more crystalline than the analogous Cp derivatives. Such ligand "tuning" is a fundamental aspect of Cp-ligated complexes, some of which will be encountered in the next section.

1.3   Group 4 Bent Metallocene Complexes

A limiting factor to the use of the cyclopentadienyl unit as an ancillary ligand is its high electron count. A formally six-electron donor as an anion, it is well suited to stabilize electron deficient early metals, but less compatible with electron-rich late members of the series. For example ferrocene is an electronically saturated 18-electron complex, which explains its remarkable stability but also restricts potential reactivity at the metal centre. To accommodate reactive ligands into a Cp_2M framework one must move to the left of the transition metal series. As shown below for Nb, the addition of ligands breaks the D_{5h} symmetry of the sandwich geometry observed in ferrocene (**A**), inducing a distortion to a bent metallocene configuration (**B**) with up to three additional ligands occupying the equatorial wedge between the two Cp rings.[6]

A   **B**
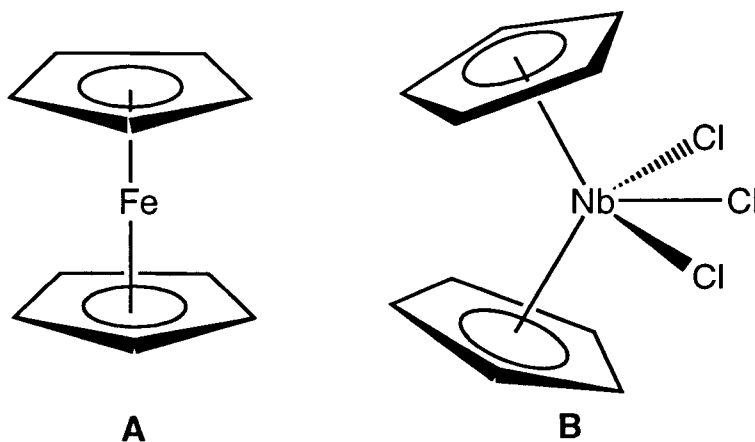
The bent metallocenes constitute a dominant fraction of the research conducted on Cp-ligated systems.[7] Foremost among these are the Group 4 derivatives Cp_2MCl_2 (M = Ti, Zr, Hf), which exhibit a rich metathesis chemistry to generate a multitude of $Cp_2MR(X)$ (R = H, alkyl; X = halide, alkoxide, etc.) and Cp_2MR_2 complexes.[8] The use of Cp* and other substituted Cp ligands has provided for additional bent metallocene derivatives.[1] The stability of these complexes in comparison to homoleptic Group 4 alkyl species (MR_4) is testimony to the ancillary ligand set, and control of the stereochemistry to the equatorial wedge permits well-

references begin on page 17

defined reactivity. Examples include the synthetically useful hydrozirconation reagent $Cp_2Zr(H)Cl$ for alkene and alkyne insertion products,[9] ring-opening olefin metathesis polymerization (ROMP) mediated by Ti alkylidene intermediates,[10,11] cycloaddition reactions at a Zr phosphinidene $Cp_2Zr(=PR)$ complex,[12] and a variety of C–C coupling reactions which are either mediated by Cp_2Zr(benzyne) complexes,[13] or conducted on the intermediate "Cp_2Zr" synthon obtained from the Negishi reagent (Cp_2ZrCl_2/ 2 ^nBuLi).[14]

Since the early 1980's the focus in Group 4 metallocene chemistry has centered on cationic alkyl species $[Cp_2ZrR]^+$, which have proven to be very active homogeneous catalysts for the Ziegler-Natta polymerization of alkenes.[15,16] Substantial efforts into the steric and electronic modification of Cp-based metallocene ligands have coincided with these developments. The impetus started with the discovery by Kaminsky[17] in 1980 that Cp_2ZrCl_2 polymerizes propylene in the presence of excess methylalumoxane $((MeAlO)_n)$ to generate high molecular weight polypropylene. These results prompted an interest to develop chiral metallocene catalysts to induce stereoregularity into the polymers obtained from prochiral α-olefins such as propylene. This was soon accomplished with the C_2-symmetric *ansa*-metallocenes (**C**), in which the indenyl rings are linked by an interannular bridge to give a rigid chiral structure.

C   **D**
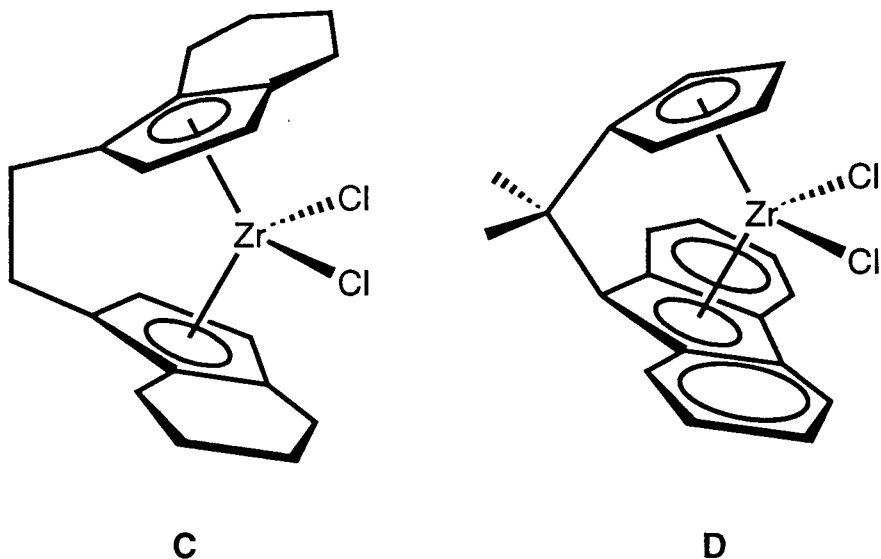
These catalysts were found to be effective in producing isotactic polypropylene,[18,19] and neutral complexes employing this ligand set have been utilized in a number of other asymmetric transformations as well. For example, Buchwald has used Ti derivatives for the hydrogenation of highly substituted alkenes,[20] and in the Pauson-Khand[21] cyclization reaction involving the intramolecular coupling of an alkene, an alkyne and CO.[22] Further modification of the metallocene ligand to a fluorenyl-Cp linkage to give a polymerization catalyst with C_s symmetry (**D**) has permitted the formation of mainly syndiotactic propylene.[23] Such ligand tuning for stereospecific α-olefin polymerization has continued steadily with the synthetic preparation of a variety of elegant ligand architectures.[24-27]

1.4   Mono(cyclopentadienyl) Complexes of Zr and Hf

In comparison to the exhaustive reports on the chemistry of the Group 4 metallocenes, there has been considerably less study into the mono(cyclopentadienyl) analogues (e.g., $CpMCl_3$). Some of this disparity stems from the synthetic difficulties encountered in accessing the latter derivatives,[28] although adducts (i.e., $CpMCl_3(DME)$)[29] can be readily prepared. There are significant differences in reactivity and structure between bis(cyclopentadienyl) Group 4 complexes and their mono(cyclopentadienyl) analogues. In comparison to the bent metallocene structure of monomeric Cp_2ZrCl_2, $CpZrCl_3$ exists as an insoluble polymer that resembles the structure of $ZrCl_4$. $ZrCl_4$ is a one-dimensional polymeric network with zigzag chains of edge-shared, chloride-bridged $ZrCl_6$ octahedra (**E**).[30] $CpZrCl_3$ is similarly a chloride-bridged one-dimensional polymer (**F**),[31] but the octahedral geometry at the Zr centre is distorted by the presence of the bulky cyclopentadienyl group, such that all equatorial Zr–Cl bonds are bent away from the Cp ring. The Cp ring also induces bond lengthening in both the terminal and bridging Zr-Cl bonds in comparison to $ZrCl_4$, presumably due to both steric and electronic factors.

Increasing the steric bulk of the Cp unit can break up the polymeric network. For example, the structure of Cp*ZrCl₃ is that of a chloride-bridged dimer,[32] in which the Zr–Cl bonds are again bent away from the ring to give a four-legged piano-stool structure. With even bulkier substituents the isolation of monomeric Cp'ZrCl₃ derivatives that exhibit a three-legged piano-stool geometry has been achieved.[33]

E

F
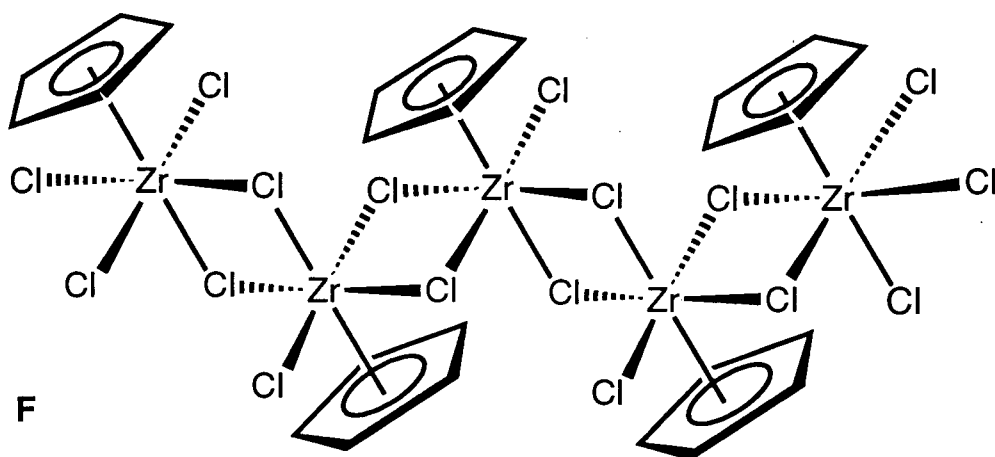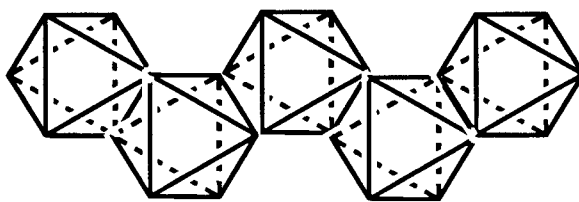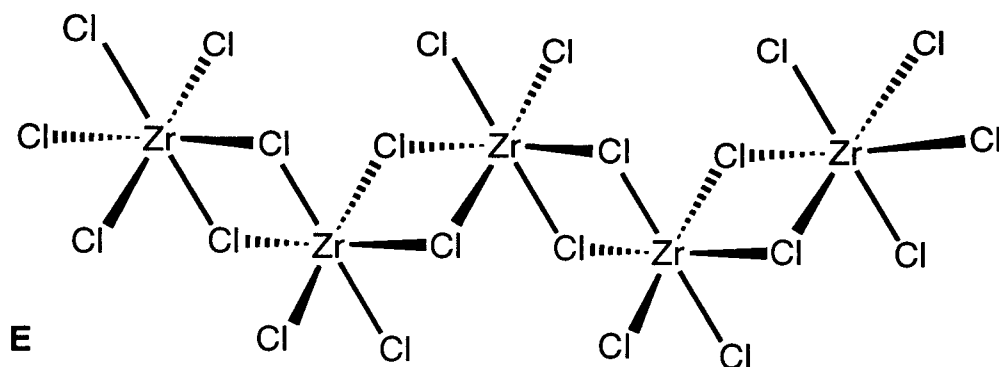
Compared to 16-electron Cp_2ZrCl_2 metallocenes, the $CpZrCl_3$ unit is formally a 12-electron species that can accommodate up to two additional two-electron donors upon break up of the polymer structure. However, the hard Lewis acidity of $CpZrCl_3$ is demonstrated by the inability to form adducts with phosphines, as opposed to harder donors such as ethers and amines. The addition of a single neutral donor gives a chloride-bridged dimer $[CpZrCl_3(L)]_2$ (i.e., L = butanone,[34] tethered ether donor[35]), while the addition of two molecules generates monomeric bis(adduct) complexes of the general formula $CpZrCl_3(L)_2$ (i.e., L = THF,[36] H_2O[37]). Analogous Hf derivatives have also been isolated.[29] All of the structurally characterized examples share the same distorted quasi-octahedral geometry (**G**), with the cyclopentadienyl donor represented as occupying a single coordination site. The distortion is evident in the equatorial bond angles, which are directed away from the Cp unit as noted above for $(CpZrCl_3)_n$ and $(Cp^*ZrCl_3)_2$. The arrangement of ligands is also consistent for each example; one neutral donor occupies an equatorial site *cis* to the Cp ring, while the axial site *trans* to the Cp group is coordinated either by the bridging chloride of the dimer, or by the second neutral donor. This axial ligand is typically labile, as evidenced by reversible dissociation of either the bridging ligand[43] or the terminal donor.[36]

G
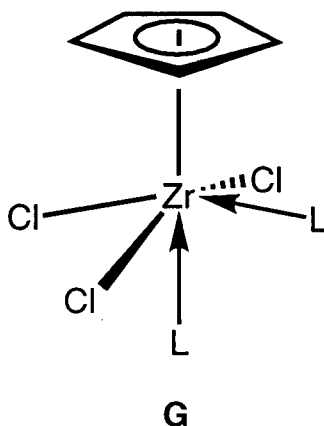
$Cp'ZrCl_3$ complexes are strong Lewis acids that have been used as catalysts for the epoxidation of alkenes,[38] in Diels-Alder reactions,[36] and in asymmetric aldol reactions[39] using chiral catalysts.[40] The bulky Cp* group has enabled the tri-alkyl complexes Cp^*ZrR_3 (R = Me,

CH_2Ph, Ph, CH_2CMe_3)[41,42] to be isolated. These species show thermal stabilities intermediate between those of the analogous metallocenes and the homoleptic MR_4 alkyls.[43] Cationic mono(cyclopentadienyl) derivatives $[Cp'MR_2]^+$ of Ti,[44-46] and to a lesser extent Zr,[44] have shown some capacity as polymerization catalysts, albeit with substantially lower activities in comparison to their metallocene counterparts. The cationic $[Cp^*ZrR_2]^+$ species are highly electrophilic and decompose readily in either CH_2Cl_2 or THF.[47] The electronic and coordinative unsaturation of the $[Cp^*MR_2]^+$ moiety is further illustrated by the ability to coordinate toluene as found in $[Cp^*HfMe_2(\eta^6\text{-PhMe})][BMe(C_6F_5)_3]$,[48] a rare example of an η^6-arene complex of a d^0 metal.

1.5   Mono(cyclopentadienyl) Complexes with Pendant Donors

Appending an anionic amide donor on a silyl link to a Cp ligand has yielded "constrained geometry" complexes (H)[49] that compare favourably with *ansa*-metallocene catalysts for the polymerization of α-olefins. One of the Cp donors of the metallocene ligand set has been replaced by a smaller amide, which combined with the short silyl bridge gives less steric and electronic saturation at the metal centre. The enhanced Lewis acidity of these amido-linked systems is indicated by their being highly active in the catalytic copolymerization of α-olefins (including styrene) with ethylene.[50,51] As with the metallocenes, the success of this system has encouraged ligand modifications. Chiral examples have been made by incorporating a chiral substituent on the amido group,[52] or by introducing planar chirality to the cyclopentadienyl ring.[53] Other modifications of this system have included the use of a linked fluorenyl-amido ligand,[54] and a few examples have been noted where the side-arm is extended further (I) to allow coordination of an additional neutral donor L, which may be either an amine[55] or an ether.[56] The latter example has been used to stabilize rare Zr complexes that possess two higher alkyl ligands that are resistant to β-hydrogen elimination. There is also a similar analogue of I in which the equatorial donor is a neutral ether instead of an amide, with an amine as the basal donor.[57] As a

mono-anionic ancillary ligand this is coordinated to a $ZrCl_3$ fragment to give an octahedral complex similar to that depicted in **G**. A different strategy for adding another donor is the use of a second side-arm from the Cp ring (**J**), for which a Sc derivative has been reported.[58]

H

I

J

K
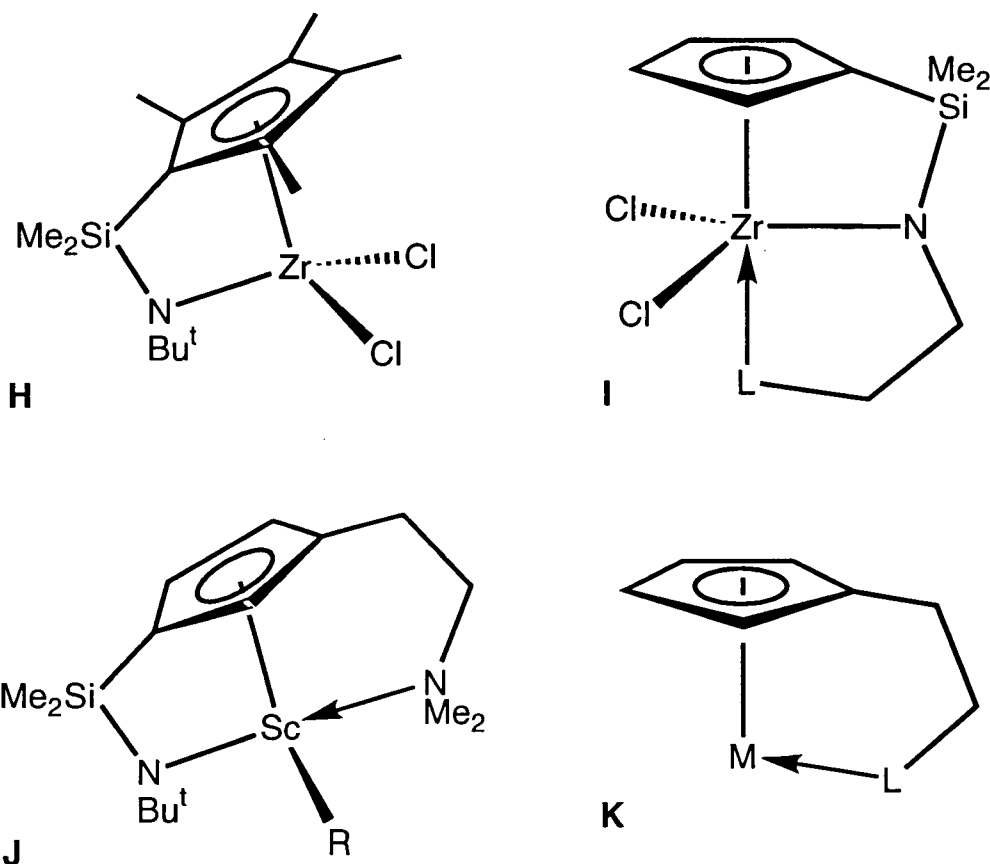
A related class of pendant donor cyclopentadienyl ligands with a less constrained two-carbon backbone (**K**) has been extensively used for a variety of metals.[59] There are also a few examples in which the chelating donors are separated by a three-carbon backbone.[60] Group 4 derivatives that incorporate pendant side-arms have included donors such as amides,[61] amines,[59,62,63] pyridines,[64] phosphines,[65] alkenes,[66] phenolates,[67] and ethers.[35,68] Chiral complexes have been prepared in which the chirality is applied either within the bridge[61] or as a substituent on the pendant donor atom.[68] Some metallocene species have been designed whereby two appended-donor Cp ligands are bound to the same metal, with intramolecular coordination of both side-arms to give a complex with helical chirality.[69,70]

Complexes with cyclopentadienyl ligands having appended side-arms can be compared to the constrained geometry polymerization catalysts. The strategy with a weak neutral side-arm donor is to enable reversible coordination, whereby a reactive cationic intermediate can be stabilized by intramolecular chelation, yet be sufficiently labile to provide an open site for reactivity.[54,73] Intramolecularly stabilized cations have been isolated that are similar to analogous cationic metallocene alkyl species that have been trapped by the formation of an adduct, as in $[Cp_2ZrR(L)]^+$ (L = THF,[71] PMe_3[72,73]). However, with one exception[74] there have not been any reports on catalytic activity, which is not surprising in view of the dampening effect the presence of donor molecules (especially phosphines) have on the catalytic activity of cationic metallocene systems.

1.6   Phosphine Complexes of Zirconium and Hafnium

Phosphine ligands (PR_3) comprise one of the most important classes of ligands in inorganic chemistry and are utilized in numerous catalytic cycles.[75] The diversity of phosphine derivatives is impressive, including a variety of chelating multidentate ligands and chiral examples for asymmetric synthesis.[76]

However, in contrast to the later metals of the transition metal series, for which phosphine complexes are common, there are correspondingly fewer examples for the early metals.[77] This is primarily due to the mismatch between metal and donor; phosphines are generally soft polarizable ligands, whereas early metals are typically in a high oxidation state and therefore favour hard N- and O-atom donors. A useful example was alluded to earlier in which $Cp*ZrCl_3$ forms stable adducts with ethers and amines but not with phosphines. For early metals in lower oxidation states (i.e., Zr(II)) the occurrence of phosphine ligands becomes more prevalent, especially with bidentate chelating or macrocyclic phosphines.[78-80] The presence of Cp ligands can assist in stabilizing these low-valent species, as electron density provided by π-donation from

the Cp ligand can be transferred to π-acceptor ligands that are usually present in these complexes.[81]

Despite the relative scarcity of phosphine coordination to high-valent early metals, representative examples illustrate the importance of this group of complexes. One of the major roles of phosphines in the chemistry of the early metals is to trap a reactive intermediate as an isolable species. Examples of this have been seen above with the isolation of cationic alkyl derivatives.[72,73,82] Other examples include the addition of phosphines to trap Zr benzyne[13] and Ti alkylidene[83] complexes. The general strategy is to supply steric and electronic saturation to the metal to stabilize a highly reactive species, potentially capturing a snapshot of an otherwise undetected intermediate.

A particularly useful aspect of phosphine ligands in organometallic complexes is the application of ^{31}P NMR spectroscopy. The phosphorus-31 nucleus (I = 1/2) is 100% abundant and possesses reasonable sensitivity (6.6% that of ^{1}H) for spectroscopic study.[84] Chemical shift values span a wide range (> 1200 ppm) and thus provide general information regarding the coordination of a phosphine to a metal centre. Spin-coupling to other nuclei can be very sensitive to the stereochemistry of a complex and may supply a more detailed analysis of the coordination sphere.

One feature that makes phosphine ligands extremely versatile is that they comprise a select group of ligands in which the steric and electronic properties can be modified by varying the substituents. Electron-releasing substituents such as alkyl groups increase the donor ability of the phosphine, while the steric bulk of a phosphine can be measured by the Tolman cone angle.[85] This combination of electronic and steric modification is the basis for "fine-tuning" a ligand to moderate the reactivity at the metal centre, which has been encountered previously with the Cp group. Therefore, combining a phosphine donor with a Cp unit in the same ligand set offers a wealth of flexibility to experiment with the chemistry of a particular system.

1.7 Cyclopentadienylphosphine Complexes of Zirconium and Hafnium

In spite of the potential mentioned above for the combination of a Cp donor with a phosphine, cyclopentadienyl ligands with pendant phosphine donors have received less attention in comparison to other members of this series. Complexes of these ligand with late metals[86] and main group elements[87] have shown intramolecular coordination of the side-arm donor. There are also examples of dinuclear structures where the side-arm phosphine bridges across to coordinate to another metal.[88] A notable utilization of this bridging feature is the incorporation of pendant phosphines on the Cp rings of ferrocene, which generates a new chelating ligand for coordination to a second metal centre. Chiral derivatives of this ligand have been successfully used in asymmetric synthesis,[89] and one strategy has taken advantage of the redox behaviour of ferrocene to give a redox-switchable hemilabile ligand for Rh complexes.[90]

Complexes of cyclopentadienylphosphine ligands with Group 4 metals are relatively few. Except for a Ti example in which the ligand coordinates the phosphine in a chelating fashion,[65] and a zirconocene cation with chelating donors appended from the Cp rings,[70] the side-arm generally remains dangling and in some instances, as noted above, this free donor can bridge to a later metal (i.e., $Fe(CO)_4$) to give a heterobimetallic complex.[91] However, these examples are all metallocene derivatives that are electronically and coordinatively unsaturated. To allow the phosphine to bind it is preferable that only one Cp ligand be present within the coordination sphere.

1.8 The Scope of this Thesis

references begin on page 17

Previous work in the Fryzuk laboratory has focused on the tridentate chelating amidodiphosphine ligand, $N(SiMe_2CH_2PR_2)_2$ [PNP].[92] The strategy of combining the hard amide donor with two soft donor phosphines within the same ligand framework was designed to effect new reactivity patterns with potential application for a variety of metals. For Zr and Hf the amide anchors the ancillary ligand to the metal while phosphine coordination is enhanced by chelation.[93] Fluxional coordination of the side-arm donors allows open sites to be temporarily available for controlled reactivity.

[PNP]   [P₂Cp]
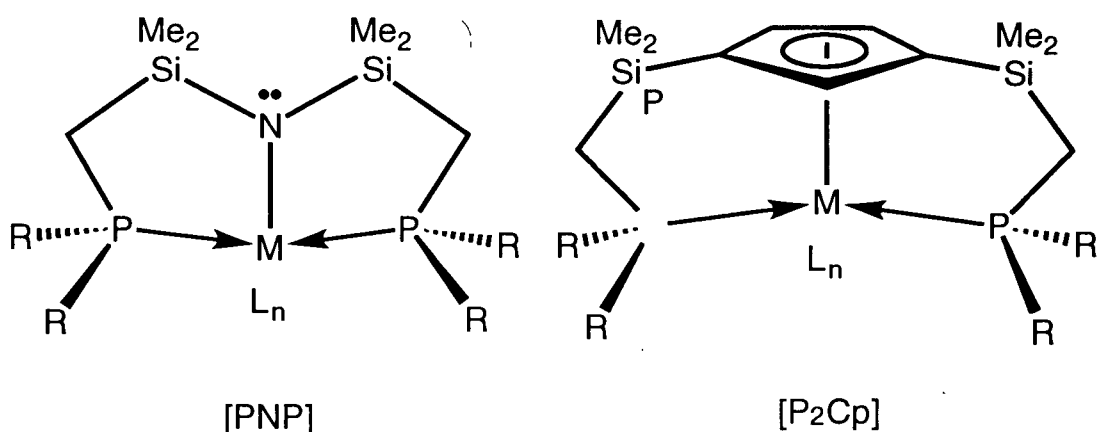
In view of the interest in cyclopentadienyl complexes of the Group 4 metals, and the scarcity of complexes with pendant phosphine donors, it was a logical extension to substitute the amide donor in [PNP] with a Cp group to give the analogous hybrid-donor ligand $1,3-C_5H_3-(SiMe_2CH_2PR_2)_2$ [P2Cp]. This is a rare example of a Cp ligand with two pendant phosphine donors,[94,95] which resembles the dianionic ligand depicted in **J**. Employing this ancillary ligand with Zr and Hf allows comparisons with other Cp complexes, in addition to a parallel comparison with results obtained with the [PNP] ligand set. One of the main differences between the two ligands arises from the steric bulk of the substituted Cp ring in [P2Cp] compared to the amide in [PNP], which extends the side-arms and introduces a different distortion in the metal–phosphine bond angles. Additionally, the steric bulk and higher electron count of the Cp donor increases saturation at the metal centre. Substituting the Cp group for the more basic

amide and removing the reactive silyl-amide linkage also adds greater hydrolytic stability to the ancillary ligand, while a further advantage is the option to modify the Cp group in addition to the phosphine substituents to change the ligand environment.

Early work with the P_2Cp ligand has enabled the isolation of the first structurally characterized zirconium alkylidene complex.[96] However, the mechanism of this reaction was not determined. An investigation into these mechanistic details may furnish insight into the role of the ancillary ligand in the formation and stabilization of this alkylidene species, in view of the relative scarcity of Group 4 alkylidenes derivatives in comparison to the number of examples from Group 5. Information obtained from this study can be applied towards the chemistry of other complexes coordinated by the P_2Cp ancillary ligand. This thesis is therefore organized into three experimental chapters, with the mechanism of formation and reactivity of the alkylidene complex serving as a central theme.

Chapter 2 introduces zirconium(IV) and hafnium(IV) halide and alkyl complexes stabilized by the isopropyl-substituted phosphine version of the ancillary ligand. Surprising differences between the Zr and Hf chloride complexes are examined. The structure of the alkyl complexes are discussed, with an emphasis on the effects of the size and number of the alkyl ligands on the fluxional coordination of the side-arm phosphines.

Conspicuously absent in the discussion of alkyl complexes in Chapter 2 are the dialkyl derivatives. In Chapter 3 it is shown that attempts to synthesize these complexes leads to an equilibrium with the mono- and tri-substituted species. Kinetic details of the subsequent thermal reaction of this mixture to give Zr and Hf alkylidene complexes are investigated. Sequential insertion reactions starting from these alkylidene species are described, along with a discussion concerning the influence of the ancillary ligand in the observed reactivity.

In view of the important role of the bulky isopropyl phosphines in the solution behaviour and reactivity of the complexes described in the preceding chapters, Chapter 4 examines the

effect of steric modification with considerably smaller methyl groups. Changes in structure, solution dynamics and reactivity are observed for the alkyl complexes with these less bulky derivatives. The reactivity of a series of Zr(II) ethylene complexes is also studied as a contrast to the insertion reactions observed in Chapter 3. Concluding remarks will summarize the results of this thesis and delineate extensions for future work to other metals and alternate strategies for ligand modification.

1.9   References

(1)   *Comprehensive Organometallic Chemistry II*; Wilkinson, G.; Stone, F. G. A.; Abel, E. W., Ed.; Pergamon Press: Oxford, 1995.

(2)   Kealy, T. J.; Pauson, P. L. *Nature* **1951**, *168*, 1039.

(3)   Miller, S. A.; Tebboth, J. A.; Tremaine, J. F. *J. Chem. Soc.* **1952**, 632.

(4)   Wilkinson, G.; Rosenblum, M.; Whiting, M. C.; Woodward, R. B. *J. Am. Chem. Soc.* **1952**, *74*, 2125.

(5)   Greenwood, N. N.; Earnshaw, A. *Chemistry of the Elements*; Pergamon Press: Oxford, England, 1993.

(6)   Lauher, J. W.; Hoffman, R. *J. Am. Chem. Soc.* **1976**, *98*, 1729.

(7)   *Comprehensive Organometallic Chemistry*; Wilkinson, G.; Stone, F. G. A.; Abel, E. W., Ed.; Pergamon Press: Oxford, 1982.

(8)   Cardin, D. J.; Lappert, M. F.; Raston, C. L. *Chemistry of Organo-Zirconium and -Hafnium Compounds*; Ellis Horwood, Ltd.: West Sussex, England, 1986.

(9)   Schwartz, J.; Labinger, J. A. *Angew. Chem., Int. Ed. Engl.* **1976**, *15*, 333.

(10)   Grubbs, R. H.; Tumas, W. *Science* **1989**, *243*, 907.

(11)   Petasis, N. A.; Fu, D.-K. *J. Am. Chem. Soc.* **1993**, *115*, 7208.

(12)   Breen, T. L.; Stephan, D. W. *J. Am. Chem. Soc.* **1995**, *117*, 11914.

(13)   Broene, R. D.; Buchwald, S. L. *Science* **1993**, *261*, 1696.

(14)   Negishi, E.; Takahashi, T. *Acc. Chem. Res.* **1994**, *27*, 124.

(15)   Jordan, R. F. *Adv. Organomet. Chem.* **1991**, *32*, 325.

(16)   Hoveyda, A. H.; Morken, J. P. *Angew. Chem., Int. Ed. Engl.* **1996**, *35*, 1262.

(17)   Sinn, H.; Kaminsky, W. *J. Organomet. Chem.* **1980**, *18*, 99.

(18)   Ewen, J. A. *J. Am. Chem. Soc.* **1984**, *106*, 6355.

(19)   Kaminsky, W.; Külper, K.; Brintzinger, H. H.; Wild, F. R. W. P. *Angew. Chem., Int. Ed. Engl.* **1985**, *24*, 507.

(20)   Broene, R. D.; Buchwald, S. L. *J. Am. Chem. Soc.* **1993**, *115*, 12569.

(21)   Khand, I. U.; Knox, G. R.; Pauson, P. L.; Watts, W. E.; Foreman, M. I. *J. Chem. Soc., Perkin Trans.1* **1973**, *1*, 973.

(22)   Hicks, F. A.; Buchwald, S. L. *J. Am. Chem. Soc.* **1996**, *118*, 11688.

(23)   Ewen, J. A.; Jones, R. L.; Razavi, A.; Ferrara, J. D. *J. Am. Chem. Soc.* **1988**, *110*, 6255.

(24)   Haltermann, R. L. *Chem. Rev.* **1992**, *92*, 965.

(25)   Coates, G. W.; Waymouth, R. M. *Science* **1995**, *267*, 217.

(26)   Herzog, T. A.; Zubris, D. L.; Bercaw, J. E. *J. Am. Chem. Soc.* **1996**, *118*, 11988.

(27)   Giardello, M. A.; Eisen, M. S.; Stern, C. L.; Marks, T. J. *J. Am. Chem. Soc.* **1995,** *117,* 12114.

(28)   Erker, G.; Berg, K.; Treschanke, L.; Engel, K. *Inorg. Chem.* **1982,** *21,* 1277.

(29)   Lund, E. C.; Livinghouse, T. *Organometallics* **1990,** *9,* 2426.

(30)   Krebs, B. *Angew. Chem., Int. Ed. Engl.* **1969,** *8,* 146.

(31)   Engelhardt, L. M.; Papasergio, R. I.; Raston, C. L.; White, A. H. *Organometallics* **1984,** *3,* 18.

(32)   Martín, A.; Mena, M.; Palacios, F. *J. Organomet. Chem.* **1994,** *480,* C10.

(33)   Winter, C. H.; Zhou, X.-X.; Dobbs, D. A.; Heeg, M. J. *Organometallics* **1991,** *10,* 210.

(34)   Erker, G. *J. Organomet. Chem.* **1990,** *400,* 185.

(35)   Zeijden, A. A. H.; Mattheis, C.; Fröhlich, R.; Zippel, F. *Inorg. Chem.* **1997,** *36,* 4444.

(36)   Erker, G.; Sarter, C.; Albrecht, M.; Dehnicke, S.; Krüger, C.; Raabe, E.; Schlund, R.; Benn, R.; Rufínska, A.; Mynott, R. *J. Organomet. Chem.* **1990,** *382,* 89.

(37)   Erker, G.; Sarter, C.; Werner, S.; Krüger, C. *J. Organomet. Chem.* **1989,** *377,* C55.

(38)   Chang, B.-H.; Grubbs, R. H.; C H Brubacker, J. *J. Organomet. Chem.* **1985,** *280,* 365.

(39)   Erker, G.; Zeijden, A. A. H. *Angew. Chem., Int. Ed. Engl.* **1990,** *29,* 512.

(40)   Erker, G.; Schamberger, J.; Zeijden, A. A. H.; Dehnicke, S.; Krüger, C.; Goddard, R.; Nolte, M. *J. Organomet. Chem.* **1993,** *459,* 107.

(41)   Wengrovius, J. H.; Schrock, R. R. *J. Organomet. Chem.* **1981,** *205,* 319.

(42)   Wolczanski, P. T.; Bercaw, J. E. *Organometallics* **1982,** *1,* 793.

(43)   Zucchini, U.; Albizzati, E.; Gianni, U. *J. Organomet. Chem.* **1971**, *26*, 357.

(44)   Pellechia, C.; Proto, A.; Longo, P.; Zambelli, A. *Macromol. Chem., Rapid Commun.* **1992**, *13*, 277.

(45)   Pindado, G. J.; Thornton-Pett, M.; Bouwkamp, M.; Meetsma, A.; Hessen, B.; Bochmann, M. *Angew. Chem., Int. Ed. Engl.* **1997**, *36*, 2358.

(46)   Ewart, S. W.; Sarsfield, M. J.; Jeremic, D.; Tremblay, T. L.; Williams, E. F.; Baird, M. C. *Organometallics* **1998**, *17*, 1502.

(47)   Crowther, D. J.; Jordan, R. F.; Baenziger, N. C.; Verma, A. *Organometallics* **1990**, *9*, 2574.

(48)   Gillis, D. J.; Tudoret, M.-J.; Baird, M. C. *J. Am. Chem. Soc.* **1993**, *115*, 2543.

(49)   Shapiro, P. J.; Bunel, E.; Schaefer, W. P.; Bercaw, J. E. *Organometallics* **1990**, *9*, 867.

(50)   Stevens, J. C.; Timmers, F. J.; Wilson, D. R.; Schmidt, G. F.; Nickias, P. N.; Rosen, R. K.; Knight, G. W.; Lai, S. Y. In *European Patent Application EP-416-815-A2*; March 1991 (Dow).

(51)   Canich, J. A. In *PCT Application WO 91/04257*; April 1991 (Exxon).

(52)   McKnight, A. L.; Masood, M. A.; Waymouth, R. M. *Organometallics* **1997**, *16*, 2879.

(53)   Okuda, J. *Chem. Ber.* **1990**, *123*, 1649.

(54)   Okuda, J.; Schattenmann, F. J.; Wocadlo, S.; Massa, W. *Organometallics* **1995**, *14*, 789.

(55)   Plooy, K. E. d.; Moll, U.; Wocadlo, S.; Massa, W.; Okuda, J. *Organometallics* **1995**, *14*, 3129.

(56)   Amor, F.; Spaniol, T. P.; Okuda, J. *Organometallics* **1997**, *16*, 4765.

20

(57)　Mu, Y.; Piers, W. E.; MacGillivray, L. R.; Zaworotko, M. J. *Polyhedron* **1995**, *14*, 1.

(58)　Mu, Y.; Piers, W. E.; MacQuarrie, D. C.; Zaworotko, M. J.; V G Young, J. *Organometallics* **1996**, *15*, 2720.

(59)　Jutzi, P.; Siemeling, U. *J. Organomet. Chem.* **1995**, *500*, 175.

(60)　Hughes, A. K.; Meetsma, A.; Teuben, J. H. *Organometallics* **1993**, *12*, 1936.

(61)　Schwink, L.; Knochel, P.; Eberle, T.; Okuda, J. *Organometallics* **1998**, *17*, 7.

(62)　Beckhaus, R.; Oster, J.; Ganter, B.; Englert, U. *Organometallics* **1997**, *16*, 3902.

(63)　Jutzi, P.; Kleimeier, J. *J. Organomet. Chem.* **1995**, *486*, 287.

(64)　Enders, M.; Rudolph, R.; Pritzkow, H. *Chem. Ber.* **1996**, *129*, 459.

(65)　LeBlanc, J. C.; Moise, C.; Maisonnat, A.; Poilblanc, R.; Charrier, C.; Mathey, F. *J. Organomet. Chem.* **1982**, *231*, C43.

(66)　Galakhov, M. V.; Heinz, G.; Royo, P. *J. Chem. Soc., Chem. Commun.* **1998**, 17.

(67)　Chen, Y.-X.; Fu, P.-F.; Stern, C. L.; Marks, T. J. *Organometallics* **1997**, *16*, 5958.

(68)　Zeijden, A. A. H.; Mattheis, C.; Fröhlich, R. *Organometallics* **1997**, *16*, 2651.

(69)　Christoffers, J.; Bergman, R. G. *Angew. Chem., Int. Ed. Engl.* **1995**, *34*, 2266.

(70)　Bosch, B. E.; Erker, G.; Fröhlich, R.; Meyer, O. *Organometallics* **1997**, *16*, 5449.

(71)　Jordan, R. F.; LaPointe, R. E.; Bradley, P. K.; Baenziger, N. *Organometallics* **1989**, *8*, 2892.

(72)　Guo, Z.; Swenson, D. C.; Jordan, R. F. *Organometallics* **1994**, *13*, 1424.

(73)   Razavi, A.; Thewalt, U. *J. Organomet. Chem.* **1993**, *445*, 111.

(74)   Flores, J. C.; Chien, J. C. W.; Rausch, M. D. *Organometallics* **1994**, *13*, 4140.

(75)   Collman, J. P.; Hegedus, L. S.; Norton, J. R.; Finke, R. G. *Principles and Applications of Organotransition Metal Chemistry*; University Science Books: Mill Valley, 1987, pp 989.

(76)   Kagan, H. B. *Asymmetric Synthesis*; Academic: New York, 1985.

(77)   Elschenbroich, C.; Salzer, A. *Organometallics;* 2nd ed.; VCH Publications: New York, 1992, pp 495.

(78)   Wielstra, Y.; Gambarotta, S.; Roedelof, J. B. *Organometallics* **1988**, *7*, 2177.

(79)   Stein, B. K.; Frerichs, S. R.; Ellis, J. E. *Organometallics* **1987**, *6*, 2017.

(80)   Fryzuk, M. D.; Love, J. B.; Rettig, S. J.; Young, V. G. *Science* **1997**, *275*, 1445.

(81)   Fryzuk, M. D.; Haddad, T. S.; Mylvaganum, M.; McConville, D. H.; Rettig, S. J. *J. Am. Chem. Soc.* **1993**, *115*, 2782.

(82)   Jordan, R. F.; Bajgur, C. S.; Dasher, W. E.; Rheingold, A. L. *Organometallics* **1987**, *6*, 1041.

(83)   Beckhaus, R. *Angew. Chem., Int. Ed. Engl.* **1997**, *36*, 686.

(84)   Harris, R. K. *Nuclear Magnetic Resonance Spectroscopy*; Pitman Books Limited: London, 1983, pp 250.

(85)   Tolman, C. A. *Chem. Rev.* **1977**, *77*, 313.

(86)   Butenschön, H.; Kettenbach, R. T.; Krüger, C. *Angew. Chem., Int. Ed. Engl.* **1992**, *31*, 1066.

(87)   Cowley, A. H.; King, C. S.; Decken, A. *Organometallics* **1995**, *14*, 20.

(88)   Lee, I.; Dahan, F.; Maisonnat, A.; Poilblanc, R. *Organometallics* **1994**, *13*, 2743.

(89)   Togni, A.; Breutel, C.; Schnyder, A.; Spindler, F.; Landolt, H.; Tijani, A. *J. Am. Chem. Soc.* **1994**, *116*, 4062.

(90)   Singewald, E. T.; Mirkin, C. A.; Stern, C. L. *Angew. Chem., Int. Ed. Engl.* **1995**, *34*, 1624.

(91)   Schore, N. E. *J. Am. Chem. Soc.* **1979**, *101*, 7410.

(92)   Fryzuk, M. D.; MacNeil, P. A.; Rettig, S. J.; Secco, A. S.; Trotter, J. *Organometallics* **1982**, *1*, 918.

(93)   Fryzuk, M. D.; Carter, A.; Westerhaus, A. *Inorg. Chem.* **1985**, *24*, 642.

(94)   Atherton, M. J.; Fawcett, J.; Holloway, J. H.; Hope, E. G.; Karaçar, A.; Russell, D. R.; Saunders, G. C. *J. Chem. Soc., Chem. Commun.* **1995**, 191.

(95)   Barthel-Rosa, L. P.; Catalano, V. J.; Maitra, K.; Nelson, J. H. *Organometallics* **1996**, *15*, 3924.

(96)   Fryzuk, M. D.; Mao, S. S. H.; Zaworotko, M. J.; MacGillivray, L. R. *J. Am. Chem. Soc.* **1993**, *115*, 5336.

Chapter 2

Halide and Alkyl Complexes of

Zirconium and Hafnium

Stabilized by the Ancillary P$_2$Cp Ligand

2.1   Introduction

In this chapter the preparation of a new type of ancillary ligand is presented, and the coordination chemistry of the isopropyl variant of this ligand is examined with zirconium (IV) and hafnium (IV), to form a series of halide and alkyl complexes. The stability conferred by the ancillary ligand to these species, and in particular the role of the side-arm phosphines, will be investigated. The sensitivity of the coordination of these pendant donors to the number and size of the alkyl substituents on the metal centre will be evaluated, and the reactivity of these complexes will also be briefly discussed. The dialkyl complexes ^{Pr}[P$_2$Cp]MClR$_2$ are omitted in the discussion of alkyl complexes in this chapter. The inability to isolate these species is the initial focus for Chapter 3, as these complexes disproportionate to give an equilibrium mixture of alkyl-substituted derivatives [P$_2$Cp]MCl$_x$R$_{3-x}$ (x = 0-2), which undergoes a thermal reaction to yield an alkylidene complex in a composite mechanism.

references begin on page 75

2.2 Synthesis of ^{R}[P$_2$Cp]Li (R = Me, Pr^i, Bu^t)

Shown below in Scheme 2.1 is the sequence of reactions in the synthesis of the ancillary ligand P$_2$Cp to be employed in the course of this study.
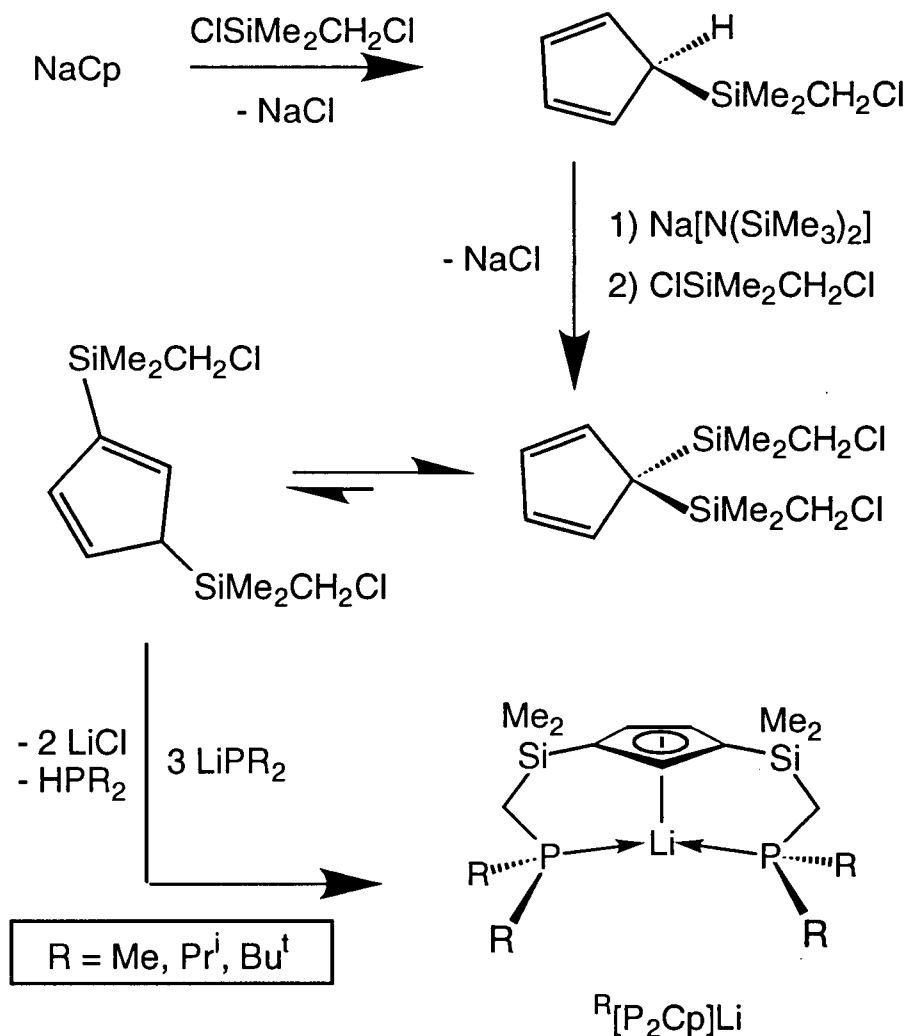
Scheme 2.1 Reaction scheme for the synthesis of the ancillary ligand ^{R}[P$_2$Cp]Li.

The preparation of this ligand involves the stepwise attachment of the two side-arms to a cyclopentadienyl anion. Each of these steps begins with deprotonation of an acidic ring proton, followed by attack of the Cp anion at the more electrophilic silyl-chloride bond. A silatropic

shift gives rise to isomeric forms as shown above, but in the last step only the 1,3-disubstituted isomer possesses an acidic proton, which yields directly to a high yield of the desired lithium salt of the ancillary ligand. The steric bulk of the ligand can be adjusted by the choice of phosphide utilized in this last synthetic step. The advantage of the silatropic shift is evident in comparison to synthetic difficulties encountered with the analogous bis(side-arm) ligand system **J** illustrated in Chapter 1.[1] Attachment of the two-carbon backbone in this latter system generates a mixture of 1,2- and 1,3-isomers in the final product, which both lowers the yield and introduces the synthetic complication of separating products.

The Pr^i and Bu^t ligand salts are both obtained as white solids while the Me derivative is isolated as a viscous reddish oil. Evidence for the coordination of both pendant donors to Li is supplied by the ^{31}P{^{1}H} NMR spectrum, which shows a distinct 1:1:1:1 quartet (for example, $^1J_{LiP}$ = 48Hz for the Bu^t complex) for equivalent phosphines coupled to a ^{7}Li centre (I = 3/2). Additional coupling to ^{6}Li (I = 1, 7.4 % natural abundance) is also observed in the same spectrum ($^1J_{LiP}$ = 48Hz).

2.3.1 Synthesis and Structure of ^{Pr}[P$_2$Cp]MCl$_3$ (M = Zr, Hf)

A stoichoimetric reaction of MCl$_4$(THT)$_2$ (M = Zr, Hf; THT = tetrahydrothiophene) with the ligand ^{Pr}[P$_2$Cp]Li in toluene produces the complex ^{Pr}[P$_2$Cp]MCl$_3$ (**1**: M = Zr,[2] **2**: M = Hf) in high yield as pale yellow (**1**) or white (**2**), air- and moisture-sensitive crystals (equation 2.1). The comparative inertness of Hf relative to Zr is apparent in the conditions used in these reactions. The formation of **1** is complete within 12 h under ambient conditions, while the Hf derivative **2** requires 24 h at 65 °C.

$$\text{MCl}_4(\text{THT})_2 + {}^{Pr}[\text{P}_2\text{Cp}]\text{Li}$$

- LiCl
- 2 THT

(2.1)
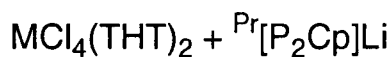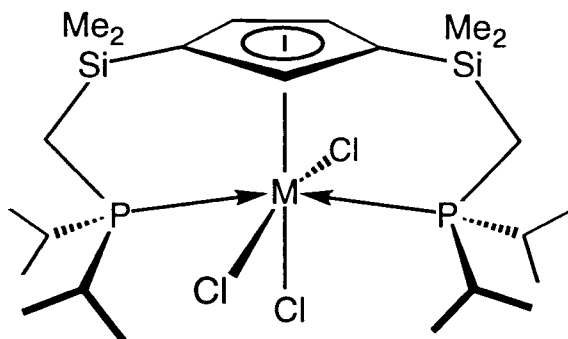
1   M = Zr

2   M = Hf

A non-coordinating solvent such as toluene is utilized in the preparation of **1**, since the same reaction conducted in THF gives an oily mixture consisting of **1**, unreacted [P$_2$Cp]Li, and an additional species characterized as the bis(ligand) complex ^{Pr}[P$_2$Cp]$_2$ZrCl$_2$.[2] The formation of ^{Pr}[P$_2$Cp]$_2$ZrCl$_2$ is obtained from the reaction of **1** with another equivalent of ^{Pr}[P$_2$Cp]Li in THF. This new species, a side-arm substituted analogue of zirconocene dichloride, is tentatively identified by assigned resonances for the ancillary ligand in the ^{1}H NMR, and a singlet in the ^{31}P{^{1}H} NMR spectrum for equivalent dangling phosphines. The formation of this species involves initial metathesis of the chloride in ZrCl$_4$(THT)$_2$ by ^{Pr}[P$_2$Cp]Li to give ^{Pr}[P$_2$Cp]ZrCl$_3$(THT)$_2$ having both phosphine arms dangling. In toluene, the THT ligands of this intermediate are replaced by the intramolecular phosphine donors to generate **1** before a further reaction can occur with ^{Pr}[P$_2$Cp]Li. In THF, rapid ligand exchange with the solvent yields the solvated species ^{Pr}[P$_2$Cp]ZrCl$_3$(THF)$_2$, which preventis the phosphines from coordinating. As this species is more soluble than MCl$_4$(THT)$_2$ it can effectively compete for a second equivalent of [P$_2$Cp]Li to generate the bis(ligand) complex ^{Pr}[P$_2$Cp]$_2$ZrCl$_2$. This synthetic complication of forming an intermediate in a coordinating solvent that is more soluble and kinetically prone to

further reactivity, before the reaction of the starting material $ZrCl_4(THF)_2$ can proceed to completion, has been noted in other instances.[3]

The trichloride derivatives **1** and **2** are isostructural, as determined by X-ray crystallography. This is not surprising, given the close similarity in size and electronic configuration between the two congeners Zr and Hf.[4] The Hf derivative **2** is depicted in Figure 2.1, and selected bond length and bond angles are presented for both **1** and **2** in Table 2.1 for comparison. Note that corresponding metal-ligand bond distances are slightly shorter for **2**, a feature that reflects a general trend in Hf complexes versus Zr analogues.[5] The overall geometry of **2** can be described as a quasi-octahedral structure of C_s symmetry, with the cyclopentadienyl ring of the ancillary ligand occupying an apical coordination site and the two pendant phosphine donors in mutually *trans* equatorial positions. A pair of *trans* chloro ligands are located in the same equatorial plane as the two phosphines, with a third chloride *trans* to the cyclopentadienyl ring. This monomeric, octahedral structure has been similarly observed in other structurally characterized adducts of the general formula $CpMCl_3(L)_2$,[6,7] including examples in which one[8] or both[9] of the donor atoms is appended to the cyclopentadienyl ring *via* a side-arm tether. However, in all of these structures the thee chlorides are in equatorial positions, with one of the neutral donors adopting the labile axial site *trans* to the cyclopentadienyl ring. Spectroscopic studies have commonly observed fluxional coordination of the donor molecule at this site.[7,10] By comparison, it is readily apparent in **2** that the constrained geometry imposed by the two chelating side-arms induces a unique orientation of the ligands within this octahedral framework, as neither phosphine can reach the axial site *trans* to the Cp ring, and the 1,3-configuration of the side-arms further restricts these pendant donors to mutually trans positions within the equatorial plane.
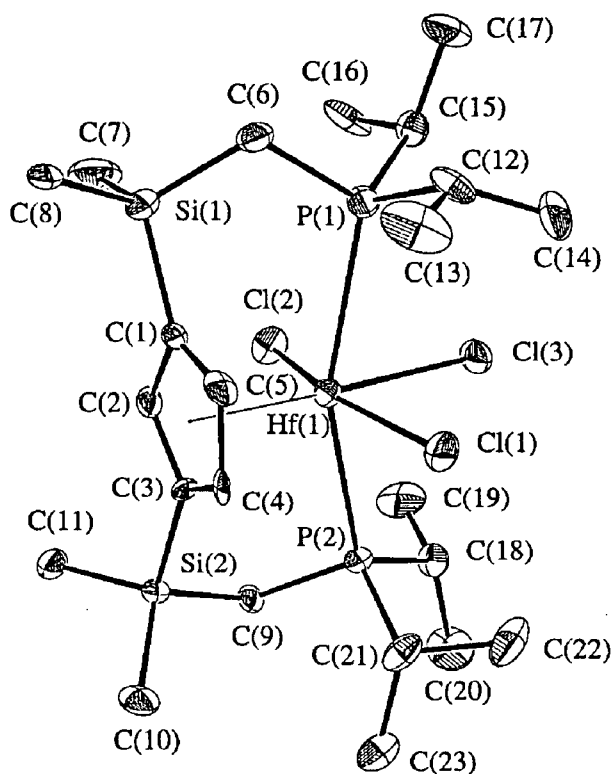
Figure 2.1 Molecular structure of ^{Pr}[P$_2$Cp]HfCl$_3$ (**2**); 33% probability thermal ellipsoids are shown. Hydrogen atoms and disorder not shown for clarity.

Table 2.1 Selected Bond Length (Å) and Bond Angles (deg) for ^{Pr}[P$_2$Cp]MCl$_3$ (**1**: M = Zr,[2] **2**: M = Hf). The numbering scheme is identical for each.

	1	2		1	2
M-Cl(1)	2.489(1)	2.466(3)	Cl(1)-M-Cl(2)	160.61(5)	160.6(1)
M-Cl(2)	2.490(1)	2.476(3)	Cl(1)-M-Cl(3)	80.79(3)	80.7(1)
M-Cl(3)	2.529(1)	2.514(3)	Cl(2)-M-Cl(3)	81.19(5)	81.1(1)
M-P(1)	2.897(1)	2.876(4)	P(1)-M-P(2)	159.53(4)	159.3(1)
M-P(2)	2.871(1)	2.847(4)	Cl(3)-M-P(1)	78.32(4)	78.1(1)
M-Cp'	2.260(5)	2.25	Cl(3)-M-P(2)	81.43(4)	81.4(1)
			Cp'-M-Cl(3)	177.50	177.4

For both **1** and **2**, the steric bulk of the Cp ring induces the equatorial M-Cl and M-P bonds to bend away from this group towards the axial chloride. The P(1)-M(1)-P(1) and Cl(1)-M(1)-Cl(2) angles are therefore distorted from ideal octahedral geometry by approximately 20°, while the axial Cp(centroid)-M-Cl(3) angle remains unaffected. As mentioned in the previous chapter this structural mode is prevalent for mono(cyclopentadienyl) complexes.[11] The substituted Cp ring in **1** is also responsible for a lengthened M(1)–Cp(centroid) distance that is generally found with bulky Cp derivatives, particularly those which have pendant side-arm donors.[12] In comparison, for complexes coordinated by unsubstituted cyclopentadienyl rings, such as polymeric $CpZrCl_3$[13] and monomeric Cp_2ZrCl_2,[14] the Zr–Cp(centroid) distances are 2.196 Å and 2.20 Å, respectively. The M–P and M-Cl bond distances in **1** are within the normal range for Zr(IV) and Hf(IV) species; of note, however, is the lengthened axial M(1)-Cl(3) bond relative to the two equatorial M-Cl bond distances due to its position *trans* to the strong Cp donor.

2.3.2 Solution Behaviour of $^{Pr}[P_2Cp]MCl_3$ (M = Zr, Hf)

It is interesting to note that although the trichloride complexes **1** and **2** possess essentially identical molecular structures in the solid state, the solution behavior of these species as measured by multinuclear NMR spectroscopy differ markedly. The $^{31}P\{^1H\}$, $^{13}C\{^1H\}$, and ^1H NMR spectra of the Zr derivative **1** are consistent with the solid state structure and remain unchanged over a wide temperature range, whereas the corresponding spectra for the Hf analogue **2** exhibit complicated temperature-dependent fluxionality. The spectral data of **1** are straightforward and will be addressed first, to provide a foundation from which the fluxional processes associated with the complicated NMR spectra of **2** can be more easily interpreted.

The $^{31}P\{^1H\}$ NMR spectrum of **1** shows a singlet at 10.7 ppm for two equivalent phosphines in a chemical shift region that is indicative of coordination to the metal centre. In the ^1H NMR spectrum there are two cyclopentadienyl proton resonances in a 2:1 ratio due to the C_s symmetry of the complex, along with two peaks for the silylmethyl (Si(CH_3)$_2$), two for the

methylene (PCH_2Si), and four for the isopropyl (PCH(CH_3)$_2$) protons of the ligand backbone (Figure 2.2). The isopropyl and methylene protons exhibit additional coupling to the phosphorus nuclei. These combined features are all in agreement with the structure of **1** depicted in Figure 2.1, and as mentioned above, these spectra remain invariant with changes in temperature, implying that any exchange process involving the side-arm phosphines is undetectable on the NMR time scale. This solution behaviour contrasts with the adduct CpZrCl$_3$(THF)$_2$,[7] a schematic structure of which is shown as **G** in Chapter 1, which undergoes rapid exchange of the THF ligand *trans* to the Cp ring with bulk solvent molecules, presumably via a dissociative process involving a CpZrCl$_3$(THF) intermediate. The absence of similar fluxional behavior in **1** attests to the stability of the chelating phosphine donors.
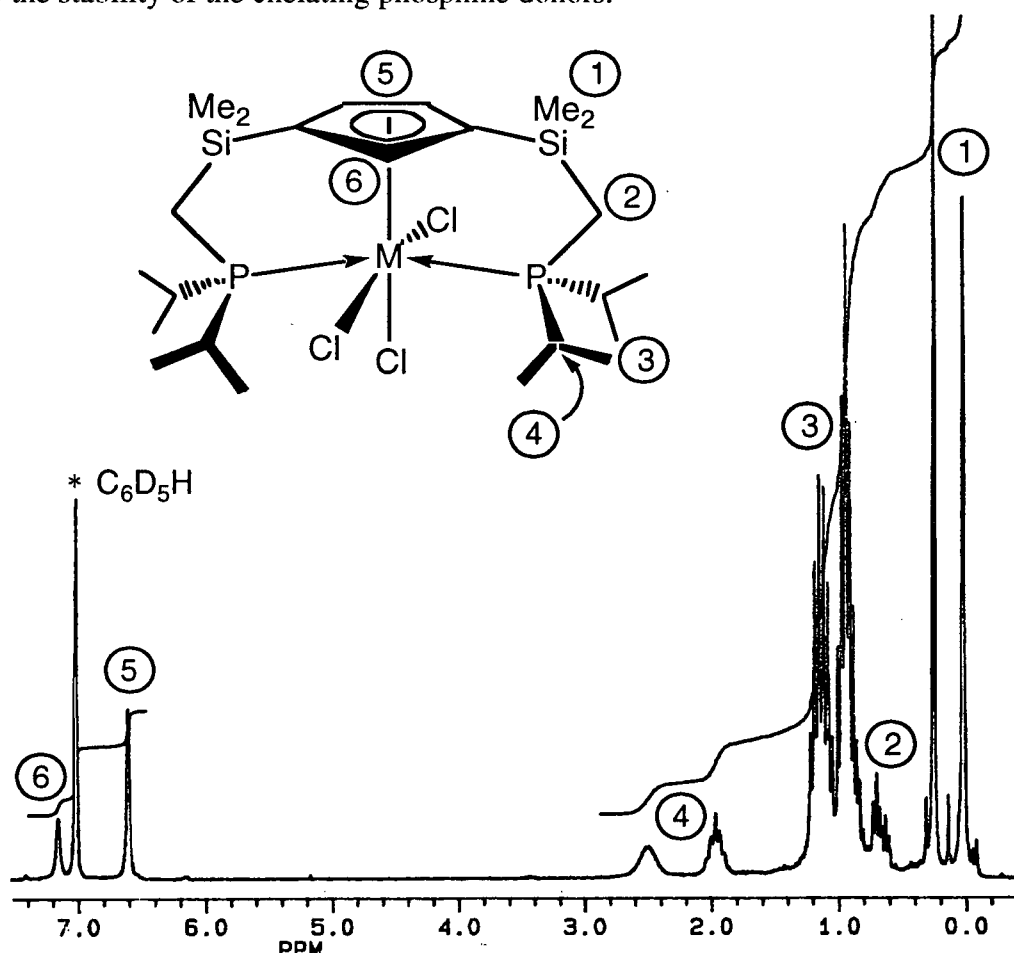
Figure 2.2   Ambient temperature ^{1}H NMR spectrum of ^{Pr}[P$_2$Cp]ZrCl$_3$ (**1**) in C$_6$D$_6$.

A curious aspect of the ^{1}H NMR spectrum of **1** is the observation that the resonance of the unique proton of the cyclopentadienyl ring (attached to C(2) in Figure 2.1) shifts from 6.0 ppm in ^{Pr}[P$_2$Cp]Li to 7.3 ppm in **1**, while the resonance due to the remaining two protons, attached to C(4) and C(5), remain at the same position of 6.4 ppm. This may be due to a weak interaction between that single proton and Cl(2). The distance between these two atoms as measured from the X-ray crystal structure is 2.7 Å, which is closer than the van der Waals H···Cl distance of 3.0 Å.[15] The sensitivity of the chemical shifts of these cyclopentadienyl protons to the chemical environment of the rest of the complex is a characteristic feature with this ancillary ligand and will be encountered further in a number of other examples.

In contrast to the routine solution behavior observed for **1**, the NMR spectroscopic features of the structurally similar Hf derivative **2** are surprising. For example, the ambient temperature ^{31}P{^{1}H}NMR spectrum of **2** shows thee exchange-broadened resonances at -4.9, 14.9, and 24.9 ppm, in an approximate 1:2:1 ratio, respectively, in comparison to the sharp singlet seen for **1**. The two equal intensity peaks at -4.9 and 24.9 ppm also share a resemblance in line shape, while the remaining peak at 14.9 ppm is somewhat narrower. Meanwhile, the ^{1}H NMR spectrum of **2** at this temperature also exhibits extremely broad resonances from which little information can be gleaned.

Variable temperature (VT) ^{31}P{^{1}H} and ^{1}H NMR spectroscopies were utilized to monitor the exchange process that is operative at room temperature, and the results are shown in Figure 2.3. As the temperature is lowered below ambient temperature the peaks in the ^{31}P NMR spectrum gradually sharpen, and the two resonances at -4.9 ppm and 24.9 ppm decrease in intensity relative to the other peak at 14.9 ppm. This trend continues until only the sharp singlet at 14.9 ppm remains below -65 °C. At this temperature the ^{1}H NMR spectrum is also straightforward, with well defined peaks for the ancillary ligand that bear a striking resemblance to the ambient temperature spectrum of **1**. Indeed, the similarity extends to the cyclopentadienyl resonances, where the same 2:1 integration ratio is observed with the peak for the unique Cp proton again located downfield.
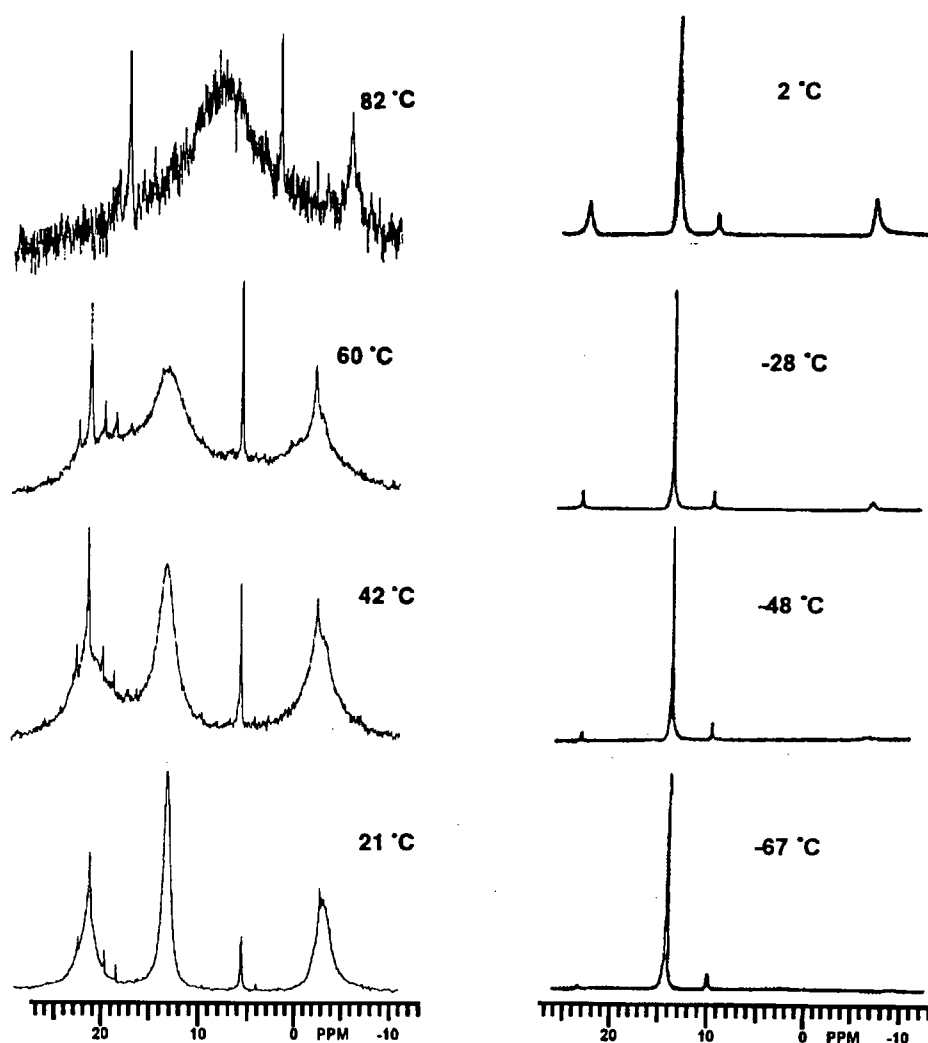
Figure 2.3   Variable Temperature ^{31}P{^{1}H} NMR spectra of ^{Pr}[P$_2$Cp]HfCl$_3$ (**2**) in C$_7$D$_8$.

If the singlet at 14.9 ppm in the ^{31}P NMR spectrum is identified with the octahedral structure shown in Figure 2.1, then the two other peaks at -4.9 and 24.9 ppm appear to belong to a single separate isomer, as they are related by equivalent line shapes and integration in each spectrum that is obtained. The structures of this second species is hinted at by the spectral data: the downfield peak at 24.9 ppm suggests a strongly coordinating phosphine donor, while the

references begin on page 75

other peak at -4.9 ppm is indicative of an unbound phosphine. A five coordinate structure as shown below (**2'**) is consistent with this data. The ^{1}H NMR spectrum also supports this proposed structure. Above -65 °C the emergence of new resonances can be discerned that are separate from those assigned to the octahedral isomer **2**. These new peaks are indicative of the low symmetry presented by 1b'. For example, separate singlets are observed for the four inequivalent silylmethyl groups, and the thee cyclopentadienyl protons are also inequivalant. Assignment of the remaining resonances for **2'** in the ^{1}H NMR spectrum is complicated by the coexistence of **2**, which results in an overlap of resonances for the methylene and isopropyl groups. Analysis of the spectrum is hampered further as the temperature is raised, since the exchange-broadening increases as coalescence is approached at 20 °C.

2'
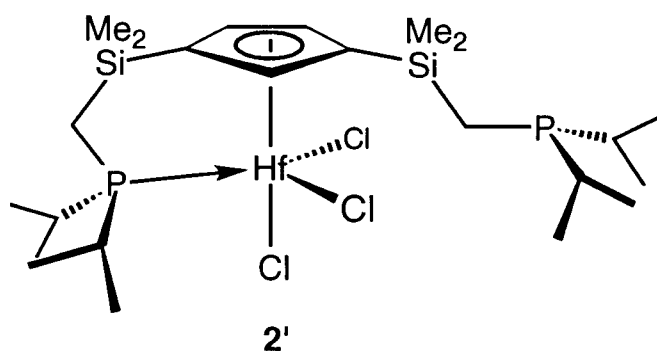
It is evident from the VT spectral data that the two isomers **2** and **2'** are in equilibrium (equation 2.2). The former is exclusively favoured at low temperatures, while the latter becomes increasingly abundant as temperature is raised. To evaluate this equilibrium, the relative concentration of each species was measured at separate temperatures in the range between -65 °C and 20 °C, for which reliable measurements could be made from integration of the ^{31}P NMR spectra. Equilibrium constants were calculated according to the equation K = [**2'**]/[**2**] and plotted as a function of temperature. The data are listed in Table 2.2 and the resulting van't Hoff plot shown in Figure 2.4, from which the thermodynamic parameters $\Delta H° = 4.9(5)$ kcal mol^{-1} and $\Delta S°$ = 17(1) cal mol^{-1}K^{-1} were obtained. The errors were estimated from separate experimental runs and indicate reproducibility. The positive entropy term is in accord with a less-ordered structure

for **2'**, represented by the dangling pendant side-arm and the overall lower symmetry of this molecule.

(2.2)
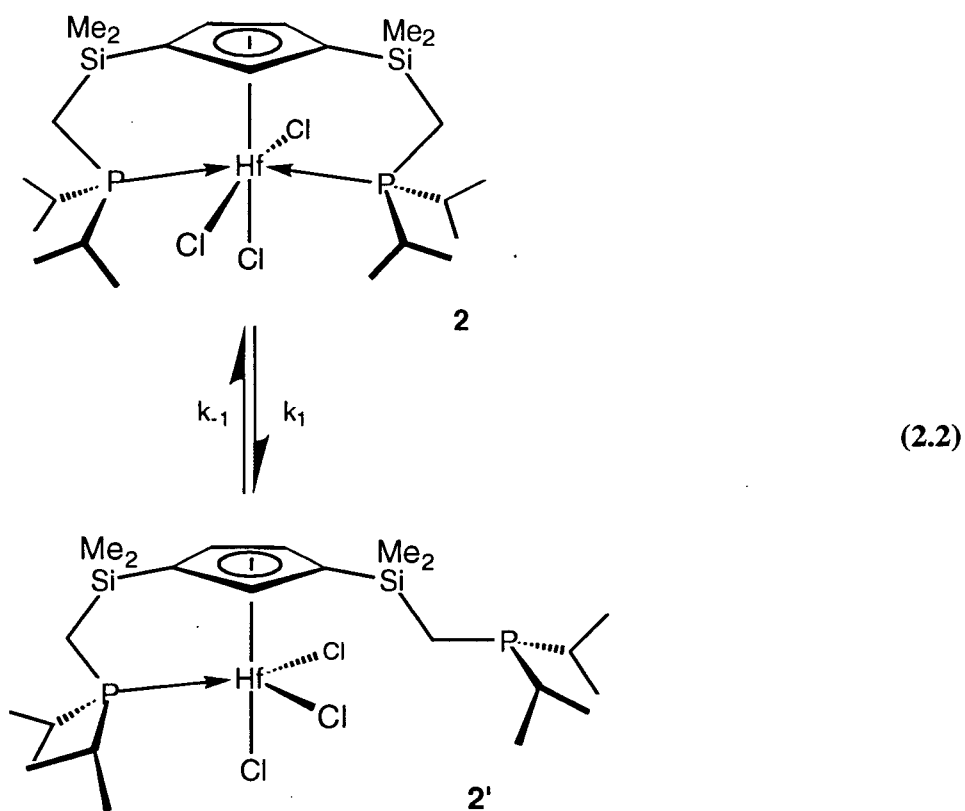
Table 2.2   Equilibrium constant (K) as a function of temperature for the two Hf

trichloride species in equation 2.2, obtained from the $^{31}P\{^{1}H\}$ NMR spectra

shown in Figure 2.6.

T (°C)	-67.1	-48.0	-28.3	2.1	24.0	36.6
K	0.04	0.08	0.19	0.60	1.22	1.54

Figure 2.4 A van't Hoff plot of the $^{31}P\{^{1}H\}$ NMR spectral data for the equilibrium shown in equation 2.2.

The resonances in the $^{31}P\{^{1}H\}$ and ^{1}H NMR spectra for this system are broadened because the fluxional process that interconverts the equilibrium species occurs at a rate comparable to the NMR time scale. The value of the equilibrium constant has a significant effect on line broadening.[16] The increase in line width (Δv) due to chemical exchange is dependent on the average lifetime (τ) that a nuclear spin-state is populated, which is directly proportional to the rate at which that spin-state is exchanged (equation 2.3).

$$\Delta v_A = 1/\tau_A \pi \qquad\qquad \text{where } \tau_A = 1/k_A \qquad\qquad (2.3)$$

For sites that are unequally populated (i.e., $K \neq 1$) the exchange rates will also differ ($K = k_1/k_{-1}$), so that the resulting line-broadening will be greater for the less abundant species. This is

36 *references begin on page 75*

observed in the present system where the lower concentration of **2'** results in proportionally wider peaks at lower temperatures relative to **2**. The peaks for **2'** show additional line broadening as the two phosphine environments within this molecule are also under exchange (Scheme 2.2).
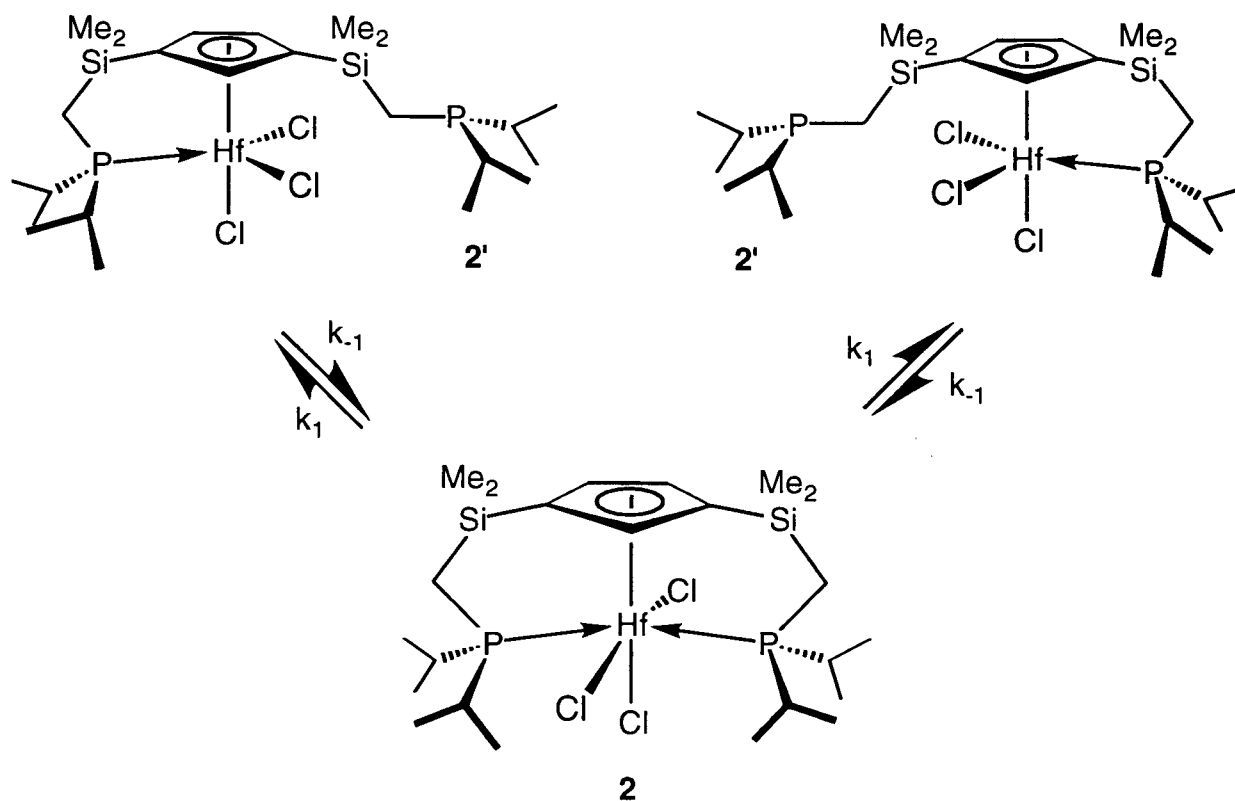
Scheme 2.2   Exchange process in the equilibrium of $^{Pr}[P_2Cp]HfCl_3$ (**2**).

In the low temperature spectrum this process is frozen out at the slow exchange limit, and distinct peaks with narrow line width can be identified for each isomer. A rise in temperature increases the rate of exchange and produces greater line broadening until coalescence (T$_c$) is reached. This point occurs at a higher temperature in the $^{31}P\{^{1}H\}$ NMR spectrum (50 °C) in comparison to the ^{1}H NMR spectrum (20 °C), for spectra obtained from the same 300 MHz instrument, because of the wider peak separation (in Hz) between the resonances under exchange (equation 2.4).[17]

at T_c, $k_{ex} = 2.22\Delta\delta$ $\Delta\delta$ = peak separation (Hz) in the slow exchange limit   **(2.4)**

A similar effect of raising the coalescence temperature is observed upon measuring the same ^{31}P NMR spectrum at higher field (i.e. $T_c = 65$ °C at 202.33 MHz).

Above the coalescence temperature the ^{31}P NMR spectrum displays a single broad signal near 15 ppm that narrows in line width as the temperature is raised. The re-emerging peaks in the ^{1}H NMR spectrum above coalescence also become increasingly sharper until assignable resonances are observable for an average chemical environment near 50 °C. This corresponds to an averaging of the chemical environments of the two species in solution in the fast exchange limit.

The different solution behavior between **1** and **2** is puzzling, as the two species are isostructural in the solid state as indicated earlier. Since the ligand coordination sphere is identical in **1** and **2**, these complexes therefore offer a unique example of the subtle electronic differences that occasionally surface between these otherwise near-identical congeners. One can speculate why **2** should display fluxional phosphine coordination in solution to generate two species in equilibrium. The metal-ligand bond distances are shorter in the Hf derivative, suggesting that stronger Hf bonding may allow the metal centre to competitively attain a stable electronic configuration with a smaller coordination number and a correspondingly lower formal electron count (as in **2'**). In addition, this more open geometry may relieve steric pressures arising from closer Hf-ligand contacts in the octahedral geometry. A similar example where a Hf analogue adopts a coordination geometry in which the electron count is lower relative to the corresponding Zr species, is observed for the tetracyclopentadienyl derivatives Cp_4M (M = Zr,[18] Hf[19]). In this instance, only two of the Cp ligands are bound facially in an η^5-fashion for the Hf structure (compared to three for the Zr complex). Again, this modification is probably an attempt to relieve a similarly crowded coordination sphere.

2.3.3 General Reactivity of ^{Pr}[P$_2$Cp]MCl$_3$ (M=Zr, Hf)

The air and moisture sensitivity of trichloride **1** is dramatically reduced in comparison to the strong Lewis acids CpZrCl$_3$[13] and Cp*ZrCl$_3$.[20] **1** is also essentially inactive as a co-catalyst for the polymerization of ethylene in the presence of MAO. The side-arm phosphine donors provide electronic and coordinative saturation, the latter significantly enhanced by the steric bulk of the substituted cyclopentadienyl ring and the isopropyl groups on the phosphines. This protection also helps to control the reactivity which is outlined below.

2.4.1 Synthesis of [P$_2$Cp]MR$_3$ (M = Zr, Hf; R = CH$_2$Ph, CH$_2$CMe$_3$, CH$_2$SiMe$_3$)

Addition of either 3 equivalents of K(CH$_2$Ph) in THF or 1.5 equivalents of Mg(CH$_2$Ph)$_2$(THF)$_2$ in toluene to ^{Pr}[P$_2$Cp]MCl$_3$ generates the tribenzyl derivatives ^{Pr}[P$_2$Cp]M(CH$_2$Ph)$_3$ (**3**: M = Zr, **4**: M = Hf) as shown below (equation 2.5).

$$^{Pr}[P_2Cp]MCl_3 \quad \xrightarrow[\text{- 3 KCl}]{\text{3 KCH}_2\text{Ph}} \quad {}^{Pr}[P_2Cp]Zr(CH_2Ph)_3$$

$$\textbf{3} \quad M = Zr$$

$$\textbf{4} \quad M = Hf$$

(2.5)
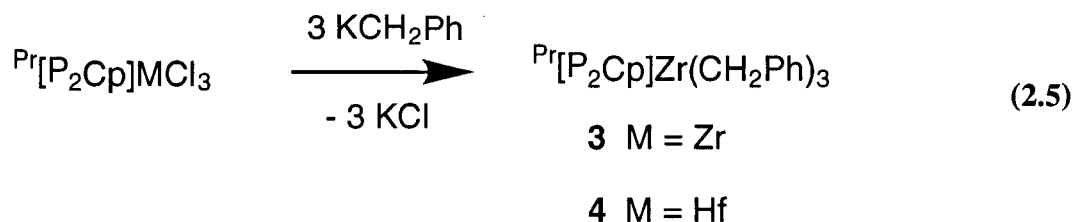
These compounds can be isolated cleanly as yellowish air- and moisture-sensitive, thermally-stable oils, that remain highly soluble in hydrocarbon solvents. In comparison to Zr(CH$_2$Ph)$_4$,[21] which decomposes rapidly in solution above 0 °C, the robust thermal stability of **2** is more in line with another tribenzyl derivative Cp*Zr(CH$_2$Ph)$_3$,[22] exemplifying the stabilizing influence provided by coordination of a bulky cyclopentadienyl donor.

The ^{1}H, ^{13}C{^{1}H}, and ^{31}P{^{1}H} NMR spectroscopic data for **3** and **4** are very similar and are both consistent with the presence of thee benzyl groups and one P$_2$Cp moiety. At ambient

temperatures, a singlet in the $^{31}P\{^1H\}$ NMR spectrum is observed for each species at -5.2 ppm (3) and -5.9 ppm (4), respectively, which as described previously is in the chemical shift range for uncoordinated phosphine donors. Further evidence that the phosphine arms of the ligand are dangling in these complexes is furnished by the absence of ^{31}P coupling for both the protons and the carbons of the benzylic CH_2 groups, which appear as singlets in the respective ^1H and $^{13}C\{^1H\}$ NMR spectra. The structure of 2 can therefore be described as a thee-legged piano stool as depicted below, with phosphine coordination to the metal prevented by the presence of thee relatively bulky alkyl ligands. In addition, all three benzyl groups are equivalent in both the ^1H and $^{13}C\{^1H\}$ NMR spectra, as only one set of resonances is observed for each of the ortho, meta, para, and benzyl groups. The benzyl ligands are therefore undergoing rapid exchange, facilitated by a lack of interference from the dangling side-arms. Multinuclear NMR spectroscopic studies showed that this behavior persists even at low temperatures.
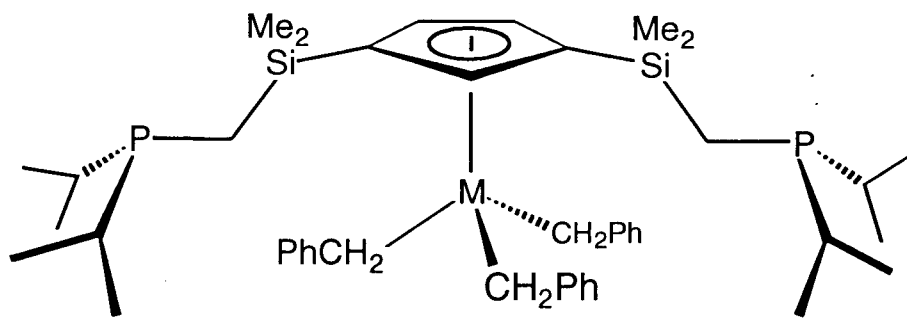
3   M = Zr

4   M = Hf

There is a tendency for benzyl ligands bound to early transition metals to depart from the conventional η^1-coordination mode of a normal σ-bond to improve electron donation.[10,23] This is accomplished either though an α-agostic[24] interaction or by increasing the hapticity to access the π-system in the phenyl ring. Both of these distortions induce shifts in the ^1H and the ^{13}C NMR spectroscopic features. A weakening of the agostic C-H bond decreases the $^1J_{CH}$ coupling (< 120 Hz) for this group, while an η^2-benzyl ligand displays upfield chemical shifts for both the methylene and ortho protons, and a corresponding upfield shift in the methylene and ipso carbon

atoms. An η^n structure is also typified by relatively large $^1J_{CH}$ coupling (> 140 Hz) for the methylenes as a result of partial rehybridization to an sp^2 electronic configuration.

There is spectroscopic evidence that the benzyl ligands in **2** may be coordinated in an η^2-interaction, which would not be unexpected given that the pendant phosphines are unable to bind in this unsaturated 14-electron complex. The ^1H NMR spectrum shows upfield resonances for the methylene and ortho protons near 1.9 and 6.6 ppm, respectively. The ipso and ortho carbon atoms are both located within an intermediate chemical shift range (near 125 ppm) in the ^{13}C NMR spectrum as are the methylene carbons at 70 ppm. The $^1J_{CH}$ value of 125 Hz for the methylene group in the coupled spectrum is within the normal range. Overall, in the absence of an X-ray structure the NMR data are inconclusive regarding the possible binding mode of these ligands, although fluxional behaviour may be responsible for averaging the values of these parameters.

The preparation of similar bulky trialkyl derivations, $^{Pr}[P_2Cp]Zr(CH_2EMe_3)_3$ (**5a:** E = C, **5b:** E = Si), could be achieved from **1a** with the appropriate alkylating reagent (equation 2.6).

$$^{Pr}[P_2Cp]ZrCl_3 \xrightarrow[- 3\ LiCl]{3\ LiCH_2EMe_3} {}^{Pr}[P_2Cp]Zr(CH_2EMe_3)_3$$

1

5a: E = C   (2.6)

5b: E = Si
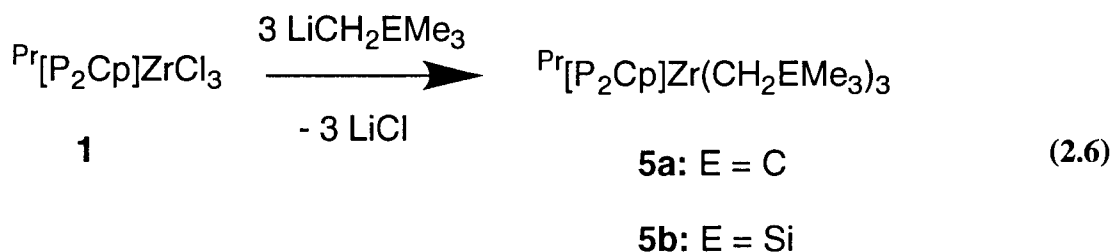
The tri-neopentyl (CH_2CMe_3) and tri-neosilyl (CH_2SiMe_3) complexes **5a** and **5b**, respectively, were both isolated cleanly as air- and moisture-sensitive, hydrocarbon-soluble oils. These species exhibit thermal stability similar to that observed for **2** and with the analogous trisubstituted derivative Cp^*ZrR_3 (R= CH_2CMe_3,[25] CH_2SiMe_3).

The ^1H NMR spectra for **3** and **4** show resonances for the methyl and methylene groups of the respective neopentyl and neosilyl ligands that integrate correctly for the stoichiometry

41

indicated. In the ^{31}P NMR spectrum a singlet is observed at -5.5 ppm for **5a** and similarly at -5.9 ppm for **5b**. These resonances remain unchanged at lower temperatures and are indicative of dangling phosphines, indicating a similar thee-legged piano stool geometry as found for **3**. It is evident that the ability of thee bulky alkyl ligands to sterically saturate the coordination sphere is a general feature with this ancillary ligand system.

2.4.2 Synthesis and Fluxional Behavior of ^{Pr}[P₂Cp]Zr(CH₃)₃

To examine the phosphine behaviour in a trialkyl species in which steric factors are minimized, the starting Zr chloride complex **1** was methylated; addition of three equivalents (or a slight excess) of MeMgBr in toluene generates the trimethyl derivative [P₂Cp]Zr(CH₃)₃ (**6**) (equation 2.7). The trimethyl derivative **6** can also be synthesized using MeLi, although this reaction is quite sensitive to reaction stoichiometry and solvent conditions. The addition of a slight excess of MeLi in ether results in decomposition of the entire reaction mixture; one of the reaction products detected in the resultant mixture is ^{Pr}[P₂Cp]Li. Similarly, adding 0.1 equiv. of MeLi to **6** induces the same decomposition process. One by-product of this reaction is ^{Pr}[P₂Cp]Li, so it is conceivable that the unstable tetramethyl species Zr(CH₃)₄ is formed, which acts as a catalyst for the decomposition of ^{Pr}[P₂Cp]Zr(CH₃)₃.

$$^{Pr}[P_2Cp]ZrCl_3 \xrightarrow[- \ 3 \ MgClBr]{3 \ MeMgBr} {}^{Pr}[P_2Cp]Zr(CH_3)_3 \qquad (2.7)$$

$$\textbf{1a} \qquad\qquad\qquad\qquad\qquad\qquad \textbf{6}$$
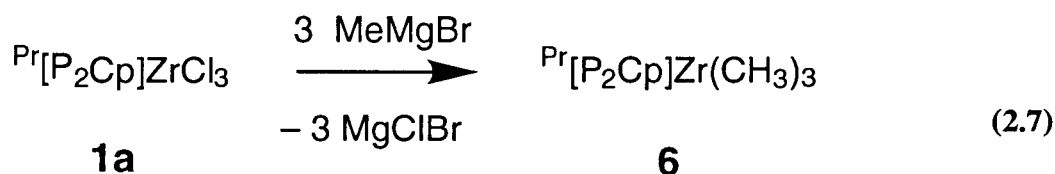
Trimethyl **6** is isolated as a yellowish air- and moisture-sensitive, slightly impure oil. This compound decomposes upon exposure to visible light within hours but has remarkable thermal stability in the dark at 100 °C, in marked contrast to the reported thermal lability of the related complex Cp*Zr(CH₃)₃.[22] The latter gradually decomposes under ambient conditions,

although the addition of external phosphine donors yields adducts (i.e., Cp*Zr(CH$_3$)$_3$(PMe$_3$)$_2$ and Cp*Zr(CH$_3$)$_3$(dmpe)) which can be isolated as thermally stable solids. It is worth noting that these adduct species comprise the same general ligand set that is present in **6**.

The ambient temperature NMR spectroscopic parameters for this trimethyl derivative are simple. A singlet at 2.3 ppm in ^{31}P{^{1}H} NMR spectrum is observed, indicative of equivalent phosphine donors, while the methyl groups attached to zirconium appear as one triplet in the ^{1}H NMR spectrum and one triplet at 42.7 ppm in the ^{13}C{^{1}H} NMR spectrum, indicating that these resonances are coupled to both phosphines. In addition, the ligand backbone resonances are also suggestive of high symmetry, giving rise to only one singlet for the silyl methyl groups and a doublet for the methylene hydrogens. The peaks due to the cyclopentadienyl protons appear in the familiar 1:2 ratio as a triplet at 6.42 ppm for the unique proton and a doublet at 6.71 ppm for the two equivalent protons.

Variable temperature experiments show that as the temperature is lowered, these simple NMR spectra broaden and become more complicated (Figure 2.4). For instance, the singlet in the ^{31}P NMR spectrum gets increasingly broader down to -33 °C, and below this temperature two very broad resonances grow out of the baseline near -37 °C. These new resonances, near -10 and 10 ppm, respectively, display similarly broad line shapes and peak intensities. A further decrease in temperature reveals an equivalent amount of narrowing in the line width of these peaks, while the other signal at 1.6 ppm shinks in relative intensity until it disappears into the baseline near -67 C. The ^{1}H and ^{13}C{^{1}H} NMR spectra also show the corresponding changes, although less clearly.
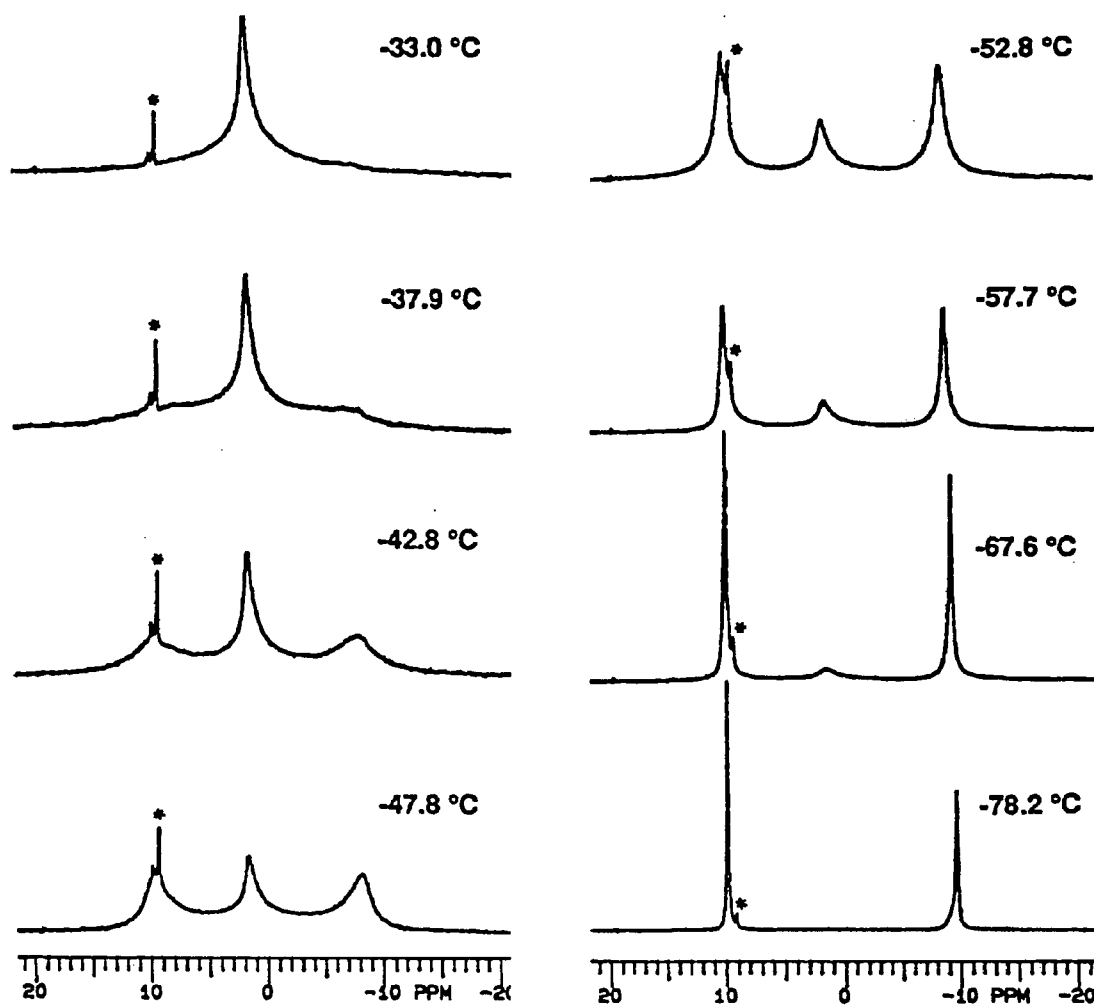
Figure 2.5 Variable temperature $^{31}P\{^1H\}$ NMR spectra of the two species in solution for $^{Pr}[P_2Cp]Zr(CH_3)_3$ (6). A minor unknown impurity is shown with an asterisk.

Aspects of this curious variable temperature behaviour parallel the complicated phenomena described earlier for the Hf trichloride **2**. Between -70 °C and -38 °C the ^{31}P NMR spectrum reveals the co-existence of two sets of resonances: one pair of related peaks for a single complex consisting of one coordinated and one uncoordinated phosphine (**6'**), and a separate singlet between these resonances belonging to a second species having equivalent phosphine donors (**6**). As with **2** the relative concentration of these species again varies according to a temperature-dependent equilibrium (equation 2.8), generating exchange broadening in the line width. Note that there is a significant difference with this equilibrium compared to the

44   *references begin on page 75*

equilibrium observed for **2**, however, in that the species favoured at lower temperatures is the asymmetric complex **6'**. At -80 °C this is the only detectable species, and additional support for the asymmetric structure is provided by the ^{1}H NMR spectrum obtained at this temperature, where three inequivalent protons are represented in the Cp region. At this temperature there are also thee distinct methyl carbon resonances at 41.0, 44.0 and 44.2 ppm, respectively. At higher temperatures the exchange rate between **6** and **6'** increases until coalescence near -33 °C, above which a broad singlet is observed in the fast exchange limit in the ^{31}P NMR spectrum, which sharpens further with rising temperature. Likewise, the highly symmetric ambient temperature ^{1}H NMR spectrum is also suggestive of an averaged chemical environment, as are the single resonances for three equivalent methyl groups in both the ^{13}C and ^{1}H NMR spectra.

(2.8)
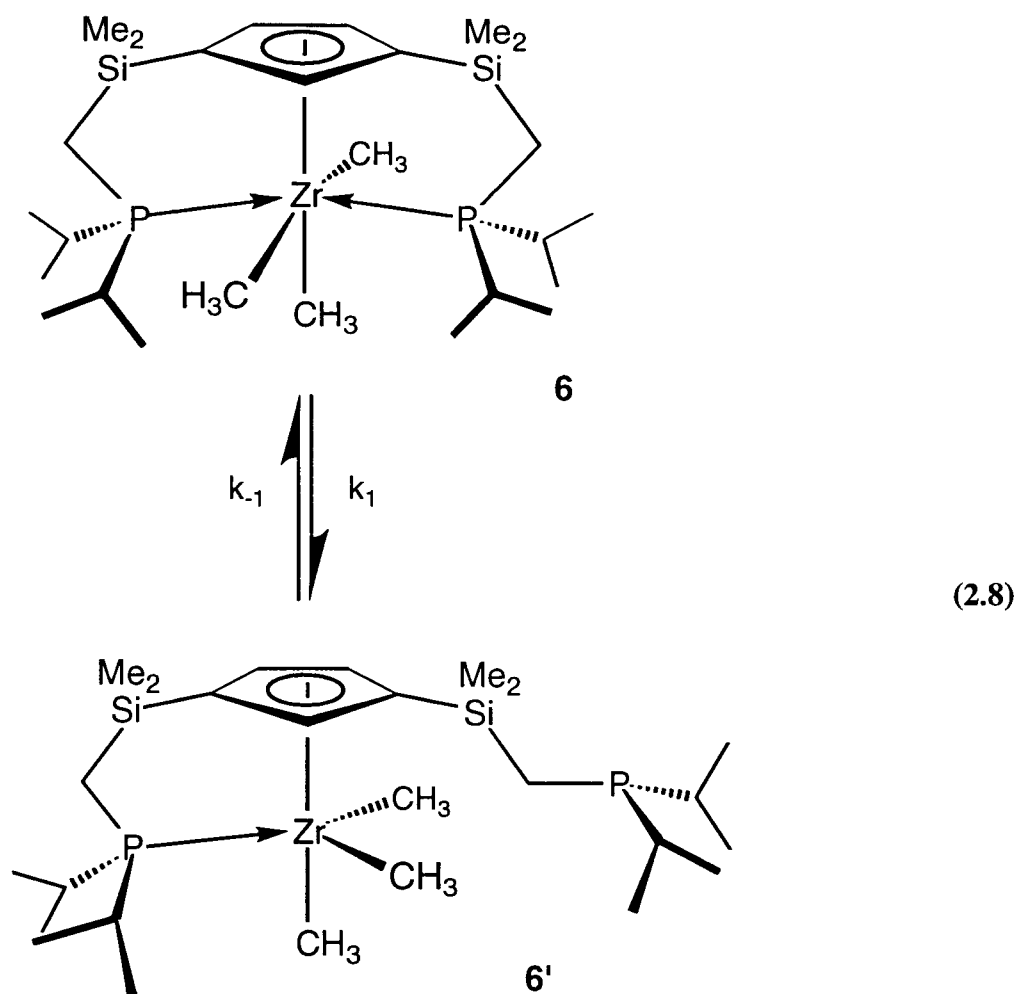
Integration of the variable temperature $^{31}P\{^1H\}$ NMR spectra between -68°C and -43°C permitted equilibrium constants to be calculated as a function of temperature from the concentration measurements for each species. The results are presented in Table 2.3, and a van't Hoff plot using these data is shown in Figure 2.5, from which values for the thermodynamic parameters $\Delta H° = 6.1(1.0)$ kcal mol^{-1} and $\Delta S° = -25(5)$ cal K^{-1} mol^{-1} were determined. It should be noted that there are relatively large error bars in the thermodynamic parameters due to the difficulty in accurately measuring the integration from the $^{31}P\{^1H\}$ NMR spectra, especially in the higher temperature region where line broadening is more pronounced. The errors were estimated from different runs and indicate reproducibility.

Table 2.3   Equilibrium data for the two trimethyl complexes. The data were taken from the $^{31}P\{^1H\}$ NMR spectra shown in Figure 2.9.

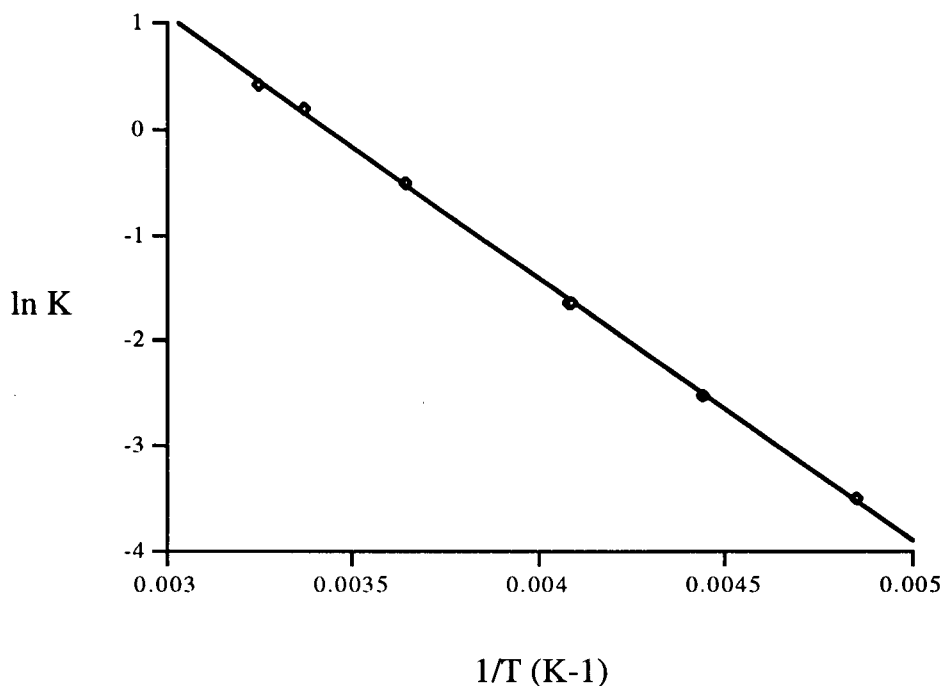| T (°C)	-67.6	-62.7	-57.7	-52.8	-47.8	-42.8
K	12.8	8.1	5.7	5.0	3.3	2.4
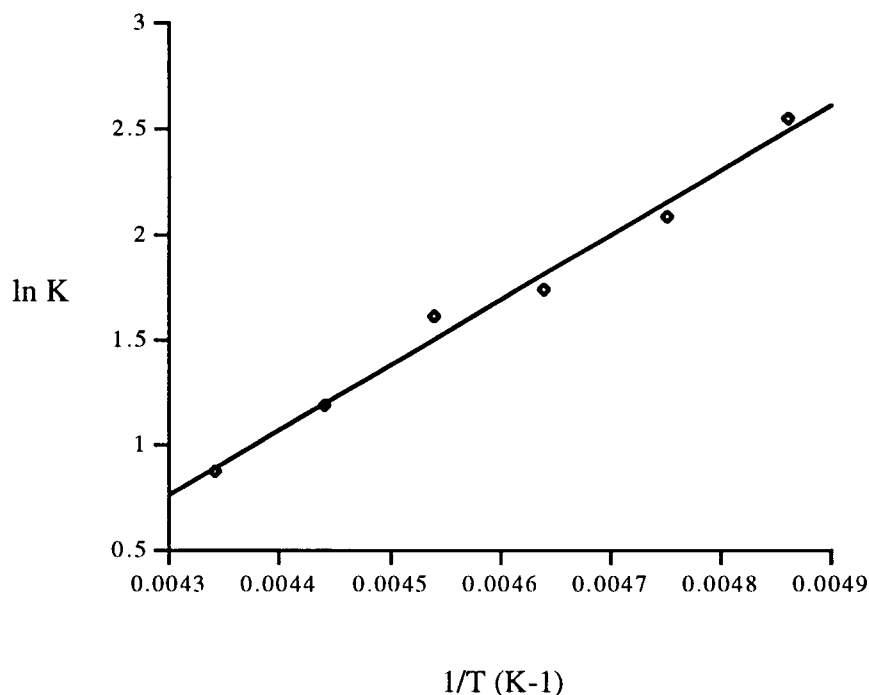
Figure 2.6 A van't Hoff plot of the $^{31}P\{^1H\}$ NMR spectral data for the equilibrium shown in equation 2.10.

An unexpected result from the van't Hoff plot shown above is the negative entropy term for the equilibrium in equation 2.8, suggesting that **6'** is the more ordered of the two complexes. It is also surprising that phosphine dissociation as observed in **6'** would be favoured at lower temperatures. One possible reconciliation of the data is that **6'** actually exists as a dimer with bridging methyl groups. The equilibrium would then be modified to the equation $K = [6']/[6]^2$, which yields $\Delta H^\circ = 11.2(1.0)$ kcal mol^{-1} and $\Delta S^\circ = -40(5)$ cal K^{-1} mol^{-1} when the concentration data are replotted. In this instance the negative entropy term would be consistent with favouring the break-up of a dimer at higher temperatures. Analogous dinuclear species with this ancillary ligand system are proposed as intermediates for intermolecular ligand exchange processes which will be encountered later.

6'
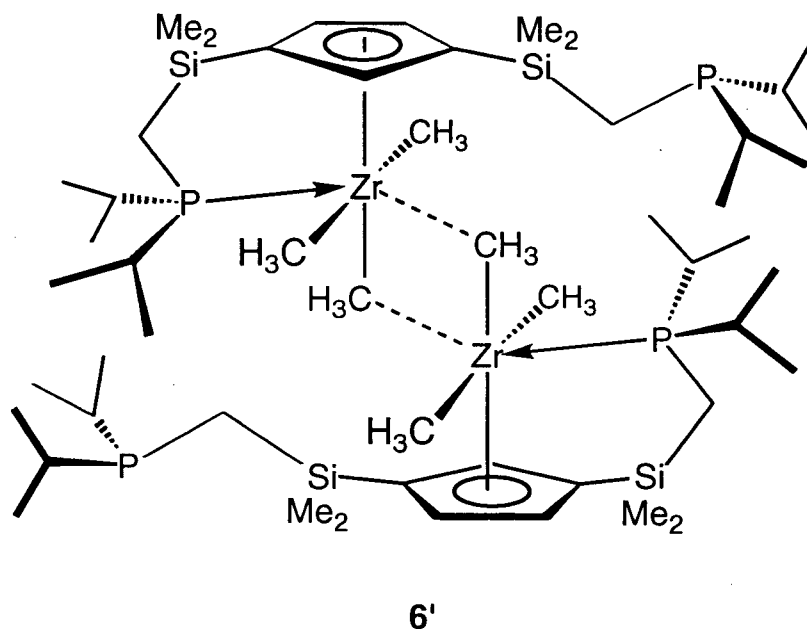
2.4.3 Reactivity of $^{Pr}[P_2Cp]MR_3$

All of the trialkyl complexes mentioned above react within hours to an atmosphere of H_2, generating putative hydride resonances in the ^1H NMR spectrum, and in the reaction of H_2 with **6** a doublet of doublets is observed in the ^{31}P NMR spectrum for a pair of mutually coupled inequivalent phosphines. However, a mixture of products is obtained in these reactions from which identifiable species could not be isolated. It was anticipated that hydrogenation of the alkyl groups might yield a $(^{Pr}[P_2Cp]ZrH_3)_n$ hydride species that could be trapped by the side-arm phosphines. However, these observations are in line with similar unsuccessful attempts to trap stable products from the hydrogenation of Cp^*ZrR_3 complexes in the presence of external phosphines.[22] In both cases the observation of multiple products may be due to a propensity of the resulting hydrides to oligomerize. Similarly, the reaction of $[P_2Cp]ZrR_3$ species with an excess of CO leads to decomposition of the whole reaction mixture. Presumably, with thee alkyl ligands to potentially undergo CO insertion there are a number of reaction pathways which could eventually lead to homolytic or heterolytic bond cleavage. These results can be contrasted with

the analogous reaction of CO with $^{Pr}[P_2Cp]ZrCl_2(CH_2Ph)$ (**13**) (see later in section 2.5.4), which offers fewer options for decomposition.

2.5.1   Synthesis of $^{Pr}[P_2Cp]ZrCl_2R$ (CH_2CMe_3, CH_2SiMe_3, Me, Et, OBu^t)

In light of the complex solution behaviour noted above for **6**, a series of mono(substituted) complexes were prepared in order to assess the electronic effects with the presence of a single alkyl ligand. Substituents of varying size were selected, ranging from the relatively bulky neopentyl and neosilyl groups to the much smaller methyl and ethyl derivatives. A large electron-withdrawing alkoxide (OBu^t) was also employed to obtain a bulky complex with similar electronic properties to **1**. However, it was anticipated that steric effects in these mono(substituted) species would be minor in comparison to the bulky trialkyl species.

The mono-alkyl complexes $^{Pr}[P_2Cp]ZrCl_2(CH_2EMe_3)$ (**7a**: E = C, **7b**: E = Si) were prepared from reactions of **1** with the appropriate stoichiometry of $LiCH_2EMe_3$ in toluene (equation 2.9).

$$^{Pr}[P_2Cp]ZrCl_3 \quad \xrightarrow[{- LiCl}]{LiCH_2EMe_3} \quad ^{Pr}[P_2Cp]ZrCl_2(CH_2EMe_3) \qquad (2.9)$$

1

7a   E = C

7b   E = Si
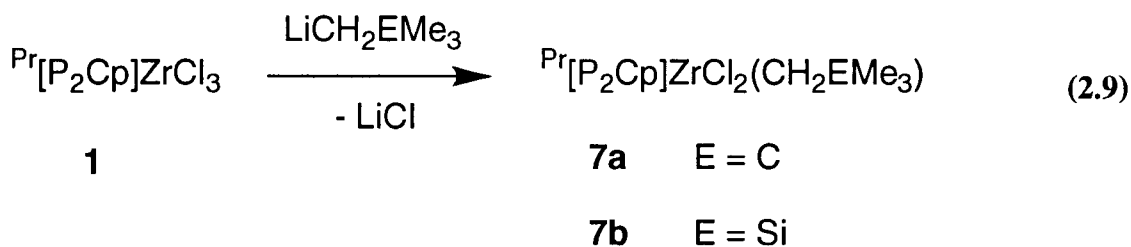
The methyl and ethyl analogues $^{Pr}[P_2Cp]ZrCl_2R$ (**8**: R = Me, **9**: R = Et) were more readily made from the corresponding Grignard (equation 2.10) as opposed to the alkyl lithium reagent.

$$^{Pr}[P_2Cp]ZrCl_3 \xrightarrow[- MgClBr]{RMgBr} \ ^{Pr}[P_2Cp]ZrCl_2R$$

$$\mathbf{1} \qquad\qquad\qquad\qquad\qquad \mathbf{8} \quad R = Me \qquad\qquad (2.10)$$

$$\mathbf{9} \quad R = Et$$
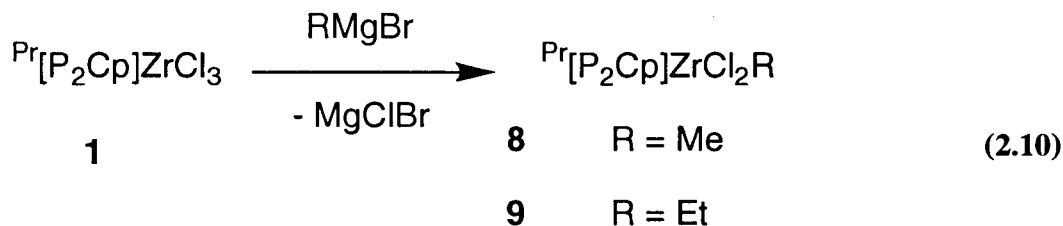
The mono(alkoxide) species $^{Pr}[P_2Cp]ZrCl_2(OBu^t)$ (**10**) was synthesized from the reaction of the alkoxide with **1** in THF (equation 2.11).

$$^{Pr}[P_2Cp]ZrCl_3 \xrightarrow[- KCl]{KOBu^t} \ ^{Pr}[P_2Cp]ZrCl_2(OBu^t)$$

$$\mathbf{1} \qquad\qquad\qquad\qquad\qquad\qquad \mathbf{10} \qquad\qquad\qquad (2.11)$$
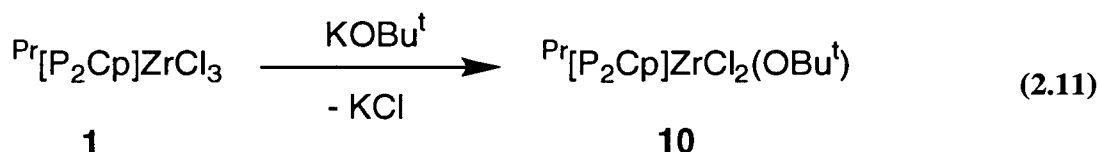
All of these reactions were conducted using high dilution to ensure that only one equivalent of reagent was added to each metal centre. Mono(alkyl) **7a,7b** and **8** were each obtained as yellow oils, **9** as a reddish oil, and **10** as a pale cream-coloured oil. None of these compounds could be isolated free of impurities (typically 5-10% by NMR spectroscopy), and all species slowly disproportionate to regenerate **1** and a number of unidentified decomposition products. A dinuclear species analogous to that proposed for **6'** is a possible intermediate in this disproportionation reaction. The analogous monoalkyl Cp^*ZrCl_2Me complex is also suspected to undergo oligomerization and/or halide exchange, and slowly decomposes in solution.[22] In contrast, Hf mono(alkyl) complexes Cp^*HfCl_2R (R = Me, Ph) are generally more thermally stable.[26]

The NMR spectra of these mono(alkyl) complexes show complicated exchanged broadened resonances that suggest a similar equilibrium process is operative as noted for **2** and **6**. For example, in **7a**, **7b**, **8** and **10** there are two small peaks near 10 and -5 ppm in the ambient temperature ^{31}P NMR spectrum associated with the five-coordinate species, and a separate resonance in the vicinity of 0 ppm for the symmetric six-coordinate complex, which is the major

isomer (> 75%) in solution. The corresponding ambient temperature spectrum of **9** is near coalescence. The equilibria for these systems are suggested by consistent changes in peak broadening and intensity as a function of temperature, although these processes could not be satisfactorily studied by VT NMR spectroscopy due to the inherent impurities present in the samples.

2.5.2 Synthesis of ^{Pr}[P$_2$Cp]MCl$_2$(CH$_2$Ph) (M = Zr, Hf)

Addition of one equivalent of KCH$_2$Ph to trichloride **1** generates the monobenzyl derivative ^{Pr}[P$_2$Cp]MCl$_2$(CH$_2$Ph) (**11**: M = Zr, **12**: M = Hf), which is obtained either as a red solid (**11**) or an orange-yellow oil (**12**) (equation 2.12).

$$^{Pr}[P_2Cp]MCl_3 \xrightarrow[- KCl]{KCH_2Ph} \quad ^{Pr}[P_2Cp]ZrCl_2(CH_2Ph)$$

$$\textbf{1}$$

$$\textbf{11: M = Zr}$$

$$\textbf{12: M = Hf}$$

(2.12)
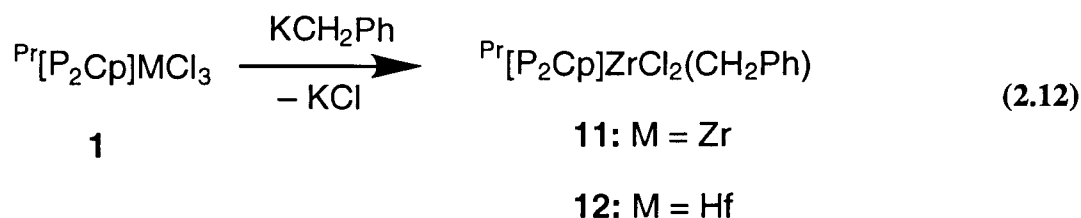
Integration of the ^{1}H NMR spectrum shows only one benzyl group per P$_2$Cp unit. The ambient temperature ^{31}P NMR spectrum for **11** shows two broad resonances which coalesce into a broad singlet near 5.8 ppm that sharpens at higher temperatures. Below room temperature these broad peaks gradually sharpen to a pair of singlets at 14.2 and -6.9 ppm, again corresponding to a five-coordinate geometry in the slow exchange limit. The variable temperature spectroscopic data show the familiar line-broadening effects as the temperature is raised to the fast exchange limit where the two phosphine sites are averaged. This averaged chemical environment is also reflected in the ^{13}C NMR spectrum, which shows a triplet for the benzylic carbon (*C*H$_2$) due to coupling to both phosphorus nuclei. No coupling was observed to phosphorus for the benzylic protons in the ^{1}H NMR spectrum.

11
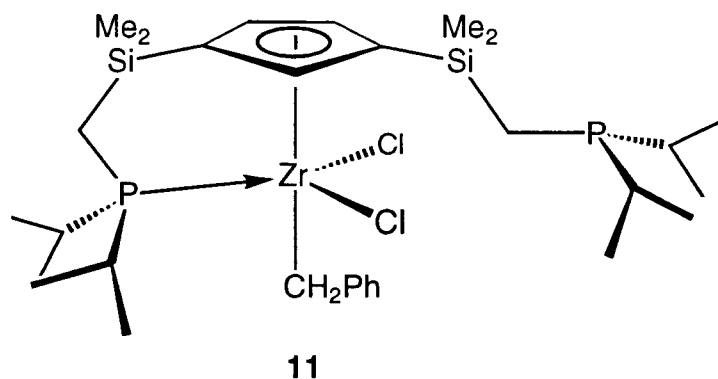
In contrast to the other fluxional complexes described previously, however, the dynamic solution behaviour of **11a** is unique in that the intermediate six-coordinate species that mediates phosphine exchange is not directly observed. Rather, instead of being present as an equilibrium species, this intermediate is inferred as an undetected transition state structure. To support this analysis, simulation of the temperature dependent $^{31}P\{^1H\}$ NMR spectra by NMR line shape analysis (DNMR-5) enabled rate constants to be calculated (Table 2.4). From the resulting Eyring plot (Figure 2.6) the following activation parameters were obtained: $\Delta H^{\ddagger} = 8.8$ kcal mol^{-1}, $\Delta S^{\ddagger} = -13.1$ cal mol^{-1}K^{-1}. The negative entropy of activation for this process is consistent with a six-coordinate structure for the transition state (Figure 2.7), implying that phosphine exchange in **11** occurs *via* the same associative pathway as found for the other fluxional systems, except that in this instance the lifetime of the six-coordinate intermediate is too fleeting to be directly observed.

Table 2.4 Rate constants of phosphine exchange for $^{Pr}[P_2Cp]ZrCl_2(CH_2Ph)$ (**11**) as obtained from line shape analysis using DNMR-5.

T (°C)	-18.4	-8.4	1.9	12.1	22.4	30.5	40.5	50.5	60.5	70.4
k	200	400	800	1500	2500	4000	6500	11000	16000	24000
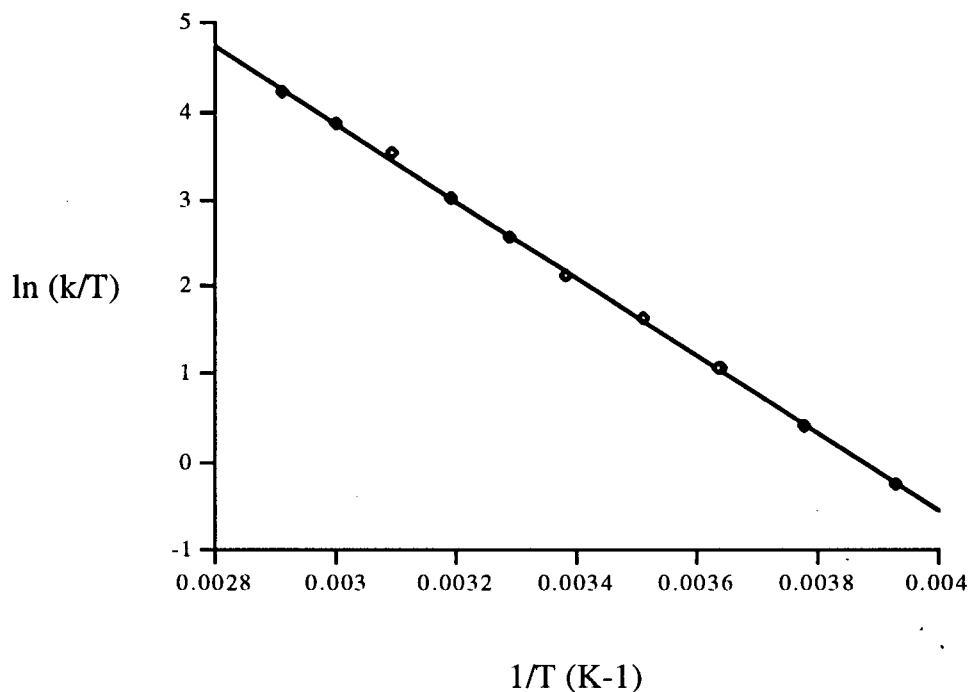
Figure 2.7 Eyring plot of ln(k/T) versus 1/T for the complex $^{Pr}[P_2Cp]ZrCl_2(CH_2Ph)$ (**11**) using the equation $k = (k_BT/h)exp(-\Delta G^{\ddagger}/RT) = (k_BT/h)exp((T\Delta S^{\ddagger}-\Delta H^{\ddagger})/RT)$; the rate constants and temperatures are taken directly from Table 2.6.
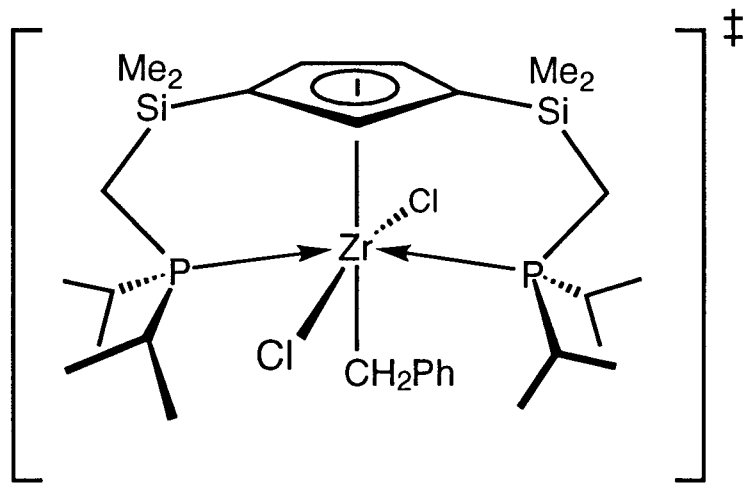
Figure 2.8 Proposed transition state structure for the interconversion of the phosphine sites in $^{Pr}[P2Cp]ZrCl_2(CH_2Ph)$ (**11**).

references begin on page 75

2.5.3   Reactivity of $^{Pr}[P_2Cp]ZrCl_2R$

Due to the inability to purify most of the alkyl derivatives described above, reactions involving these species generally did not lead to clean products. For example, attempts to alkylate alkoxide **10** (prepared in situ) with KCH_2Ph does yield two main products as observed in the ^{31}P NMR spectrum at -3.5 and -5.5 ppm, but a number of organic byproducts are also formed, hampering efforts to isolate or identify these compounds. Analogous reactions to form mixed alkyl species for a series of cross-over experiments will be discussed in the next chapter. In comparison, monobenzyl **11** can be obtained as a pure compound suitable for reactivity studies. However, except for the CO insertion reaction outlined below, the reaction of **11** with reagents such as H_2 and CO_2 led to decomposition products.

2.5.4   Synthesis of $^{Pr}[P_2Cp]ZrCl_2(\eta^2\text{-}C(O)CH_2Ph)$ (13)

Exposure of a toluene solution of mono(benzyl) **11** to an atmosphere of CO under ambient conditions for 6 h affords the acyl-ylide complex $^{Pr}[P_2Cp]ZrCl_2(\eta^2\text{-}C(O)CH_2Ph)$ **(13)** as pale yellow, air- and moisture-sensitive crystals (equation 2 13). The open site for initial coordination of a CO molecule prior to migratory insertion into the Zr-benzyl σ-bond is made available by fluxional phosphine dissociation in the exchange process described above for **11**. Despite the electrophilic nature of the acyl carbon in early metal acyl complexes, similar reports of adduct formation to give an ylide species are relatively rare. A Ta silaacyl complex, $Cp^*TaCl_3(\eta^2\text{-}C(O)SiMe_3)$,[27] forms adducts with pyridine, $P(OMe)_3$, and PEt_3, and there is an example similar to **13** of a Zr formyl-ylide complex that is stabilized by intramolecular coordination of a pendant donor of a chelating amidodiphosphine (PNP) ligand.[28]

$$^{Pr}[P_2Cp]ZrCl_2(CH_2Ph) \quad \text{(2.13)}$$

11

13
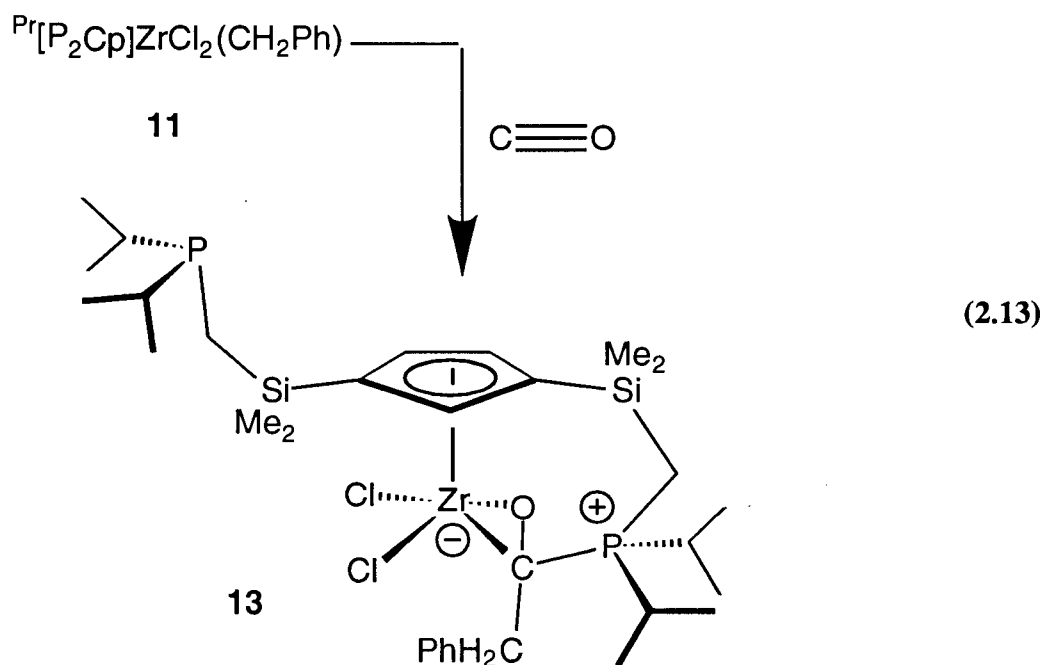
The X-ray crystal structure of **13** is shown in Figure 2.8, with selected bond length and bond angles listed in Table 2.5. The unusual arrangement of the ancillary ligand has one pendant phosphine attached to the acyl carbon to generate a zwitterionic ylide moiety and a chiral carbon centre, while the other side-arm is directed well away from the coordination sphere and remains dangling. The main structural features of interest in **13** are associated with the acyl-ylide unit. Although the η^2-binding mode in **13** is typical for oxophilic early metal acyl complexes (**I**),[29] the increased electron density supplied to the electrophilic acyl carbon from intramolecular phosphine coordination results in modest changes in the bond length and bond angles. For example, relative to other Zr acyl complexes (i.e., $Cp_2ZrMe(\eta^2\text{-}C(O)Me)$),[30] in **13** the Zr(1)-C(24) and C(24)-O(1) bond distances are comparatively longer, the Zr(1)-O(1) distance is shorter, and the Zr(1)-C(24)-O(1) angle is smaller. These effects indicate an increase in the Zr-O bonding interaction as the bonding contribution to the metal from the phosphine-stabilized acyl carbon is lessened, and point to a significant oxycarbene character in this moiety (**II**). The reduced C-O bond order is also reflected in the lack of an obvious carbonyl stretch in the IR spectrum. The strength of the P(1)-C(24) bond is suggested by the fact that the other P-C single

bonds associated with this phosphonium centre are actually slightly longer in comparison. The Zr-Cl bond distances are comparable to the equatorial Zr-Cl bonds in **1**.
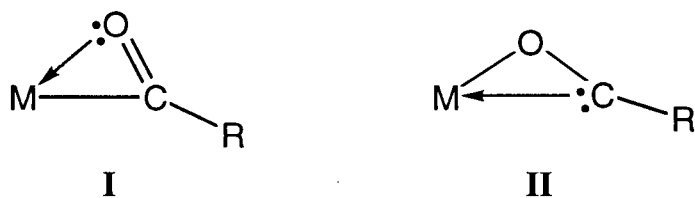
Table 2.5 Selected Bond Length (Å) and Bond Angles (deg) for

$^{Pr}[P_2Cp]ZrCl_2(\eta^2\text{-}C(O)CH_2Ph)$ **(13)**

		Cl(1)-Zr(1)-Cl(2)	94.77(8)
Zr(1)-Cl(1)	2.463(2)		
		Cl(1)-Zr(1)-O(1)	92.0(1)
Zr(1)-Cl(2)	2.470(2)		
		Cl(1)-Zr(1)-C(24)	113.1(2)
Zr(1)-O(1)	2.037(5)		
		Cl(1)-Zr(1)-Cp'	117.4
Zr(1)-C(24)	2.284(9)		
		Cl(2)-Zr(1)-O(1)	129.7(2)
Zr(1)-Cp'(1)	2.21		
		Cl(2)-Zr(1)-C(24)	93.4(2)
P(1)-C(6)	1.809(7)		
		Zr(1)-C(24)-O(1)	61.3(4)
P(1)-C(10)	1.811(8)		
		Zr(1)-C(24)-P(1)	132.8(4)
P(1)-C(13)	1.815(8)		
		O(1)-C(24)-C(25)	111.0(6)
P(1)-C(24)	1.779(8)		
		P(1)-C(24)-O(1)	111.2(5)
O(1)-C(24)	1.476(9)		
		P(1)-C(24)-C(25)	116.8(6)
C(24)-C(25)	1.54(1)		

C(19) C(20)
C(18)
P(2)
C(22)
C(21)
C(7)
C(23)
C(16)
Si(2)
C(3)
C(17)
C(4)
C(5) C(9)
C(2)
Cl(1) Zr(1) C(1)
Si(1)
Cl(2) C(8)
O(1) C(24)
P(1)
C(27) C(25) C(11)
C(14) C(10)
C(28) C(26) C(13) C(15)
C(29) C(31) C(12)
C(30)
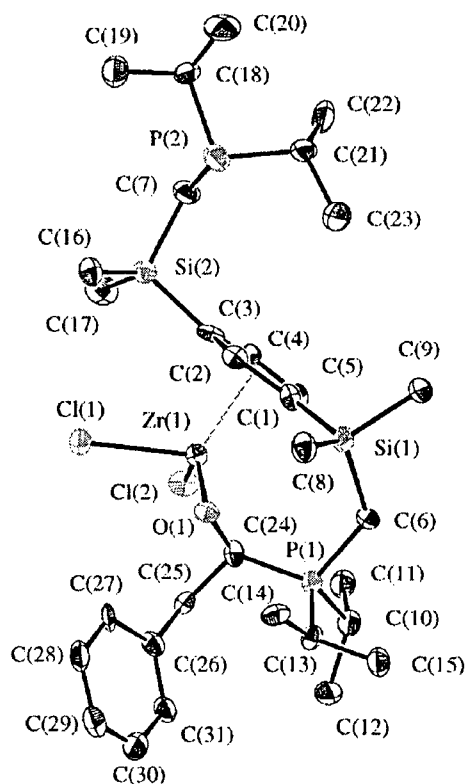
Figure 2.9   Molecular structure of $^{Pr}[P_2Cp]ZrCl_2(\eta^2$-C(O)CH$_2$Ph) (**13**); 33% probability thermal ellipsoids are shown. Hydrogen atoms not shown for clarity.

Two isomers are observed in solution for **13** with a slight excess of one species relative to the other. Each isomer displays a separate singlet near 47 ppm in the ^{31}P{^{1}H} NMR spectrum for the ylide phosphorus nucleus, and a second peak near -5 ppm for the dangling phosphine. The ylide resonance is located downfield relative to the normal chemical shift range (0-20 ppm) for a metal-bound phosphine with this ligand system, and is consistent with the chemical environment of a phosphonium centre. A doublet ($^1J_{PC}$ = 57Hz) for the acyl carbon is observed near 79 ppm in the ^{13}C{^{1}H} NMR spectrum for each ^{13}C-labeled isotopomer. In comparison to other Zr acyl complexes (δ > 200 ppm), this peak resonates considerably further upfield in the region for a typical sp^3-hybridized carbon atom with a C-O single bond,[31] in agreement with the molecular structure. The $^1J_{PC}$ coupling is similar to that found in the analogous intramolecular Zr formyl-ylide complex ($^1J_{PC}$ = 55Hz). Contrasting with the reported coupling for a Ta adduct

($^1J_{PC}$ = 8Hz), in which the ylide results from attack by an intermolecular phosphine, the larger values for the two Zr examples may be due to steric effects associated with the chelating side-arms.

The ^{1}H NMR spectrum of **13** is complicated by the asymmetry of the molecule and by the presence of two diastereomers. The effect of the chiral centre is particularly evident in the resonances of the diastereotopic geminal protons of the benzyl group, which have a chemical shift separation of nearly 1 ppm. This generates an AMX splitting pattern for each unique benzyl proton originating from $^1J_{HH}$ and $^3J_{PH}$ coupling, and additional $^3J_{PH}$ coupling is observed to the ^{13}C-labeled acyl carbon (Figure 2.9). These values re listed in Table 2.6; note the significant differences between H_A and H_M in their respective coupling to the phosphorus and carbon nuclei. The low C_1 symmetry of this complex is also evident in the cyclopentadienyl region where thee separate peaks are seen in the ^{1}H NMR spectrum for each isomer. These resonances could be individually assigned from cross-peaks in the 2D-COSY NMR spectrum. The resonances associated with the dangling side-arm exhibit are isochronous, due to the remoteness of these groups from the chiral centre.
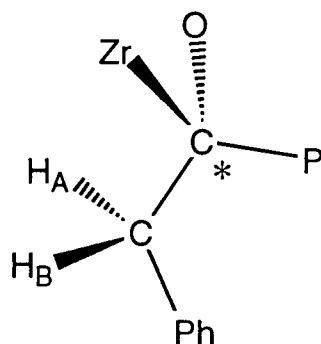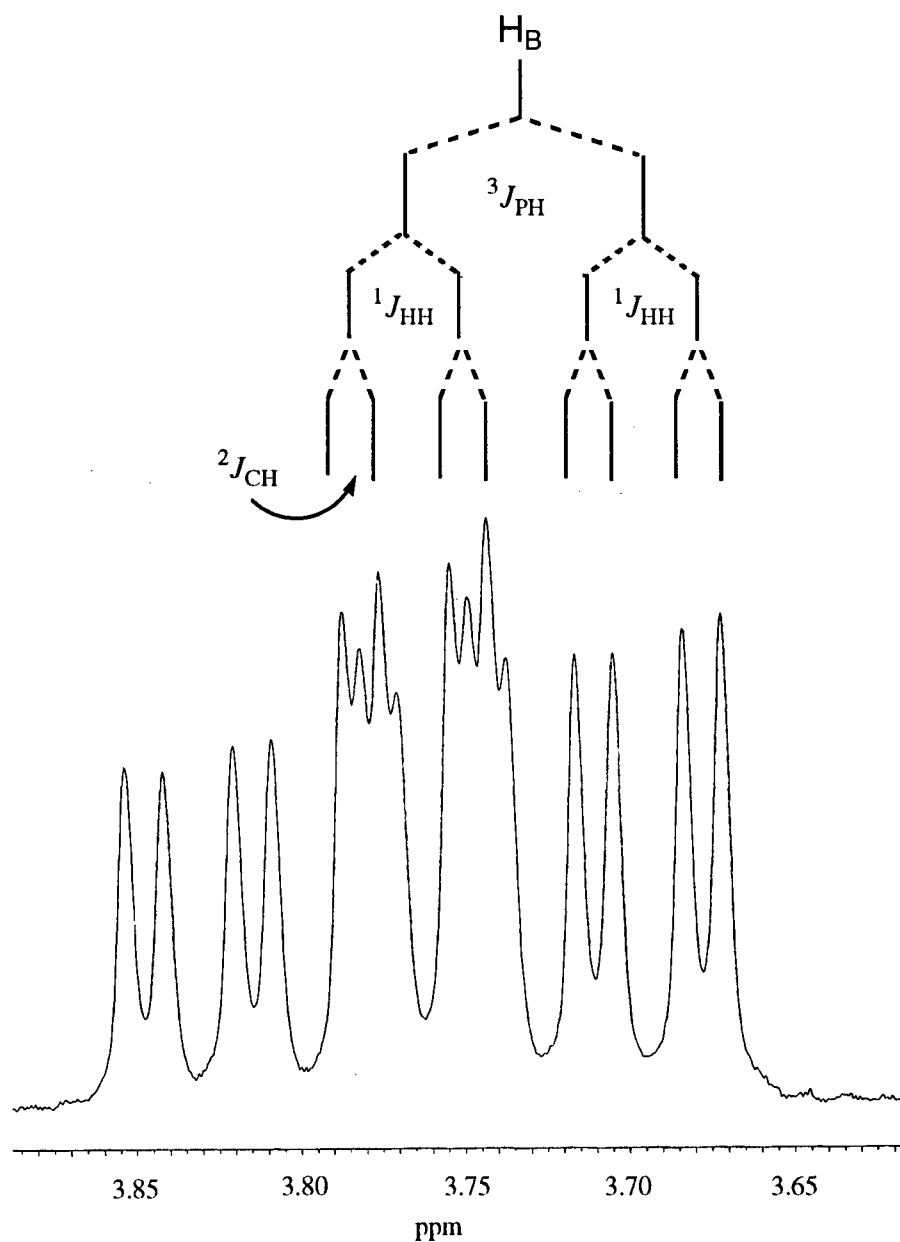
Figure 2.10 Region in ^{1}H NMR spectrum of ^{Pr}[P$_2$Cp]ZrCl$_2$(η^2-C(O)CH$_2$Ph) (**13**) showing

one of the diastereotopic protons (two isomers present).

Table 2.6 Coupling constants (Hz) for the benzylic (CH_2Ph) protons in **13**.

	H$_A$	H$_M$
$^1J_{HH}$	16.5	16.5
$^2J_{CH}$	< 1	5.7
$^3J_{PH}$	2.0	36.2

59

The two diastereomers seen for **13** likely differ in the relative orientation of the coordinated acyl unit. A similar feature has been observed in other early metal η^2-acyl complexes. For example, the kinetic product from the insertion reaction of CO with Cp$_2$ZrMe$_2$ is oriented as shown in **A**, which isomerizes upon heating at 50 °C to give the thermodynamically favoured product **B**, where steric interactions between the two methyl groups are eliminated (equation 2.14).[32] Theoretical calculations suggest that this transformation may proceed via an η^1-intermediate with subsequent rotation about the M-O bond axis.[33]

(2.14)

A   **B**
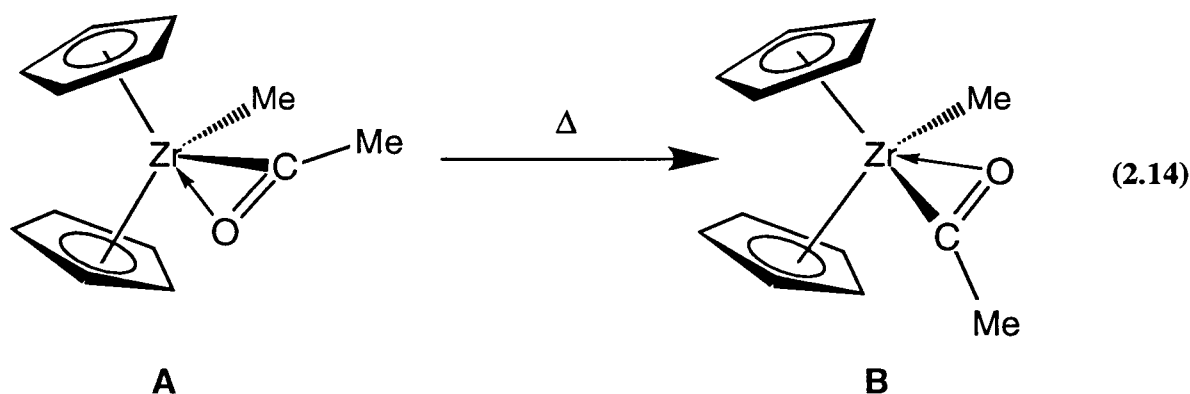
In the case of **13**, it is not obvious that one isomer should be energetically preferred over the other; hence, it is reasonable that both species should co-exist in nearly equal proportions in solution (equation 2.15).

(2.15)
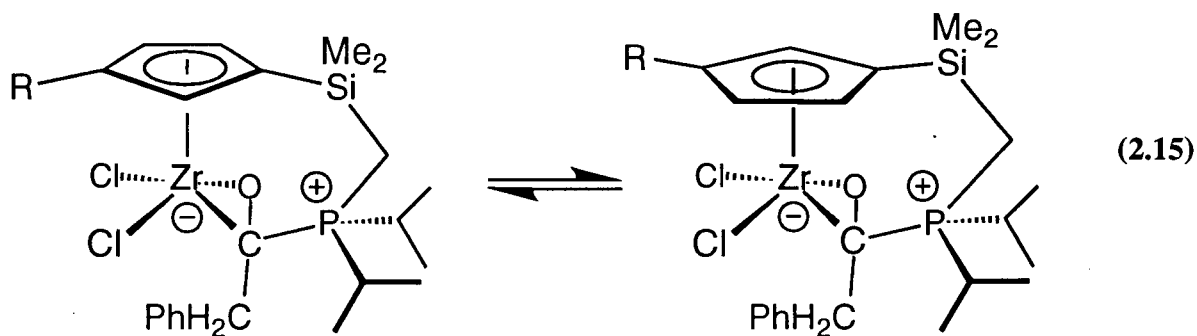
2.6   Summary and conclusions

A potentially chelating hybrid-donor ligand system consisting of a central cyclopentadienyl ring with two pendant side-arm phosphines has been developed. The steric properties of the ligand can be varied depending on the alkyl substituents (Me, Pr^i, Bu^t) on the phosphines. The variant of the ligand with isopropyl groups on the phosphines has been employed to examine its coordination chemistry with zirconium(IV) and hafnium (IV). The trichloride complexes [P₂Cp]MCl₃ (**1**: M = Zr, **2**: M = Hf) have been prepared; these derivatives serve as versatile starting materials for the synthesis of a series of alkyl complexes. What emerges from this study is that coordination of the pendant phosphine arms becomes less favorable as the electron density at the metal increases. For example, the electron-withdrawing ligands in trichloride **1** and alkoxide **10** encourage the coordination of both phosphine donors. The introduction of a single electron-releasing alkyl ligand at zirconium is sufficient to increase the tendency for phosphine dissociation such that the low temperature limiting structure for **8** is five-coordinate with a dangling side-arm. A further consequence of this reduced tendency for phosphine binding is that fluxional processes become prevalent for these mono-substituted alkyl complexes. Indeed, the subtle electronic balance that influences the coordination mode of the pendant phosphines is perhaps best illustrated by a comparison of the trichloride derivatives **1** and **2**. A similar mononuclear solid state structure is observed for both **1** and **2** with two pendant phosphine donors coordinated to the metal centre. However, while the solution behavior of **1** remains consistent with the solid state structure at all temperatures studied, NMR spectroscopic studies reveal fluxional processes for **2** involving the side-arm phosphines. The divergent solution behavior of these otherwise identical species is perhaps attributed to the capacity for Hf to form comparatively stronger bonds, thus enabling the metal to be competitively saturated electronically with a lower coordination number.

The coordination mode of the side-arms in the trialkyl derivatives is dependent on the size of the alkyl groups. Sterically bulky ligands (i.e., CH_2Ph, CH_2CMe_3, CH_2SiMe_3) crowd the metal centre and prevent the phosphines from binding, resulting in a thee-legged piano stool geometry. With three small methyl groups in **5** (i.e., comparable in size to the chloride ligands in

1), there is ample space for the phosphines to access the metal; therefore, electronic factors dominate and an equilibrium mixture of species ensues, as observed for **2** and a few of the mono(alkyl) derivatives. These systems all undergo similar exchange processes for the phosphines that reflect the subtle electronic factors mentioned above.

There is a difference in the thermal stability of the mono- versus tri-alkyl complexes. Except for mono(benzyl) **11** there is a tendency for the mono-substituted derivatives (including alkoxide **10**) to disproportionate over time to give trichloride **1** and a number of unidentified decomposition products. The mechanism for the disproportionation of these species may involve ligand exchange via a binuclear intermediate. The trialkyl complexes are considerably more robust, and the resistance of these species to thermal decomposition will be addressed again in the next chapter.

2.7 Experimental

2.7.1 General Considerations

Unless otherwise stated all manipulations were performed under an atmosphere of pre-purified dinitrogen in a Vacuum Atmospheres HE-553-2 glove box equipped with a MO-40-2H purification system, or in standard Schlenk-type glassware on a dual vacuum/dinitrogen line. The glove box was also equipped with a -40 °C freezer. Reactions involving gaseous reagents were conducted in Pyrex vessels (bombs) designed to withtand pressures up to and including 4 atm. ^{1}H NMR spectroscopy was performed on either a Bruker AC-200 instrument operating at 200.1 MHz, or a Bruker AM-500 instrument operating at 500.33 MHz, depending on the complexity of the particular spectrum. ^{1}H NMR spectra were referenced to internal C_6D_5H (7.15 ppm) or $C_6D_5CD_2H$ (2.09 ppm). ^{13}C NMR spectroscopy was performed on either a Bruker AC-200 instrument operating at 50.3 MHz, or a Varian XL-300 instrument operating at 75.4 MHz. ^{13}C NMR spectra were referenced to internal C_6D_6 (128.0 ppm) or $C_6D_5CD_3$ (137.5

ppm). $^{31}P\{^1H\}$ NMR spectroscopy was performed on either a Bruker AC-200 instrument operating at 81.0 MHz, a Varian XL-300 instrument operating at 121.4 MHz, or a Bruker AM-500 instrument operating at 202.3 MHz. $^{31}P\{^1H\}$ NMR spectra were referenced to external $P(OMe)_3$ (141.0 ppm). Variable temperature experiments were performed on either the Varian XL-300 or the Bruker AM-500 instrument. All chemical shifts are reported in ppm and all coupling constants are reported in Hz. Microanalyses (C, H, N) were performed by Mr. P. Borda within this department.

2.7.2 Materials

$^{Pr}[P_2Cp]ZrCl_3$[2] was prepared according to published procedures. $HfCl_4(THT)_2$ was prepared according to the analogous published procedure for $HfCl_4(THF)_2$,[34] substituting THT for THF. $NaCp(THF)$,[35] KCH_2Ph,[36] $LiCH_2CMe_3$,[37] $LiCH_2SiMe_3$,[38] were prepared according to published procedures. MeMgBr (1.4 M solution in toluene/THF), EtMgBr (3.0 M solution in ether), and MeLi (1.4 M solution in ether) were purchased from Aldrich and used as received. $KOBu^t$ was purchased from Aldrich and sublimed before use.

Hexanes, tetrahydrofuran (THF), ether, and toluene were pre-dried over CaH_2 followed by distillation under argon from either sodium metal or sodium-benzophenone ketyl. Pentane and hexamethyldisiloxane were distilled from sodium-benzophenone ketyl. The deuterated solvents C_6D_6 and $C_6D_5CD_3$ were dried over molten sodium metal, vacuum transferred to a bomb, and degassed by thee freeze-pump-thaw cycles before use. Ethylene and carbon monoxide were obtained as lecture bottles from Matheson and dried over P_2O_5 before use. Labeled ^{13}CO (Cambridge Isotopes) was used as received. Hydrogen was purchased from Matheson and purified by passage though a column of activated 4Å molecular sieves and MnO supported on vermiculite.

2.7.3   Synthesis

2.7.3.1   Ligand synthesis

C₅H₅SiMe₂CH₂Cl

A 0.85 M THF solution of NaCp prepared *in situ* (200 mL, 170 mmol) maintained at -30 °C was added dropwise *via* cannula over a period of 30 minutes to a cooled (-78 °C) stirring solution of ClSiMe₂CH₂Cl (25.0 g, 174 mmol) dissolved in 300 mL of THF. The solution gradually turned viscous and pale cream in colour. The mixture was allowed to slowly warm to room temperature and stirred for 1 h. The solvent was removed under vacuum and 100 mL water added to the flask, and extracted with four aliquots (25 mL) of diethyl ether. The ether layer was dried over MgSO₄ and filtered, and the solvent subsequently removed to give a yellow oil. Vacuum distillation yielded a clear liquid (bp 30-35 °C, 10^{-2} Torr) consisting mainly of one isomer (> 85 % by ^{1}H NMR spectroscopy). Yield: (21.7 g, 74 %). ^{1}H NMR (20 °C, CDCl₃): δ 0.0 (s, 6H, Si(C*H₃*)₂), 2.59 (s, 2H, SiC*H₂*Cl), 3.41 (very br, 1H, Cp-*H*Si), 6.7 (overlapping br, 4H, Cp-*H*).

C₅H₄(SiMe₂CH₂Cl)₂

A solution of NaN(SiMe₃)₂ (22.3 g, 122 mmol) in 150 mL of THF was added dropwise over a period of 15 minutes to a cooled (-90 °C) stirring solution of C₅H₅SiMe₂CH₂Cl (21.0 g, 122 mmol) dissolved in 150 mL of THF. The temperature of the ethanol/liquid N₂ cooling bath was maintained below -85 °C during this addition. The mixture was stirred at -90 °C for another 30 minutes after the addition was complete, and then added dropwise over a period of 20 minutes to a cooled (-78 °C) stirring solution of ClSiMe₂CH₂Cl (18.0 g, 126 mmol) in 300 mL of THF. The reaction mixture became viscous during the course of the addition. The solution was slowly warmed to room temperature and stirred for 2 h, the solvent was then removed under vacuum and 80 mL water added to the flask, and extracted with four aliquots (25 mL) of diethyl ether. The ether layer was dried over MgSO₄ and filtered, and the solvent subsequently removed to

give a clear yellow oil. Vacuum distillation yielded some of the starting $C_5H_5SiMe_2CH_2Cl$ (bp 34-41 °C, 10^{-2} Torr) and a viscous pale yellow oil (bp 95-100 °C, 10^{-2} Torr) consisting primarily (> 90 % by ^{1}H NMR spectroscopy) of the 1,1-substituted isomer. Yield: (19.8 g, 58 %). Anal. Calcd. for $C_{11}H_{20}Si_2Cl_2$: C, 47.29; H, 7.22. Found: C, 46.96; H, 7.25. ^{1}H NMR (20 °C, $CDCl_3$): δ 0.0 (s, 12H, Si(CH_3)$_2$), 2.38 (s, 4H, SiCH_2Cl), 6.20 and 6.59 (m, 4H, Cp-*H*). ^{13}C{^{1}H} NMR (20 °C, $CDCl_3$): -3.7 (Si(CH_3)$_2$), 30.2 (SiCH_2Cl), 100.5 (*C*(Si(CH$_3$)$_2$CH$_2$)$_2$), 132.2 (Cp), 134.5 (Cp).

^{Me}[P$_2$Cp]Li

A solution of $C_5H_4(SiMe_2CH_2Cl)_2$ (4.88 g, 17.4 mmol) dissolved in a mixture of 10 mL of toluene and 60 mL of THF was added dropwise to a heated (50 °C) stirring solution of LiPMe$_2$ (3.56 g, 52.4 mmol) dissolved in 60 mL of THF. The green colour of the phosphide solution was immediately discharged upon addition of the last drops, and shortly afterward turned pink. The reaction mixture was immediately removed from the heating bath, cooled to room temperature, and the solvent removed under vacuum. The red oily residue was extracted with hexanes and filtered, and the solvent removed to yield a viscous pink gel. Yield: (5.50 g, 94 %). ^{1}H NMR (20 °C, C_6D_6): δ 0.42 (s, 12H, Si(CH_3)$_2$), 0.51 and 1.02 (d, 2H, $^2J_{HH}$ = 8Hz, SiCH_2P), 0.73 (s, 12H, P(CH_3)$_2$), 6.46 (t, 1H, $^4J_{HH}$ = 1Hz, Cp-*H*), 6.53 (d, 2H, $^4J_{HH}$ = 1Hz, Cp-*H*). ^{31}P NMR (20 °C, C_6D_6): δ -54.0 (s).

^{Pr}[P$_2$Cp]Li

The procedure followed was as above, adding $C_5H_4(SiMe_2CH_2Cl)_2$ (5.00 g, 17.8 mmol) to a heated (65 °C) solution of LiPPr^i$_2$ (6.66 g, 53.6 mmol). A white solid was obtained from a cold (-40 °C) saturated hexanes solution. Yield: (6.78 g, 84 %). Anal. Calcd. for $C_{23}H_{47}LiP_2Si_2$: C, 61.57; H, 10.56. Found: C, 61.54; H, 10.77. ^{1}H NMR (20 °C, C_6D_6): δ

0.49 (d, 2H, $^2J_{PH}$ = 4Hz, SiCH_2P), 0.52 (s, 12H, Si(CH_3)$_2$), 0.91 (m, 24H, CH(CH_3)$_2$), 1.60 (sept, 4H, $^3J_{HH}$ = 7Hz, CH(CH$_3$)$_2$), 6.51 (t, 1H, $^4J_{HH}$ = 1Hz, Cp-H), 6.56 (d, 2H, $^4J_{HH}$ = 1Hz, Cp-H). ^{31}P NMR (20 °C, C$_6$D$_6$): δ 0.2 (quartet, $^1J_{LiP}$ = 55Hz). ^{13}C{^{1}H} NMR (20 °C, C$_6$D$_6$): δ -0.6 (Si(CH_3)$_2$), 8.1 (SiCH$_2$P), 19.7 and 23.8 (CH(CH$_3$)$_2$), 114.5 (CH(CH$_3$)$_2$), 115.8 and 117.8 Cp), 137.4 (CpSi).

^{Bu}[P$_2$Cp]Li

The procedure followed was again as above, adding C$_5$H$_4$(SiMe$_2$CH$_2$Cl)$_2$ (3.31 g, 11.8 mmol) to a heated (65 °C) solution of LiPBu$^t_2$ (5.40 g, 35.5 mmol). A white crystalline solid was obtained from a cold (-40 °C) saturated hexanes solution. Yield: (4.60 g, 77 %). Anal. Calcd. for C$_{27}$H$_{55}$LiP$_2$Si$_2$: C, 64.24; H, 10.98. Found: C, 64.33; H, 11.03. ^{1}H NMR (20 °C, C$_6$D$_6$): δ 0.38 (s, 12H, Si(CH_3)$_2$), 0.86 and 0.91 (d, 18H, $^3J_{PH}$ = 8Hz, C(CH_3)$_3$), 6.41 (t, 1H, $^4J_{HH}$ = 1Hz, Cp-H), 6.44 (d, 2H, $^4J_{HH}$ = 1Hz, Cp-H). ^{31}P NMR (20 °C, C$_6$D$_6$): δ 24.4 (quartet, $^1J_{LiP}$ = 48Hz).

2.7.3.2 ^{Pr}[P$_2$Cp]HfCl$_3$ (2).

100 mL of toluene was added to an intimate mixture of [P$_2$Cp]Li (1.82 g, 4.06 mmol) and HfCl$_4$·(THT)$_2$ (2.02 g, 4.08 mmol) at 0 °C. The mixture was heated to 65 °C and stirred at that temperature for 24 h, during which the yellowish colour of the ligand gradually diminished to give a pale buff yellow solution. The solution was filtered and the solvent reduced to with 10 mL, from which pale yellow crystals were obtained at -78 °C. The crystals were washed with cold hexanes and dried. Yield: (1.99 g, 67 %). Anal. Calcd. for C$_{23}$H$_{47}$Cl$_3$HfP$_2$Si$_2$: C, 38.02; H, 6.52. Found: C, 38.40; H, 6.70. In solution, **2** exists as an equilibrium mixture consisting of two complexes of the same formula.

isomer 2: ^{1}H NMR (-40 °C, C_7D_8): δ 0.12 and 0.38 (s, 6H, Si(CH_3)$_2$), 0.84 (dd, 4H, $^2J_{HH}$ = 6Hz, $^2J_{PH}$ = 4Hz, SiCH_2P), 0.99 and 1.34 (m, 12H, CH(CH_3)$_2$), 2.15 and 2.77 (sept., 2H, $^3J_{HH}$ = 7Hz, CH(CH$_3$)$_2$), 6.51 (d, 2H, $^4J_{HH}$ = 1Hz, Cp-H), 7.18 (t, 1H, $^4J_{HH}$ = 1Hz, Cp-H). ^{31}P NMR (-40 °C, C_7D_8): δ 14.9 (s).

isomer 2': ^{1}H NMR (-40 °C, C_7D_8): δ 0.08, 0.30, 0.68 and 0.71 (s, 3H, Si(CH_3)$_2$), 1.08 and 1.17 (m, 12H, CH(CH_3)$_2$), 1.52 and 1.84 (m, 2H, CH(CH$_3$)$_2$), 6.62, 6.66 and 7.12 (m, 1H, Cp-H). ^{31}P NMR (-40 °C, C_7D_8): δ -4.9 and 24.9 (br s).

2.7.3.3 ^{Pr}[P$_2$Cp]Zr(CH$_2$Ph)$_3$ (3).

A solution of Mg(CH$_2$Ph)$_2$(THF)$_2$ (82 mg, 0.23 mmol) in 10 mL of toluene was added dropwise over a period of 15 minutes to a cooled (-78 °C) stirring solution of **1** (100 mg, 0.16 mmol) dissolved in 60 mL of toluene. The colour of the solution immediately changed from pale yellow to orange. The solution was allowed to slowly warm to room temperature, the volatiles were then removed under vacuum and the residue extracted with hexanes and filtered. Removal of the solvent under vacuum yielded a hydrocarbon soluble yellowish oil. ^{1}H NMR (20 °C, C_6D_6): δ 0.36 (s, 12H, Si(CH_3)$_2$), 0.58 (d, 4H, $^2J_{PH}$ = 4Hz, SiCH_2P), 0.96 (m, 24H, CH(CH_3)$_2$), 1.53 (d of sept, 4H, $^2J_{HH}$ = 7Hz, $^2J_{PH}$ = 3Hz, CH(CH$_3$)$_2$), 1.91 (s, 6H, CH_2Ph), 6.40 (d, 2H, $^4J_{HH}$ = 2Hz, Cp-H), 6.68 (d, 6H, $^3J_{HH}$ = 7Hz, o-C_6H_5), 6.93 (t, 3H, $^3J_{HH}$ = 7Hz, p-C_6H_5), 6.96 (t, 1H, $^3J_{HH}$ = 2Hz, Cp-H), 7.11 (t, 6H, $^3J_{HH}$ = 7Hz, m-C_6H_5). ^{31}P{^{1}H} NMR (20 °C, C_6D_6): δ -5.2 (s). ^{13}C{^{1}H} NMR (20 °C, C_6D_6): δ -0.2 and -0.1 (s, Si(CH_3)$_2$), 7.7 (d, $^1J_{PC}$ = 40Hz, SiCH_2P), 18.7, 19.1, 19.6 and 20.0 (s, CH(CH_3)$_2$), 24.9 and 25.2 (d, $^1J_{PC}$ = 17Hz, CH(CH$_3$)$_2$), 69.2 (s, CH$_2$Ph), 123.4 (s, Cp), 123.6 (s, Cp), 128.9 (s, o-C_6H_5), 129.8 (s, m-C_6H_5), 144.9 (s, p-C_6H_5).

67

2.7.3.4 $^{Pr}[P_2Cp]Hf(CH_2Ph)_3$ (4)

A solution of KCH_2Ph (19 mg, 0.24 mmol) in 30 mL of toluene was added dropwise over a period of 20 minutes to a cooled (-78 °C) stirring solution of **2** (156 mg, 0.24 mmol) dissolved in 60 mL of toluene. The solution was allowed to slowly warm to room temperature and stirred for 12 h, during which the colourless Hf solution gradually turned bright yellow. The volatiles were then removed under vacuum and the residue extracted with hexanes and filtered. Removal of the solvent under vacuum yielded a hydrocarbon soluble yellowish oil. ^1H NMR (20 °C, C_6D_6): δ 0.34 (s, 12H, Si($CH_3)_2$), 0.56 (d, 4H, $^2J_{PH}$ = 5Hz, SiCH_2P), 0.95 (m, 24H, CH($CH_3)_2$), 1.50 (sept, 4H, $^2J_{HH}$ = 7Hz, CH(CH$_3$)$_2$), 1.90 (s, 6H, CH_2Ph), 6.28 (d, 2H, $^4J_{HH}$ = 2Hz, Cp-H), 6.69 (t, 1H, $^3J_{HH}$ = 2Hz, Cp-H), 6.78 (d, 6H, $^3J_{HH}$ = 7Hz, o-C_6H_5), 6.87 (t, 3H, $^3J_{HH}$ = 7Hz, p-C_6H_5), 7.17 (t, 6H, $^3J_{HH}$ = 7Hz, m-C_6H_5). $^{31}P\{^1H\}$ NMR (20 °C, C_6D_6): δ -5.6 (s). $^{13}C\{^1H\}$ NMR (20 °C, C_6D_6): δ -0.2 and 0.2 (s, Si(CH_3)$_2$), 8.1 (d, $^1J_{PC}$ = 35Hz, SiCH_2P), 16.5, 17.2, 17.4 and 18.0 (s, CH(CH_3)$_2$), 26.0 and 26.4 (d, $^1J_{PC}$ = 15Hz, CH(CH$_3$)$_2$), 70.1 (s, CH_2Ph), 121.6 (s, Cp), 130.1 (s, o-C_6H_5), 131.7 (s, m-C_6H_5), 140.9 (s, p-C_6H_5).

2.7.3.5 $^{Pr}[P_2Cp]Zr(CH_2CMe_3)_3$ (5a)

A solution of $LiCH_2CMe_3$ (56 mg, 0.72 mmol) in 30 mL of toluene was added dropwise to a cooled (-78 °C) stirring solution of **1** (154 mg, 0.24 mmol) dissolved in 60 mL of toluene. The colour of the solution immediately turned bright yellow upon addition. The mixture was warmed to room temperature, and stirring was continued for 30 minutes. The solvent was then removed in vacuo, and the oily residue extracted with hexanes and filtered. The filtrate was reduced under vacuum to give **5a** as a bright yellow oil which remained soluble in pentane even at -40 °C, precluding the isolation of crystalline material. Yield: (130 mg, 72 %). ^1H NMR (20 °C, C_6D_6): δ 0.48 and 0.49 (s, 6H, Si(CH_3)$_2$), 0.70 (dd, 4H, $^2J_{HH}$ = 6Hz, $^2J_{PH}$ = 4Hz, SiCH_2P),

0.99 (m, 24H, CH(CH_3)$_2$), 1.21 (s, 6H, CH_2C(CH$_3$)$_3$), 1.22 (s, 27H, CH$_2$C(CH_3)$_3$), 1.55 (m, 4H, CH(CH$_3$)$_2$), 6.68 (d, 2H, $^4J_{HH}$ = 1Hz, Cp-H), 6.94 (t, 1Hz, $^4J_{HH}$ = 1H, Cp-H). ^{31}P NMR (20 °C, C$_6$D$_6$): δ -5.5 (s).

2.7.3.6 ^{Pr}[P$_2$Cp]Zr(CH$_2$SiMe$_3$)$_3$ (5b)

A solution of LiCH$_2$SiMe$_3$ (82 mg, 0.87 mmol) in 30 mL of toluene was added dropwise to a cooled (-78 °C) stirring solution of **1** (185 mg, 0.29 mmol) dissolved in 60 mL of toluene. The mixture was warmed to room temperature and left to stir for 2 h, during which the colour of the solution slowly turned pale yellow. The solvent was then removed in vacuo, and the oily residue extracted with hexanes and filtered. The filtrate was reduced under vacuum to give a pale yellow, hydrocarbon-soluble oil. Yield: (176 mg, 76 %). ^{1}H NMR (20 °C, C$_6$D$_6$): δ 0.28 (s, 27H, CH$_2$Si(CH_3)$_3$), 0.29 and 0.45 (s, 6H, Si(CH_3)$_2$), 0.32 and 0.63 (d, 2H, $^2J_{HH}$ = 6Hz, SiCH_2P), 0.68 (s, 6H, CH_2Si(CH$_3$)$_3$), 1.00 (m, 24H, CH(CH_3)$_2$), 1.59 (m, 4H, CH(CH$_3$)$_2$), 6.74 (d, 2H, $^4J_{HH}$ = 2Hz, Cp-H), 6.91 (t, 1H, $^4J_{HH}$ = 2Hz, CpH). ^{31}P NMR (20 °C, C$_6$D$_6$): δ -5.9 (s).

2.7.3.7 ^{Pr}[P$_2$Cp]Zr(CH$_3$)$_3$ (6)

A solution of 1.4 M MeMgBr (3.91 mL, 5.47 mmol) was diluted in 310 mL of toluene and added dropwise to a cooled (-78 °C) stirring solution of **1** (1.00 g, 1.56 mmol) dissolved in 50 mL of toluene. The pale yellow solution gradually turned pale yellow over the course of the addition. The solution was warmed to room temperature, covered with metal foil, and stirred for 12 h, after which the solvent was removed under vacuum and the residue extracted with hexanes and filtered. Removal of the solvent under vacuum yielded approximately 0.6 g of trimethyl **5** as a slightly impure (impurities total less than 5% by ^{31}P NMR spectroscopy) yellowish oil . ^{1}H NMR (20 °C, C$_6$D$_6$): δ 0.37 (s, 12H, Si(CH_3)$_2$), 0.54 (t, 9H, $^3J_{PH}$ = 2Hz, ZrCH_3), 0.70 (d, 4H, $^2J_{PH}$ = 7Hz, SiCH_2P), 1.00 (m, 24H, CH(CH_3)$_2$), 1.62 (d of sept, 4H, $^3J_{HH}$ = 7Hz, $^2J_{PH}$ = 3Hz,

CH(CH$_3$)$_2$), 6.42 (t, 1H, $^4J_{HH}$ = 2Hz, Cp-H), 6.71 (d, 2H, $^4J_{HH}$ = 2Hz, Cp-H). ^{13}C{^{1}H} NMR (20 °C, C$_6$D$_6$): δ -0.6 (d, $^3J_{PC}$ = 5Hz, Si(CH_3)$_2$), -0.2 (d, $^3J_{PC}$ = 4Hz, Si(CH_3)$_2$), 10.3 (d, $^1J_{PC}$ = 24Hz, SiCH_2P), 19.2 and 19.6 (d, $^2J_{PC}$ = 8Hz, CH(CH_3)$_2$), 25.7 (d, $^1J_{PC}$ = 8Hz, CH(CH$_3$)$_2$), 42.7 (t, $^2J_{PC}$ = 3Hz, ZrCH_3), 121.5 (Cp), 121.9 (d, Cp), 125.35 (d, $^3J_{PC}$ = 4Hz, Cp). ^{31}P{^{1}H} NMR (20 °C, C$_6$D$_6$): δ 2.3 (s).

2.7.3.8 ^{Pr}[P$_2$Cp]ZrCl$_2$(CH$_2$CMe$_3$) (7a)

A solution of LiCH$_2$CMe$_3$ (19 mg, 0.24 mmol) in 30 mL of toluene was added dropwise over a period of 20 minutes to a cooled (-78 °C) stirring solution of **1** (156 mg, 0.24 mmol) dissolved in 50 mL of toluene. The colour of the solution gradually changed from pale to bright yellow. The solution was stirred at -78°C to 0°C for another 30 minutes, and then allowed to warm slowly to room temperature. The solvent was then removed in vacuo, and the oily residue extracted with hexanes and filtered. The filtrate was reduced to yield 0.87 g of a slightly impure (by ^{1}H and ^{31}P NMR spectroscopy) yellow oil consisting of **7a** as the main (>90%) product. ^{1}H NMR (20 °C, C$_6$D$_6$): δ 0.26 and 0.36 (s, 6H, Si(CH_3)$_2$), 0.70 (dd, 4H, $^2J_{HH}$ = 6Hz, $^2J_{PH}$ = 7Hz, SiCH_2P), 1.00 (m, 24H, CH(CH_3)$_2$), 1.20 (d, 2H, $^3J_{PH}$ = 7Hz, CH_2C(CH$_3$)$_3$), 1.47 (s, 9H, CH$_2$C(CH_3)$_3$), 1.52 (m, 4H, CH(CH$_3$)$_2$), 1.68 (s, 2H, CH_2C(CH$_3$)$_3$), 6.54 (t, 1H, $^4J_{HH}$ = 1Hz, Cp-H), 6.98 (d, 2H, $^4J_{HH}$ = 1Hz, Cp-H). ^{31}P NMR (20 °C, C$_6$D$_6$): δ 0.7 (very br) (isomer 1 - 75%); -6.8 and 8.7 (br s) (isomer 2 - 25%).

2.7.3.9 ^{Pr}[P$_2$Cp]ZrCl$_2$(CH$_2$SiMe$_3$) (7b)

A solution of LiCH$_2$SiMe$_3$ (27 mg, 0.29 mmol) in 30 mL of toluene was added dropwise over a period of 20 minutes to a cooled (-78 °C) stirring solution of **1** (185 mg, 0.29 mmol) dissolved in 50 mL of toluene. The solution was allowed to warm slowly to room temperature and stirred for another 2 h, during which the pale yellow solution brightened somewhat. The

solvent was then removed in vacuo, and the oily residue extracted with hexanes and filtered. The solvent was removed under vacuum to yield 0.90 g of a slightly impure (by ^{1}H and ^{31}P NMR spectroscopy) yellow oil consisting of **7b** as the main (>85%) product. ^{1}H NMR (20 °C, C$_6$D$_6$): δ 0.31 (s, 9H, CH$_2$Si(CH_3)$_3$), 0.38 and 0.50 (s, 6H, Si(CH_3)$_2$), 0.69 (s, 2H, CH_2Si(CH$_3$)$_3$), 0.71 (dd, 4H, $^2J_{HH}$ = 6Hz, $^2J_{PH}$ = 7Hz, SiCH_2P), 1.05 (m, 24H, CH(CH_3)$_2$), 1.61 (m, 4H, CH(CH$_3$)$_2$), 6.50 (t, 1H, $^4J_{HH}$ = 1Hz, Cp-H), 7.05 (d, 2H, $^4J_{HH}$ = 1Hz, Cp-H). ^{31}P NMR (20 °C, C$_6$D$_6$):δ 1.5 (very br) (isomer 1 - 85%); -6.5 and 9.0 (br s) (isomer 2 - 15%).

2.7.3.10 ^{Pr}[P$_2$Cp]ZrCl$_2$(CH$_3$) (8)

A solution of 1.4 M MeLi (0.54 mL, 0.76 mmol) was diluted in 10 mL of ether and added dropwise to a cooled (-78 °C) stirring solution of **1** (481 mg, 0.75 mmol) dissolved in 40 mL of toluene. The solution turned yellow during the course of the addition. The reaction mixture was then warmed to room temperature, covered with metal foil, and stirred for 2 h. The solvent was subsequently removed in vacuo, the oily residue extracted with a toluene/hexanes mixture, and filtered. The filtrate was reduced under vacuum to yield 0.39 g of a slightly impure (by ^{1}H and ^{31}P NMR spectroscopy) yellow oil consisting of **8** as the main (>85%) product. This material slowly decomposed over a period of weeks at (-78 °C) to give the starting trichloride **1** and a variety of unidentified products. ^{1}H NMR (20 °C, C$_6$D$_6$): δ 0.21 and 0.26 (s, 6H, Si(CH_3)$_2$), 0.56 and 0.62 (dd, 2H, $^2J_{HH}$ = 3Hz, $^2J_{PH}$ = 6Hz, SiCH_2P), 0.91 (m, 24H, CH(CH_3)$_2$), 1.01 (br, 3H, ZrCH_3), 1.50 (m, 4H, CH(CH$_3$)$_2$), 1.51 (6.71 (d, 2H, $^3J_{HH}$ = 1Hz, Cp-H), 6.75 (t, 1H, $^4J_{HH}$ = 2Hz, Cp-H). ^{31}P NMR (20 °C, C$_6$D$_6$): δ 1.3 (very br) (isomer 1 - 90%); -7.4 and 8.6 (br s) (isomer 2 - 10%).

2.7.3.11 ^{Pr}[P$_2$Cp]ZrCl$_2$(CH$_2$CH$_3$) (9)

A solution of 3.0 M EtMgBr (0.12 mL, 0.36 mmol) was diluted in 10 mL of toluene and added dropwise over a period of 15 min to a cooled (-78 °C) stirring solution of **1** (225 mg, 0.35 mmol) dissolved in 50 mL of toluene. The solution turned bright yellow during the course of the addition. The reaction mixture was stirred at this temperature for 30 min, then warmed to room temperature and stirred for 6 h. The colour of the solution changed gradually from bright yellow to a dull reddish-brown. The solvent was removed in vacuo and the oily residue extracted with hexanes and filtered. The filtrate was reduced under vacuum to yield 0.17 g of a slightly impure (by ^{1}H and ^{31}P NMR spectroscopy) dark red oil consisting of **9** as the main (>90%) product. This material slowly decomposed over a period of weeks at (-78 °C) to give the starting trichloride **1** and a variety of unidentified products. ^{1}H and ^{31}P{^{1}H} NMR spectra of this are near coalescence at room temperature. ^{1}H NMR (60 °C, C$_6$D$_6$): δ 0.3 and 0.4 (br, 6H, Si(CH_3)$_2$), 0.9 (br, SiCH_2P), 1.1 (br, 24H, CH(CH_3)$_2$), 1.8 (br, 4H, CH(CH$_3$)$_2$), 1.9 (br quartet, 3H, CH$_2$CH_3), 6.8 (br, 1H, Cp-H), 6.9 (br, 2H, Cp-H). ^{31}P{^{1}H} NMR (20 °C, C$_6$D$_6$): δ -5 and 11 (very br - near coalescence).

2.7.3.12 ^{Pr}[P$_2$Cp]ZrCl$_2$(OBu^t) (10)

A solution of KO^{t}Bu (39 mg, 0.35 mmol) in 10 mL of THF was added dropwise with stirring to a cooled (-78 °C) solution of **1** (221 mg, 0.35 mmol) dissolved in 30 mL of THF. The pale yellow colour of the chloro complex gradually dissipated after the addition was complete. The solution was slowly warmed to room temperature and stirred for another 24 hours. The solvent was then removed in *vacuo*, and the residue extracted with hexanes and filtered to give a hydrocarbon-soluble yellowish-white oil, which slowly decomposed at (-78 °C) to give the starting trichloride **1** and a variety of unidentified products. ^{1}H NMR (20 °C, 400 MHz, C$_6$D$_6$): δ 0.28 and 0.39 (s, 6H, Si(CH_3)$_2$), 0.62 and 0.72 (dd, 2H, $^2J_{HH}$ = 7Hz, $^2J_{PH}$ = 6Hz, SiCH_2P), 0.98 (m, 24H, CH(CH_3)$_2$), 1.26 (s, 9H, OC(CH_3)$_3$), 1.61 (m, 4H, CH(CH$_3$)$_2$), 6.71 (d, 2H, $^3J_{HH}$

= 1Hz, Cp-H), 6.75 (t, 1H, $^4J_{HH}$ = 2Hz, Cp-H). ^{31}P NMR (20 °C, C_6D_6): δ 0.6 (br s) (isomer 1 - 95%); -7.8 and 8. (br s) (isomer 2 - 5%).

2.7.3.13 ^{Pr}[P$_2$Cp]ZrCl$_2$(CH$_2$Ph) (11)

A solution of KCH$_2$Ph (115 mg, 0.8 mmol) in 30 mL of THF was added dropwise to a cooled (-78 °C) stirring solution of **1** (156 mg, 0.24 mmol) dissolved in 60 mL of THF. The colourless solution immediately turned yellowish-orange. The mixture was allowed to warm to room temperature and then stirred for 2 h, during which the colour of the solution gradually turned red. The volatiles were then removed under vacuum and the residue extracted with hexanes and filtered. Red crystals were obtained from slow evaporation of a concentrated hexamethyldisiloxane solution. Anal. Calcd. for $C_{23}H_{47}Cl_2P_2Si_2Zr$: C, 56.43; H, 6.53. Found: C, 55.45; H, 6.72. ^{1}H NMR (20 °C, C_6D_6): δ 0.22 (s, 12H, Si(CH_3)$_2$), 0.41 and 0.61 (d, 2H, $^2J_{PH}$ = 4Hz, SiCH_2P), 0.98 (m, 24H, CH(CH_3)$_2$), 1.63 (m, 4H, CH(CH$_3$)$_2$), 2.90 (s, 2H, CH_2Ph), 6.54 (d, 2H, $^4J_{HH}$ = 2Hz, Cp-H), 6.92 (t, 1H, $^3J_{HH}$ = 7Hz, p-C_6H_5), 6.95 (t, 1H, $^4J_{HH}$ = 2Hz, Cp-H), 7.32 (t, 2H, $^3J_{HH}$ = 7Hz, m-C_6H_5), 7.55 (d, 1H, $^3J_{HH}$ = 7Hz, o-C_6H_5). ^{31}P{^{1}H} NMR (-20 °C, C_7D_8): δ -6.9 (s), 14.2 (s); (20 °C, C_7D_8): δ 5.8 (s). ^{13}C{^{1}H} NMR (20 °C, C_7D_8): δ -1.2 (d, $^3J_{PC}$ = 4Hz, Si(CH$_3$)$_2$), -0.3 (d, $^3J_{PC}$ = 6Hz, Si(CH$_3$)$_2$), 9.8 (br, SiCH$_2$P), 18.4, 19.1, 19.3 and 19.5 (CH(CH_3)$_2$), 25.5 (d, $^1J_{PC}$ = 7Hz,CH(CH$_3$)$_2$), 25.9 (d, $^1J_{PC}$ = 5Hz, CH(CH$_3$)$_2$), 75.7 (t, $^2J_{PC}$ = 9Hz, CH_2Ph), 121.6 (s, Cp), 123.5 (s, Cp), 126.1 (s, Cp), 127.9 (s, o-C_6H_5), 130.3 (s, m-C_6H_5), 146.8 (s, p-C_6H_5).

2.7.3.14 ^{Pr}[P$_2$Cp]HfCl$_2$(CH$_2$Ph) (12)

A solution of KCH$_2$Ph (115 mg, 0.8 mmol) in 30 mL of THF was added dropwise to a cooled (-78 °C) stirring solution of **2** (156 mg, 0.24 mmol) dissolved in 60 mL of THF. The colourless Hf solution gradually turned yellowish-orange. The mixture was allowed to warm to

room temperature and then stirred for 12 h. The volatiles were then removed under vacuum and the residue extracted with hexanes and filtered. Removal of the solvent under vacuum yielded a yellowish oil, soluble in pentane. ^{1}H NMR (20 °C, C_6D_6): δ 0.02 (s, 12H, Si(CH_3)$_2$), 0.24 and 0.60 (d, 2H, $^2J_{PH}$ = 5Hz, SiCH_2P), 0.91 (m, 24H, CH(CH_3)$_2$), 1.55 (m, 4H, CH(CH$_3$)$_2$), 2.42 (s, 2H, CH_2Ph), 6.38 (d, 1H, $^4J_{HH}$ = 2Hz, Cp-H), 6.74 (t, 1H, $^4J_{HH}$ = 1Hz, Cp-H), 6.79 (t, 1H, $^3J_{HH}$ = 7Hz, p-C_6H_5), 7.23 (t, 2H, $^3J_{HH}$ = 7Hz, m-C_6H_5), 7.42 (d, 1H, $^3J_{HH}$ = 7Hz, o-C_6H_5). ^{31}P{^{1}H} NMR (-20 °C, C_7D_8): δ 0 and 19 (very br).

2.7.3.15 ^{Pr}[P$_2$Cp]ZrCl$_2$(η^2-C(O)CH$_2$Ph) (13)

A solution of **11** (170 mg, 0.24 mmol) in 30 mL of toluene was placed in a 200 mL bomb and affixed to a dual vacuum/nitrogen line. A small portion of solvent was removed under vacuum, and an atmosphere of carbon monoxide introduced at -30 °C. The reaction mixture was warmed to room temperature and left to stir for 2 h, during which the red colour of the solution gradually changed to a pale orange-yellow. The solvent was reduced to 3 mL, and from this saturated solution pale yellow prisms were obtained. The crystals were washed with cold hexanes and dried. Yield 138 mg (78 %). Anal. Calcd. for $C_{31}H_{54}Cl_2OP_2Si_2Zr$: C, 51.50; H, 7.53. Found: C, 51.53; H, 7.55.

isomer 1 (55%): ^{1}H NMR (20 °C, 400 MHz, C_6D_6): δ 0.13 and 0.36 (s, 6H, Si(CH_3)$_2$), 0.84 (dd, 4H, $^2J_{HH}$ = 6Hz, $^2J_{PH}$ = 4Hz, SiCH_2P), 1.03 (m, 24H, CH(CH_3)$_2$), 1.60 and 1.81 (m, 2H, CH(CH$_3$)$_2$), 3.02 (dd, 1H, $^2J_{HH}$ = 16Hz, $^3J_{PH}$ = 3Hz, CH_AHPh), 3.82 (dd, 1H, $^2J_{HH}$ = 16Hz, $^3J_{PH}$ = 35Hz, CHH_BPh), 6.63 (dd, 1H, $^3J_{HH}$ = 2Hz, Cp-H), 6.87 (t, 1H, $^4J_{HH}$ = 2Hz, Cp-H), 7.46 (dd, 1H, $^3J_{HH}$ = 2Hz, Cp-H), 7.10 and 7.56 (m, 5H, overlapping phenyl resonances). ^{31}P NMR (20 °C, C_6D_6): δ -5.1 (s), 44.4 (s).

isomer 2 (45%): ^{1}H NMR (20 °C, 400 MHz, C_6D_6): δ 0.09 and 0.23 (s, 6H, Si(CH_3)$_2$), 0.52 (dd, 4H, $^2J_{HH}$ = 6Hz, $^2J_{PH}$ = 10Hz, SiCH_2P), 1.03 (m, 24H, CH(CH_3)$_2$), 1.50 (m, 4H,

CH(CH$_3$)$_2$), 2.95 (dd, 1H, $^2J_{HH}$ = 16Hz, $^3J_{PH}$ = 2Hz, CH_AHPh), 3.89 (dd, 1H, $^2J_{HH}$ = 16Hz,

$^3J_{PH}$ = 35Hz, CH_BHPh), 6.63 (dd, 1H, $^3J_{HH}$ = 2Hz, Cp-H), 6.74 (t, 1H, $^4J_{HH}$ = 2Hz, Cp-H), 7.26

(dd, 1H, $^3J_{HH}$ = 2Hz, Cp-H), 7.10 and 7.56 (m, 5H, overlapping phenyl resonances). ^{31}P NMR

(20 °C, C$_6$D$_6$): δ -5.4 (s), 45.9 (s).

2.8   References

(1)   Mu, Y.; Piers, W. E.; MacQuarrie, D. C.; Zaworotko, M. J.; V G Young, J. *Organometallics* **1996**, *15*, 2720.

(2)   Fryzuk, M. D.; Mao, S. S. H.; Duval, P. B.; Rettig, S. J. *Polyhedron* **1995**, *14*, 11.

(3)   Plooy, K.E.; Moll, U.; Wocadlo, S.; Massa, W.; Okuda, J. *Organometallics* **1995**, *14*, 3129.

(4)   Cotton, F. A.; Wilkinson, G. *Advanced Inorganic Chemistry;* 5th ed.; John Wiley & Sons: Toronto, 1988.

(5)   *Comprehensive Organometallic Chemistry II*; Wilkinson, G.; Stone, F. G. A.; Abel, E. W., Ed.; Pergamon Press: Oxford, 1995.

(6)   Lund, E. C.; Livinghouse, T. *Organometallics* **1990**, *9*, 2426.

(7)   Erker, G.; Sarter, C.; Albrecht, M.; Dehnicke, S.; Krüger, C.; Raabe, E.; Schlund, R.; Benn, R.; Rufínska, A.; Mynott, R. *J. Organomet. Chem.* **1990**, *382*, 89.

(8)   Zeijden, A. A. H. v. d.; Mattheis, C.; Fröhlich, R.; Zippel, F. *Inorg. Chem.* **1997**, *36*, 4444.

(9)   Mu, Y.; Piers, W. E.; MacGillivray, L. R.; Zaworotko, M. J. *Polyhedron* **1995**, *14*, 1.

(10)   Crowther, D. J.; Jordan, R. F.; Baenziger, N. C.; Verma, A. *Organometallics* **1990**, *9*, 2574.

(11)   Winter, C. H.; Zhou, X.-X.; Dobbs, D. A.; Heeg, M. J. *Organometallics* **1991**, *10*, 210.

(12)   Jutzi, P.; Kleimeier, J. *J. Organomet. Chem.* **1995**, *486*, 287.

(13)   Engelhardt, L. M.; Papasergio, R. I.; Raston, C. L.; White, A. H. *Organometallics* **1984**, *3*, 18.

(14)   Prout, K.; Cameron, T. S.; Forder, R. A.; Critchley, S. R.; Denton, B.; Rees, G. V. *Acta Crystallogr.* **1974**, *B30*, 2290.

(15)   Bondi, A. *J. Phys. Chem.* **1964**, *68*, 441.

(16)   Hore, P. J. *Nuclear Magnetic Resonance*; Oxford University Press: Oxford, 1995.

(17)   Sanders, J. K. M.; Hunter, B. K. *Modern NMR Spectroscopy;* 2nd ed.; Oxford University Press: Oxford, 1993.

(18)   Rogers, R. D.; Bynum, R. V.; Atwood, J. L. *J. Am. Chem. Soc.* **1978**, *100*, 5238.

(19)   Rogers, R. D.; Bynum, R. V.; Atwood, J. L. *J. Am. Chem. Soc.* **1981**, *103*, 692.

(20)   Martín, A.; Mena, M.; Palacios, F. *J. Organomet. Chem.* **1994**, *480*, C10.

(21)   Berthold, H. J.; Groh, G. *Angew. Chem., Int. Ed. Engl.* **1966**, *5*, 516.

(22)   Wolczanski, P. T.; Bercaw, J. E. *Organometallics* **1982**, *1*, 793.

(23)   Legzdins, P.; Jones, R.H.; Phillips, E.C.; Yee, V.C.; Trotter, J.; Einstein, F.W.B. *Organometallics* **1991**, *10*, 986.

(24)   Brookhart, M.; Green, M. L. H.; Wong, L. L. *Prog. Inorg. Chem.* **1988**, *36*, 1.

(25) Wengrovius, J. H.; Schock, R. R. *J. Organomet. Chem.* **1981**, *205*, 319.

(26) Roddick, D. M.; Santarsiero, B. D.; Bercaw, J. E. *J. Am. Chem. Soc.* **1985**, *107*, 4670.

(27) Arnold, J.; Tilley, T. D.; Rheingold, A. L.; Geib, S. J.; Arif, A. M. *J. Am. Chem. Soc.* **1989**, *111*, 149.

(28) Fryzuk, M. D.; Mylvaganum, M.; Zaworotko, M. J.; MacGillivray, L. R. *Organometallics* **1996**, *15*, 1134.

(29) Crabtree, R. H. *The Organometallic Chemistry of the Transition Metals;* 2nd ed.; John Wiley & Sons: USA, 1994, pp 487.

(30) Fachinetti, G.; Floriani, C.; Marchetti, F.; Merlino, S. *J. Chem. Soc., Chem. Commun.* **1976**, 552.

(31) Williams, D. H.; Fleming, I. *Spectroscopic Methods in Organic Chemistry;* 4th ed.; McGraw-Hill: London, 1989.

(32) Erker, G. *Acc. Chem. Res.* **1984**, *17*, 103.

(33) Tatsumi, K.; Nakumura, A.; Hofmann, P.; Stauffert, P.; Hoffmann, R. *J. Am. Chem. Soc.* **1985**, *107*, 4440.

(34) Manzer, L. E. *Inorg. Synth.* **1982**, *21*, 137.

(35) King, R. B.; Stone, F. G. A. *Inorg. Synth.* **1963**, *7*, 99.

(36) Schlosser, M.; Hartmann, J. *Angew. Chem., Int. Ed. Engl.* **1973**, *12*, 508.

(37) Schrock, R. R.; Fellman, J. D. *J. Am. Chem. Soc.* **1978**, *100*, 3359.

(38) Schrock, R. R. *J. Organomet. Chem.* **1976**, *122*, 209.

Chapter 3

Zirconium and Hafnium Alkylidene Complexes:

Mechanism of Formation and Reactivity

3.1   Introduction

The previous chapter surveyed the synthesis and solution structure of a series of mono- and tri-substituted alkyl complexes of Zr and Hf coordinated by the ancillary P2Cp ligand. The trialkyl derivatives were found to possess considerable thermal stability in comparison to the monoalkyl species, which were prone to disproportionate over time. Fluxional coordination of the side-arm phosphine was seen to be a prevalent trait in several of these complexes.

In this chapter the focus shifts to the solution dynamics and thermal reactivity of the dialkyl complexes. The conversion of these species to rare Zr and Hf alkylidene merits special attention, so the composite mechanism involved in this high yield reaction will be investigated, with an emphasis towards evaluating the role of the ancillary ligand. The extension of this mechanism to the formation of other alkylidene derivatives will also be tested.

The reactivity of the resulting alkylidene complexes will also be explored. If the side-arm phosphines are an integral factor in the stability of these complexes, they nevertheless allow controlled reactivity at the metal centre by virtue of their labile coordination, which provides an open site for substrate activation to occur. However, it is evident that slower reaction rates are

observed in comparison to other alkylidene derivatives, and the steric bulk of the ligand also limits the size of reactants that can access the metal.

3.2.1 NMR spectroscopic identification of ^{Pr}[P$_2$Cp]ZrCl(CH$_2$Ph)$_2$

In the previous chapter the preparation of benzyl derivatives [P$_2$Cp]M(CH$_2$Ph)$_3$ (**3**: M = Zr, **4**: M = Hf) and ^{Pr}[P$_2$Cp]MCl$_2$(CH$_2$Ph) (**11**: M = Zr, **12**: M = Hf) were described. In contrast to these results, treating the starting trichloride complex **1** or **2** with 2 equivalents of KCH$_2$Ph in THF (or 1 equiv of Mg(CH$_2$Ph)$_2$(THF)$_2$ in toluene) does not give the anticipated dibenzyl complex ^{Pr}[P$_2$Cp]MCl(CH$_2$Ph)$_2$ (**14**: M = Zr, **15**: M = Hf) as the sole product, but instead yields a thermally and photochemically labile greenish-orange oil consisting of a mixture of mono-, di-, and tri-benzyl species, which occur in a 5 : 4 : 5 ratio, respectively, at room temperature (equation 3.1):

$$^{Pr}[P_2Cp]MCl_3 \quad \xrightarrow[-2\ KCl]{2\ KCH_2Ph}$$

1 M= Zr
2 M = Hf

(3.1)

$$^{Pr}[P_2Cp]MCl_2(CH_2Ph) \ + \ ^{Pr}[P_2Cp]MCl(CH_2Ph)_2 \ + \ ^{Pr}[P_2Cp]M(CH_2Ph)_3$$

11 M= Zr
12 M = Hf

14 M= Zr
15 M = Hf

3 M= Zr
4 M = Hf
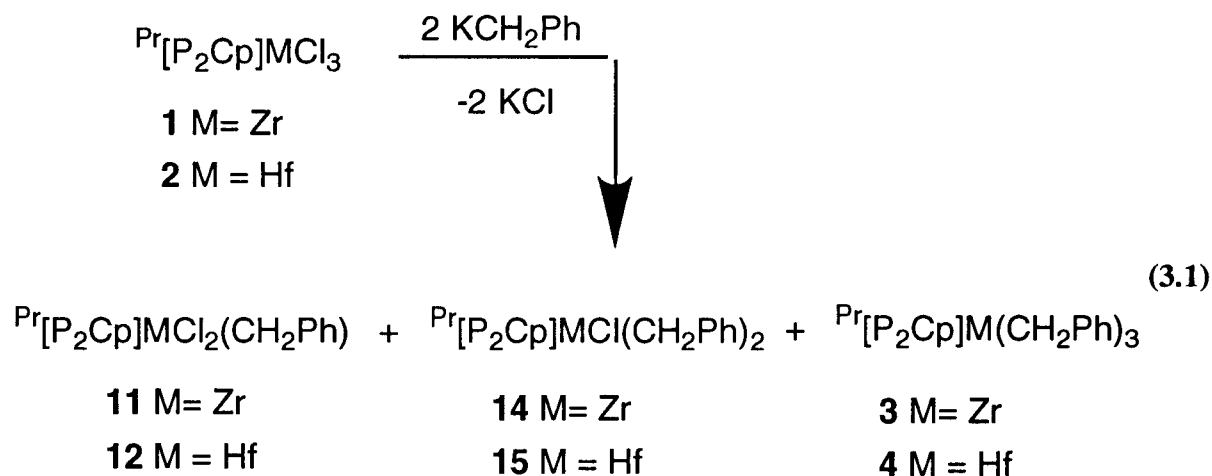
These are all observed together as products of this reaction as long as the stoichiometry of KCH$_2$Ph reacted with **1** is greater than 1 equivalent and less than 3 equivalents, the relative proportion of tribenzyl present in the mixture increasing with the amount of benzyl reagent used. Attempts to separate individual species from this mixture have repeatedly proved unsuccessful.

The subsequent thermal and photochemical decomposition of this ensemble to produce the benzylidene complex ^{Pr}[P$_2$Cp]M=CHPh(Cl) (**16**: M = Zr, **17**: M = Hf) will be discussed later.

The following discussion will centre on the Zr system as it has been more extensively studied. Familiarity with the ^{1}H and ^{31}P{^{1}H} NMR spectroscopic features of tribenzyl **3** and monobenzyl **11** assists in the interpretion of the NMR spectra of the reaction mixture obtained in equation 3.1. The coexistence of all three species in solution generates a complicated ^{1}H NMR spectrum with some peaks overlapping, even when conducted on the 500 MHz instrument. This renders some of the resonances unassignable, although separating those peaks attributed to known **3** and **11** permits the identification of **14** from the remaining diagnostic resonances. Integration of the benzyl protons relative to those of the ancillary ligand supports the stoichiometry of **14** as the dibenzyl complex. In the complicated ^{13}C{^{1}H} NMR spectrum the benzylic carbon resonance for **14** can be identified at 71 ppm.

A cursory examination of the ambient temperature ^{31}P{^{1}H} NMR spectrum of the reaction mixture (Figure 3.1) suggests that only two species are present in solution, in approximately equal proportions. However, there is an additional pair of resonances that are almost completely broadened into the baseline, associated with **11** and resulting from the previously described fluxional process for this complex in Chapter 2, which is near coalescence at this temperature. The reappearance of diagnostic peaks upon raising or lowering the temperature from the coalescence point is in agreement with the VT behavior identified with this species. Therefore, of the two distinct singlets seen in the ^{31}P{^{1}H} NMR spectrum in Figure 3.1, one at -5.6 ppm is attributed to **3**, leaving the other at 0.5 ppm assigned to **14**. The singlet for **14** in the ambient temperature ^{31}P{^{1}H} NMR spectrum at 0.5 ppm sharpens as the temperature is elevated to 95 °C. Below room temperature, this peak gradually broadens as the temperature is lowered until it disappears into the baseline near -70 °C, beyond which a reappearance of new peaks is not observed down to the experimental temperature limit in C$_7$D$_8$ at -95 °C. These observations are consistent with fluxional coordination of the side-arm phosphines to the metal

centre, as previously noted with **11**. However, the inability to detect resonances at any temperature below coalescence precluded a kinetic study of this process by line shape analysis.
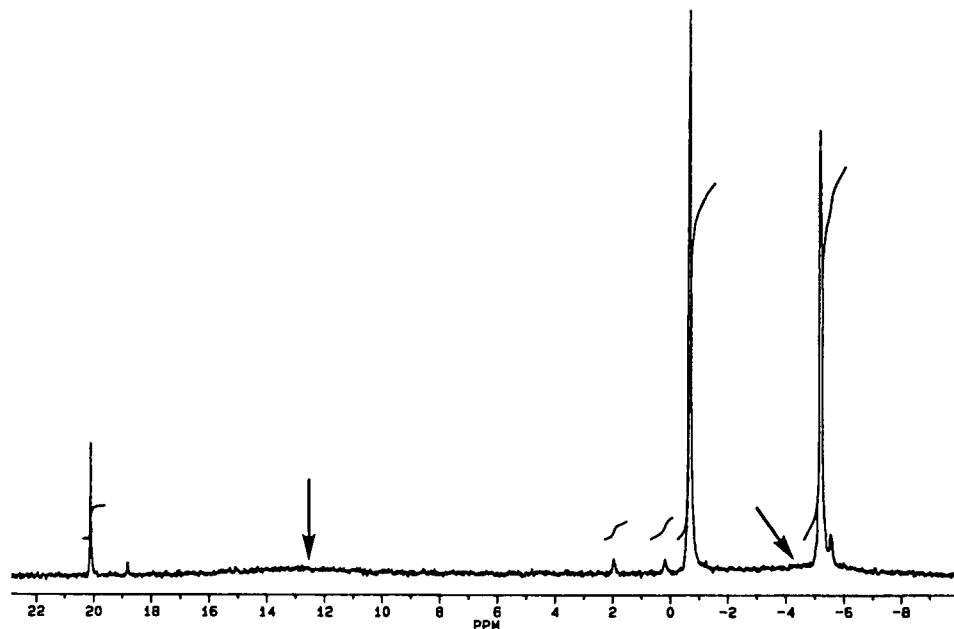
Figure 3.1 $^{31}P\{^{1}H\}$ NMR spectrum of the reaction mixture from

equation 3.1 in C_7D_8 at 30 °C. Arrows refer to presence of **11** in the spectrum.

The benzylic (CH_2Ph) protons of **14** also exhibit fluxional behavior in the ^{1}H NMR spectrum. This region of the spectrum is relatively unobscured, thus permitting a variable temperature study which is summarized below (Figure 3.2).

references begin on page 141
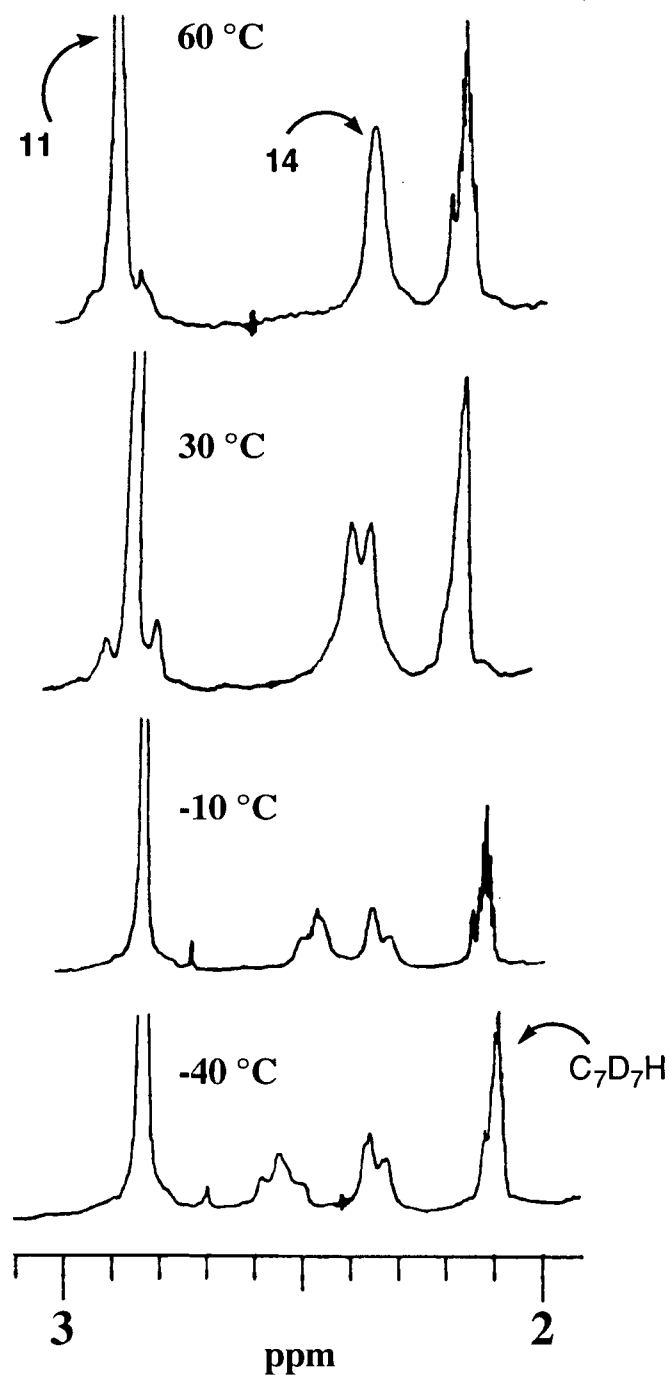
Figure 3.2 Variable temperature ^{1}H NMR spectrum for ^{Pr}[P$_2$Cp]ZrCl(CH$_2$Ph)$_2$ (**14**) from 2-3 ppm in C$_7$D$_8$.

At -40 °C the benzylic protons appear as a pair of unresolved multiplets centered near 2.45 ppm. As the temperature is raised to -10 °C these multiplets evolve into a doublet of doublets, which

references begin on page 141

gradually converges to two broad singlets at 30 °C. Eventually these peaks coalesce as the temperature approaches 40 °C, and a further temperature increase gradually sharpens this singlet further. To account for these observations, it is apparent that in any structural configuration of **14** the benzyl ligands are chemically inequivalent, although these groups could exchange via a fluxional process involving dissociation of the pendant phosphine donors, as hinted at by the variable temperature ^{31}P NMR spectra mentioned above. Therefore, the low temperature ^{1}H NMR spectrum corresponding to the slow exchange limit shows two multiplets, one for each benzyl group. As the temperature is raised the rate of ligand exchange gradually increases until it coincides with the NMR time scale at coalescence, and eventually in the fast exchange limit of this process a singlet is observed as an average of two chemical environments.

3.2.2 Equilibrium between [P$_2$Cp]ZrCl$_2$(CH$_2$Ph) (11), [P$_2$Cp]ZrCl(CH$_2$Ph)$_2$ (14), and [P$_2$Cp]Zr(CH$_2$Ph)$_3$ (3)

Given that monobenzyl **11** and tribenzyl **3** are each isolable in high yield from reactions conducted under the appropriate stoichiometric conditions, it is interesting to note that dibenzyl **14** cannot be isolated. A possible explanation for the coexistence of all three alkyl derivatives from the reaction in equation 3.1 is that **14** could undergo some degree of ligand redistribution to form **3** and **11** (equation 3.2):

$$2 \ ^{Pr}[P_2Cp]ZrCl(CH_2Ph)_2 \longrightarrow$$

14

$$^{Pr}[P_2Cp]ZrCl_2(CH_2Ph) \ + \ ^{Pr}[P_2Cp]Zr(CH_2Ph)_3 \qquad (3.2)$$

11   **3**
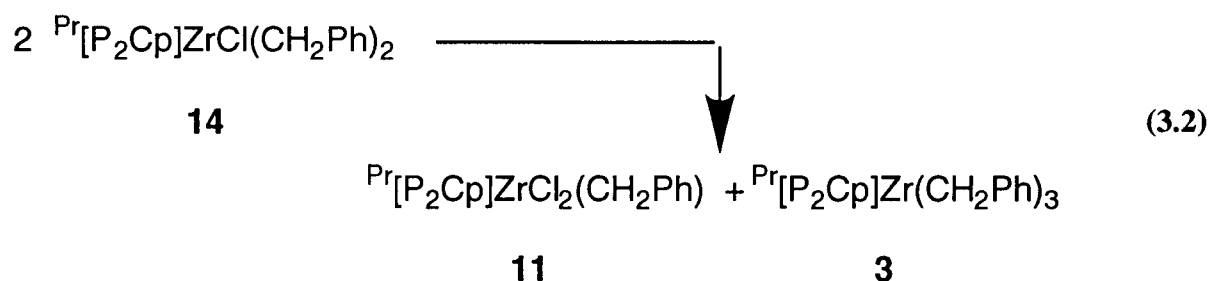
That the initial ratio of products remains constant indefinitely (i.e., the disproportionation of **14** does not continue to completion) suggests the reverse reaction of equation 3.2 must also occur, indicating that an equilibrium is established between these species in solution. In support of this hypothesis, combining solutions of tribenzyl **3** and monobenzyl **11** immediately shows the formation of dibenzyl **14**, irrespective of the order of addition, to regenerate a mixture of all three compounds. Again, the ratio of species observed depends on the relative amounts of **3** and **11** initially added. Table 3.1 shows the equilibrium concentrations obtained from separate prepared solutions in which the initial proportions of **3** and **11** added together were varied. From the data below it is evident that these species are indeed in equilibrium (equation 3.3) with an equilibrium constant (K = $[14]^2/[3][11]$) equal to 0.7(1) at 25 °C. The estimated uncertainty in K is a function of the imprecision in the integration measurements of the ^1H NMR spectra, as evaluated from repetitive experiments.

Table 3.1 Equilibrium concentrations of $^{Pr}[P_2Cp]ZrCl_2(CH_2Ph)$ (**11**), $^{Pr}[P_2Cp]ZrCl$-$(CH_2Ph)_2$ (**14**) and $^{Pr}[P_2Cp]Zr(CH_2Ph)_3$ (**3**) from mixed solutions at 295 K, and the equilibrium constant (K) calculated according to equation 3.3.

[11] (M)	[14] (M)	[3] (M)	K
0.55	0.12	0.04	0.7
0.23	0.10	0.07	0.6
0.15	0.11	0.17	0.7
0.04	0.07	0.17	0.7

$$^{Pr}[P_2Cp]ZrCl_2(CH_2Ph) + {}^{Pr}[P_2Cp]Zr(CH_2Ph)_3$$

$$\mathbf{11} \qquad\qquad \mathbf{3}$$

$$k_{-1} \Big\updownarrow k_1 \qquad\qquad (3.3)$$

$$2\ {}^{Pr}[P_2Cp]ZrCl(CH_2Ph)_2$$

$$\mathbf{14}$$
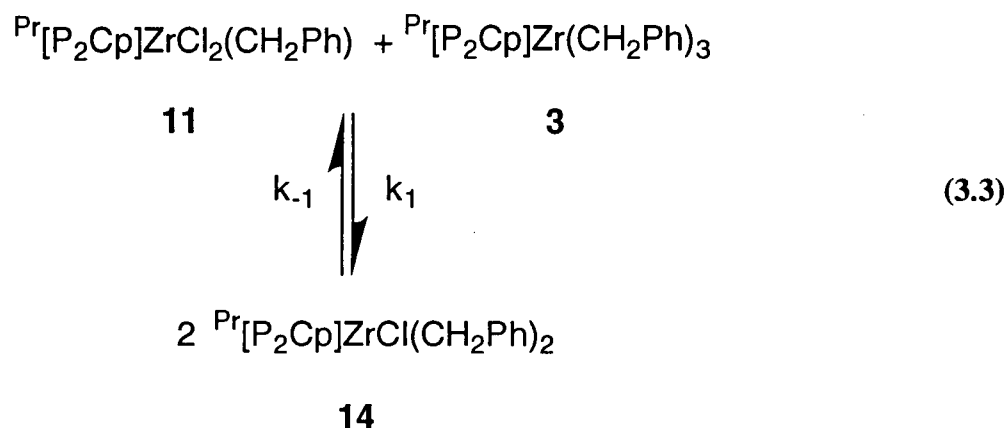
VT NMR experiments were conducted on sample mixtures to obtain thermodynamic information from the temperature-dependence of the equilibrium constant pertaining to equation 3.3. Precise integration measurements of the spectra obtained were hampered, however, by a combination of the fluxional behaviour of various species and by the temperature-induced migration of some resonances, leading to broadened and/or overlapping peaks at various temperatures. As a result, the van't Hoff plots obtained were subject to considerable uncertainty in the linear fits. Therefore, reproducible values for the thermodynamic parameters $\Delta H°$, $\Delta S°$, and $\Delta G°$ could not be calculated. However, the measurements are sufficiently reliable to be able to discern a small increase in the concentration of dibenzyl **14** relative to **3** and **11** as the temperature is increased over a wide (-65 °C to 60 °C) range. Therefore, a qualitative assessment of the thermodynamics in this reaction can be offered. The minimal temperature-dependence of the equilibrium constant apparent from the results suggests that the magnitude of $\Delta H°$ is fairly small, a positive value being inferred from the observed increase in K with temperature. Also, since the species on either side of equation 3.3 are equal in number and approximately similar in structure, one could argue that $\Delta S°$ is also relatively small. Overall, this would give a low value for $\Delta G°$ in this reaction, although admittedly there is a degree of uncertainty associated with the assumptions made in this analysis. A similar generalization can be made regarding the rates k_1 and k_{-1} of this reversible reaction, as the peaks in the NMR spectra do not show appreciable line

broadening, even in the high temperature regime, indicating that the slow exchange limit is still

maintained (i.e., rate constants are relatively small)

$$^{Pr}[P_2Cp]ZrCl_2(CH_2Ph) + {}^{Pr}[P_2Cp]Zr(CH_2Ph)_3$$

11   **3**

path a   fast   slow

‡

A

path b   slow   fast

$$2 \ {}^{Pr}[P_2Cp]ZrCl(CH_2Ph)_2$$

14
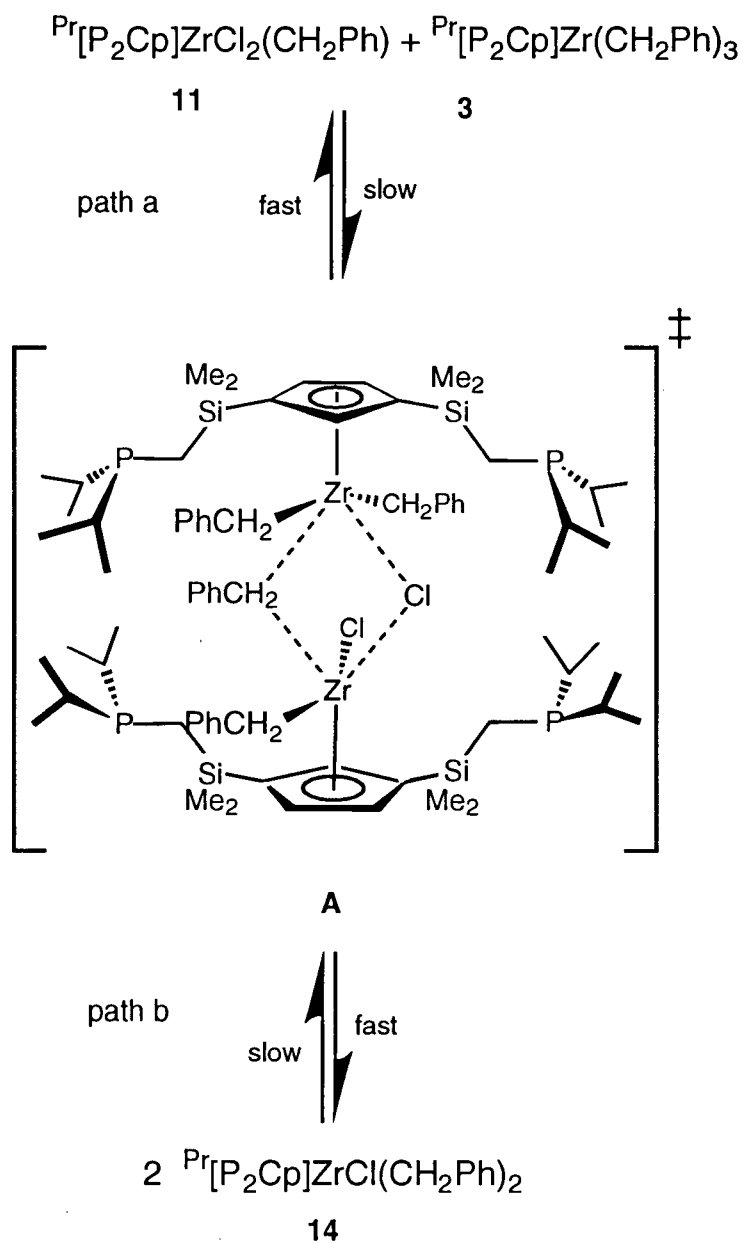
Scheme 3.1   Proposed intermediate in the ligand exchange mechanism for the

equilibrium in equation 3.3.

The mechanism that interconverts monobenzyl **11** and tribenzyl **3** to 2 equivalents of

dibenzyl **14** involves a mutual exchange of benzyl and chloro ligands. An intermediate is not

observed in this reaction, but a plausible candidate could be the binuclear adduct **A** shown in Scheme 3.1. There are two options for dissociation of the bridging ligands in complex **A**: path (a) regenerates **3** and **11**, while path (b) leads to the formation of two equivalents of **14**; both pathways are consistent with the reaction in equation 3.3. Since the equilibrium concentrations are established relatively quickly (within minutes), this places a lower limit on the exchange rates ($k > 0.001$ s^{-1}), suggesting that the energy barrier to transition state **A** is fairly low in this system.

It should be stated at this point that both monomeric **14** and binuclear adduct **A** possess an identical stoichiometry of two benzyl ligands for each P_2Cp group. The distinction that identifies **14** as the observed equilibrium species in the NMR spectra instead of **A**, thereby designating the latter as an undetected intermediate, is made from the relative equilibrium concentrations shown in Table 3.1. This set of data is not in accord with a process involving binuclear **A** in direct equilibrium with tribenzyl **3** and monobenzyl **11** (i.e., in which path b in Scheme 3.1 is omitted). The equilibrium constant calculated using this relationship ($K = [A]/[3][11]$), where the value for [A] determined by integration of the NMR spectra would equal one-half the value listed for **14** in Table 3.1, shows poor correlation between the separate sample mixtures. Further, if this equilibrium were in effect then high dilution of the reaction mixture should induce further disproportionation of **A** to restore the equilibrium, a feature that is not observed.

3.3.1 Synthesis and Structure of $^{Pr}[P_2Cp]M=CHPh(Cl)$ (M = Zr, Hf)

As briefly mentioned in section 3.3.2, thermolysis of a toluene solution of the equilibrium mixture consisting of tribenzyl **3**, dibenzyl **14** and monobenzyl **11** produces the alkylidene[1] complex $^{Pr}[P_2Cp]M=CHPh(Cl)$ (**16**: M = Zr,[2] **17**: M = Hf) in high yield (equation 3.5). The conditions differ dramatically for each derivative: the reaction that forms **16** is complete within

12 hours at 65 °C, while the Hf analogue **17** requires 6 days at 95 °C. Both species are thermally stable and can be isolated as moderately air- and moisture-sensitive crystals.

$$0.5 \ ^{Pr}[P_2Cp]M(CH_2Ph)Cl_2 \ + \ 0.5 \ ^{Pr}[P_2Cp]M(CH_2Ph)_3$$

11 $k_{-1} \uparrow\downarrow k_1$ **3**

$$^{Pr}[P_2Cp]M(CH_2Ph)_2Cl$$

14

(3.4)

$- \ PhMe \ \Big\downarrow \ \Delta$

$$^{Pr}[P_2Cp]M{=}CHPh(Cl)$$

16: M = Zr

17: M = Hf
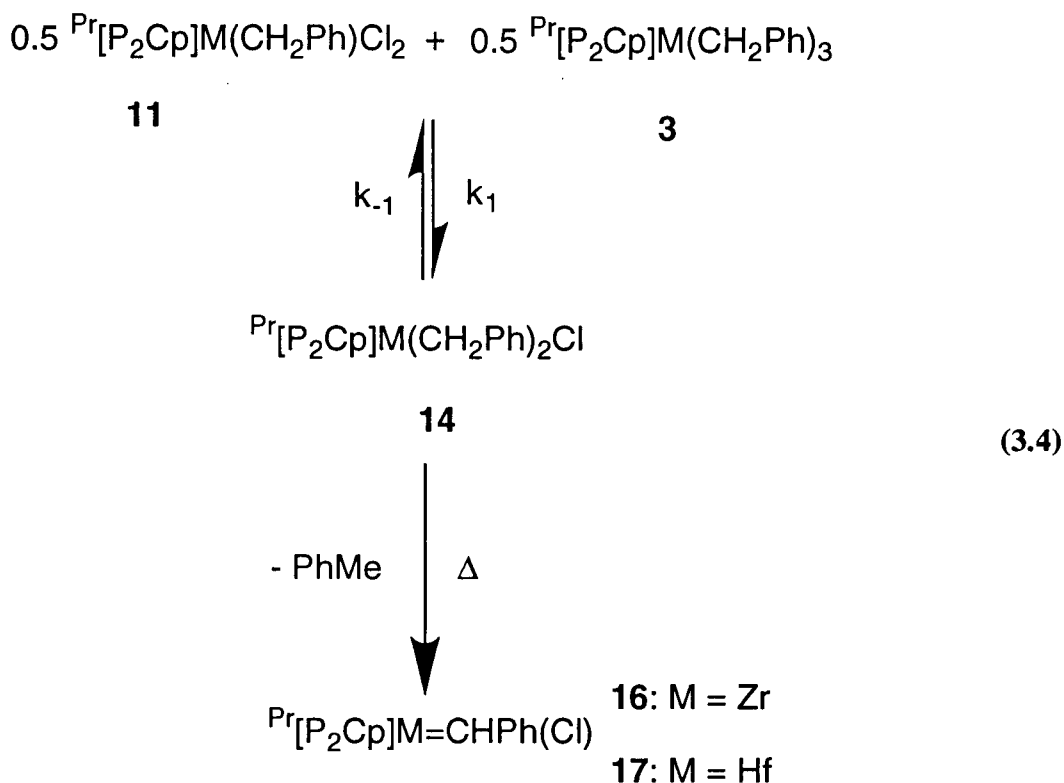
These are the first examples of Zr and Hf alkylidene complexes to be structurally characterized by X-ray diffraction.[3] As with trichlorides **1** and **2**, the molecular structures of **16** and **17** are nearly identical; the Hf example is depicted below (Figure 3.3), with bond distances and bond angles listed for both derivatives in Table 3.2 for comparison.
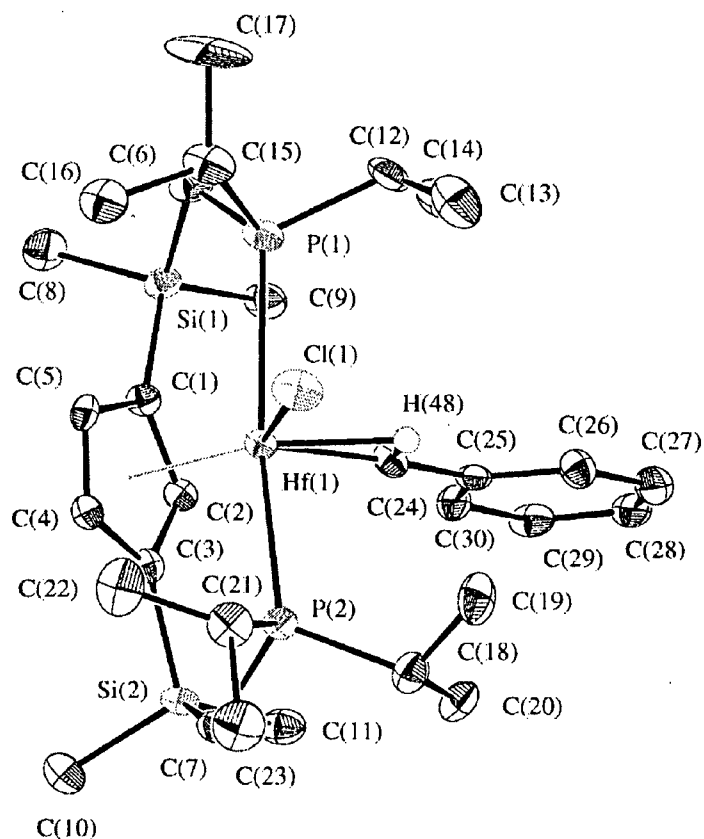
Figure 3.3 Molecular structure of $^{Pr}[P_2Cp]Hf=CHPh(Cl)$ (**17**); 33% probability thermal ellipsoids are shown. All hydrogen atoms other than the α-agostic hydrogen atom are omitted for clarity.

Table 3.2 Selected Bond Lengths (Å) and Bond Angles (") for $^{Pr}[P_2Cp]M=CHPh(Cl)$ (**16**: M = Zr, **17**: M = Hf). The numbering scheme is identical for each.

	16	17		16	17
M-Cl(1)	2.5418(13)	2.5068(11)	Cl(1)-M-P(1)	77.23(4)	75.90(4)
M-P(1)	2.8299(16)	2.8038(14)	Cl(1)-M-P(2)	76.35(4)	76.79(4)
M-P(2)	2.8425(17)	2.7986(13)	P(1)-M-P(2)	153.58(4)	152.68(4)
M-C(24)	2.024(4)	1.994(4)	Cl(1)-M-C(24)	110.11(11)	108.87(13)
C(24)-C(25)	1.456(5)	1.481(5)	M-C(24)-C(25)	169.2(3)	167.8(4)
M-Cp'	2.234	2.22	M-C(24)-H(48)	79.8(23)	71.6(17)
M···H(48)	2.07(4)	1.93(3)			

Once again, as in the trichloride derivatives, the bond lengths are slightly shorter for the corresponding Hf complex. The alkylidene unit in **17** is indicated by the very short Hf(1)-C(24) bond distance of 1.994(4) Å. For comparison, a typical Hf-C single bond averages approximately 2.3 Å.[4] The analogous Zr=C bond distance of 2.024(4) Å is also considerably short for that metal. A characteristic feature of unsaturated metal alkylidene complexes is an α-agostic C-H interaction to the metal;[5] in **16** and **17**, this interaction orients the alkylidene unit such that the phenyl ring points toward the cyclopentadienyl portion of the ancillary ligand. For both alkylidene derivatives the position of the α-hydrogen atom was located and refined (for **17**, this atom was refined with restraints). The short M···H contact is indicative of an α-agostic bond, which is reflected in an open M-C$_\alpha$-C$_\beta$ bond angle of nearly 170° for each complex. The phenyl ring is aligned perpendicular to the Cp ring, both to minimize steric interactions with the bulky isopropyl groups on the phosphines, and to maximize orbital overlap with the metal. The structure also has the alkylidene group pointed *syn* to the unique carbon atom of the cyclopentadienyl ring. The absence of an axial ligand in these alkylidenes (compensated somewhat by the agostic interaction in the direction of this open site) results in a modified geometry approaching that of a typical piano stool. Therefore the angular distortion of the equatorial bonds away from the Cp ring is increased in **17** relative to trichloride **2**, and is particularly evident with the *trans* chloride and alkylidene ligands, where the Cl-M-C bond angle is near 110°. The decrease in the coordination number also is responsible for shorter bond lengths in comparison to **2**.

The NMR spectroscopic data for the alkylidene complexes are consistent with the solid state structure. A singlet is seen in the ^{31}P{^{1}H} NMR spectrum (18.8 ppm for **16**, 23.4 ppm for **17**) for a pair of equivalent metal-bound phosphines. Diagnostic of the alkylidene unit are the downfield resonances for both the α-carbon atom (229.4 ppm in **16**, 210 ppm in **17**) and α-hydrogen atom (8.08 ppm in **16**, 7.33 ppm in **17**) in the respective ^{13}C and ^{1}H NMR spectra. The small $^{1}J_{CH}$ value of 87 Hz determined for the Zr complex indicates a weakening of this C-H

bond as a result of the agostic interaction. In a NOEDIFF ^{1}H NMR experiment, irradiation of the unique Cp proton was observed to enhance the signal of the ortho protons of the phenyl ring in the ^{1}H NMR spectrum, but did not affect the alkylidene proton resonance. In comparison, irradiation of the signal corresponding to the two equivalent Cp protons yielded no change (enhancement) in any of the peaks associated with the alkylidene group. These results signify both that the stereochemical preference observed in the solid state is maintained in solution, and that the agostic interaction is also unbroken, with no sign of rotation about the Zr=C bond axis.

3.3.2 Mechanistic studies of the formation of ^{Pr}[P$_2$Cp]Zr=CHPh(Cl) (16)

The unusual transformation of this mixture of benzyl species to produce alkylidene **16** prompted an investigation of the reaction mechanism employed, especially given the stark contrast between the paucity of Group 4 alkylidene complexes[6] in comparison to the number of examples known for Group 5.[5] This difference has been attributed to the mechanism by which these complexes are formed, whereby a sterically congested precursor decomposes *via* a thermally induced α-abstraction reaction involving two presumably *cis* alkyl ligands (Scheme 3.2).[7] For Group 5 this arrangement can be satisfactorily met either with bulky homoleptic alkyl complexes like Ta(CH$_2$CMe$_3$)$_5$[1] or similar derivatives such as Cp*TaCl$_2$(CH$_2$CMe$_3$)$_2$.[8] Conversely, the analogous group 4 complexes contain at least one less alkyl ligand and hence are at a considerable disadvantage to achieve a similarly crowded coordination sphere.[9] Therefore, all group 4 alkylidene complexes reported thus far have required the addition of either inter- or intramolecular phosphine donors, and of these examples,[10] only a handful of Ti derivatives have been isolated as thermally stable compounds. [11,12] It is reasonable to suggest that the presence of two intramolecular phosphine donors appended to a bulky Cp ligand is a major factor in the formation and thermal stability of both **16** and **17**.

$$\text{Ta(CH}_2\text{CMe}_3)_5 \longrightarrow \left[\begin{array}{c} \text{Np}_3\text{Ta}\text{-----}\text{C}\,\text{H}_2\text{CMe}_3 \\[2pt] | \quad\quad | \\[2pt] \text{Me}_3\text{C}\text{--}\text{C}\text{-----}\text{H} \\[2pt] | \\ \text{H} \end{array} \right]^{\ddagger}$$

$$-\text{CMe}_4 \quad \Big\downarrow \quad \Delta$$

$$\text{Ta=CHCMe}_3(\text{CH}_2\text{CMe}_3)_3$$
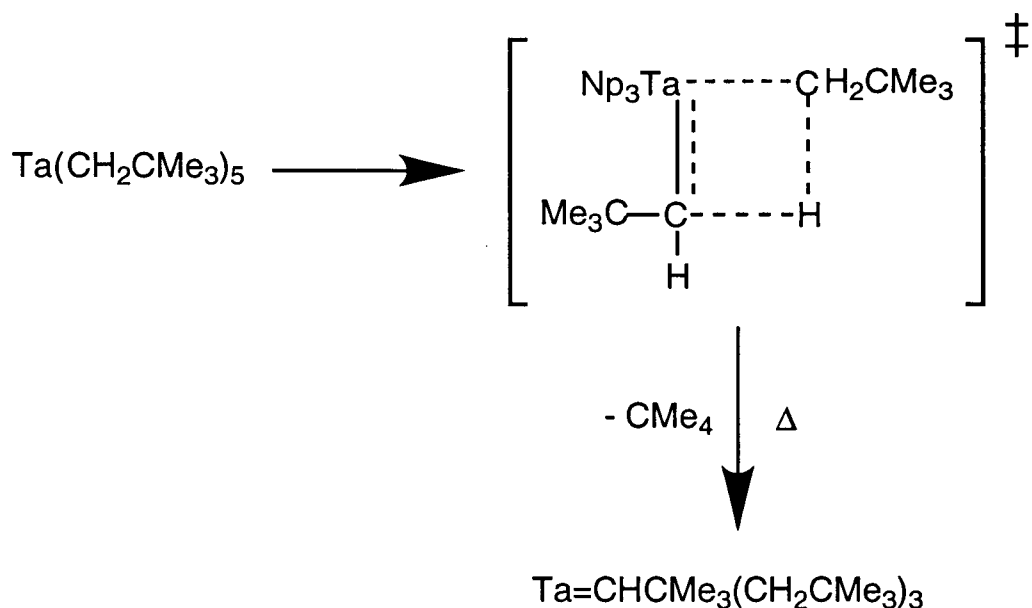
Scheme 3.2   Mechanism of α-hydrogen abstraction to yield an alkylidene complex.

The results of the mechanistic study into the Zr system that forms **16** are outlined here. Of importance, neither tribenzyl **3** nor monobenzyl **11** are independently reactive under the conditions that generate alkylidene **16**. The dibenzyl complex **14** is therefore a likely precursor to undergo α-abstraction and give **16** and one equivalent of toluene, as shown in Scheme 3.3. Accordingly, the continued depletion of **14** in forming **16** would perturb the pre-equilibrium, thus prompting the conversion of additional tribenzyl **3** and monobenzyl **11** to replenish **14**, eventually resulting in the observed high yield production of **16**. Added support that **14** is the reactive species is provided by heating reaction mixtures prepared from unequal proportions of **3** and **11**. In each case the formation of **16** ceases when the precursor **14** can no longer be replenished, which occurs once the limiting component (either **3** or **11**) as a source for **14** has been consumed.

$$0.5 \; {}^{Pr}[P_2Cp]ZrCl_2(CH_2Ph) \quad + \quad 0.5 \; {}^{Pr}[P_2Cp]Zr(CH_2Ph)_3$$

11 k_{-1} $\Big\updownarrow$ k_1 **3**

$${}^{Pr}[P_2Cp]ZrCl_3 \xrightarrow{\text{2 KCH}_2\text{Ph}} {}^{Pr}[P_2Cp]ZrCl(CH_2Ph)_2 \quad \textbf{14}$$

1

k_2 Δ

fast

− PhMe

$${}^{Pr}[P_2Cp]Zr=CHPh(Cl)$$

16

$$\left[\begin{array}{c} \text{Me}_2\text{Si} \quad \text{Me}_2\text{Si} \\ \text{P} \rightarrow \text{Zr} \leftarrow \text{P} \\ \text{Cl} \\ \text{PhHC} \quad \text{CH}_2\text{Ph} \\ \text{H} \end{array} \right]^{\ddagger}$$
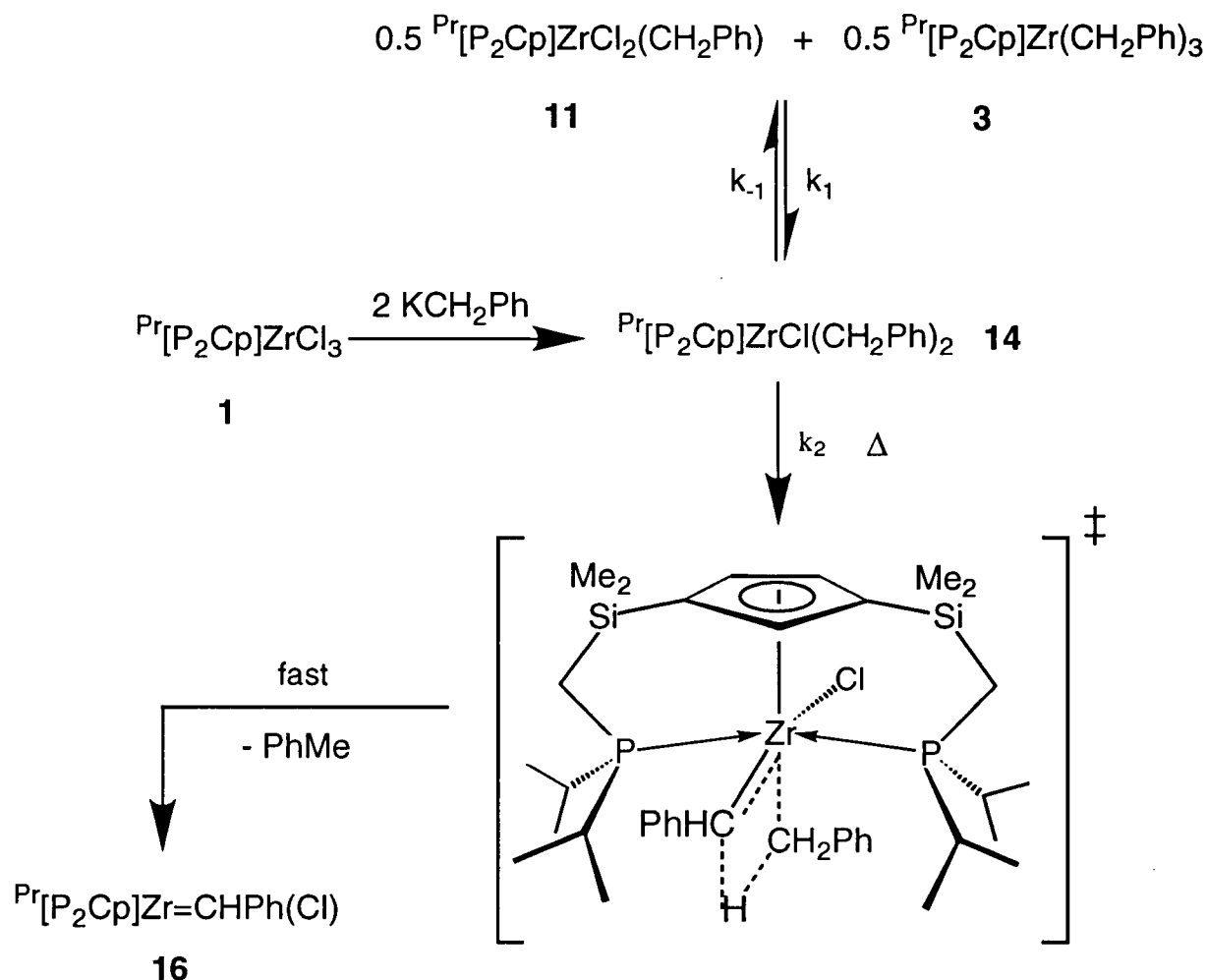
Scheme 3.3   Proposed reaction scheme for the formation of **16** from the mixture of

benzyl species **3**, **11** and **14**.

A kinetic analysis of the thermal decomposition of this reaction mixture was conducted by monitoring the $^{31}P\{^1H\}$ NMR spectra for separate reactions performed at 70, 80, 85 and 95 °C, respectively. A similar study was also conducted at 70 °C on the perdeuterated analogue $[P_2Cp]ZrCl(CD_2C_6D_5)_2$ **(14-d₇)** to examine a possible kinetic isotope effect. In all instances the decline in **[14]** followed a pattern as shown in Figure 3.4. The non-linear fit of the plot of ln[**14**] versus time illustrates a departure from first-order kinetics. The pre-equilibrium in this composite mechanism is likely responsible for these complicated results. The steep initial

decrease in the concentration of **14** corresponds more closely to the actual first-order α-abstraction reaction rate, but curvature in the ln plot in Figure 3.4 arises due to a steady decrease in the observed rate (k_{obs}) as the continued lowering in the concentrations of the equilibrium species makes it more difficult to replenish **14** from bimolecular collisions of **3** and **11**.

To evaluate the complicating factor of the pre-equilibrium, the results were simulated (Chemical Kinetics Simulator®) from input of the initial concentrations and the kinetic parameters k_1, k_{-1} and k_{-2}. Knowledge of the approximate equilibrium constant K gives the ratio k_1/k_{-1}, with limits for these values set ($1 < k < 10^{-3}$ s^{-1}) by the spectroscopic data as outlined in the discussion of this equilibrium in the previous section. A more precise estimate of these parameters, as well as the rate constant k_2 for the irreversible α-abstraction step, could be made by iteration of the simulation results to give the best agreement with the experimentally determined changes in [**3**], [**14**] and [**16**] as a function of time. The simulations show that including the pre-equilibrium in the analysis reproduces the experimental results depicted in Figure 3.4.
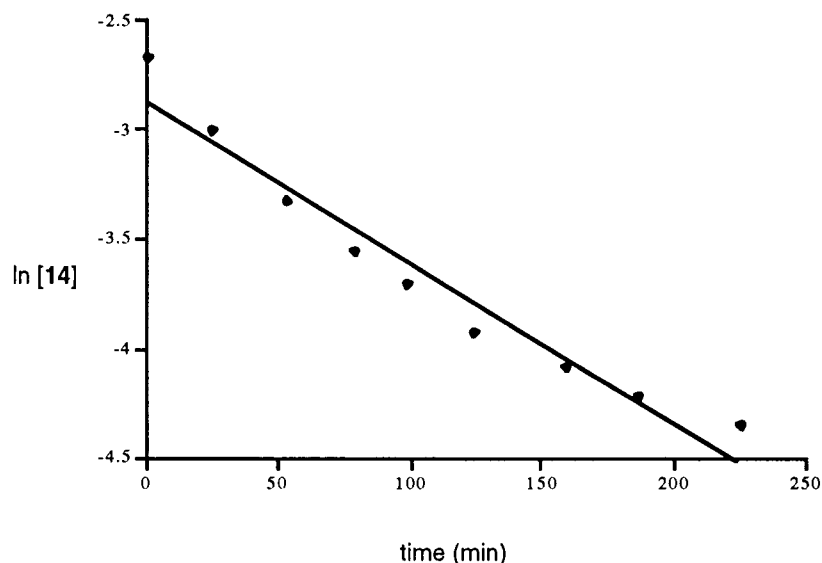
Figure 3.4   Non-linear fit to the first-order decomposition of ^{Pr}[P$_2$Cp]ZrCl(CH$_2$Ph)$_2$ (**14**).

Table 3.3   Estimated rate constants for the first-order α-abstraction of

$^{Pr}[P_2Cp]ZrCl(CH_2Ph)_2$ (**14**).

T (K)	$k_2 \times 10^{-5}$ (s^{-1})
343(1)	3.7(3)
353(1)	4.8(3)
363(1)	7.7(4)
373(1)	9.7(5)
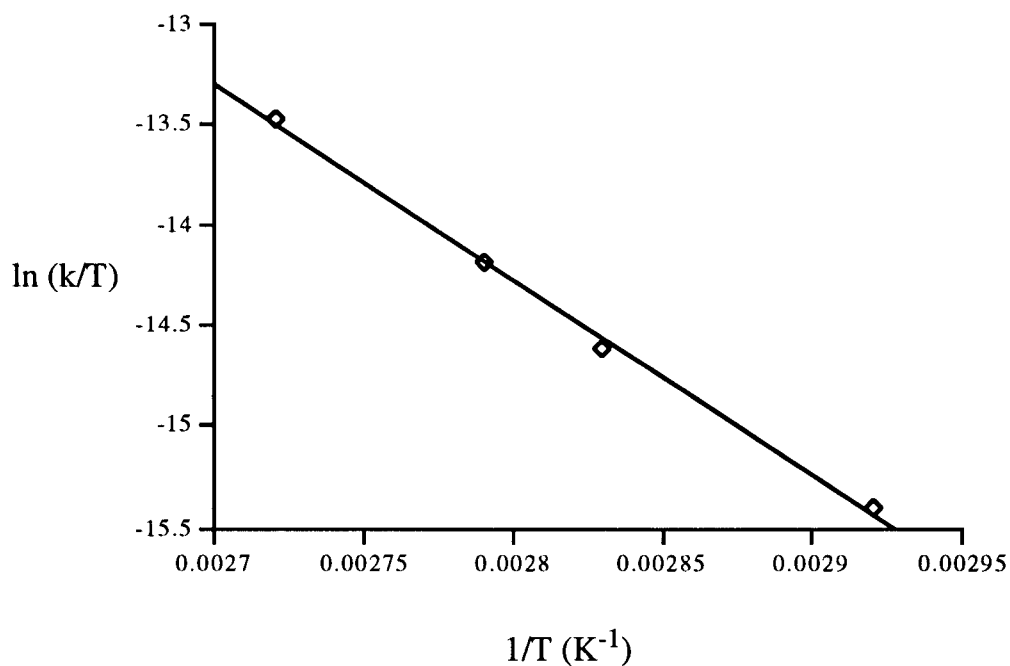
Figure 3.5   Eyring plot of the first-order portion of the decomposition of

$^{Pr}[P_2Cp]ZrCl(CH_2Ph)_2$ (**14**).

The rate constants (k_2) obtained for each temperature from the simulated data are shown in Table 3.3; a kinetic isotope effect of 3.0(0.5) was observed at 70 °C for the perdeuterated

95

species, in support of rate-determining C-H bond activation[7] in a concerted four-centred transition state as shown in Scheme 3.2. From the Eyring plot in Figure 3.5 the activation parameters $\Delta H^{\ddagger} = 19(1)$ kcal mol^{-1} and $\Delta S^{\ddagger} = -22(5)$ cal mol^{-1} K^{-1} were obtained. The value for $\Delta H^{\ddagger}$ is in accord with kinetic studies conducted on other systems involving alkylidene formation and related C-H activation processes.[13-15] In those studies $\Delta H^{\ddagger}$ ranges between 20 to 30 kcal mol^{-1}. However, the experimentally determined value of $\Delta S^{\ddagger}$ for **14** is rather large in comparison to these other systems (typically between 0 and -10 cal mol^{-1} K^{-1}), although the decomposition of Ti(CH$_2$CMe$_3$)$_4$ via an alkylidene intermediate has a similar large negative $\Delta S^{\ddagger}$ = -16 cal mol^{-1} K^{-1}.[9] An in-depth analysis of the kinetic results for **14** will be given in conjunction with the analogous results for the α-abstraction of ^{Pr}[P$_2$Cp]ZrCl(CH$_2$SiMe$_3$)$_2$ (**19b**) to give alkylidene ^{Pr}[P$_2$Cp]Zr=CHSiMe$_3$(Cl) (**18b**).

3.3.3 Other alkylidene analogues ^{Pr}[P$_2$Cp]Zr=CHEMe$_3$(Cl) (E = C, Si)

In view of the success in synthesizing and isolating both a Zr and a Hf example of a benzylidene complex, we were interested in testing both the generality of this reaction mechanism and the versatility of the P$_2$Cp ligand in stabilizing other Zr alkylidene complexes. Two examples of bulky alkyl groups with α-hydrogens that have been commonly chosen for the synthesis of early transition-metal alkylidene complexes are the neopentyl (CH$_2$CMe$_3$)[5] and neosilyl (CH$_2$SiMe$_3$) ligands.[7] Treating **1** with 2 equivalents of LiCH$_2$EMe$_3$ (E = C, Si) in toluene at -78 °C yields a bright yellow oil after workup. Thermolysis of this material in toluene at 95 °C generates the corresponding alkylidene complex ^{Pr}[P$_2$Cp]Zr=CHEMe$_3$(Cl) (**18a**: E = C, **18b**: E = Si) (equation 3.5). The formation of **18a** requires 6 days at 95°C, while the analogous reaction to produce **18b** is complete within 3 days under the same conditions.

$$\text{Pr}[P_2Cp]ZrCl_3 \xrightarrow[\text{- 2 LiCl}]{2\ LiCH_2EMe_3} \text{bright yellow oil}$$

1

$$\text{- EMe}_4 \downarrow \Delta$$

$$\text{Pr}[P_2Cp]Zr{=}CHEMe_3(Cl)$$

(3.5)

18a E = C

18b E = Si
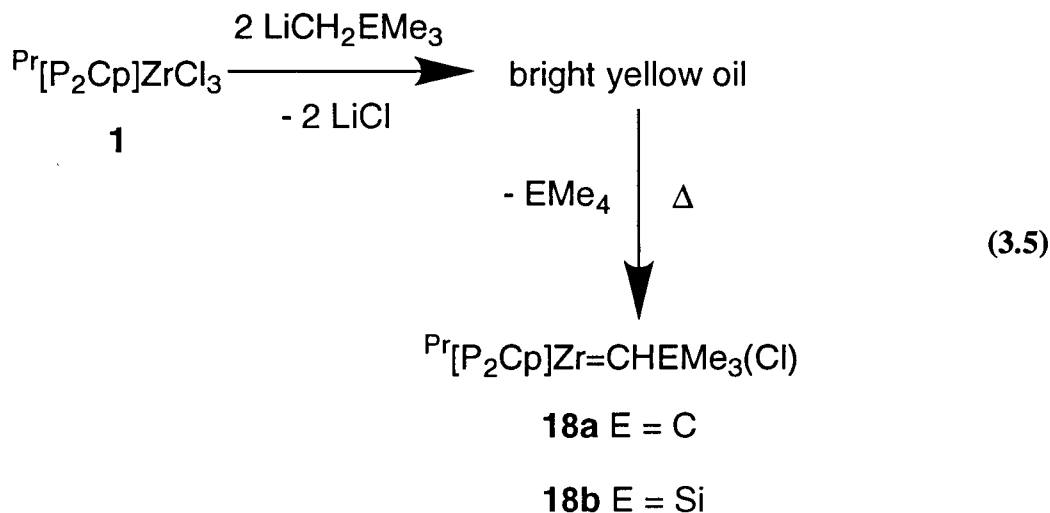
A green oil is obtained for **18a**, which is accompanied by inseparable side-products (approximately 20% by NMR spectroscopy) accumulated over the prolonged duration of the thermolysis. This complex is identified by assignable resonances in the ^1H, $^{13}C\{^1H\}$, and $^{31}P\{^1H\}$ NMR spectra; of note are a singlet observed at 8.56 ppm in the ^1H NMR spectrum and a triplet at 209 ppm in the $^{13}C\{^1H\}$ NMR spectrum, for the alkylidene proton (Zr=C*H*CMe₃) and carbon, respectively. In contrast, **18b** can be isolated as thermally stable, air- and moisture-sensitive yellow crystals in very good yield from cold hexanes. Spectroscopic data for **18b** reveal a singlet in the ^1H NMR spectrum at 8.99 ppm for the alkylidene proton (Zr=C*H*SiMe₃) and a triplet at 225 ppm in the $^{13}C\{^1H\}$ NMR spectrum for the alkylidene carbon (Zr=C*H*SiMe₃), arising from $^2J_{PC}$ coupling to two equivalent phosphines.

An X-ray structure determination of **18b** was undertaken, and the molecular structure is shown in Figure 3.6, with selected bond lengths and bond angles given in Table 3.4. The very short Zr-C bond distance of 2.015(9) Å is similar to that of 2.024(4) Å for Zr benzylidene **16**. As also observed for **16**, the alkylidene fragment in **18b** is oriented *syn* to the unique cyclopentadienyl carbon, with the α-hydrogen atom directed below the metal centre to form the same type of agostic C-H interaction. This hydrogen was located and refined, and the Zr···H

97

distance of 2.28(8) Å, together with the distorted Zr-C-Si angle of 164.3(6)°, is characteristic of an α-agostic C-H bond. All other bond lengths and angles are similar to those in the corresponding alkylidene **16**.
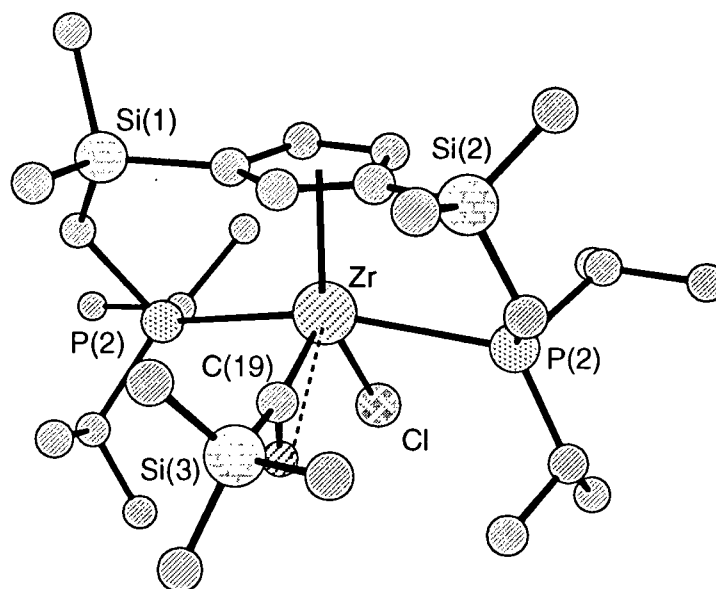
Figure 3.6   A Chem 3D® view of the molecular structure of **18b**. All hydrogen atoms except the α-agostic hydrogen are omitted for clarity.

Table 3.4   Selected Bond Lengths (Å) and Bond Angles (°) for $^{Pr}[P_2Cp]Zr=CHSiMe_3(Cl)$ (**18b**).

Zr-Cl	2.508(3)	P(1)-Zr-P(2)	154.91(8)
Zr-P(1)	2.838(3)	Cl-Zr-C(19)	108.0(3)
Zr-P(2)	2.820(3)	Cl-Zr-P(1)	76.48(8)
Zr-C(19)	2.015(9)	Cl-Zr-P(2)	76.44(9)
Zr-Cp'	2.2557(13)	Zr-C(19)-Si(3)	164.3(6)
Zr···H(19)	2.28(8)	Zr-C(19)-H(19)	89(5)
Si(3)-C(19)	1.848(9)	Cp'-Zr-Cl	141.23(8)
C(19)-H(19)	1.10(8)		

3.3.4 Mechanistic studies of the formation of $^{Pr}[P_2Cp]Zr=CHEMe_3(Cl)$ (E = C, Si)

An examination of the yellow oil obtained from the reaction of **1** with 2 equivalents of $LiCH_2EMe_3$ prior to the thermolysis reveals the presence of trialkyl $^{Pr}[P_2Cp]Zr(CH_2EMe_3)_3$ (**5a**: E = C, **5b**: E = Si), monoalkyl $^{Pr}[P_2Cp]ZrCl_2(CH_2EMe_3)$ (**7a**: E = C, **7b**: E = Si), and another species which is observed as a singlet in the ^{31}P NMR spectrum and identified from the integration of peaks in the ^1H NMR spectrum as the dialkyl derivative $[P_2Cp]ZrCl(CH_2EMe_3)_2$ (**19a**: E = C, **19b**: E = Si). It seems that a similar equilibrium (equation 3.6) is established between all three alkyl species for both the neopentyl and neosilyl systems as has been observed for the benzyl derivative, since combining together separate samples of the trialkyl and monoalkyl species again generates the dialkyl complex to produce a similar mixture of all three alkyl species.

$$^{Pr}[P_2Cp]ZrCl_2(CH_2EMe_3) \ + \ ^{Pr}[P_2Cp]Zr(CH_2EMe_3)_3$$

| **7a** E = C | **5a** E = C |
| **7b** E = Si | **5b** E = Si |

$$k_{-1} \quad\Big\updownarrow\quad k_1 \qquad\qquad (3.6)$$

$$^{Pr}[P_2Cp]ZrCl(CH_2EMe_3)_2$$

19a E = C
19b E = Si
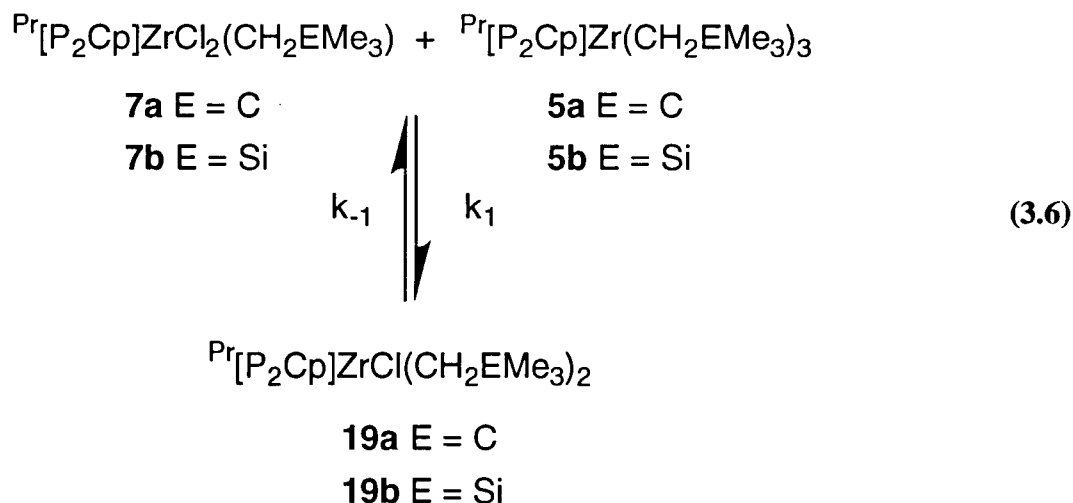
Detailed analyses of these equilibria were precluded by the overlap of peaks in the ^1H and $^{31}P\{^1H\}$ NMR spectra for various species at separate temperatures. However, it could be

ascertained that below the temperature at which one observes alkylidene formation, the equilibrium increasingly favours ligand distribution of the dialkyl species **19** as the temperature is raised (i.e., the value of K decreases with an increase in temperature), in contrast to the observations for **14** in the equilibrium of equation 3.3.

It is evident that the mechanistic details for the formation of the neopentyl and neosilyl alkylidene complexes **18** are similar to those previously outlined for benzylidene **13**. For example, heating either the trialkyl **5** or monoalkyl **7** derivatives independently does not generate an alkylidene complex, and the production of alkylidene from the thermolysis of the equilibrium mixture in equation 3.5 ceases when the supply of dialkyl precursor **19** has been exhausted. Once again this points to a mechanism analogous to that in Scheme 3.2, where the dialkyl complex **19** is the thermally labile species that leads directly to the alkylidene product in a first order mechanism.

Experimental complications associated with the long reaction time and the formation of interfering impurities precluded a kinetic study of the neopentyl system. However, an analysis of the reaction kinetics for the thermal decomposition of neosilyl **19b** was conducted by ^{31}P NMR spectroscopy, for reactions performed at 80, 95, 110 and 125 °C. In all instances the same pattern for the decrease in [**19b**] over time was observed as has been noted for benzyl **14** in Figure 3.4. Therefore, the results for **19b** were simulated by the same iterative procedure followed for **14**, from which the first-order rate constant (k_2) was obtained for each temperature (Table 3.5). The corresponding Eyring plot is shown in Figure 3.7, from which the activation parameters $\Delta H^{\ddagger}$ = 6.2 kcal mol^{-1} and $\Delta S^{\ddagger}$ = -60 cal mol^{-1} K^{-1} were obtained;these values are significantly different to the parameters obtained for **14**.

Table 3.5 Rate constants for the first-order portion of the decomposition of

$[P_2Cp]ZrCl(CH_2SiMe_3)_2$ (**19b**)

T (K)	$k_2 \times 10^{-5}$ (s^{-1})
353(1)	3.7(3)
368(1)	4.8(3)
383(1)	7.7(4)
398(1)	9.7(5)
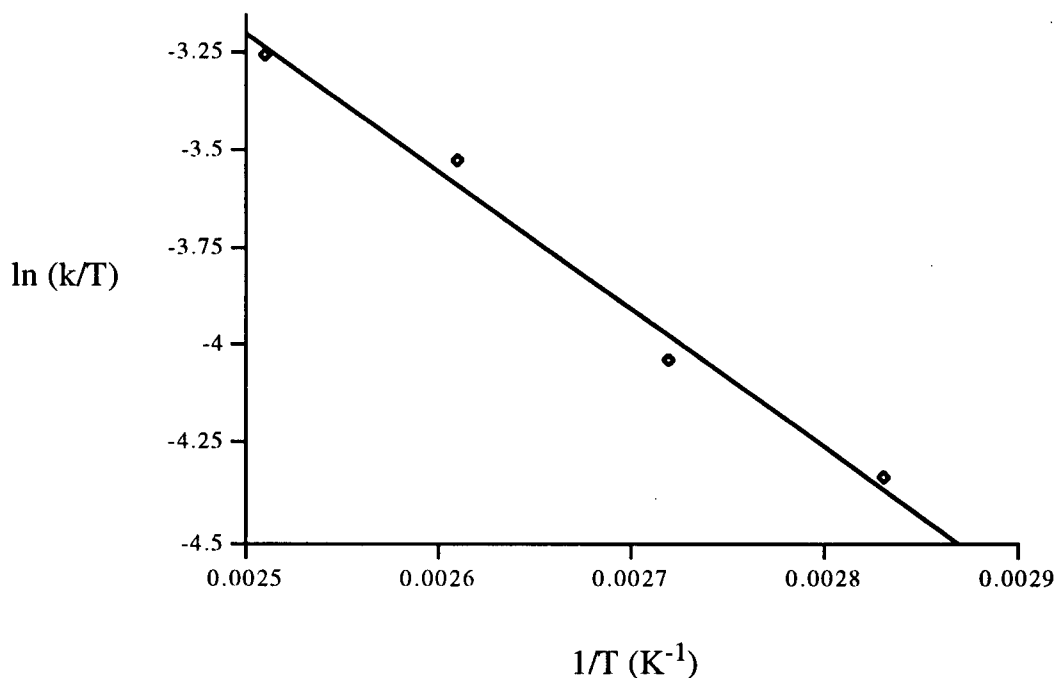
Figure 3.7 Eyring plot of the first-order decomposition of **19b**.

The trend reported in the literature for the relative rates of alkylidene complex formation follows the order neopentyl > neosilyl > benzyl, which reflects faster rate-determining α-abstraction for complexes bound by alkyl ligands that can provide greater steric congestion at the

references begin on page 141

metal centre. For example, for the first-order decomposition of $Ta(CH_2R)_5$ (R = Ph, $SiMe_3$, CMe_3), the rate constants follow the order k = 4.3 x 10^{-5} (at 313 K) < 3.5 x 10^{-4} (311 K) < too fast to monitor, for R = Ph,[16] $SiMe_3$,[7] and CMe_3,[7] respectively. Our results indicate a *reversal* of this trend for the complexes studied here. The neopentyl system that produces alkylidene **18a** was found to be too slow to study, and a comparison of the first order rate constants in Table 3.3 and Table 3.4 for the dialkyl species studied reveals the slower thermal reactivity of neosilyl **19b** versus benzyl **14**. This surprising observation may be partially related to the unusual pre-equilibrium step associated with the postulated mechanism (Scheme 3.2), where ligand distribution of the dialkyl species is favoured at higher temperatures for the bulkier derivatives, in competition with the irreversible step leading to alkylidene formation. However, the effect of the pre-equilibrium is evidently secondary in comparison to the activation parameters, particularly $\Delta S^{\ddagger}$, associated with the rate determining α-abstraction step. As mentioned above, both near-zero and negative values (0 to -10 cal mol^{-1} K^{-1}) have been typically observed for the majority of C-H bond activation processes that have been studied. The results from this work show considerable departure from these values, especially with the large negative $\Delta S^{\ddagger}$ of -62 cal mol^{-1} K^{-1} for **19b**, which has been rarely seen for a first-order process. To account for this remarkable difference it is useful to examine the proposed transition state structure ($\ddagger$) in this reaction as shown below:
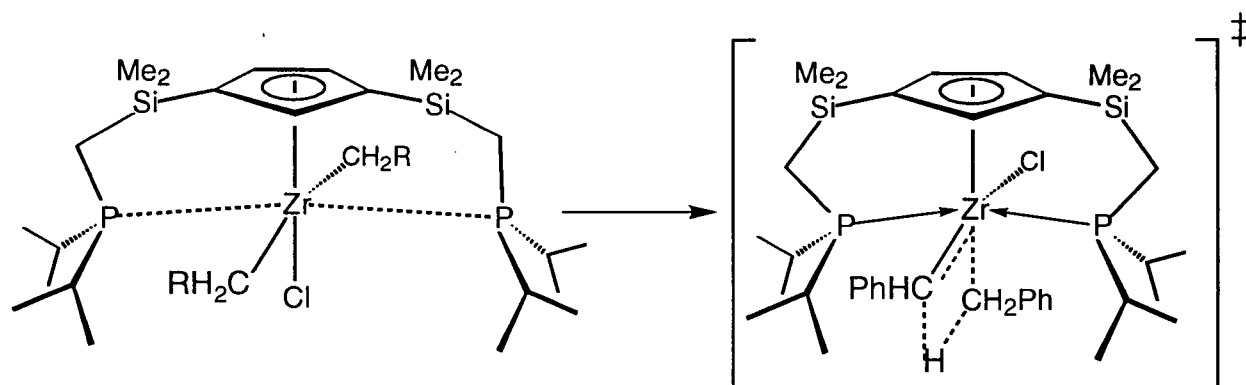
There are two features that indicate a significantly more ordered structure in the transition state in comparison to the ground state structure of the dialkyl derivatives, which could generate a large negative $\Delta S^{\ddagger}$ term. The first is the coordination of both bulky side-arm phosphines, considered to help lower the activation energy by increasing steric saturation at the metal centre to induce α-abstraction as a means of relieving the steric pressure. The second feature is the necessity for the two alkyl ligands to attain a *cis* configuration in order to permit the concerted abstraction step to proceed *via* the four-centred transition state. However, if the phosphines are coordinated then a mutually *trans* arrangement of the bulky alkyl ligands is perhaps sterically favoured, as supported by structural evidence from $^{Me}[P_2Cp]Cl(CH_2Ph)_2$ (**27**), a dibenzyl derivative with methyl groups attached to the phosphines, which is discussed separately in the next chapter. The steric difficulties that must be surmounted to reach the transition state are more pronounced for the bulkier dialkyl species **19b**. For example, the singlet in the $^{31}P\{^1H\}$ NMR spectrum for **19b** at -4.5 ppm is indicative of phosphine donors that are at best only weakly interacting with the metal. Overall, these factors could account for a much larger negative value of $\Delta S^{\ddagger}$ for the bulkier alkyl derivatives and hence the observed reversal of the reactivity trend, which arises from entropic factors. These factors also help to explain the otherwise contradictory observation that the bulky trialkyl derivatives are thermally unreactive, as these complexes are paradoxically less sterically hindered in comparison to the dialkyl analogues because the bulky phosphines are unable to coordinate in the trialkyl species.

3.3.7 Crossover experiments

Crossover experiments were conducted as a further test for the general mechanism proposed for the alkylidene reaction, and as an attempt to compare competitive α-abstraction rates for various alkyl groups. Accordingly, solutions of monobenzyl **11** and tris(neosilyl) **7b** were combined as shown in Scheme 3.3 in an attempt to generate the mixed alkyl species (**B**).

$$^{Pr}[P_2Cp]ZrCl_2(CH_2Ph) + {}^{Pr}[P_2Cp]Zr(CH_2SiMe_3)_3$$

11   **7b**

$$^{Pr}[P_2Cp]ZrCl(CH_2Ph)(CH_2SiMe_3) + {}^{Pr}[P_2Cp]ZrCl\ (CH_2SiMe_3)_2$$

- SiMe$_4$ **B**   - SiMe$_4$ **19b**

$$^{Pr}[P_2Cp]Zr{=}CHPh(Cl)$$

16

- PhMe

$$^{Pr}[P_2Cp]Zr{=}CHSiMe_3(Cl)$$

18b
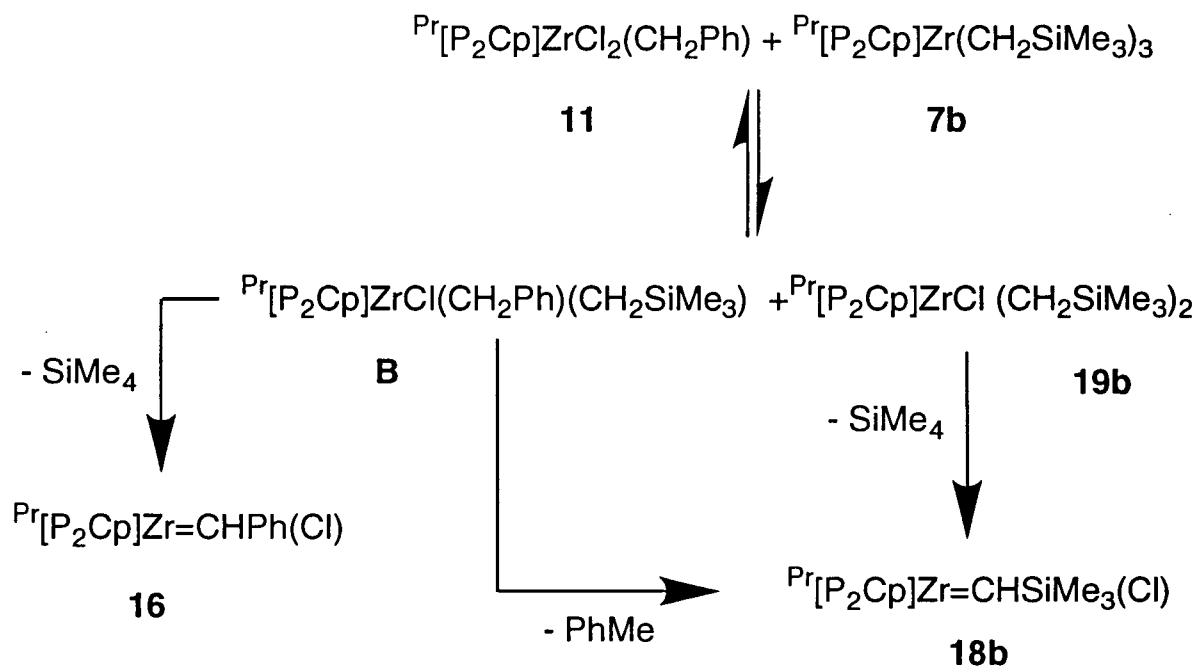
Scheme 3.3   Alkylidene products arising from crossover experiments.

Additional recombination products were also formed in small amounts. Thermolysis of such a mixture offers two competing α-abstraction pathways for **B**, offering a route to two different alkylidene products. Indeed, both products were observed, providing additional support for the ligand redistribution mechanism in the pre-equilibrium step detailed above in Scheme 3.2.

3.4.   Reactivity of $^{Pr}[P_2Cp]Zr{=}CHR(Cl)$ (R = Ph, SiMe$_3$)

Early metal alkylidene complexes continue to attract considerable attention by virtue of the diverse reactivity arising from the metal-carbon multiple bond.[4] These species have been utilized as catalysts in a number of transformations involving alkenes[17-20] and alkynes,[21] and in stoichiometric Wittig-like olefination reactions with organic carbonyl functionalities.[22-24] Probably the most notable catalytic reaction is the olefin metathesis process[10] for which the ring

opening version has had a huge impact in polymer chemistry,[25] while the ring closing version is an exciting new synthetic method in organic synthesis.[26] As the alkylidene complexes discussed in the previous sections are to our knowledge the only stable zirconium and hafnium derivatives, an investigation of the their reactivity patterns provides a unique opportunity to examine the results in comparison to the reactivity trends that have been noted for Group 5 and 6 alkylidene complexes. Again, the role of the hemilabile phosphines in moderating the reactivity of these complexes is shown in their capacity to provide an open coordination site for reactivity to occur. Importantly, this hemilabile coordination of the phosphines moderates and controls the reactivity (i.e., controlled reactivity).

3.4.1 Reactivity of ^{Pr}[P$_2$Cp]Zr=CHR(Cl) with alkenes (R = Ph, SiMe$_3$)

An orange toluene solution of ^{Pr}[P$_2$Cp]Zr=CHR(Cl) (**16**: R = Ph, **18b**: R = SiMe$_3$) reacts slowly (12 h for **16**, 8 h for **18b**) with ethylene under ambient conditions to generate a dark red solution consisting of a 9:1 ratio of the two isomers of the ethylene complex ^{Pr}[P$_2$Cp]Zr(η^2-CH$_2$=CH$_2$)Cl (**20**) (equation 3.7). Each isomer of **20** displays a singlet in the ^{31}P{^{1}H} NMR spectrum and corresponding resonances in the ^{1}H NMR spectrum, consistent with a structure in which the orientation of the ethylene unit is directed either *syn* or *anti* with respect to the unique Cp carbon of the ancillary ligand.

The organic by-products that accompany the formation of **20** were detected by ^{1}H NMR spectroscopy and identified by GC-MS. For example, from benzylidene **16** the major product (approx. 70 %) is the terminal alkene PhCH$_2$CH=CH$_2$, while the *cis* and *trans* isomers of the internal alkene PhCH=CHCH$_3$ are obtained in approximately equal quantity. Similar results for **18b** are observed.

16 R = Ph
18b R = SiMe₃

$H_2C\!=\!\!=\!\!CH_2$

syn-**20** + *anti*-**20**

(3.7)
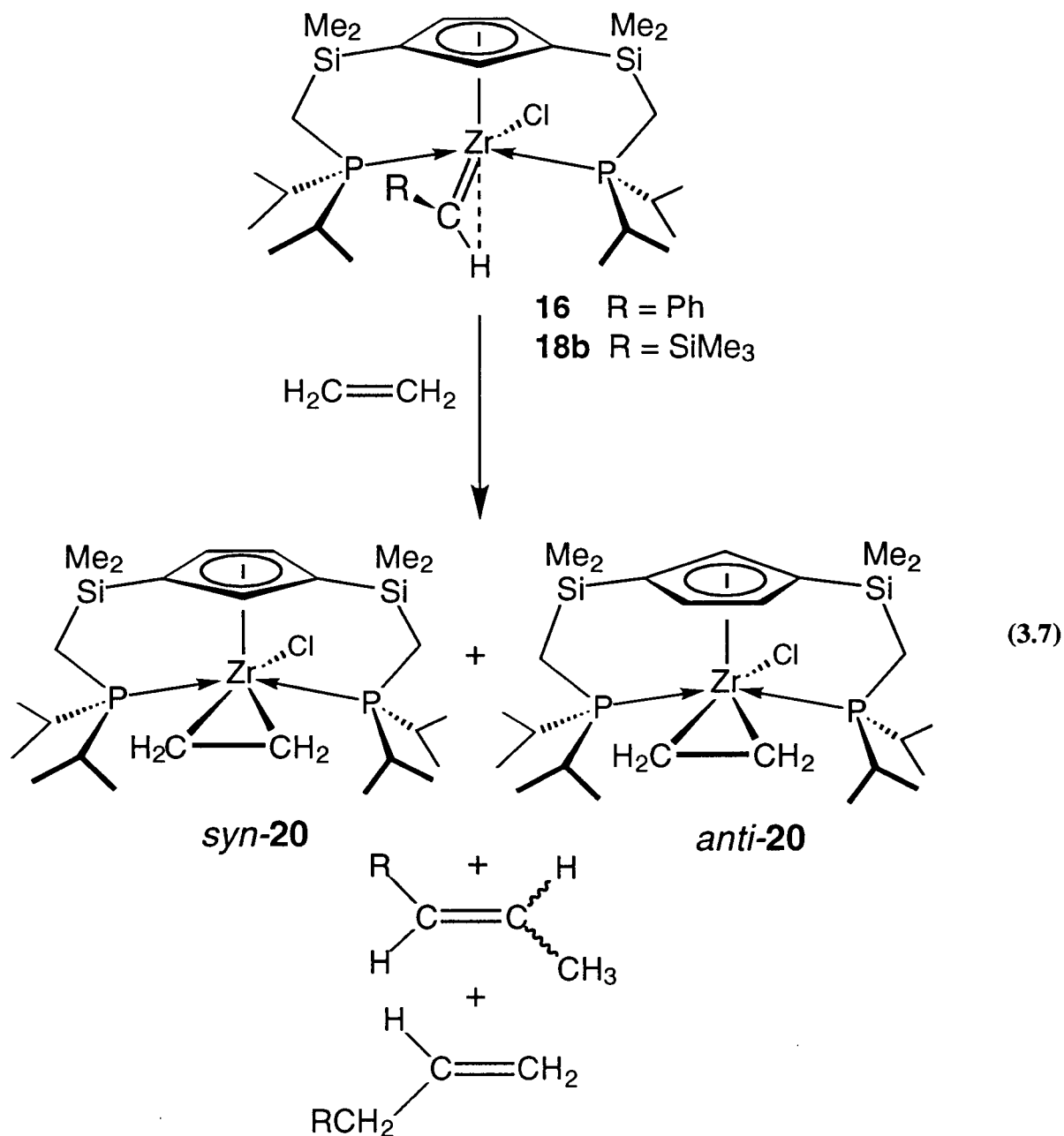
In the $^{13}C\{^1H\}$ NMR spectrum of **20** (only peaks due to the major *syn* isomer are observed), the ethylene carbon resonances are located upfield at 35 ppm with a $^1J_{CH}$ value of 142 Hz, consistent with hybridization intermediate between sp² and sp³.[27] The ethylene protons give rise to a complex multiplet centred near 1.0 ppm in the ^1H NMR spectrum, originating from an AA'BB'XX' spin system due to additional $^3J_{PH}$ coupling from the side-arm phosphines. This

coupling pattern remains unchanged even at higher temperatures, indicating that the ethylene unit is firmly bound with no evidence for rotation about the metal-ethylene bond axis on the NMR time scale. A C=C stretch in the IR spectrum for the coordinated ethylene unit was also not observed. These spectroscopic data are similar to those of other early-metal ethylene complexes[13,28-31] and are consistent with a formulation of **20** as a Zr(IV) zirconacyclopropane complex rather than as a Zr(II) adduct. However, aspects of the solid state structure and the reactivity of this species, to be outlined later, suggest a fair degree of Zr(II) character still extant in this molecule.

Attempts to determine the major isomer in solution by ^{1}H NMR spectroscopy by irradiating the Cp proton resonances to examine a possible nuclear Overhauser enhancement (nOe) on the protons of the coordinated ethylene fragment were inconclusive. However, as will be discussed in the following chapter, an analogous ethylene complex can be prepared by an independent route, ^{Me}[P2Cp]Zr(η^2-CH2=CH2)Br (**32**), in which the isopropyl substituents on the phosphines are replaced by methyl groups. Only the *syn* isomer is observed in this species, and by extrapolating the ^{1}H NMR spectrum of this derivative to **20**, especially with excellent correlation seen in the sensitive Cp region, it is evident that the major isomer in solution corresponds to *syn*-**20**.

Further insight into the Zr-ethylene bonding interaction was furnished by a crystal structure determination of *syn*-**20**. The molecular structure is shown in Figure 3.9, with relevant bond distances and bond angles given in Table 3.6. The C(19)-C(20) bond distance of 1.433(17) Å is lengthened relative to free ethylene (1.337 Å)[32] and is comparable (albeit somewhat shorter) to that of the only other monomeric Zr(II) ethylene complex that has been structurally characterized, Cp2Zr(η^2-CH2=CH2)(PMe3),[33] which has a corresponding C-C bond length of 1.486(8) Å for the ethylene unit. This distance range is indicative of significant back-bonding from the metal and supports the metallacyclopropane bonding depiction for **20**. Also consistent with this formalism are the Zr-C bond lengths (average 2.319(11) Å) in **20**, which are

considerably shorter than the Zr-C distance of 2.68(2) in a cationic Zr(IV) olefin complex in which d-π^* back-bonding is necessarily absent.[34] The orientation of the ethylene unit parallel to the Cp ring not only reduces steric interactions with the Cp ring, but also situates the π^*-orbital to overlap favourably with the metal d_{xy} orbital. Investigations into bonding interactions in electron-rich complexes with piano-stool geometries, of which this formally Zr(II) species is a suitable example, suggest that it is the metal d_{xy} orbital that offers the best donation to a π-acceptor ligand.[35,36] These studies also indicate that π-donor ligands (such as a chloride) are better located further away from the Cp group, which is supported by the wider Cp'-Zr-Cl angle in **20** (152°) as found in alkylidene **18b** (141°).
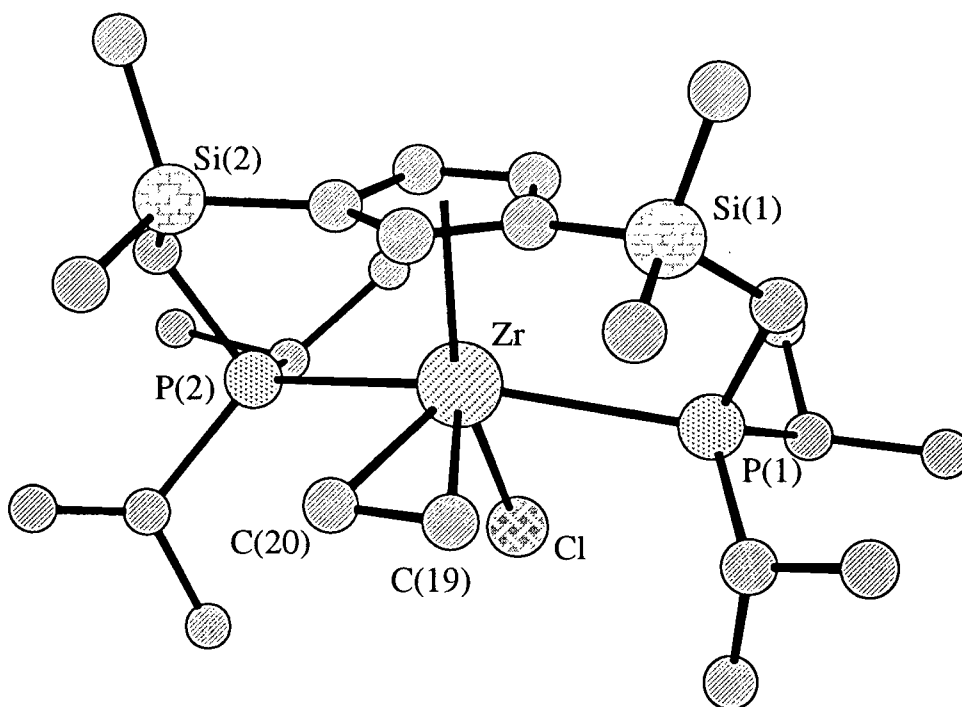
Figure 3.8   A Chem 3D® view of the molecular structure of $^{Pr}[P_2Cp]Zr(\eta^2$-$CH_2=CH_2)Cl$ **(20)**. Hydrogen atoms are omitted for clarity.

Table 3.6   Selected Bond Lengths (Å) and Bond Angles (°) for $^{Pr}[P_2Cp]Zr(\eta^2\text{-}CH_2{=}CH_2)Cl$ **(20)**.

Zr-Cl	2.500(4)	P(1)-Zr-P(2)	153.45(11)
Zr-P(1)	2.872(4)	Cl-Zr-P(1)	77.85(12)
Zr-P(2)	2.850(4)	Cl-Zr-P(2)	77.42(12)
Zr-C(19)	2.326(11)	Cl-Zr-C(19)	98.8(3)
Zr-C(20)	2.318(11)	Cl-Zr-C(20)	100.6(3)
Zr-Cp'	2.2361(16)	Cp'-Zr-Cl	152.23(10)
C(19)-C(20)	1.433(17)		

3.4.2   Kinetic study into the formation of 20

Kinetic experiments were conducted to investigate the mechanism of the formation of the ethylene complex **20** from alkylidene **16**. Figure 3.9 illustrates a plot of ln[**16**] vs. time for reactions carried out to between two and three half-lives for a number of different ethylene concentrations. In all instances the ethylene concentration remained unchanged during the course of the reaction, so that the results shown in Figure 3.9 exhibit pseudo first-order behaviour consistent with overall second order kinetics, where the observed rate = k_o[**16**][C$_2$H$_4$].

Although intermediates in the transformation of alkylidenes **16** or **18b** to ethylene **20** were not observed, the second-order kinetics, together with the organic by-products from reaction 3.7, are consistent with the reaction mechanism depicted in Scheme 3.5. The initial coordination of ethylene to the alkylidene is likely assisted by dissociation of either the agostic interaction or one of the potentially labile side-arm phosphines. Subsequent cycloaddition of the coordinated ethylene with the alkylidene moiety gives a four-membered metallacycle (**M**), an intermediate that has been trapped and isolated[11,17,37] in analogous reactions between alkylidene

complexes and certain alkenes. β-hydride elimination of zirconacyclobutane **M** can occur via two pathways; in Scheme 3.5, only the pathway that generates the terminal alkene $RCH_2CH=CH_2$, the product of the more kinetically favored route, is shown. In the presence of excess ethylene, the zirconium centre is trapped by a second equivalent of ethylene, to generate the final product **20**. It is noteworthy that products resulting from alkene metathesis $(RCH=CH_2)$ were not detected, an indication of the presumed rapid rate for the β-elimination process. This particular mechanism has been generally observed in the reaction of alkylidene complexes with ethylene,[11,12,38] although further coupling from an additional equivalent of ethylene to give a metallacyclopentane[28,39] complex has also been noted. However, this feature is not observed for **20**, which does not react further with additional ethylene.
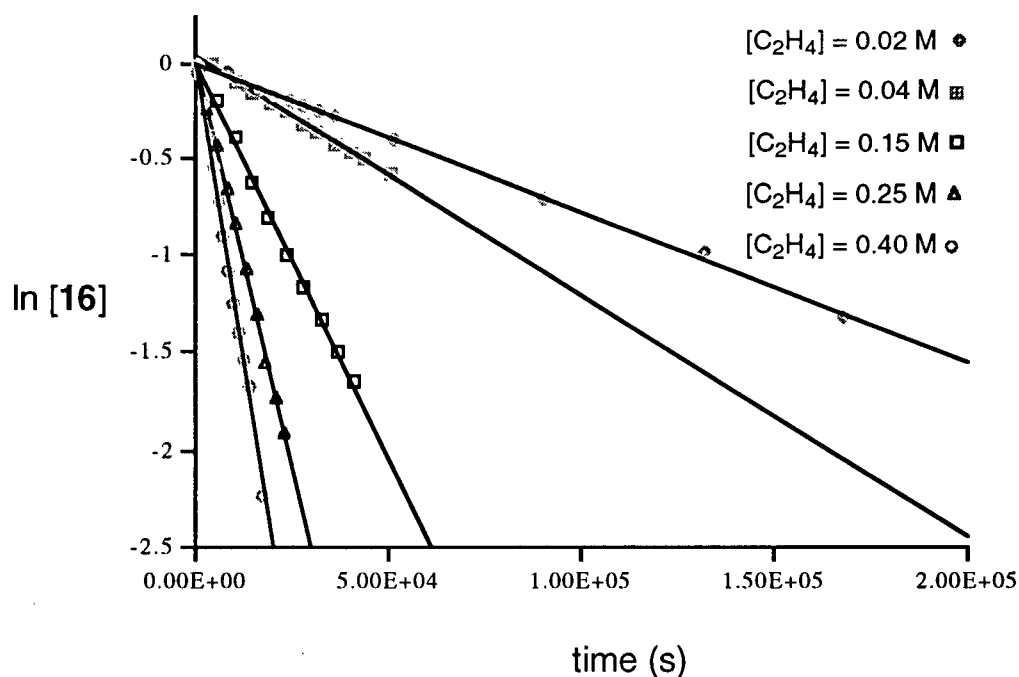
Figure 3.9   Pseudo first-order kinetics in the reaction of **16** with ethylene to give **20**.

16 R = Ph
18b R = SiMe₃
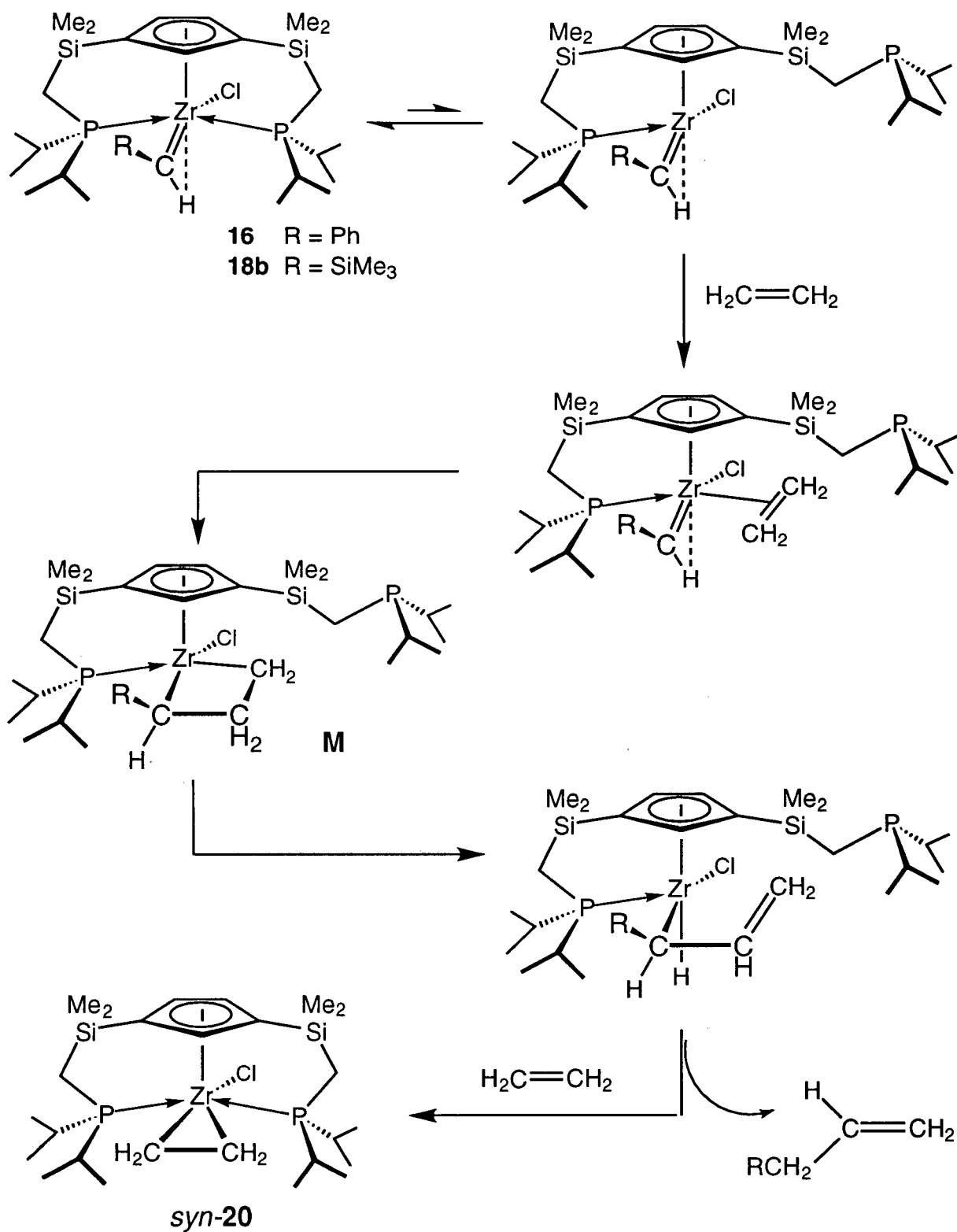
Scheme 3.5 Proposed mechanistic steps in the formation of **20**.

111

3.4.3   Reactivity of ^{Pr}[P$_2$Cp]Zr=CHR(Cl) with larger substrates

In comparison with some group 5 alkylidene systems,[39] the slow reaction with ethylene that produces **20** indicates the steric and electronic saturation at the Zr centre in alkylidenes **16** and **18b**. When the slightly larger and more weakly binding olefin propylene is employed the reaction is considerably slower, eventually yielding unidentified paramagnetic products after more than one week. However, the organic by-product observed in this reaction is almost exclusively the terminal alkene RCH$_2$C(Me)=CH$_2$, which again is consistent with β-H elimination from an analogous zirconacyclobutane intermediate. The predominant elimination of only one alkene from this reaction signifies two points. First, the propylene addition with either **16** or **18b** is highly regioselective, with the substituted portion of the double bond adding to the alkylidene carbon. Second, the kinetic preference noted earlier for the elimination of a terminal alkene rather than an internal alkene is magnified in the propylene reaction. The significantly longer duration needed for the this reaction, together with the apparent instability of the resulting propylene adduct, points to steric factors. It is evident that steric crowding from the ancillary ligand restricts the size of molecules that can access the metal centre, even with the advent of side-arm phosphine dissociation. This property is accentuated by the equally slow reaction of these alkylidenes with the relatively small cumulene allene, and the total inability to react with larger activated substrates like norbornene, butadiene, and internal alkynes.

Another reaction that is characteristic of early metal alkylidene complexes is a parallel of the Wittig reaction,[23] and an example is shown below in the reaction of either **16** or **18b** with acetone (equation 3.8). The alkene RCH=C(CH$_3$)$_2$ was isolated and identified by GC-MS, but unfortunately, a Zr containing species could not be isolated from this reaction. The ^{31}P{^{1}H} NMR spectrum of this reaction mixture shows a variety of unidentified species, presumably due to decomposition of the putative oxo species ^{Pr}[P$_2$Cp]ZrO(Cl).

$$16 \quad R = Ph$$
$$18a \quad R = SiMe_3$$

(3.8)
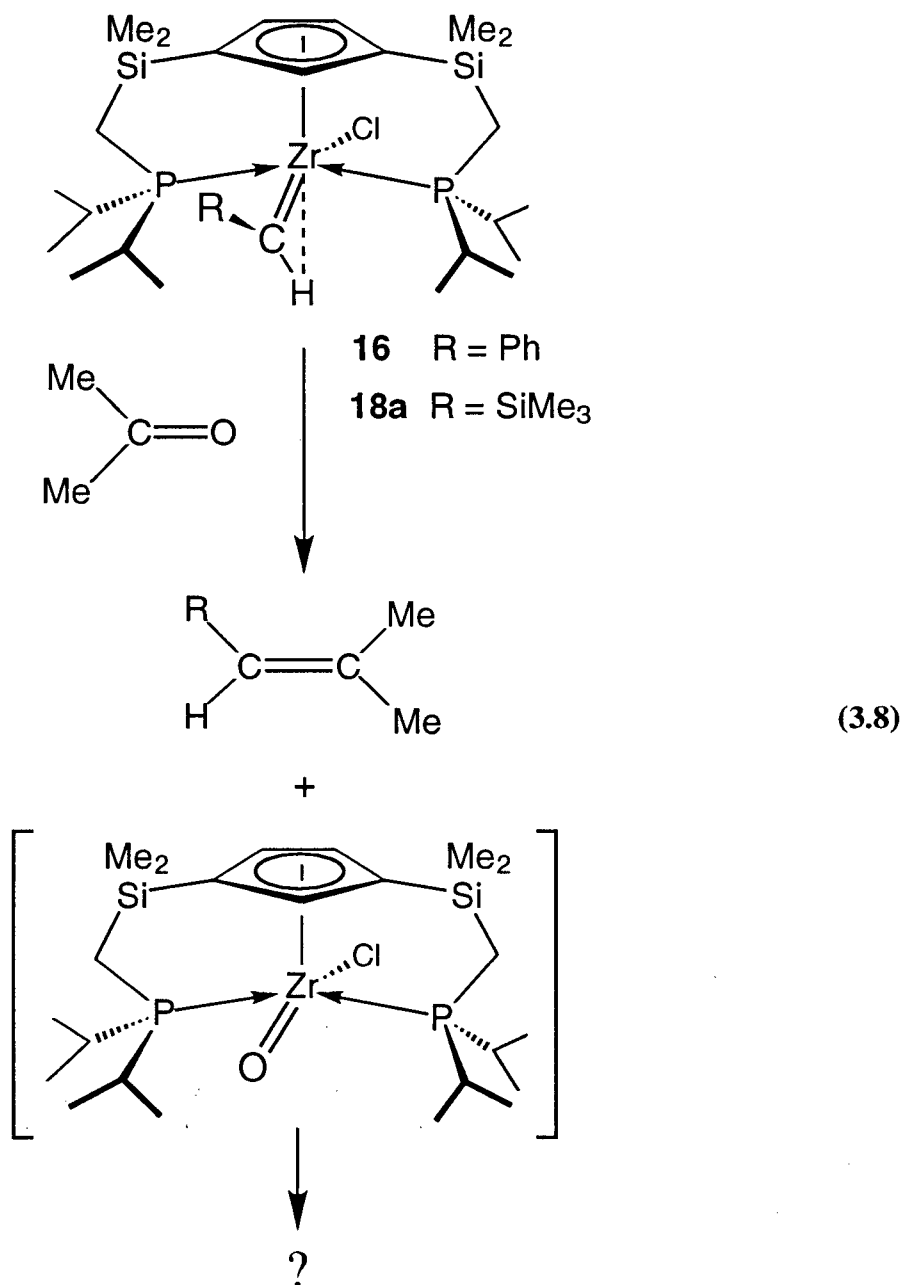
3.4.4 Preparation of ketene and ketenimine complexes $^{Pr}[P_2Cp]Zr(\eta^2\text{-}C(X)\text{=}CHR$

$(X = O, NBu^t)$

In comparison to the extensive chemistry of alkylidene complexes with alkenes and organic carbonyls, much less attention has been directed towards their reactivity with carbon

monoxide and isonitriles. This is somewhat surprising, given that these reactions have been noted to yield unusual ketene and ketenimine complexes,[11,40,41] species that have demonstrated their synthetic utility in a variety of organic transformations.[42-44] Of the ketene complexes obtained by the insertion reaction of metal alkylidenes and CO, structural analysis of the products detailing the mode of insertion have not been reported.

A toluene solution of the alkylidene complex **16 or 18b** reacts with CO under ambient conditions over a period of 24 hours to yield the thermally stable ketene complex $^{Pr}[P_2Cp]Zr(\eta^2\text{-}C(O)=CHR(Cl)$ (**21a**: R = Ph, **21b**: R = SiMe$_3$) in moderate yield (equation 3.9). Orange crystals of **21a** can be isolated from cold hexanes whereas **21b** is obtained as an orange oil which remains soluble in hydrocarbon solvents.

16 R = Ph

18b R = SiMe$_3$

C≡O

(3.9)

syn-**21** *anti*-**21**
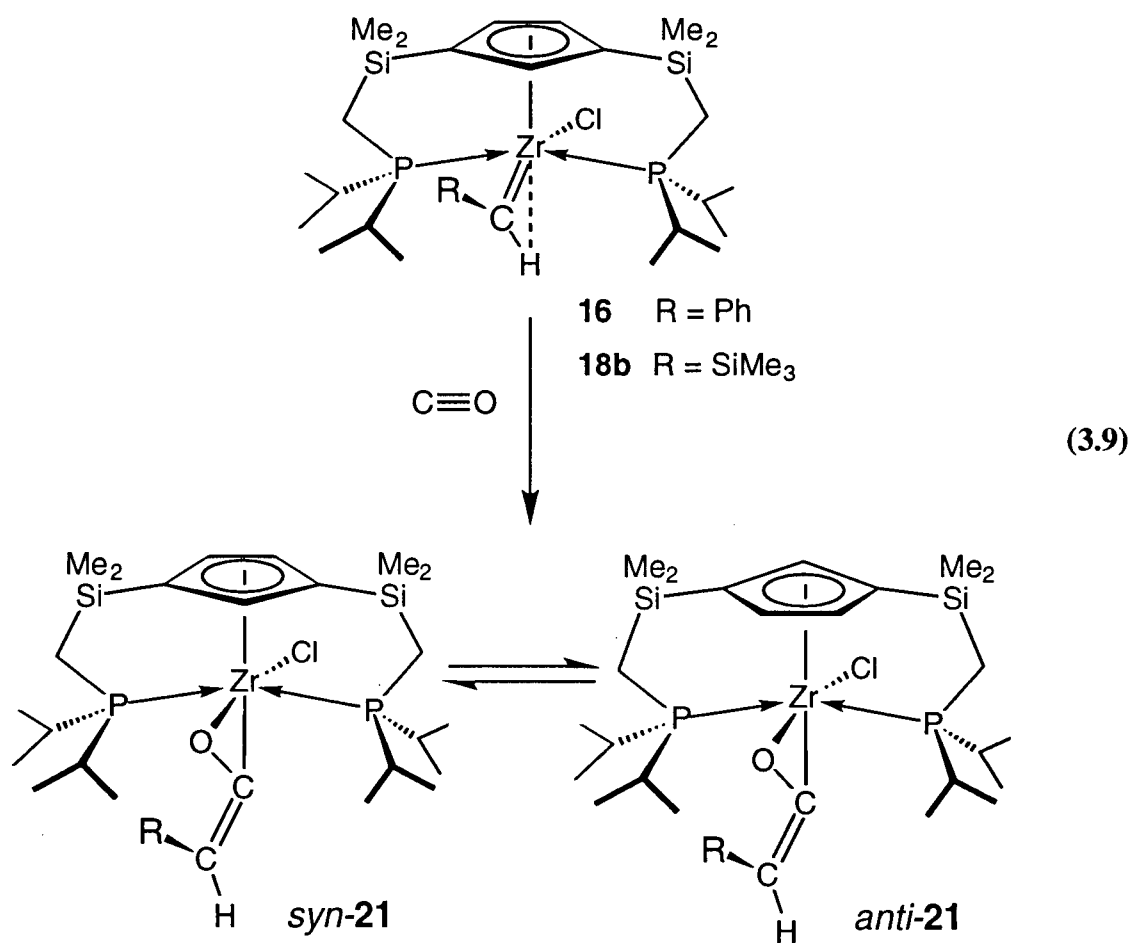
Similar to the solution behaviour noted previously for **20**, both **21a** and **21b** exhibit two stereoisomers each, either in a 4:1 (**21a**) or 2:1 (**21b**) ratio at room temperature. These species are identified by separate singlets in the $^{31}P\{^1H\}$NMR spectrum and by corresponding resonances in the ^1H NMR spectrum. Additionally, for each isomer there is a triplet located downfield in the $^{13}C\{^1H\}$ NMR spectrum for the ketene carbon, the observed splitting due to $^2J_{PC}$ coupling to two equivalent phosphines. For **21a** these resonances are at 192 ppm (minor isomer) and 205 ppm (major isomer), while **21b** exhibits triplets at 203 ppm (major isomer) and 216 ppm (minor isomer), respectively. **21a** also shows a strong peak in the IR spectrum for the ketene moiety at 1495 cm^{-1}. Again, as with **20** these stereoisomers are likely the structures *syn*-**21** and *anti*-**21**, which differ in the relative orientation of the ketene unit with respect to the ancillary ligand. It is evident that both species are in equilibrium, as variable temperature NMR spectroscopy reveals a smooth temperature dependent variation in the relative concentrations (the major isomer is present in lesser amounts at higher temperature), and an increase in line broadening in the $^{31}P\{^1H\}$ NMR spectrum is observed as the temperature is raised, due to a faster exchange rate between the two structures. However, it could not be unambiguously determined which species is the *syn* isomer as the spectroscopic data are unable to distinguish between the two structures in solution. It is not possible to examine a nuclear Overhauser enhancement (nOe) between the Cp ring protons and protons within the ketene unit as these nuclei are too far apart. Attempts to introduce an NMR active nucleus closer to the Cp ring protons by substituting the chloride of **21** with either a fluoride or an alkyl group were unsuccessful, and a heteronuclear nOe experiment conducted on a sample of **21b** containing a ^{13}C-labeled ketene carbon was also inconclusive. Regarding the method of interconversion of the *syn* and *anti* isomers of **21** (and presumably of **20** as well), it is likely that dissociation of both phosphines is followed by a 180° rotation of the ancillary ligand around the Zr-Cp axis occurs (Scheme 3.6).
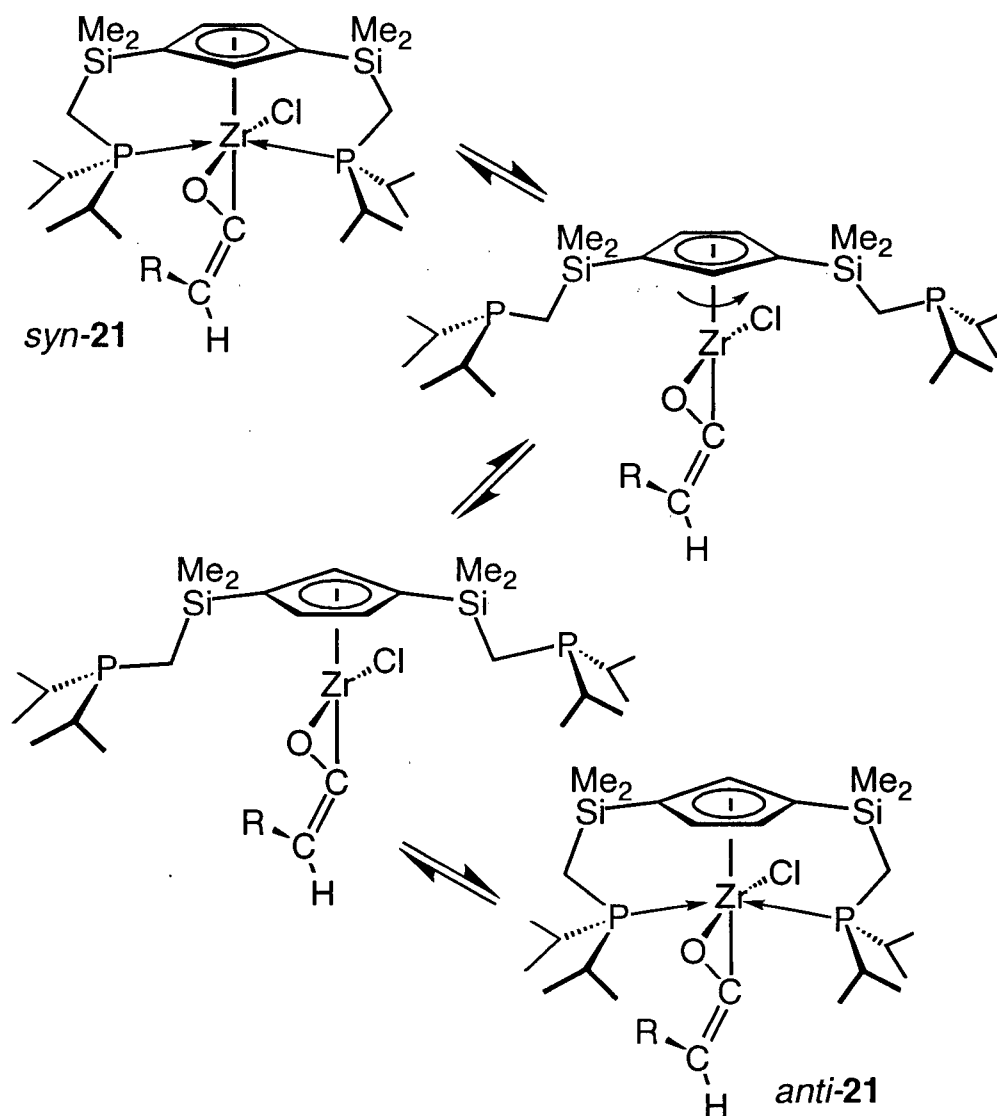
Scheme 3.6 Proposed mechanism for the interconversion of stereoisomers in **20**.

Crystals suitable for X-ray structure determination were obtained for benzylidene ketene **21a**, and the molecular structure is shown in Figure 3.10. Selected bond distances and bond angles are given in Table 3.7. The mononuclear structure arises from the steric bulk of the ancillary ligand, a feature in common with analogous early metal ketene complexes where bulky

substituents are required to prevent dimerization.[45-49] The η^2-C,O coordination of the ketene fragment is also a typical binding mode to oxophilic metals,[47,48,50,51] and is exhibited here by the short Zr-C(24) and Zr-O distances of 2.172(3) Å and 2.027(2) Å, respectively, and a correspondingly long C-O distance of 1.374(3) Å. These parameters are similar to the analogous bond distances in another monomeric Zr ketene complex, Cp*$_2$Zr(py)(η^2-C(O)=CH$_2$),[47] which are 2.181(2) Å, 2.126(1) Å, and 1.338(2) Å, respectively. The C(24)-C(25) distance of 1.349(4) is indicative of a double bond, and the coplanarity of the ketene moiety is illustrated by the dihedral angle of 2° between O(1), C(24), C(25), and C(26). Additionally, the phenyl ring is also nearly coplanar with the ketene fragment with a tilt angle of 8°, an alignment that presumably optimizes delocalization of electron density over the organic fragment and reduces steric interactions with the ancillary ligand.
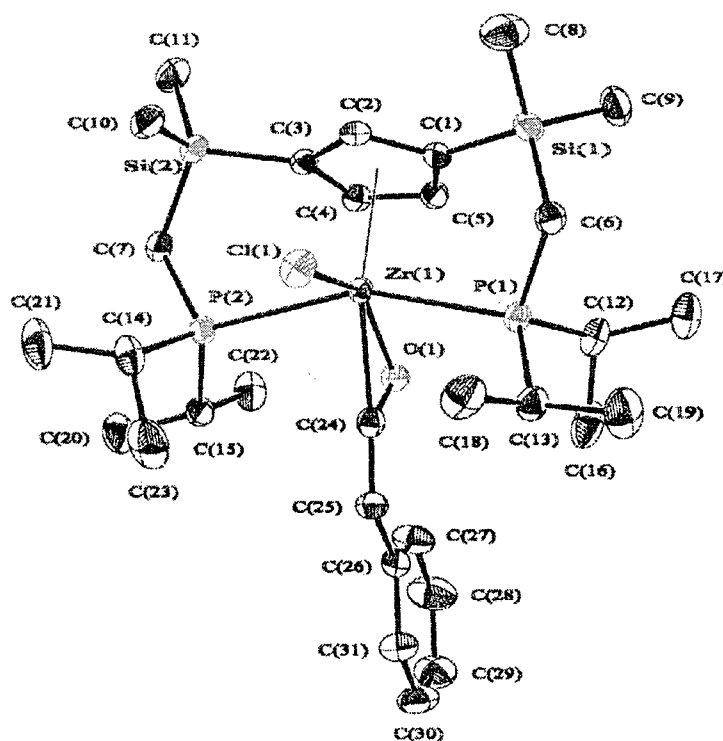
Figure 3.10 Molecular structure of ^{Pr}[P$_2$Cp]Zr(η^2-C(O)=CHPh)(Cl) **(21a)**; 33% probability thermal ellipsoids are shown. Hydrogen atoms are omitted for clarity.

117   *references begin on page 141*

Table 3.7   Selected Bond Lengths (Å) and Bond Angles (°) for

^{Pr}[P$_2$Cp]Zr(η^2-C(O)=CHPh)(Cl) (**21a**).

Zr(1)-Cl(1)	2.4976(8)	Cl(1)-Zr(1)-P(1)	87.66(3)
Zr(1)-P(1)	2.8261(8)	Cl(1)-Zr(1)-P(2)	86.54(3)
Zr(1)-P(2)	2.8517(8)	Cl(1)-Zr(1)-O(1)	141.42(6)
Zr(1)-O(1)	2.027(2)	Cl(1)-Zr(1)-C(24)	103.43(8)
Zr(1)-C(24)	2.172(3)	Cl(1)—Zr(1)—Cp	107.1
Zr(1)-Cp	2.25	P(1)-Zr(1)-P(2)	156.25(2)
C(24)-C(25)	1.349(4)	Zr(1)-C(24)-O(1)	65.3(1)
O(1)-C(24)	1.374(3)	O(1)-Zr(1)-C(24)	37.99(8)
		Zr(1)-C(24)-C(25)	169.5(2)

Two points can be made regarding the solid state structure of **21a** in comparison to that of the precursor benzylidene **16** (see Figure 3.3 for the isostructural Hf analogue **16**). First, the observed molecular structure of the ketene complex corresponds to the *anti* stereoisomer of **21**, a reversal of the orientation noted for **16**. Presumably, *anti*-**21** is the least soluble isomer of the two ketene species in equilibrium. The second point is that the α-hydrogen involved in the agostic interaction in **16** is still oriented below the zirconium in **21a**, resulting in an E-geometry for the ketene unit. In other words, insertion of CO proceeds with retention of stereochemistry about the zirconium-carbon double bond. This geometry arises from the lack of rotation previously noted in the Zr=C bond of the precursor alkylidene. Furthermore, no E/Z isomerization is observed for the ketene complexes **21**, and this contrasts some other early metal ketene complexes that have been studied.[50,51] Without this isomerization process, an exo orientation of the ketene unit relative to the Cp ring is adopted to minimize steric interactions between the phenyl group and the ancillary ligand.

exo   endo
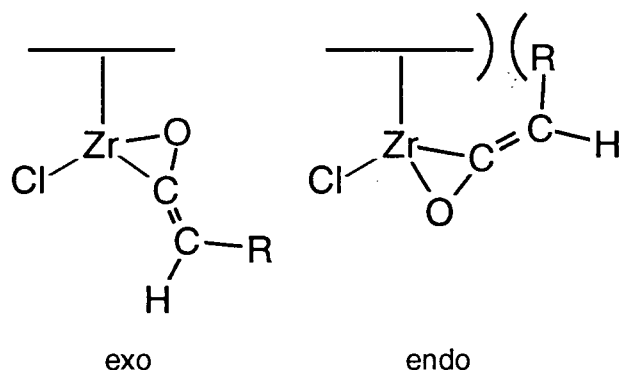
As an extension of the insertion reaction that produces **21,** a toluene solution of tert-butyl isocyanide reacts with **16** to give the analogous ketenimine[52-55] complex ^{Pr}[P$_2$Cp]Zr(η^2-C,N-C(NBu^t)=CHPh)Cl (**22**) as dark red crystals (equation 3.10). To our knowledge this is the first example of a ketenimine complex obtained from the insertion of an isocyanide into an early-metal alkylidene complex.

Bu^t—N≡C

(3.10)

16

*anti-***22**
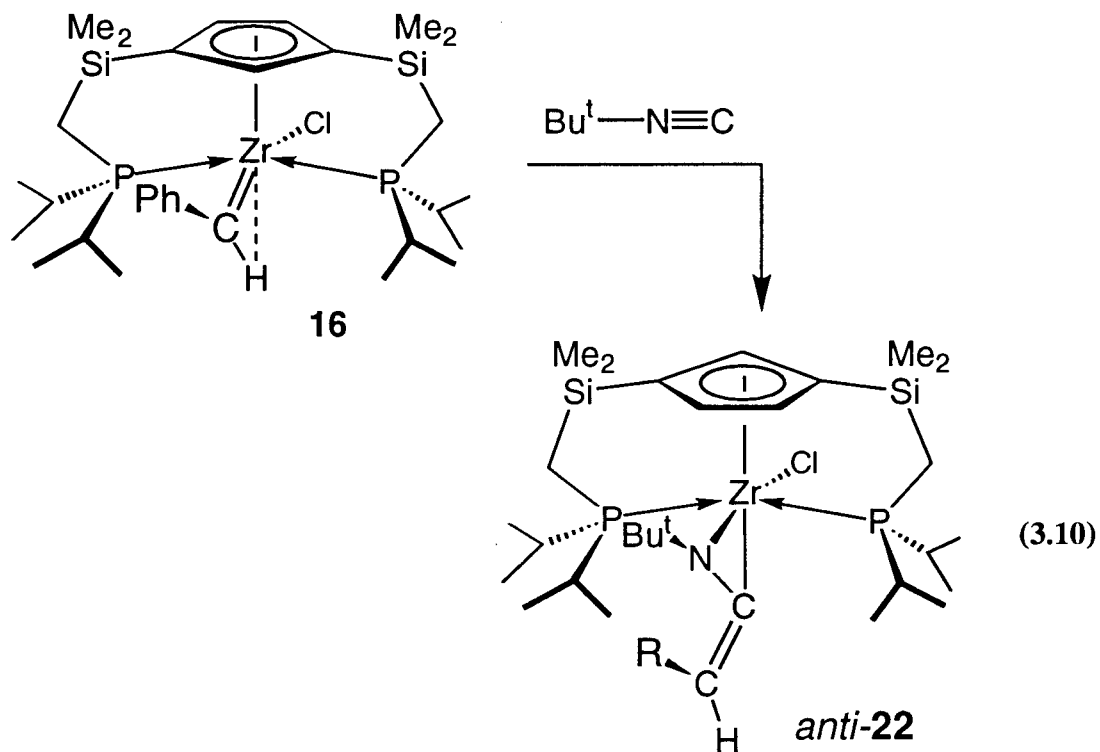
The stoichiometry of this reaction is important as an excess of the isonitrile reacts further with **22**. The spectroscopic parameters for ketenimine **21** are similar to those of the analogous ketene complex; for example, the ketenimine moiety shows a peak in the IR spectrum at 1504 cm^{-1} and the ketenimine carbon displays a downfield resonance in the $^{13}C\{^{1}H\}$ NMR spectrum at 204 ppm. In contrast to **21a**, however, only a single isomer is observed for **22** in solution (i.e., a single resonance is present in the $^{31}P\{^{1}H\}$ NMR spectrum), presumably because the isomerization mechanism mediated by Cp rotation (Scheme 3.6) is impeded by the tert-butyl group. A ^{1}H NOEDIFF NMR experiment conducted on **22** established that the isomer obtained is *anti*-**22**, since irradiating the methyl resonance of the tert-butyl group leads to an enhancement of the peak assigned to the two equivalent Cp protons, but no effect is observed for the resonance ascribed to the unique Cp proton. However, if neither the precursor alkylidene **16** nor the product ketenimine **22** undergo *syn/anti* isomerization, then the transformation from *syn*-**16** to *anti*-**22** must occur *during* the migratory insertion of the isocyanide into the Zr-C alkylidene bond (Scheme 3.7). In this instance the bulky tert-butyl group is directed away from the ancillary ligand until the final step when the nitrogen atom binds to give the $\eta^{2}(C, N)$-coordinated ketenimine complex. The same mechanism is likely involved in the formation of ketene **21**, although as mentioned previously this complex is capable of isomerizing after the product is formed.

The steric effects of the large Bu^{t} group are also apparently manifested in a pronounced broadening of peaks in the ^{1}H NMR spectrum in **22** for the ortho protons on the phenyl ring (and to a lesser extent the meta protons as well), and the resonances of the portion of the ancillary ligand that is *syn* to the ketenimine unit. However, all of these peaks are narrow in the low temperature spectrum (-25 °C), suggesting that some dynamic process is frozen out at low temperature, perhaps rotation of the phenyl ring restricted by steric interaction with the tert-butyl group, and begins exchanging chemical environments as the molecule is heated.
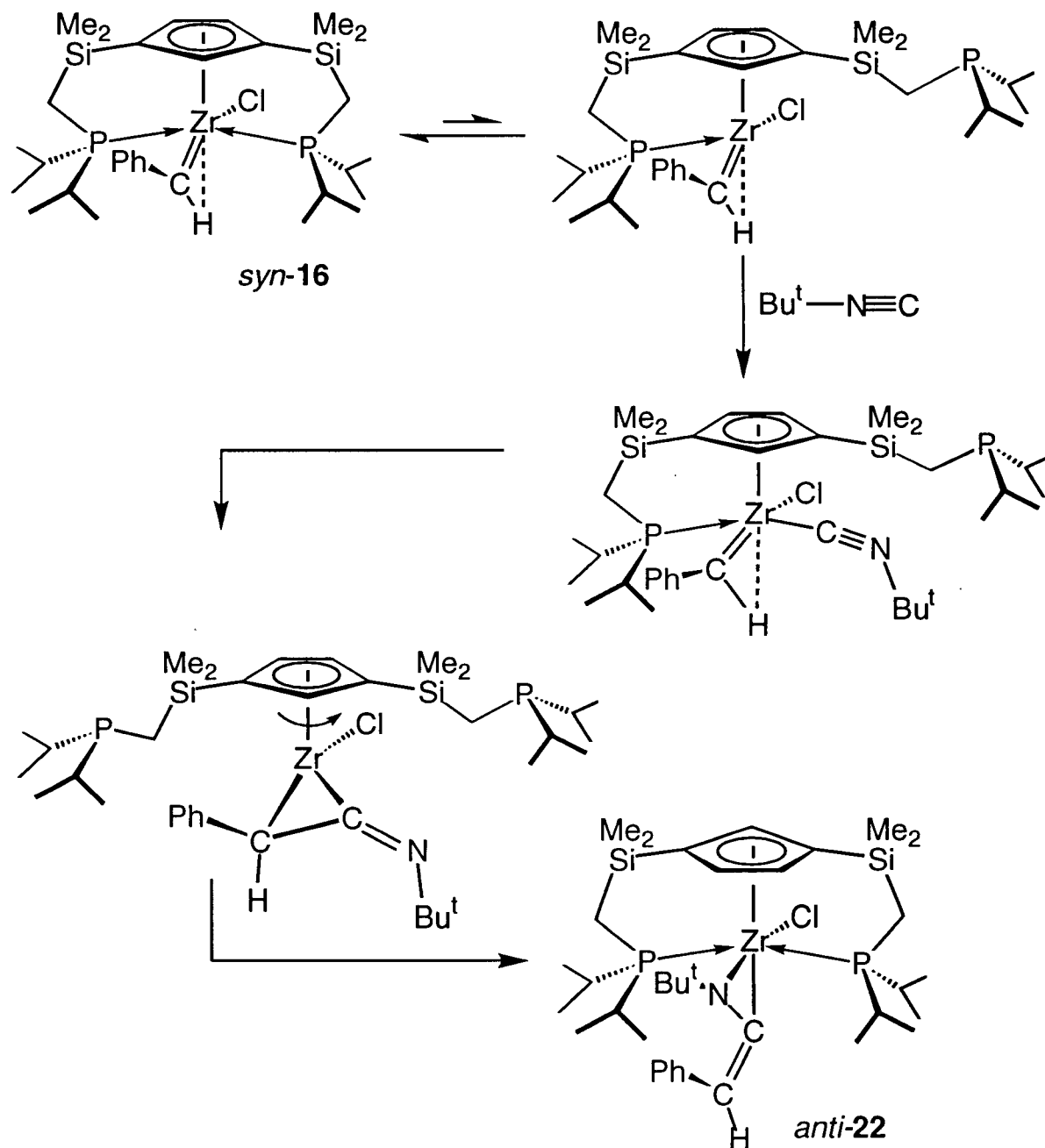
Scheme 3.7   Proposed mechanism for the formation of *anti*-**22** from *syn*-**16**.

3.4.5 Insertion reactivity of ketene $^{Pr}[P_2Cp]Zr(\eta^2\text{-}C(O)=CHR)Cl$

A toluene solution of **21** reacts with ethylene under ambient conditions over a period of two days to give the insertion product $^{Pr}[P_2Cp]Zr(\eta^2\text{-}CH_2CH_2C(O)=CHR)Cl$ (**23a:** R = Ph, **23b:** R = SiMe₃; equation 3.11).
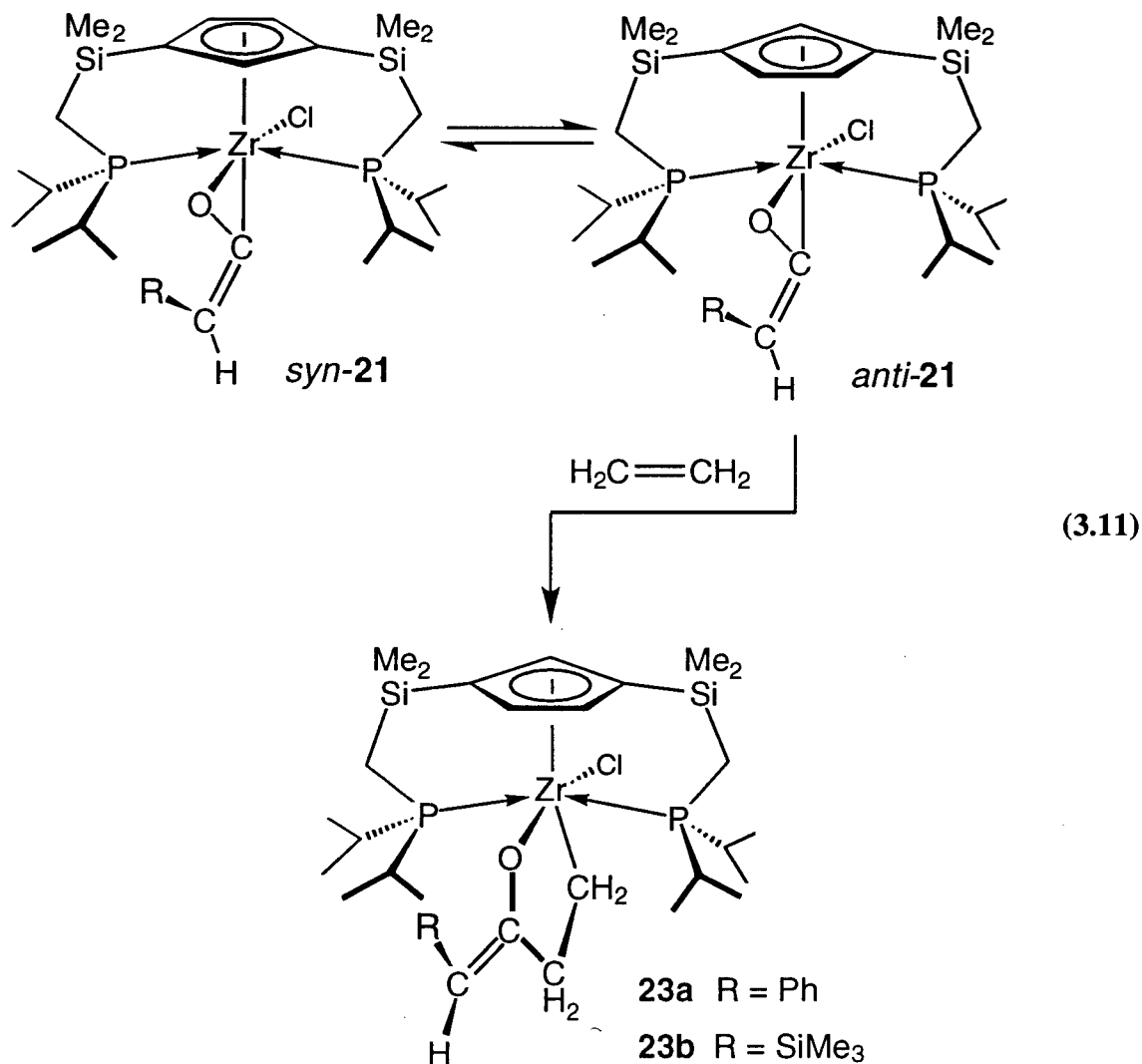
The ¹H and ³¹P{¹H} NMR spectra reveal that both **23a** and **23b** exist as a single species in solution, despite the fact that the precursor **21** consists of an equilibrium mixture of two stereoisomers. This suggests either that one isomer of **21** is kinetically more reactive, or that

both possible stereoisomers of **23** are initially formed, followed by complete conversion of the less stable isomer to the thermodynamically-favored observed product.

We were able to isolate crystals of **23b** suitable for X-ray structure determination, and the molecular structure is shown in Figure 3.11. The X-ray data of selected bond distances and bond angles are given in Table 3.8.
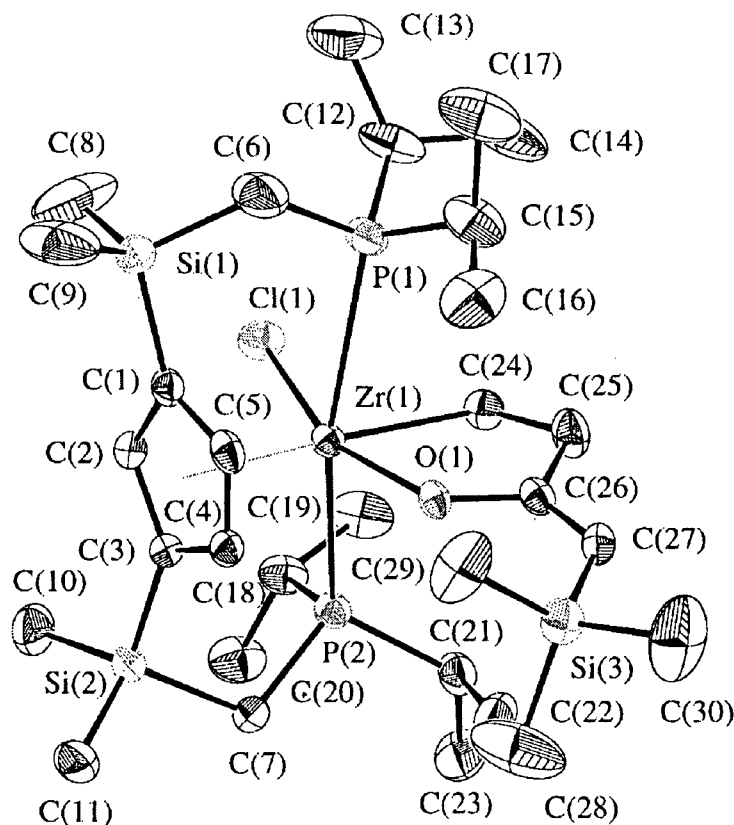
Figure 3.11 Molecular structure of $^{Pr}[P_2Cp]Zr(\eta^2\text{-}CH_2CH_2C(O)\text{=}CHR)Cl$ (**23b**); 33% probability thermal ellipsoids are shown. Hydrogen atoms are omitted for clarity.

Figure 3.11 shows that one ethylene molecule has inserted into the Zr-C bond of the ketene unit, which is now bound to Zr solely *via* the oxygen atom as an enolate fragment, to give a five-membered metallacycle. The short C(26)-C(27) distance of 1.329(5) Å is a relic of the Zr=C

bond from the original alkylidene **18b**. The overall configuration of **23b** is retained from the precursor ketene complex and resembles the isomer pertaining to *anti*-**21**. Therefore if the observed stereoselectivity is due to a kinetic factor then this implies that *anti*-**21** is the more reactive of the two ketene isomers with respect to ethylene insertion. The stereochemical preference for one orientation over the other is a recurring theme for many of the complexes involving the P_2Cp ligand, as noted previously with the alkylidene complexes and with **22**, and is somewhat puzzling, given that the apparent differences between the two sides of the ligand are unremarkable. The steric differences are almost negligible, so it seems likely that subtle electronic factors are involved in favoring a particular configuration.

Table 3.8   Selected Bond Lengths (Å) and Bond Angles (°) for

$^{Pr}[P_2Cp]Zr(\eta^2\text{-}CH_2CH_2C(O)=CHR)Cl$ (**23b**).

Zr(1)—Cl(1)	2.5234(10)	Cl(1)-Zr(1)-P(1)	81.39(3)
Zr(1)-P(1)	2.9527(11)	Cl(1)-Zr(1)-P(2)	86.31(3)
Zr(1)-P(2)	2.9007(11)	Cl(1)-Zr(1)-O(1)	156.64(6)
Zr(1)-O(1)	2.036(2)	Cl(1)-Zr(1)-C(24)	82.83(9)
Zr(1)-C(24)	2.172(3)	Cl(1)—Zr(1)—Cp	107.1
Zr(1)-Cp	2.30	P(1)-Zr(1)-P(2)	159.21(3)
C(26)-C(27)	1.329(5)	O(1)-Zr(1)-C(24)	74.10(10)
O(1)-C(24)	1.374(3)	Zr(1)-O(1)-C(26)	128.4(2)
C(24)-C(25)	1.519(5)	Zr(1)-C(24)-C(25)	110.4(2)

Monomeric ketene complexes are generally more reactive to substrates such as alkenes,[23,43] alkynes,[56] and H_2[47] than are the corresponding dimeric derivatives.[56] However, except for the reaction noted above with ethylene, the monomeric ketene complex **20** is comparatively inert, showing no reactivity with either internal alkynes, butadiene, alkylating reagents, or H_2. Again, the bulk of the ancillary ligand may contribute to this lack of reactivity.

In line with this idea, the even more sterically encumbered ketenimine complex **22** undergoes a considerably slower reaction with ethylene (approximately 5 days), and a clean product could not be isolated.

3.4.6 Formation of acyl-ylide complexes

Metallacycle **23** reacts with carbon monoxide to yield an η^2-acyl-ylide complex[57] (**24a:** R = Ph, **24b:** R = SiMe$_3$) in which the metallacycle has expanded to a six-membered ring to accommodate the insertion of CO (equation 3.12):

$$Me_2 \quad Me_2$$

23a R = Ph
23b R = SiMe$_3$

$$C\equiv O$$

(3.12)

24a R = Ph
24b R = SiMe$_3$
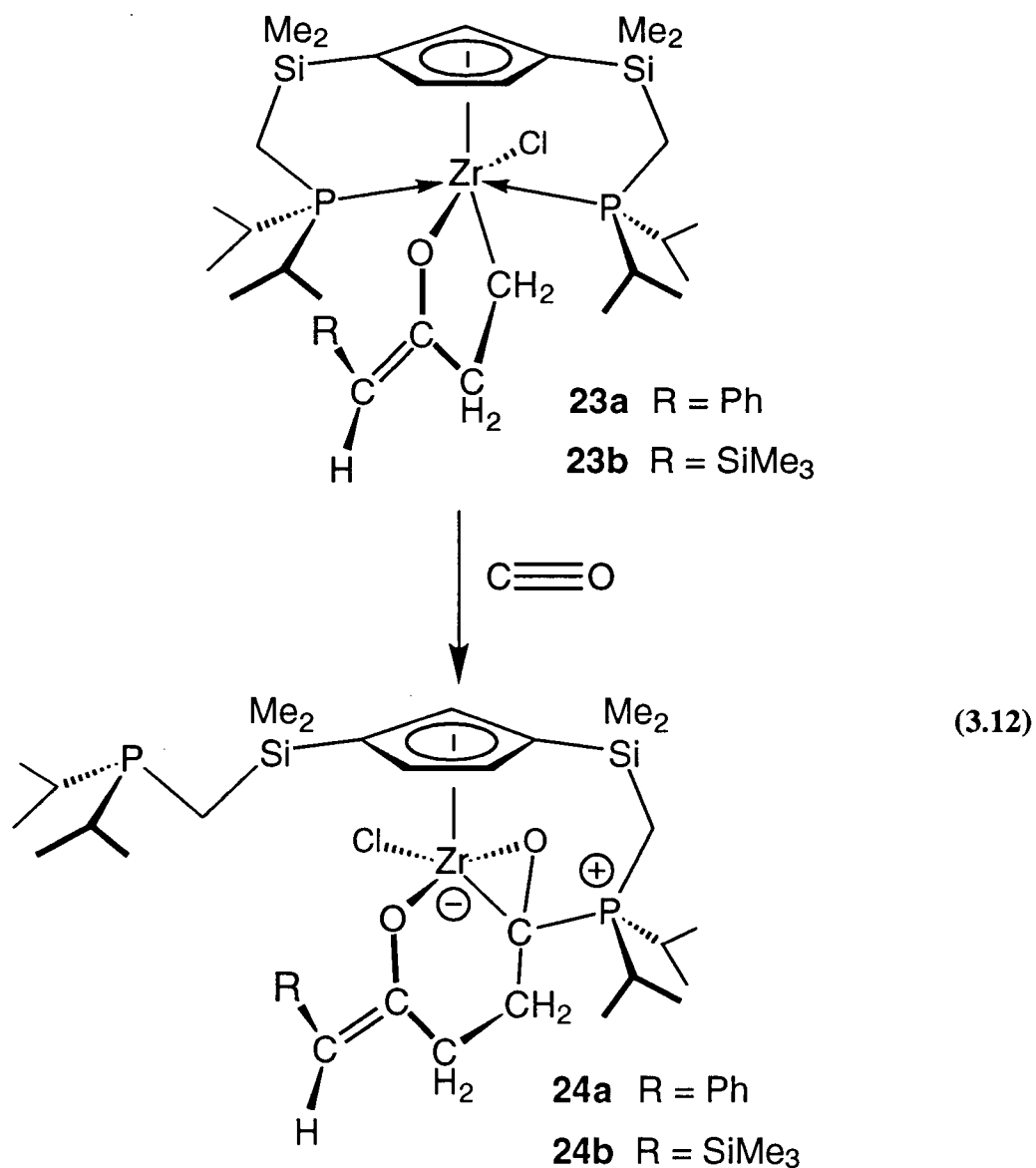
A single isomer is observed in solution for **24a**, while two species are evident in a 9:1 ratio for **24b**. The η^2-coordination mode of the acyl unit resembles that found in ketene **21**, except the carbonyl carbon of the latter is saturated electronically by the double bond to C(22), a feature that is absent in **24**. To compensate for this discrepancy, one of the side-arm phosphines coordinates not to the metal but instead stabilizes the electrophilic acyl carbon. The other pendant side-arm remains dangling, so that two singlets are observed in the $^{31}P\{^1H\}$ NMR spectrum, one located downfield near 46 ppm for the ylide phosphine, and an upfield peak near 7 ppm corresponding to a free phosphine. The ^1H NMR spectrum reveals a complicated second order splitting pattern for the diastereotopic protons of the ethylene portion of the metallacycle. For the two protons α to the chiral acyl carbon this pattern is further complicated by $^3J_{PH}$ coupling, which could be identified by decoupling the phosphorus resonance near 46 ppm. The low C_1 symmetry of this complex is also evident in the cyclopentadienyl region where three separate resonances are seen in the ^1H NMR spectrum. However, the dangling side-arm is further removed from the chiral carbon centre and these protons belie a more symmetric environment in the ^1H NMR spectrum.

The unusual acyl-ylide structure of **24** recalls the structurally characterized acyl-ylide **13** encountered in the previous chapter, obtained from the analogous insertion reaction of CO into the monobenzyl species **11**. The NMR spectroscopic features of **13** and **24** are quite similar. The resemblance between the two structures originates from the similarity between the precursors, where the general ligand set for each comprises CpL_2MX_2R, if the vinyl alkoxide fragment in **23** is regarded as a pseudo-halide. Therefore, it is not surprising that the products obtained from the insertion of CO into either **11** or **23** have the same generic structure. The only difference between the two is the cyclic unit in **24**, which is inherited from the precursor metallacycle.

The sequence of insertion reactions beginning with the alkylidene complexes ceases with the acyl-ylide **24**, which does not react with ethylene. The preceding insertion reactions required

in each case the predissociation of a pendant phosphine to create an available coordination site for the incoming substrate prior to insertion. For alkylidene **16** and **18b**, ketene **21**, and metallacycle **23** this process was possible, but in **24** one phosphine is firmly bound to the acyl carbon while the other is already uncoordinated, thereby leaving the metal centre without a labile ligand.

3.5 Summary and conclusions

The ancillary ligand P_2Cp has been utilized in the synthesis of the first reported examples of stable zirconium and hafnium alkylidene complexes, which are isolated in high yield as crystalline solids. The structural parameters are similar for each and the solid state structure is maintained in solution. Both complexes are monomeric with C_s symmetry, and the alkylidene units are oriented in the same configuration with respect to the ancillary ligand. An agostic interaction between the alkylidene C-H moiety and the metal centre is also present in both compounds, a common feature for unsaturated alkylidene complexes.

The alkylidene complexes **16, 17** and **18** are formed via the thermal decomposition of the corresponding bis(alkyl) precursors **14, 15** and **19**, respectively. The reaction mechanism is complicated by a pre-equilibrium route in which the dialkyl species undergo reversible disproportionation, presumably *via* a bridging binuclear adduct, to give the corresponding mono- and tri-alkyl species (Scheme 3.2). Kinetic studies show that the decomposition of **14** and **18b** follow first order kinetics, indicating that the rates associated with the equilibrium are rapid and do not interfere with the irreversible thermal reaction. The activation parameters obtained from the reaction are consistent with an intramolecular α-abstraction process, as is the kinetic isotope effect of 3.0 (0.5) obtained for the benzyl derivative. However, in the systems studied here the reaction rates follow the order benzyl > neosilyl > neopentyl, exactly opposite to that found previously in other systems. We believe that our results reflect a subtle balance between the

steric crowding imposed by the alkyl ligands and the side-arm phosphines of the ancillary ligand. The bulkier neopentyl ligands crowd the metal centre to a greater extent than do the benzyl groups, thus providing less opportunity for the bulky phosphines to coordinate. As alkylidene formation is hastened by phosphine coordination, this may account for the faster rates observed for the less bulky benzyl derivative, in addition to the otherwise surprising lack of thermal reactivity of the trialkyl species, where phosphine coordination remains absent under all conditions.

The rarity of alkylidene complexes found in Group 4 is striking in comparison to the number of examples known for the group 5 metals . These differences are largely based on the added coordinative saturation available to the precursor complexes of the group 5 congeners, due to the presence of an extra alkyl ligand. All Group 4 derivatives reported thus far have required the additional steric saturation of a phosphine donor. Clearly this steric requirement is adequately met with the P_2Cp ligand, by employing bulky chelating bis(phosphines) appended to a substituted cyclopentadienyl ring, to stabilize alkylidenes **16**, **17** and **18**.

The alkylidene complexes undergoes cycloaddition and insertion reactions with a variety of unsaturated substrates. The reactivity at the Zr=C bond is moderated by the bulky ancillary ligand, which induces slow reaction rates and imposes a limit on the size of substrates that can access the metal. Although unreactive with larger olefins and internal alkynes, a reaction of alkylidene **16** with ethylene follows first-order kinetics in both alkylidene and ethylene to yield the ethylene complex **20** . **16** also inserts molecules such as CO and CN^tBu to yield η^2-coordinated ketene and ketenimine complexes, **21** and **22**, respectively. Ketene **21** in turn reacts with ethylene to give metallacycle **23**, which undergoes a final insertion of CO to give the zwitterionic η^2-acyl-ylide species **24**.

All of the reactions noted above involve an insertion into a Zr-C bond, and a monomeric structure is observed for each product due to the large isopropyl substituents on the pendant phosphines of the ancillary ligand. The labile phosphines also play an important role in

providing an open coordination site for these insertion reactions to occur, which accounts for the absence of further insertion chemistry with **24**, where phosphine dissociation to create a reactive site at the metal is not available .

A characteristic feature of all of these complexes is associated with the C_s symmetry of the P$_2$Cp ligand. As depicted in the schematic of the ligand backbone below, there are two possible configurations with this ligand set, *syn* or *anti* with respect to the unique Cp carbon, which seem to present very similar steric and electronic environments for a given R group. Indeed, some of the complexes reported here (**20**, **21**) exhibit both configurations in equilibrium with each other, apparently isomerizing in solution by the mechanism in Scheme 3.6. Alternately, other complexes (**16**, **22**, **23**) exclusively favor one configuration over the other. Furthermore, while **16** adopts the *syn* structure, the chosen structure for **23** corresponds to the *anti* derivative. The factors responsible for a given configuration are evidently more subtle than the simplified diagram below suggests.

syn　　　　　　　*anti*
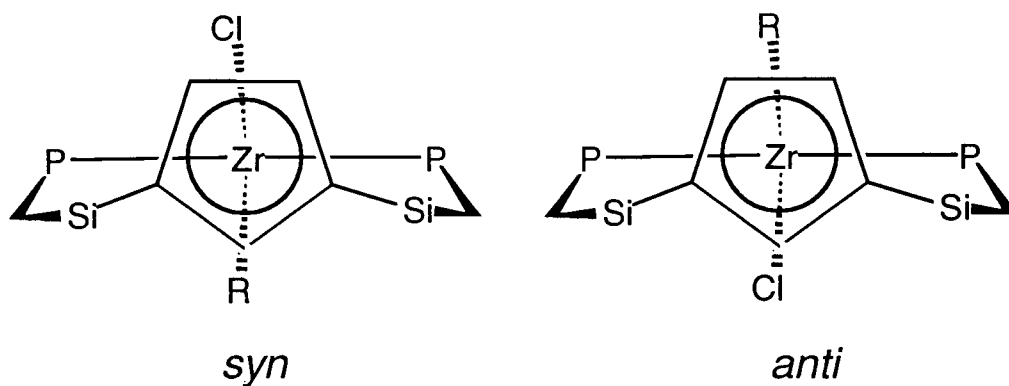
3.6 Experimental Section

3.6.1 Procedures and materials

Unless otherwise stated, general procedures were performed according to Section **2.7.1**. $KCD_2C_6D_5$ was prepared according to the same procedure followed for KCH_2Ph in Chapter 2. Tert-butyl isonitrile (Aldrich) was prepared as a toluene solution (0.88 M). The procedures for the preparation of $^{Pr}[P_2Cp]Zr=CHPh(Cl)$ (**15**) has been described elsewhere.[2]

3.6.2 Syntheses

3.6.2.1 $^{Pr}[P_2Cp]ZrCl(CH_2Ph)$ (14)

(a) From $^{Pr}[P_2Cp]ZrCl_3$ (1) and KCH_2Ph: A solution of KCH_2Ph (0.100 mg, 0.43mmol) in 10 mL of THF was added with stirring to a cooled (-78 °C) solution of **1** (65 mg, 0.23 mmol) dissolved in 30 mL of THF. The dark red colour of the KCH_2Ph solution was discharged upon addition and the colour of the reaction mixture became greenish-orange. The mixture was allowed to slowly warm to room temperature, whereupon all the volatiles were then removed under vacuum and the residue extracted with hexanes and filtered. The filtrate was reduced under vacuum to give a thermally and photochemically labile sensitive orange oil. NMR spectra of this oil indicate the presence of **14**, in addition to both tribenzyl **3** and monobenzyl **12**.

(b) From $^{Pr}[P_2Cp]ZrCl_2(CH_2Ph)$ (12) and $^{Pr}[P_2Cp]Zr(CH_2Ph)_3$ (3). Mixing together stoichiometric benzene-d_6 solutions of **3** and **12** produced a mixed solution with the same spectroscopic results as observed for procedure **(a)** above.

The assignment of peaks in the ^1H, $^{13}C\{^1H\}$ and $^{31}P\{^1H\}$ NMR spectra for **14** is provided by eliminating the known resonances for **3** and **12**. Note that some peaks for **14** are

obscured by overlapping resonances arising from the coexistence of all three benzyl species. ^{1}H NMR (20 °C, C$_6$D$_6$): δ 0.33 and 0.44 (s, 6H, Si(CH_3)$_2$), 0.89 (m, 4H, SiCH_2P), 1.23 (m, 24H, CH(CH_3)$_2$), 2.34 (m, 4H, CH_2Ph), 6.49 (d, 2H, $^4J_{HH}$ = 1Hz, Cp-H), 6.65 (d, 4H, $^4J_{HH}$ = 7Hz, o-C$_6$H$_5$), 6.87 (t, 1H, $^4J_{HH}$ = 1Hz, Cp-H), 7.03 (t, 4H, $^3J_{HH}$ = 7Hz, m-C$_6$H$_5$), 7.22 (t, 2H, $^3J_{HH}$ = 7Hz, p-C$_6$H$_5$). ^{31}P{^{1}H} NMR (20 °C, C$_6$D$_6$): δ 0.1 (s).

3.6.2.2 ^{Pr}[P$_2$Cp]Hf=CHPh(Cl) (17)

A solution of KCH$_2$Ph (68 mg, 0.55 mmol) in 20 mL of THF was added dropwise with stirring to a cooled (-78 °C) solution of 2 (400 mg, 0.55 mmol) dissolved in 20 mL of THF. The colour of the solution slowly changed to bright yellow. The solution was warmed to room temperature and then stirred for another 3 hours. The solvent was then removed in vacuo, and the residue extracted with hexanes and filtered. The filtrate was reduced under vacuum to give a yellow oil which was redissolved in 30 mL of toluene. This solution was placed in a 95 °C oilbath for 6 days, after which no further reaction could be detected by NMR spectroscopy (for a corresponding NMR scale reaction). The solvent was removed, and the oil extracted with hexane to give a bright yellow solid, which yielded crystals suitable for X-ray diffraction from a toluene/hexanes solution mixture at -40 °C. Yield: (307 mg, 75 %). ^{1}H NMR (20 °C, C$_6$D$_6$): δ 0.12 and 0.31 (s, 6H, Si(CH_3)$_2$), 0.42 and 0.49 (dd, 4H, $^2J_{HH}$ = 5Hz, $^2J_{PH}$ = 7Hz, SiCH_2P), 0.79, 0.96, 1.33 and 1.14 (dd, 6H, $^3J_{HH}$ = 7Hz, $^3J_{PH}$ = 6Hz, CH(CH_3)$_2$), 1.73 and 2.43 (m, 2H, CH(CH_3)$_2$), 6.11 (t, 1H, $^4J_{HH}$ = 1Hz, Cp-H), 6.67 (t, 1H, $^3J_{HH}$ = 7Hz, p-C$_6$H$_5$), 7.09 (d, 2H, $^4J_{HH}$ = 1Hz, Cp-H), 7.16 (t, 2H, $^3J_{HH}$ = 7Hz, m-C$_6$H$_5$), 7.33 (s, 1H, CHPh), 7.45 (d, 2H, $^4J_{HH}$ = 7Hz, o-C$_6$H$_5$). ^{31}P NMR (20 °C, C$_6$D$_6$): δ 23.4 (s). Anal. Calcd. for C$_{30}$H$_{53}$ClHfP$_2$Si$_2$(C$_7$H$_8$)$_{0.5}$: C, 50.81; H, 7.25 Found: C, 50.86; H, 7.51.

3.6.2.3 ^{Pr}[P$_2$Cp]Zr=CHCMe$_3$(Cl) (18a)

A solution of LiCH$_2$CMe$_3$ (51 mg, 0.65 mmol) in 20 mL of toluene was added dropwise with stirring to a cooled (-78 °C) solution of **1** (210 mg, 0.33 mmol) dissolved in 60 mL of toluene. The colour of the solution immediately changed to bright yellow. The solution was stirred at -78 °C to 0 °C for another 30 minutes, and then for another 3 hours at room temperature. The solvent was then removed in vacuo, and the residue extracted with hexanes and filtered. The filtrate was reduced under vacuum to give a green oil which was redissolved in 30 mL of toluene. This solution was placed in a 95 °C oilbath for 6 days, after which no further reaction could be detected by NMR spectroscopy. The solvent was removed, and the oil extracted with pentane to give a green oil, containing **18a** and other unidentified products. Repeated attempts to obtain crystals from cold pentane were unsuccessful. Estimated yield: (65% by ^{31}P NMR spectroscopy). ^{1}H NMR (20 °C, C$_6$D$_6$): δ 0.38 and 0.40 (s, 6H, Si(CH_3)$_2$), 0.80 (dd, 4H, $^2J_{HH}$ = 6Hz, $^2J_{PH}$ = 7Hz, SiCH_2P), 1.10 and 1.30 (m, 12H, CH(CH_3)$_2$), 1.50 (s, 9H, CHC(CH_3)$_3$), 2.10 (m, 4H, CH(CH$_3$)$_2$), 6.60 (d, 2H, $^4J_{HH}$ = 1Hz, C$_5H$), 7.41 (t, 1H, $^4J_{HH}$ = 1Hz, C$_5H$), 8.20 (s, 1H, CHC(CH_3)$_3$). ^{31}P NMR (20 °C, C$_6$D$_6$): δ 14.0 (s).

3.6.2.4 ^{Pr}[P$_2$Cp]Zr=CHSiMe$_3$(Cl) (18b)

A solution of LiCH$_2$SiMe$_3$ (155 mg, 1.64 mmol) in 30 mL of toluene was added dropwise with stirring to a cooled (-78 °C) solution of **1** (525 mg, 0.82 mmol) dissolved in 90 mL of toluene. The colour of the solution immediately changed from pale yellow to bright yellowish green. The solution was stirred at -78 °C to 0 °C for another 30 minutes, and then for another 2 hours at room temperature. The solvent was then removed, and the residue extracted with hexanes and filtered. The filtrate was reduced under vacuum to give a greenish yellow oil which was redissolved in 60 mL toluene. This solution was placed in a 95 °C oilbath for 3 days, after which the volume was reduced under vacuum to 1 mL and 5 mL hexanes added. Bright yellow

crystals were slowly obtained from this concentrated solution at -40 °C. The supernatant solution was filtered away, and the crystals washed twice with cold hexanes and dried under vacuum. More crystalline material could be obtained from the mother liquor. Yield: (440 mg, 82 %). ^{1}H NMR (20 °C, C_6D_6): δ 0.21 and 0.53 (s, 6H, Si(CH_3)$_2$), 0.32 (s, 9H, CHSi(CH_3)$_3$), 0.68 and 0.72 (dd, 4H, $^2J_{HH}$ = 6Hz, $^2J_{PH}$ = 7Hz, SiCH_2P), 1.04 and 1.48 (m, 12H, CH(CH_3)$_2$), 2.11 and 2.29 (m, 2H, CH(CH$_3$)$_2$), 6.07 (d, 2H, $^4J_{HH}$ = 1Hz, C$_5H$), 7.30 (t, 1H, $^4J_{HH}$ = 1Hz, C$_5H$), 8.99 (s, , CHSi(CH_3)$_3$). ^{31}P NMR (20 °C, C_6D_6): δ 16.2 (s). ^{13}C NMR (20 °C, C_6D_6): δ 5.9 and 11.1 (Si(CH_3)$_2$), 7.9 (CH(CH_3)$_2$), 16.5 (SiCH_2P), 25.6 and 30.9 (CH(CH_3)$_2$), 26.6 (CHSi(CH_3)$_3$), 35.4 and 35.5 (CH(CH$_3$)$_2$), 119.0 (Cp), 121.9 (Cp), 129.5 (Cp), 213.8 (t, $^2J_{PC}$ = 12Hz, CHSi(CH$_3$)$_3$). Anal. Calcd. for $C_{27}H_{57}ClP_2Si_3Zr$: C, 49.54; H, 8.78; Cl, 5.42. Found: C, 49.58; H, 8.71; Cl, 5.65.

3.6.2.5 ^{Pr}[P$_2$Cp]ZrCl(CH$_2$CMe$_3$)$_2$ (19a)

A solution of LiCH$_2$CMe$_3$ (1.09 mg, 0.24 mmol) in 60 mL of toluene was added dropwise to a cooled (-78 °C) stirring solution of **1** (350 mg, 0.58 mmol) dissolved in 60 mL of toluene. The colour of the solution immediately changed in intensity from pale to bright yellow. The solution was allowed to warm slowly to room temperature and stirred for another 2 hours. The solvent was then removed in vacuo, and the residue extracted with hexanes and filtered. The filtrate was reduced to give a bright yellow oil consisting of **19a**, in addition to trialkyl **5a** and monoalkyl **7a**. The assignment of resonances for **19a** is based on the known resonances for **5a** and **7a** obtained by independent syntheses. ^{1}H NMR (20 °C, C_6D_6): δ 0.45 and 0.47 (s, 6H, Si(CH_3)$_2$), 0.63 (d, 4H, $^2J_{HH}$ = 6Hz, SiCH_2P), 0.89 (m, 24H, CH(CH_3)$_2$), 1.23 (s, 18H, CH$_2$C(CH_3)$_3$), 1.31 and 1.78 (d, 2H, $^2J_{HH}$ = 8Hz, CH_2C(CH$_3$)$_3$), 1.55 (m, 4H, CH(CH$_3$)$_2$), 6.82 (d, 2H, $^4J_{HH}$ = 1Hz, Cp-H), 7.03 (t, 1H, $^4J_{HH}$ = 1Hz, Cp-H). ^{31}P NMR (20 °C, C_6D_6): δ -5.9 (s).

3.6.2.6 $^{Pr}[P_2Cp]ZrCl(CH_2SiMe_3)_2$ (19b)

The procedure followed is analogous to that for **19a** above, using $LiCH_2SiMe_3$ (117 mg, 1.24 mmol) and **1** (398 mg, 0.62 mmol). The resulting greenish oil consists of **19b**, trialkyl **5b**, and monoalkyl **7b**. Again, the assignment for **7b** is based on integration of the ^1H NMR spectrum. ^1H NMR (20 °C, C_6D_6): δ 0.32 (s, 18H, $CH_2Si(CH_3)_3$), 0.41 and 0.43 (s, 6H, $Si(CH_3)_2$), 0.63 (d, 4H, $^2J_{HH}$ = 6Hz, $SiCH_2P$), 0.70 and 1.14 (d, 2H, $^2J_{HH}$ = 12Hz, $CH_2Si(CH_3)_3$), 0.99 (m, 24H, $CH(CH_3)_2$), 1.57 (m, 4H, $CH(CH_3)_2$), 6.81 (t, 1H, $^4J_{HH}$ = 1Hz, Cp-*H*), 6.86 (d, 2H, $^4J_{HH}$ = 1Hz, Cp-*H*). ^{31}P NMR (20 °C, C_6D_6): δ -4.5 (s).

3.6.2.7 $^{Pr}[P_2Cp]Zr(\eta^2-CH_2=CH_2)Cl$ (20)

A solution of Zr alkylidene **16** (1.932 g, 2.93 mmol) in 60 mL of toluene was placed in a 200 mL reactor equipped with a needle valve and affixed to a dual vacuum/nitrogen line. A small portion of solvent was removed under vacuum, and an atmosphere of ethylene introduced at -78 °C. The reaction mixture was warmed to room temperature and left to stir for 12 h, during which time the colour of the solution gradually changed from bright yellowish-orange to dark red. The solvent was then removed in vacuo, and the oily residue extracted with pentane and filtered. Reducing the solution to 7 mL and cooling to -40 °C produced dark red crystals. Yield 1.61 g (92 %).

Method 2. The procedure was identical to that for **16** above, reacting Zr alkylidene **18b** with ethylene. A reaction conducted on the same scale as above was complete within 8 h.

^1H NMR (20°C, C_6D_6): δ 0.22 and 0.23 (s, 6H, $Si(CH_3)_2$), 0.78 and 0.83 (d, 2H, $^2J_{PH}$ = 5Hz, $SiCH_2P$), 0.99 and 1.04 (m, 2H, $ZrCH_2=CH_2$), 1.08, 1.17, 1.22 and 1.29 (dd, 6H, $^3J_{PH}$ = 9Hz, $^2J_{HH}$ = 7Hz, $CH(CH_3)_2$), 2.19 (m, 4H, $^2J_{HH}$ = 7Hz, $^2J_{PH}$ = 7Hz, $CH(CH_3)_2$), 4.32 (t, 1H,

$^4J_{HH}$ = 1Hz, Cp-*H*), 6.29 (d, 2H, $^4J_{HH}$ = 1Hz, Cp-*H*). ^{31}P{^{1}H} NMR (20°C, C_6D_6): δ 19.5 (s). ^{13}C{^{1}H} NMR (20°C, C_6D_6): δ -2.0 and 1.6 (Si(*CH*$_3$)$_2$), 9.3 (Si*CH*$_2$P), 9.3, 13.5, 22.7 and 25.4 (CH(*CH*$_3$)$_2$), 31.4 (Zr*CH*$_2$), 31.5 (CH(*CH*$_3$)$_2$), 106.8 (Cp-CH), 125.9 (Cp-CH). Anal. Calcd. for C$_{25}$H$_{51}$ClP$_2$Si$_2$Zr: C, 50.34; H, 8.62. Found: C, 50.35; H, 8.51.

3.6.2.8 ^{Pr}[P$_2$Cp]ZrC(O)=CHPh(Cl) (21a)

A solution of **16** (1.390 g, 2.11 mmol) in 60 mL of toluene was placed in a 200 mL bomb and affixed to a dual vacuum/nitrogen line. A small portion of solvent was removed under vacuum, and an atmosphere of carbon monoxide introduced. The reaction mixture was left to stir at room temperature for 48 hrs, during which the colour of the solution gradually changed from bright yellowish-orange to reddish-orange. The solution was then filtered, and the filtrate reduced to 3 mL and layered with hexanes . Orange crystals were obtained from this solution at -40 °C. Yield 1.26 g (87 %). ^{1}H NMR (20 °C, C_6D_6): δ 0.20 and 0.46 (s, 6H, Si(*CH$_3$*)$_2$), 0.70 (dd, 4H, $^2J_{HH}$ = 6Hz, $^2J_{PH}$ = 7Hz, Si*CH$_2$*P), 0.67, 0.95, 1.20, and 1.36 (dd, 6H, $^3J_{PH}$ = 9Hz, $^2J_{HH}$ = 7Hz, CH(*CH$_3$*)$_2$), 2.10 (m, 4H, C*H*(CH$_3$)$_2$), 5.96 (s, 1H, C*H*Ph), 6.60 (d, 2H, $^4J_{HH}$ = 1Hz, Cp-*H*), 7.09 (t, 1H, $^3J_{HH}$ = 7Hz, p-C$_6$H$_5$), 7.14 (t, 1H, $^4J_{HH}$ = 1Hz, Cp-*H*), 7.39 (t, 2H, $^3J_{HH}$ = 7Hz, m-C$_6$H$_5$), 8.09 (d, 2H, $^3J_{HH}$ = 7Hz, o-C$_6$H$_5$). ^{31}P NMR (20 °C, C_6D_6): δ 9.5 (s). ^{13}C NMR (20 °C, C_6D_6): δ -1.4 and 0.7 (Si(*CH$_3$*)$_2$), 9.9 (Si*CH$_2$*P), 17.5, 19.9, 26.2 and 30.9 (CH(*CH$_3$*)$_2$), 102.3 (*C*HPh), 117.1 (CpSi), 122.3 (Cp-CH2), 125.1 (p-C$_6$H$_5$), 126.3 (Cp-CH), 129.2 (m-C$_6$H$_5$), 142.0 (o-C$_6$H$_5$), 205.1 (t, $^2J_{CP}$ = 14Hz, *C*(O)=C). Anal. Calcd. for C$_{31}$H$_{53}$ClOP$_2$Si$_2$Zr: C, 54.23; H, 7.78. Found: C, 54.35; H, 7.85.

3.6.2.9 $^{Pr}[P_2Cp]ZrC(O)=CHSiMe_3(Cl)$ (21b)

The procedure followed was similar to that for **21a**, by reacting **18b** (0.98 g, 1.50 mmol) in an atmosphere of CO. The reaction mixture was left to stir at room temperature for 48 hrs, during which no colour change in the solution was noted. The solvent was then removed in vacuo, and the oily residue extracted with hexanes and filtered, yielding a hydrocarbon-soluble orange oil from which crystals could not be obtained. Yield 0.87 g (85%); spectroscopic data for the major isomer: ^{1}H NMR (20 °C, C_6D_6): δ 0.18 and 0.41 (s, 6H, Si(CH_3)$_2$), 0.48 (s, 9H, CHSi(CH_3)$_3$), 0.82 (dd, 4H, $^2J_{HH}$ = 5Hz, $^2J_{PH}$ = 7Hz, SiCH_2P), 1.12 (m, 24H, CH(CH_3)$_2$), 2.38 (m, 4H, CH(CH$_3$)$_2$), 4.39 (s, 1H, CHSi(CH$_3$)$_3$), 6.18 (t, 1H, $^4J_{HH}$ = 1Hz, Cp-H), 6.43 (d, 2H, $^4J_{HH}$ = 1Hz, Cp-H). ^{31}P NMR (20 °C, C_6D_6): δ 11.9 (s).

3.6.2.10 $^{Pr}[P_2Cp]ZrC(N^tBu)=CHPh(Cl)$ (22)

A toluene solution of 0.088 M tert-butyl-isocyanide (6.4 mL, 0.56 mmol) was added dropwise with stirring to a cooled (0 °C) solution of **16** (366 mg, 0.56 mmol) dissolved in 60 mL of toluene. The reaction mixture was stirred at 0 °C for another 30 minutes, and then slowly warmed to room temperature, during which colour of the solution gradually changed from bright orange to dark red. The solution was stirred at room temperature for another 12 hours, the solvent then removed in *vacuo*, and the residue extracted with hexanes and filtered. The solution was reduced to 5 mL, from which dark red crystalline needles were obtained at -40 °C. Yield 320 mg (77%). ^{1}H NMR (20 °C, C_6D_6): δ 0.20 (br s, 6H, Si(CH_3)$_2$), 0.40 (s, 6H, Si(CH_3)$_2$), 0.69 (m, 4H, SiCH_2P), 1.03 (m, 24H, CH(CH_3)$_2$), 1.57 (s, 9H, N(CH_3)$_3$), 1.82 (m, 2H, CH(CH$_3$)$_2$), 2.49. (br m, 2H, CH(CH$_3$)$_2$), 6.55 (s, 1H, CHPh), 6.80 (d, 2H, $^4J_{HH}$ = 1Hz, C_5H), 6.89 (t, 1H, $^4J_{HH}$ = 1Hz, C_5H), 7.02 (t, 1H, $^3J_{HH}$ = 7Hz, p-C_6H_5), 7.37 (t, 2H, $^3J_{HH}$ = 7Hz, m-C_6H_5), 8.20 (br m, 2H, o-C_6H_5). ^{31}P NMR (20 °C, C_6D_6): δ 11.8 (s). Anal. Calcd. for $C_{35}H_{62}ClNP_2Si_2Zr$: C, 56.68; H, 8.43; N, 1.89. Found: C, 56.85; H, 8.49; N 1.91.

3.6.2.11 [P₂Cp]ZrCH₂CH₂C(O)=CHPh(Cl) (23a)

A solution of **21a** (1.09 g, 1.59 mmol) in 60 mL of toluene was placed in a bomb and affixed to a dual vacuum line. The head space was partially evacuated, and an atmosphere of ethylene introduced. The solution was left to stir at room temperature for 48 hrs, during which the orange colour of the solution slowly turned red. The solvent was then removed in vacuo, and the oily residue extracted with hexanes and filtered. The solution was reduced to 5 mL, from which orange crystals were obtained at -40 °C. Yield 0.87 g (77%). ^{1}H NMR (20 °C, C₆D₆): δ 0.24 and 0.49 (s, 6H, Si(CH_3)₂), 0.72 (dd, 4H, $^2J_{HH}$ = 6Hz, $^2J_{PH}$ = 7Hz, SiCH_2P), 0.97 and 1.17 (m, 12H, CH(CH_3)₂), 1.50 (m, 2H, ZrCH_2CH₂), 2.09 and 2.21 (m, 2H, CH(CH₃)₂), 3.41 (t, 2H, $^3J_{HH}$ = 7Hz, ZrCH₂CH_2), 5.43 (s, 1H, CHPh), 6.79 (d, 2H, $^4J_{HH}$ = 2Hz, Cp-H), 7.01 (t, 1H, $^4J_{HH}$ = 1Hz, Cp-H), 7.06 (t, 1H, $^3J_{HH}$ = 7Hz, p-C₆H₅), 7.42 (t, 2H, $^3J_{HH}$ = 7Hz, m-C₆H₅), 8.05 (d, 2H, $^3J_{HH}$ = 7Hz, o-C₆H₅). ^{31}P NMR (20 °C, C₆D₆): δ 7.8 (s). Anal. Calcd. for C₃₃H₅₇ClOP₂Si₂Zr: C, 55.47; H, 8.04. Found: C, 55.67; H, 8.19.

3.6.2.12 ^{Pr}[P₂Cp]ZrCH₂CH₂C(O)=CHSiMe₃(Cl) (23b)

The procedure followed was analogous to that for **23a** above, reacting **21b** (0.80 g, 1.17 mmol) with an atmosphere of ethylene. The reaction mixture was left to stir at room temperature for 36 hrs, during which there was no colour change to the orange solution. The solution was concentrated to 2 mL and layered with hexanes, from which orange crystals were obtained at -40 °C from a solution consisting of toluene/hexanes in a 1:1 mixture. Yield 0.66 g (79 %). ^{1}H NMR (20 °C, C₆D₆): δ 0.28 and 0.48 (s, 6H, Si(CH_3)₂), 0.47 (s, 18H, CHSi(CH_3)₃), 0.91 (d, 4H, $^2J_{HH}$ = 6Hz, SiCH_2P), 1.11 (m, 24H, CH(CH_3)₂), 1.39 (m, 2H, ZrCH_2CH₂), 2.21 (m, 4H, CH(CH₃)₂), 3.34 (t, 2H, $^3J_{HH}$ = 7Hz, ZrCH₂CH_2), 4.22 (s, 1H, CHSi(CH₃)₃), 6.59 (d, 2H, $^4J_{HH}$

= 1Hz, Cp-*H*), 6.90 (t, 1H, $^4J_{HH}$ = 1Hz, Cp-*H*). ^{31}P NMR (20 °C, C$_6$D$_6$): δ 8.2 (s). Anal. Calcd. for C$_{30}$H$_{61}$ClOP$_2$Si$_3$Zr: C, 50.70; H, 8.65. Found: C, 50.60; H, 8.57.

3.6.2.13 ^{Pr}[P$_2$Cp]ZrC(O)CH$_2$CH$_2$C(O)=CHPh(Cl) (24a)

A solution of **23a** (0.64 g, 0.90 mmol) in 30 mL of toluene was placed in a bomb and affixed to a dual vacuum line. An atmosphere of carbon monoxide was introduced at -78 °C, and the reaction mixture was warmed to room temperature and stirred for 24 hrs, during which the reddish solution gradually faded to an orange-yellow colour. The solvent was then reduced to 5 mL and layered with hexanes, from which yellow crystals were obtained at -40 °C. Yield 0.54 g (80%). ^{1}H NMR (20 °C, C$_6$D$_6$): δ 0.01 and 0.28 (s, 6H, Si(C*H$_3$*)$_2$), 0.61 (dd, 2H, $^2J_{HH}$ = 6Hz, $^2J_{PH}$ = 6Hz, SiC*H$_2$*P), 0.71 (dd, 2H, $^2J_{HH}$ = 6Hz, $^2J_{PH}$ = 6Hz, SiC*H$_2$*P), 0.91 (m, 24H, CH(C*H$_3$*)$_2$), 1.62 (m, 4H, C*H*(CH$_3$)$_2$), 2.19 (m, 2H, C=CC*H$_2$*), 2.75 (m, 2H, ZrCC*H$_2$*), 5.06 (s, 1H, C*H*Ph), 6.72 (dd, 1H, Cp-*H*), 6.83 (dd, 1H, Cp-*H*), 7.02 (t, 1H, $^3J_{HH}$ = 7Hz, p-C$_6$H$_5$), 7.23 (dd, 1H, Cp-*H*), 7.30 (t, 2H, $^3J_{HH}$ = 7Hz, m-C$_6$H$_5$), 7.94 (d, 2H, $^3J_{HH}$ = 7Hz, o-C$_6$H$_5$), . ^{31}P NMR (20 °C, C$_6$D$_6$): δ 46.8 (s), -5.1 (s). Anal. Calcd. for C$_{34}$H$_{57}$ClO$_2$P$_2$Si$_3$Zr(C$_7$H$_8$)$_{0.5}$: C, 57.11; H, 7.80. Found: C, 57.30; H, 7.80.

3.6.2.14 ^{Pr}[P$_2$Cp]ZrC(O)CH$_2$CH$_2$C(O)=CHSiMe$_3$(Cl) (24b)

The procedure followed was similar to that for **24a**, by reacting **23b** (0.50 g, 0.70 mmol) with an atmosphere of CO. There was no obvious colour change to the orange solution after stirring at room temperature for 48 hrs. The solvent was then removed and the residue extracted with hexanes and filtered. A yellow-orange crystalline solid was isolated from a cold, concentrated hexanes solution. Yield: (0.39 mg, 76 %). ^{1}H NMR (20 °C, C$_6$D$_6$): δ 0.02, 0.19, 0.32 and 0.49 (s, 3H, Si(C*H$_3$*)$_2$), 0.48 (s, 9H, CHSi(C*H$_3$*)$_3$), 0.60 (dd, 4H, $^2J_{HH}$ = 7Hz, $^2J_{PH}$ =

7Hz, SiCH_2P), 0.85 and 1.09 (m, 12H, CH(CH_3)$_2$), 1.62 (m, 1H, C=CCH_2), 1.67 (m, 4H, CH(CH$_3$)$_2$), 2.04 (dd, 1H, C=CCH_2), 2.21 (dd, 1H, ZrCCH_2), 2.74 (dd, 1H, ZrCCH_2), 4.04 (s, 1H, CHSi(CH$_3$)$_3$), 6.71 (dd, 1H, Cp-H), 6.83 (dd, 1H, Cp-H), 7.10 (dd, 1H, Cp-H). ^{31}P NMR (20 °C, C$_6$D$_6$): δ 46.2 (s), -5.9 (s). Anal. Calcd. for C$_{31}$H$_{61}$ClO$_2$P$_2$Si$_3$Zr: C, 50.40; H, 8.32. Found: C, 50.42; H, 8.35.

3.6.3 NMR study of the equilibrium between 3, 12, and 14

Separate stock solutions of [3] and [12] were prepared in benzene-d_6, the concentrations of which were determined by comparing the integrated intensity of the CH_2Ph signals relative to external ferrocene. Incrementally varied proportions of these initial solutions were combined together to generate mixed solutions consisting of 3, 12 and 14. The concentrations were calculated from the integration of the CH_2Ph signals in the ^{1}H NMR spectra with respect to that of the ferrocene standard.

3.6.4 Kinetic studies of the formation of alkylidene 16 and 18b

A sample of the equilibrium mixture consisting of monobenzyl 12, dibenzyl 14 and tribenzyl 3 was dissolved in toluene-d_8 and used as a stock solution for kinetic study. The initial concentrations in this solution were calculated from the integration of the ^{31}P NMR signals of a representative sample with respect to that of the internal standard PPh$_3$. The disappearance of 14 and 3 (and the concomitant appearance of 16) as recorded by ^{31}P\{^{1}H\} NMR spectroscopy was monitored for a period of at least three half-lives; samples with an internal PPh$_3$ reference were employed to calibrate the measurements. Separate kinetic runs were conducted on the Varian 300-XL instrument at temperatures set to 70, 80, 85 and 90 °C. The uncertainty in the temperature settings was estimated to be +/- 1 °C. Similar experiments with the CD$_2$C$_6$D$_5$

labeled complexes were performed at 70 °C to examine kinetic isotope effects (KIE) associated with the proposed mechanism. Each experiment was repeated at least once to indicate reproducibility. For the duration of the kinetic experiments, all sample tubes were protected from light sources where possible using metal foil wrap to minimize the competitive photochemical transformation of **14** to **16**.

A similar procedure was followed for the study into the formation of neosilyl **18b**, except the $^{31}P\{^1H\}$ NMR spectra were conducted at 20 °C, as the resonances due to dialkyl **19b** and trialkyl **7b** merge together at higher temperatures. For a typical run, a 0.5 mL sample of the toluene solution was placed in a 5mm NMR tube, the solution frozen and degassed, and the tube then flame sealed and placed in a constant temperature oil bath (uncertainty in the temperature measurements estimated to be 1 °C). The tube was removed from the bath after a period of 1.5 hours and immersed in an ice bath to quench the reaction. A $^{31}P\{1H\}$ NMR spectrum was recorded at 20 °C on the Bruker-AMX 500 MHz instrument, and the tube returned to the oil bath. This procedure was repeated with further 1.5 hour heating intervals, and the disappearance of **5b** and **19b** (and the concomitant appearance of **18b**) as recorded by $^{31}P\{^1H\}$ NMR spectroscopy was monitored for a period of at least three half-lives. Kinetic experiments were conducted at four different temperatures (80 °C, 95 °C, 110 °C, and 125 °C) to obtain separate reaction rates.

3.7   References

(1)   Schrock, R. R. *J. Am. Chem. Soc.* **1974**, *96*, 6796.

(2)   Fryzuk, M. D.; Mao, S. S. H.; Zaworotko, M. J.; MacGillivray, L. R. *J. Am. Chem. Soc.* **1993**, *115*, 5336.

(3)   Schwartz, J.; Gell, K. I. *J. Organomet. Chem.* **1980**, *184*, C1.

(4)   *Comprehensive Organometallic Chemistry*; 2 ed.; Wilkinson, G.; Stone, F. G. A.; Abel, E. W., Ed.; Pergamon: New York, 1995; Vol. 3.

(5)   Schrock, R. R. *Acc . Chem. Res.* **1979**, *12*, 98.

(6)   Wengrovius, J. H.; Schrock, R. R. *J. Organomet. Chem.* **1981**, *205*, 319.

(7)   Li, L.; Hung, M.; Xue, Z. *J. Am. Chem. Soc.* **1995**, *117*, 12746.

(8)   Wood, C. D.; McLain, S. J.; Schrock, R. R. *J. Am. Chem. Soc.* **1979**, *101*, 3210.

(9)   Cheon, J.; Rogers, D. M.; Girolami, G. S. *J. Am. Chem. Soc.* **1997**, *119*, 6804.

(10)   Beckhaus, R. *Angew. Chem., Int. Ed. Engl.* **1997**, *36*, 686.

(11)   Doorn, J. A. v.; Heijden, H. v. d.; Orpen, A. G. *Organometallics* **1995**, *14*, 1278.

(12)   Sinnema, P.-J.; Veen, L.; Spek, A. L.; Veldman, N.; Teben, H. H. *Organometallics* **1997**, *16*, 4245.

(13)   Thorn, M. G.; Hill, J. E.; Waratuke, S. A.; Johnson, E. S.; Fanwick, P. E.; Rothwell, I. P. *J. Am. Chem. Soc.* **1997**, *119*, 8630.

(14)   Vaughan, W. M.; Abboud, K. A.; Boncella, J. M. *J. Am. Chem. Soc.* **1995**, *117*, 11015.

(15)   McDade, C.; Green, J. C.; Bercaw, J. E. *Organometallics* **1982**, *1*, 1629.

(16)   Malatesta, V.; Ingold, K. U.; Schrock, R. R. *J. Organomet. Chem.* **1978**, *152*, C53.

(17)   Wallace, K. C.; Liu, A. H.; Dewan, J. C.; Schrock, R. R. *J. Am. Chem. Soc.* **1988**, *110*, 4964.

(18)   Schrock, R. R. *Acc. Chem. Res.* **1990**, *23*, 158.

(19)   Herrmann, W. A.; Stumpf, A. W.; Priermeier, T.; Bogdanovic, S.; Dufaud, V.; Basset, J.-M. *Angew. Chem., Int. Ed. Engl.* **1996**, *35*, 2803.

(20)   Schuster, M.; Blechert, S. *Angew. Chem., Int. Ed. Engl.* **1997**, *36*, 2036.

(21)   Wallace, K. C.; Liu, A. H.; Davis, W. M.; Schrock, R. R. *Organometallics* **1989**, *8*, 644.

(22)   Aguero, A.; Kress, J.; Osborn, J. A. *J. Chem. Soc., Chem. Commun.* **1986**, 531.

(23)   Schrock, R. R.; dePue, R. T.; Feldman, J.; Schaverien, C. J.; Dewan, J. C.; Liu, A. H. *J. Am. Chem. Soc.* **1988**, *110*, 1423.

(24)   Fujimura, O.; Fu, G. C.; Rothemund, P. W. K.; Grubbs, R. H. *J. Am. Chem. Soc.* **1995**, *117*, 2355.

(25)   Schrock, R. R. *Pure App. Chem.* **1994**, *66*, 1447.

(26)   Grubbs, R. H.; Miller, S. J.; Fu, G. C. *Acc Chem Res* **1997**, *28*, 446.

(27)   Elschenbroich, C.; Salzer, A. *Organometallics;* 2nd ed.; Verlagsgesellschaft: Weinham, 1992.

(28)   McLain, S. J.; Wood, C. D.; Schrock, R. R. *J. Am. Chem. Soc.* **1979**, *101*, 4558.

(29)   Takahashi, T.; Murakama, M.; Kunishige, M.; Saburi, M.; Uchida, Y.; Kozawa, K.; Uchida, T.; Swanson, D. R.; Negishi, E. *Chem. Lett.* **1989**, 761.

(30)   Takahashi, T.; Suzuki, N.; Kageyama, M.; Nitto, Y.; Saburi, M.; Negishi, E. *Chem. Lett.* **1991**, 1579.

(31)   Poole, A. D.; Gibson, V. C.; Clegg, W. *J. Chem. Soc., Chem. Commun.* **1992**, 237.

(32)   Bartell, L. S.; Roth, E. A.; Hollowell, C. D.; Kuchitsu, K.; Young, J. E. *J. Chem. Phys.* **1965**, *42*, 2683.

(33)   Alt, H. G.; Denner, C. E.; Thewalt, U.; Raush, M. D. *J. Organomet. Chem.* **1988**, *356*, C83.

(34)   Wu, Z.; Jordan, R. F.; Petersen, J. L. *J. Am. Chem. Soc.* **1995**, *117*, 5867.

(35)   Kubácek, P.; Hoffmann, R.; Havias, Z. *Organometallics* **1982**, *1*, 180.

(36)   Poli, R. *Organometallics* **1990**, *9*, 1892.

(37)   Wallace, K. C.; Dewan, J. C.; Schrock, R. R. *Organometallics* **1986**, *5*, 2162.

(38)   Fellman, J. D.; Schrock, R. R.; Rupprecht, G. A. *J. Am. Chem. Soc.* **1981**, *103*, 5752.

(39)   McLain, S. J.; Wood, C. D.; Schrock, R. R. *J. Am. Chem. Soc.* **1977**, *99*, 3519.

(40)   Cramer, R. E.; Maynard, R. B.; Paw, J. C.; Gilje, J. W. *Organometallics* **1982**, *1*, 869.

(41)   Meinhart, J. D.; Anslyn, E. V.; Grubbs, R. H. *Organometallics* **1989**, *8*, 583.

(42)   Sierra, M. A.; Hegedus, L. S. *J. Am. Chem. Soc.* **1989**, *111*, 2335.

(43)   Anderson, B. A.; Wulff, W. D.; Rheingold, A. L. *J. Am. Chem. Soc.* **1990**, *112*, 8615.

(44)   Brandvold, T. A.; Wulff, W. D.; Rheingold, A. L. *J. Am. Chem. Soc.* **1990**, *112*, 1645.

(45)   Meinhart, J. D.; Santarsiero, B. D.; Grubbs, R. H. *J. Am. Chem. Soc.* **1986**, *108*, 3318.

(46) Bristow, G. S.; Hitchcock, P. B.; Lappert, M. F. *J. Chem. Soc., Chem. Commun.* **1982**, 462.

(47) Moore, E. J.; Straus, D. A.; Armantrout, J.; Santarsiero, B. D.; Grubbs, R. H.; Bercaw, J. E. *J. Am. Chem. Soc.* **1983**, *105*, 2068.

(48) Fachinetti, G.; Biran, C.; Floriani, C. *J. Am. Chem. Soc.* **1978**, *100*, 1921.

(49) Scott, M. J.; Lippard, S. J. *J. Am. Chem. Soc.* **1997**, *119*, 3411.

(50) Fermin, M. C.; Hneihen, A. S.; Maas, J. L.; Bruno, J. W. *Organometallics* **1993**, *12*, 1845.

(51) Antiñolo, A.; Otero, A.; Fajardo, M.; López-Mardomingo, C.; Lucas, D.; Mugnier, Y.; Lanfranchi, M.; Pellinghelli, M. *J. Organomet. Chem.* **1992**, *435*, 55.

(52) Antiñolo, A.; Fajardo, M.; López-Mardomingo, C.; Otero, A.; Mourad, Y.; Mugnier, Y.; Aparicio, J.; Fonseca, I.; Florencio, F. *Organometallics* **1990**, *9*, 2919.

(53) Antiñolo, A.; Fajardo, M.; Gil-Sanz, R.; López-Mardomingo, C.; Martín-Villa, P.; Otero, A.; Kubicki, M.; Mugnier, Y.; Krami, S.; Mourad, Y. *Organometallics* **1993**, *12*, 381.

(54) Antiñolo, A.; Fajardo, M.; Gil-Sanz, R.; López-Mardomingo, C.; Otero, A.; Atmani, A.; Kubicki, M.; Krami, S.; Mugnier, Y.; Mourad, Y. *Organometallics* **1994**, *13*, 1200.

(55) Fandos, R.; Lanfranchi, M.; Otero, A.; Pellinghelli, M.; Ruiz, M.; Teuben, J. *Organometallics* **1997**, *16*, 5283.

(56) Straus, D. A.; Grubbs, R. H. *J. Am. Chem. Soc.* **1982**, *104*, 5499.

(57) Fryzuk, M. D.; Mylvaganum, M.; Zaworotko, M. J.; MacGillivray, L. R. *Organometallics* **1996**, *15*, 1134.

Chapter 4

Effects of Ligand Modification on

Structure and Reactivity

4.1   Introduction

In the previous two chapters the solution behaviour and reactivity of zirconium and hafnium complexes stabilized by the $^{Pr}[P_2Cp]$ ancillary ligand were detailed. This final chapter will cover preliminary efforts to examine the effects on structure and reactivity resulting from modifications of this general system. There are two areas where alterations of the ligand can be made. The first strategy involves replacement of the isopropyl substituents with smaller methyl groups. The steric bulk of the isopropyl group has been demonstrated to be advantageous in the stabilization of alkylidene and ketene complexes, but at the expense of imposed limitations in the reactivity of these complexes. The sterically hindered phosphines exhibit complicated fluxional coordination in several of the alkyl species, which is a factor in the inability to isolate dialkyl derivatives. The increased aliphatic content of the isopropyl groups also contributes to increased solubility in organic solvents and introduces complications in separation and characterization. Employing methyl substituents is anticipated to improve the ability of the phosphines to coordinate, thus reducing the tendency for fluxional solution behaviour and introducing different steric and electronic influences on the reactivity.

One of the topics for future work will address a second direction for ligand modification, which entails placing a bulky substituent on the Cp ring to force the side-arms away from the 1,3-configuration to adjacent 1,2-positions on the ring. Preliminary results assess whether this

change induces the phosphines to switch from *trans* to *syn* positions in the coordination sphere, and will lead to a brief structural comparison of a few Zr(III) derivatives. Another approach to changing the system is to extend the coordination chemistry of this ancillary ligand with other metals. The ligand framework is such that the appendment of two side-arms to a central Cp donor creates a wide chelate that is a potentially compatible fit with a larger metal ion such as Th(IV).

4.2 Preparation of $^{Me}[P_2Cp]$ ZrCl$_3$

A toluene solution of the ancillary ligand $^{Me}[P_2Cp]Li$ reacts with $ZrCl_4(THT)_2$ to give the trichloride complex $^{Me}[P_2Cp]ZrCl_3$ (**25**) as colourless crystals (equation 4.1). The $^{31}P\{^1H\}$ NMR spectrum shows a singlet at -21.0 ppm for two equivalent coordinated phosphines, while the ^1H NMR spectrum resembles that found in the Pr^i derivative **1**, with a nearly identical pattern for the Cp resonances in the downfield region of the spectrum. The structure of **25** is thus considered to have the same C_s-symmetric quasi-octahedral geometry as determined previously for **1**.

(4.1)

25
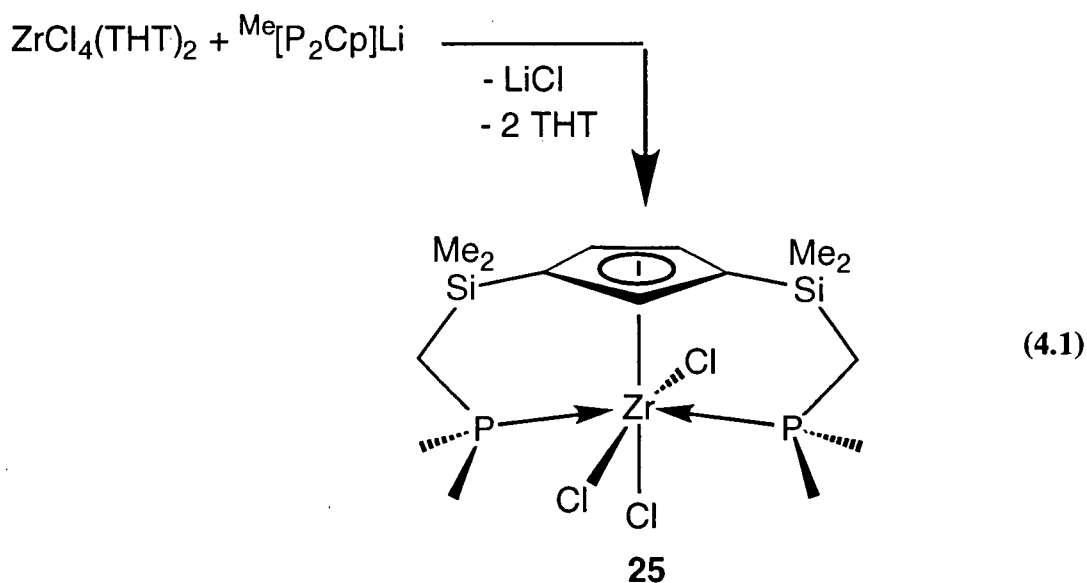
This compound has considerably lower solubility in toluene in comparison to **1**; therefore the reactions outlined below are all conducted in THF solvent.

4.3.1 Preparation of ^{Me}[P$_2$Cp]ZrCl$_2$(CH$_2$Ph)

The addition of 1 equivalent of KCH$_2$Ph to a THF solution of trichloride **25** generates the monobenzyl complex ^{Me}[P$_2$Cp]ZrCl$_2$(CH$_2$Ph) (**26**) as a red solid (equation 4.2). The ^{1}H NMR spectrum is consistent with the stoichiometry of one benzyl group per P$_2$Cp unit. As with the ^{Pr}[P$_2$Cp] analogue **12**, the methylene protons of the benzyl ligand show a downfield broadened singlet near 3.25 ppm. The ambient temperature ^{31}P{^{1}H} NMR spectrum for **26** shows a singlet at -19.0 ppm for two equivalent phosphine donors, which remains unchanged down to -40 °C. This observation contrasts with the fluxional phosphine dissociation seen for the **12**, and is indicative of a greater inclination for the methyl substituted phosphines to coordinate.

$$^{Me}[\text{P}_2\text{Cp}]\text{ZrCl}_3 \xrightarrow[\text{- KCl}]{\text{KCH}_2\text{Ph}} {}^{Me}[\text{P}_2\text{Cp}]\text{ZrCl}_2(\text{CH}_2\text{Ph}) \qquad (4.2)$$

$$\textbf{25} \qquad\qquad\qquad\qquad\qquad\qquad\qquad \textbf{26}$$
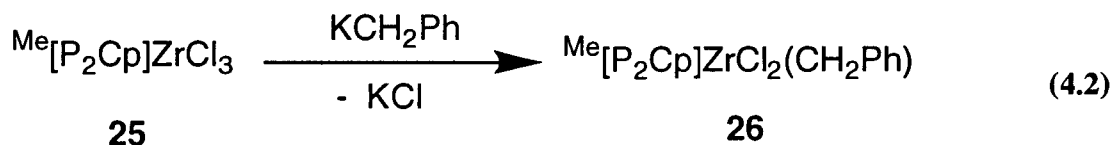
4.3.2 Isolation of ^{Me}[P$_2$Cp]ZrCl(CH$_2$Ph)$_2$

A conspicuous theme of the previous chapter was the lack of success in isolating dialkyl complexes with the ^{Pr}[P$_2$Cp] ancillary ligand, where disproportionation of the intended product yielded an equilibrium mixture of alkyl species. By contrast, adding 2 equivalents of KCH$_2$Ph to a THF solution of trichloride **25** produces the dibenzyl complex ^{Me}[P$_2$Cp]ZrCl(CH$_2$Ph)$_2$ (**27**), an exceedingly air- and moisture-sensitive species, that can be isolated in moderate yield as red crystals (equation 4.3).

$$^{Me}[P_2Cp]ZrCl_3 \xrightarrow[\text{- 2 KCl}]{\text{2 KCH}_2\text{Ph}} {}^{Me}[P_2Cp]ZrCl(CH_2Ph)_2 \qquad (4.3)$$

$$\textbf{25} \qquad\qquad\qquad\qquad\qquad\qquad \textbf{27}$$
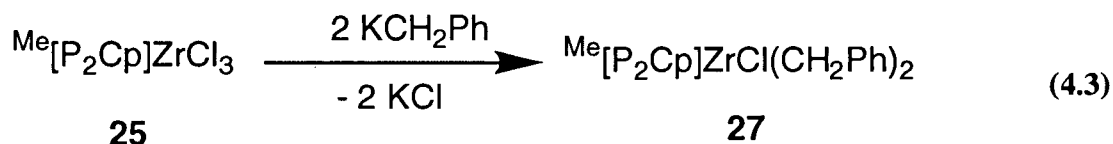
An X-ray crystal structure determination was performed on **27**, and the molecular structure is shown in Figure 4.1, with selected bond lengths and bond angles given in Table 4.1.

Figure 4.1   Molecular structure of $^{Me}[P_2Cp]ZrCl(CH_2Ph)_2$ (**27**); 33% probability thermal ellipsoids are shown. Hydrogen atoms are omitted for clarity.

The six-coordinate geometry shows distortion of the equatorial ligands away from the Cp donor, in common with trichloride **1** and metallacycle **23**. The benzyl ligands are coordinated *trans* to each other, presumably to minimize steric interactions within this crowded geometry.

148

Each benzyl ligand is bound in an η^1-mode; the Zr(1)-C(16)-C(17) and Zr(1)-C(23)-C(24) bond angles of 114.15(14)° and 106.47(13)°, respectively, are both consistent with the geometry of a normal sp^3-hybridized carbon centre, in contrast to the angular distortion observed in η^2-benzyl complexes like $Zr(CH_2Ph)_4$ (average corresponding $M-C_\alpha-C_{ipso}$ bond angle of 92°).[1] The Zr(1)-C(16) and Zr(1)-C(23) bond lengths of 2.404(2) Å and 2.407(2) Å, respectively, are approximately 0.06 Å longer than the corresponding distance in analogous η^2-benzyl complexes.[2] Unlike most Zr benzyl species, the coordination of two phosphines in **27** helps to saturate the metal so that it is unnecessary for the benzyl ligands to increase hapticity in order to improve their electron donor ability. In **27** the steric congestion is reflected in the two Zr-P bond distances differing by approximately 0.7 Å, which may result from the phenyl rings of both benzyl ligand being directed towards the same phosphine, which in turn forces this donor further away from the metal.

Table 4.1   Selected Bond Lengths (Å) and Bond Angles (°) for $^{Me}[P_2Cp]ZrCl(CH_2Ph)_2$ (**27**).

Zr(1)-Cl(1)	2.5379(5)	Cl(1)-Zr(1)-P(1)	86.41(2)
Zr(1)-P(1)	2.8079(6)	Cl(1)-Zr(1)-P(2)	78.75(2)
Zr(1)-P(2)	2.8757(6)	P(1)-Zr(1)-P(2)	164.79(2)
Zr(1)-C(16)	2.407(2)	Cl(1)-Zr(1)-C(16)	78.86(5)
Zr(1)-C(23)	2.404(2)	Cl(1)-Zr(1)-C(23)	80.52(5)
		C(16)-Zr(1)-C(23)	140.21(8)
		Zr(1)-C(16)-C(17)	114.15(14)
		Zr(1)-C(23)-C(24)	106.47(13)

The $^{31}P\{^1H\}$ NMR spectrum of **27** displays a singlet at -18.5 ppm for a pair of equivalent coordinated phosphines, in the same chemical shift region as found for trichloride **25** and for monobenzyl **26**. This spectrum remains unchanged at low temperature (-60 °C), indicating that any fluxional process involving the side-arm phosphines is undetected in the NMR time scale.

The ^{1}H NMR spectrum is consistent with the approximate C_s symmetry of the solid state structure. However, the two benzyl groups in **27** are chemically inequivalent in Figure 4.1 (or in any geometry in which the two phosphines are bound). Therefore, the prominent broad peak near 2.8 ppm for the methylene protons of the benzyl group indicates chemical exchange occurring at a rate that is comparable to the NMR time scale. This process likely involves dissociation of one or both side-arms, although as noted above this is not detected in the ^{31}P$\{^1$H$\}$ NMR spectra. At -20 °C the benzylic region of the ^{1}H NMR spectrum shows two separate multiplets, one for each set of methylene protons, indicating that the fluxional process is at the slow exchange limit at this temperature. The downfield chemical shifts of the methylene (2.83 ppm) and ortho (7.66 ppm) protons of the benzyl ligands are consistent with the η^1-coordination of these groups being maintained in solution. This contrasts with the upfield location of these resonances for the tribenzyl species **3**, where as discussed in section 2.4.1 the benzyl ligands in this complex are suspected of coordinating in an η^2-fashion to compensate for the absence of phosphine coordination.

4.3.3   Formation of toluyne ^{Me}[P$_2$Cp]Zr(η^2-C$_6$H$_3$Me)Cl from thermolysis of ^{Me}[P$_2$Cp]ZrCl(CH$_2$Ph)$_2$

The ability to isolate dibenzyl **27** in the absence of a complicating equilibrium is in sharp contrast with the disproportionation behaviour of **14**, which stems from the tendency for phosphine dissociation in the latter species. That the phosphines are more strongly bound in **27** also accounts for the absence of fluxional isomerization that is seen in several of the alkyl complexes encountered in Chapter 2. The smaller methyl substituents likely encourage phosphine coordination in **27** as a result of reduced steric conflict with the other ligands, despite the presence of two bulky benzyl groups. As will be noted in the next section there is probably also an electronic component to the superior coordination of the ^{Me}[P$_2$Cp] ligand.

Given the thermal reaction of dibenzyl **14** to generate alkylidene **16**, we were interested in determining whether the same result would obtain for the less bulky analogue **27**. The results in the previous chapter hinted that the α-abstraction mechanism for alkylidene formation is promoted by phosphine coordination. Dibenzyl **27** clearly meets these criteria and provides a unique opportunity to directly test this hypothesis. Further, a kinetic study should be facilitated since the suspected precursor is a isolable crystalline solid, as opposed to one component in an inseparable equilibrium mixture, as is the case with **14**.

Thermolysis of a toluene solution of **27** for 12 hours at 70 °C eliminates one equivalent of toluene to form a new complex, but instead of the anticipated benzylidene species the new product is a toluyne complex $^{Me}[P_2Cp]Zr(\eta^2-C_6H_3Me)Cl$ (**28**), which is obtained in two isomeric forms in a 2:1 ratio as shown below (equation 4.4). The major isomer can be separated as pale yellow crystals, which when redissolved regenerates the same single product in solution, indicating that although both isomers of **28** are formed together during the thermal decomposition of dibenzyl **27**, these species are not in equilibrium.

(4.4)
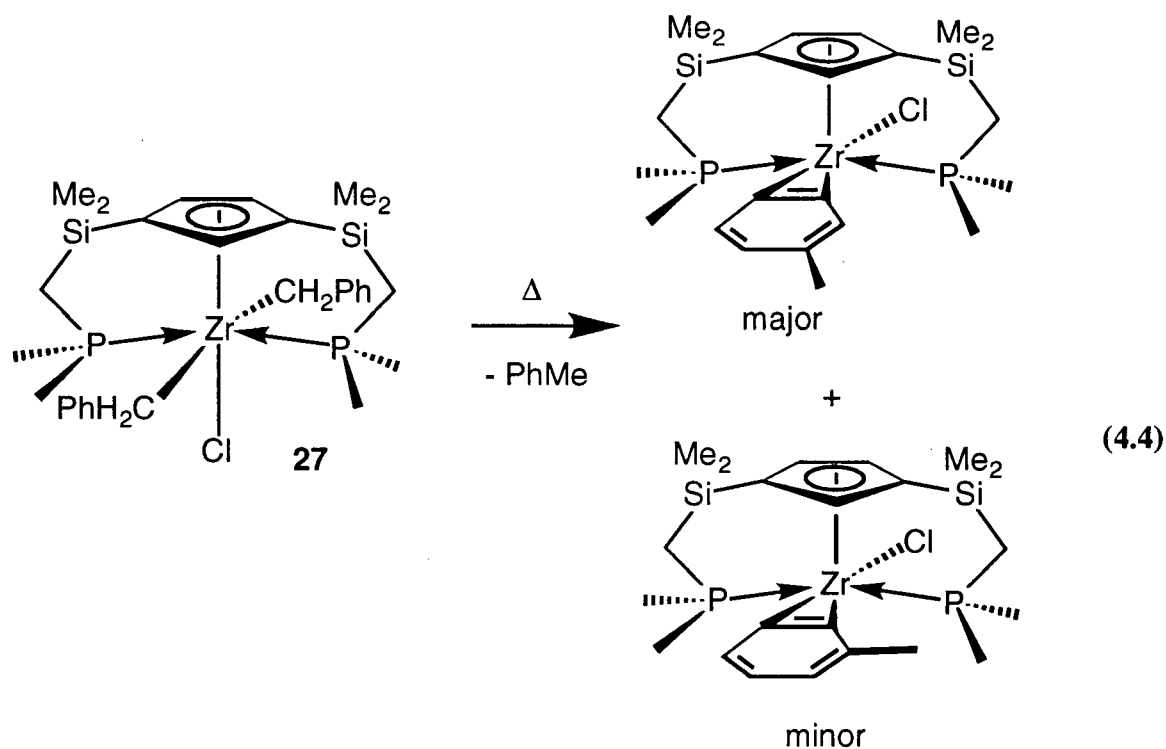
An X-ray crystal structure analysis was obtained for the major isomer of **28**. The molecular structure is depicted in Figure 4.2, with selected bond lengths and bond angles given in Table 4.2. The structure in Figure 4.3 shows the methyl group of the toluyne fragment in the sterically favoured position furthest from the metal. The planar phenyl ring is oriented parallel to the Cp ring to minimize steric congestion, as similarly observed for the ethylene complex **20**. The bonding parameters are consistent with the depiction of the toluyne ligand as an ortho-phenylene unit as shown in equation 4.4. The C(17)-C(18) bond length is similar to the other C-C bonds in the phenyl ring, and the short Zr(1)-C(17) and Zr(1)-C(18) bond distances of 2.222(2) Å and 2.213(2) Å, respectively, are indicative of Zr-C σ-bonds. These distances are similar to the parameters of analogous Zr benzyne complexes. For example, in $Cp_2Zr(\eta^2\text{-}C_6H_4)(PMe_3)$[3] the Zr-C bond lengths to the benzyne ligand average 2.25 Å.
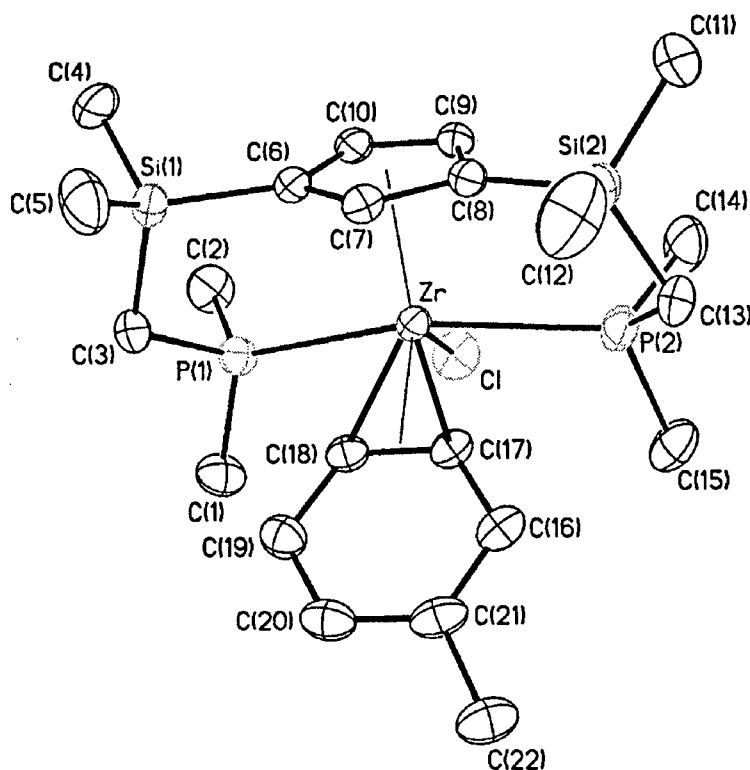
Figure 4.2 Molecular structure of $^{Me}[P_2Cp]Zr(\eta^2\text{-}C_6H_3Me)Cl$ (**28**); 33% probability thermal ellipsoids are shown. Hydrogen atoms are omitted for clarity.

Table 4.2   Selected Bond Lengths (Å) and Bond Angles (°) for $^{Me}[P_2Cp]Zr(\eta^2-C_6H_3Me)Cl$ **(28)**.

Zr(1)-Cl(1)	2.5385(8)	Cl(1)-Zr(1)-P(1)	77.41(3)
Zr(1)-P(1)	2.7192(7)	Cl(1)-Zr(1)-P(2)	77.50(3)
Zr(1)-P(2)	2.7194(8)	P(1)-Zr(1)-P(2)	154.03(3)
Zr(1)-C(17)	2.222(2)	Cl(1)-Zr(1)-C(17)	116.70(7)
Zr(1)-C(18)	2.213(2)	Cl(1)-Zr(1)-C(18)	117.12(7)
C(17)-C(18)	1.366(3)	C(17)-Zr(1)-C(18)	35.87(9)
C(18)-C(19)	1.410(4)	C(16)-C(17)-C(18)	120.3(2)
C(19)-C(20)	1.375(4)	C(16)-C(21)-C(22)	123.6(3)

NMR spectroscopic data for the two isomers of **28** are straightforward. A singlet is seen in the $^{31}P\{^1H\}$ NMR spectrum for both the major (-7.0 ppm) and minor species (-7.3 ppm). The methyl group on the toluyne fragment is prominent for each isomer in the ^1H NMR spectrum at 2.43 ppm (major) and 2.67 ppm (minor), respectively. The position of this methyl substituent on the phenyl ring with respect to the coordinated toluyne ligand gives rise to a distinctive pattern in the downfield region. For the major isomer there is a singlet at 7.82 ppm for the sole ring proton adjacent to both the methyl group and the metal-bound carbon atom, and a doublet for each of the other two ring protons. In comparison, the minor isomer shows a triplet and two doublets in the same downfield region of the NMR spectrum for the three aryl protons of the toluyne fragment.

Benzyne complexes are reactive species that have found synthetic utility with insertion reactions involving alkenes, alkynes, and other unsaturated substrates.[4-6] In contrast however, toluyne **28** is surprisingly unreactive with ethylene even at 90 °C.

The unexpected result that yields toluyne **28** from dibenzyl **27** prompted consideration of the reaction mechanism. Zr benzyne complexes are conveniently generated from a thermally induced abstraction of an aryl C-H bond by on adjacent alkyl or aryl ligand (equation 4.5).[7,8] The product is isolated with the addition of a trapping phosphine.

$$
\underset{\Delta,\ PR_3}{\overset{\displaystyle \text{L}_n\text{M}-\text{R} \cdots \text{H (aryl)}}{\longrightarrow}} \quad \text{L}_n\text{M}(\eta^2\text{-benzyne})(PR_3) \qquad (4.5)
$$

$$- RH$$
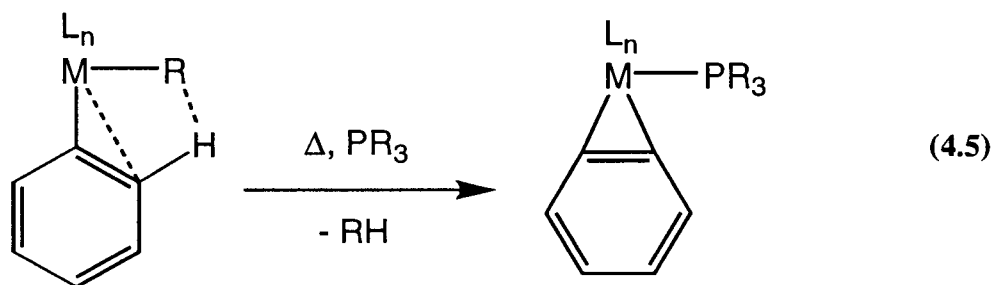
The pendant phosphines of the P_2Cp ancillary ligand are well suited to stabilize the toluyne product **28**. An appropriate intermediate that resembles the precursor indicated in equation 4.5 could be derived from the expected alkylidene complex, as shown in Scheme 4.1. Since the thermolysis was conducted in toluene the intermediate alkylidene species could possibly activate a solvent molecule to generate the aryl-alkyl species **C**, which leads directly to the toluyne complex (in Scheme 4.1 a benzyne complex should be formed).

However, the same toluyne complex **28**, not the benzyne species shown in Scheme 4.1, is obtained when the reaction is conducted in benzene, indicating that the reaction mechanism does not proceed *via* intermolecular activation of the solvent by an alkylidene species.[9-12] Therefore, an alternate intramolecular process,[13] perhaps still involving an intermediate alkylidene, is the most likely route to toluyne **28**. An examination of the photochemical decomposition of dibenzyl **27** detailed below may shed light on the thermal reaction.

154
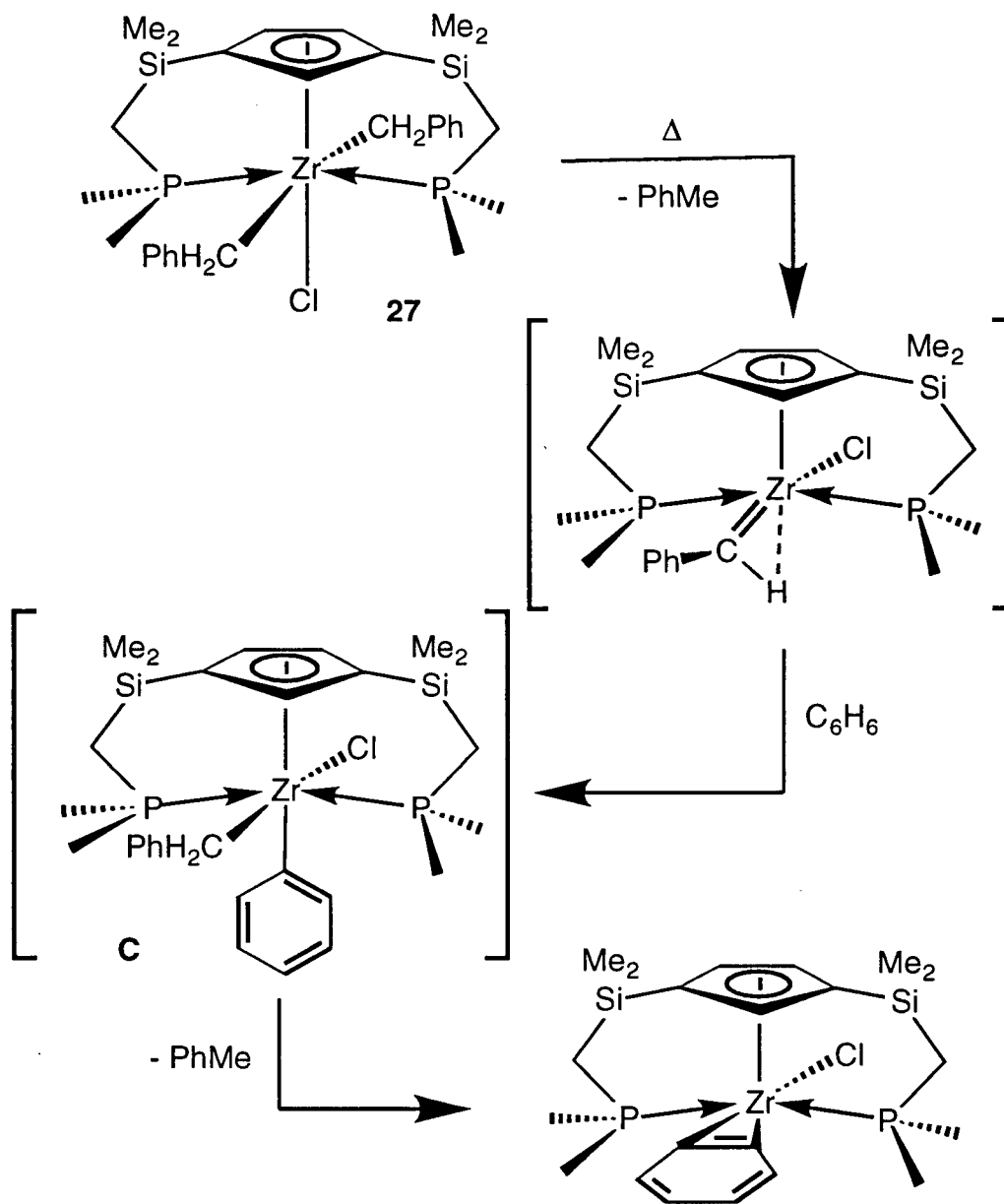
Scheme 4.1 Possible mechanistic route to a benzyne complex via C-H activation of a solvent

molecule by an intermediate alkylidene complex.

4.3.4 Photolysis of $^{Me}[P_2Cp]ZrCl(CH_2Ph)_2$

Red dibenzyl **27** is stable upon prolonged exposure to visible light. The UV-VIS spectrum of this complex shows a strong λ_{max} near 310 nm, however, and irradiation of **27** including this wavelength generates a new species in a clean reaction within 6 hours (equation 4.6). Unfortunately, this product is thermally sensitive and could not be isolated under the reaction conditions employed.

$$(4.6)$$
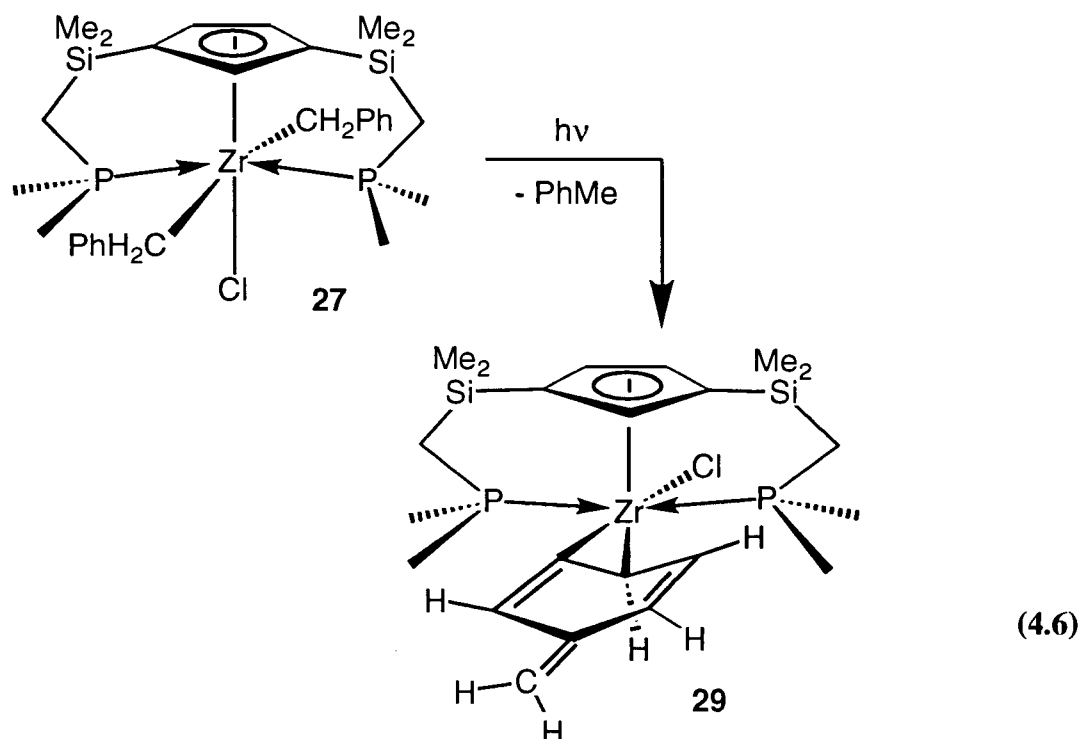
The ^1H NMR spectrum shows that one equivalent of toluene is also produced in this reaction. An AB doublet of doublets for **29** in the $^{31}P\{^1H\}$ NMR spectrum ($^2J_{PP} = 76$ Hz) at -18.6 and -18.9 ppm is indicative of two inequivalent, mutually coupled phosphine donors coordinated to the metal centre, suggesting an asymmetric molecular structure. This observation is supported by the corresponding ^1H NMR spectrum, which shows four resonances for the silylmethyl protons and another four peaks for the methyl groups attached to the phosphines, in addition to three separate peaks for the Cp protons. There are also six additional resonances

ranging between 2.8 and 6.0 ppm, each corresponding to a single proton and exhibiting a second-order splitting pattern. The combination of a 2D COSY ^{1}H NMR spectrum and the ^{1}H{^{31}P} NMR spectrum enabled the following assignments to be made in Table 4.3, consistent with the structure shown in equation 4.6.

Table 4.3 Assignments for the ^{1}H NMR spectrum of 29 between 2.8 and 6.0 ppm.

proton	chemical shift (δ)	coupled to	splitting pattern
H$_A$	2.78	H$_B$, H$_C$	dd
H$_B$	3.08	H$_A$, H$_E$	dd
H$_C$	3.17	H$_B$, H$_D$, P	m
H$_D$	3.52	H$_C$, H$_F$, P	m
H$_E$	5.04	H$_B$, H$_F$	dd
H$_F$	5.99	H$_D$, H$_E$	dd
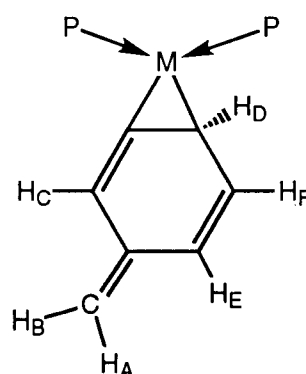
A common result from the irradiation of photochemically sensitive organometallic complexes is M-C bond homolysis.[14] In the case of Zr(CH$_2$Ph)$_4$ the benzyl radical generated is not observed to react with the toluene solvent (i.e., bibenzyl PhCH$_2$CH$_2$Ph is not formed), but instead remains within the coordination sphere in a radical cage mechanism.[15] A similar mechanism may be operative in the formation of **29** (Scheme 4.2). The benzyl radical that is generated is resonance-stabilized, and one of these resonance forms could recombine with the Zr(III) intermediate to give a suitable precursor **D**. Abstraction of an aryl C-H bond by the remaining benzyl ligand would produce the observed equivalent of toluene and the final product

references begin on page 208

29.[16] This intramolecular process may be reflected in a similar mechanism for the thermal reaction that forms **28**.
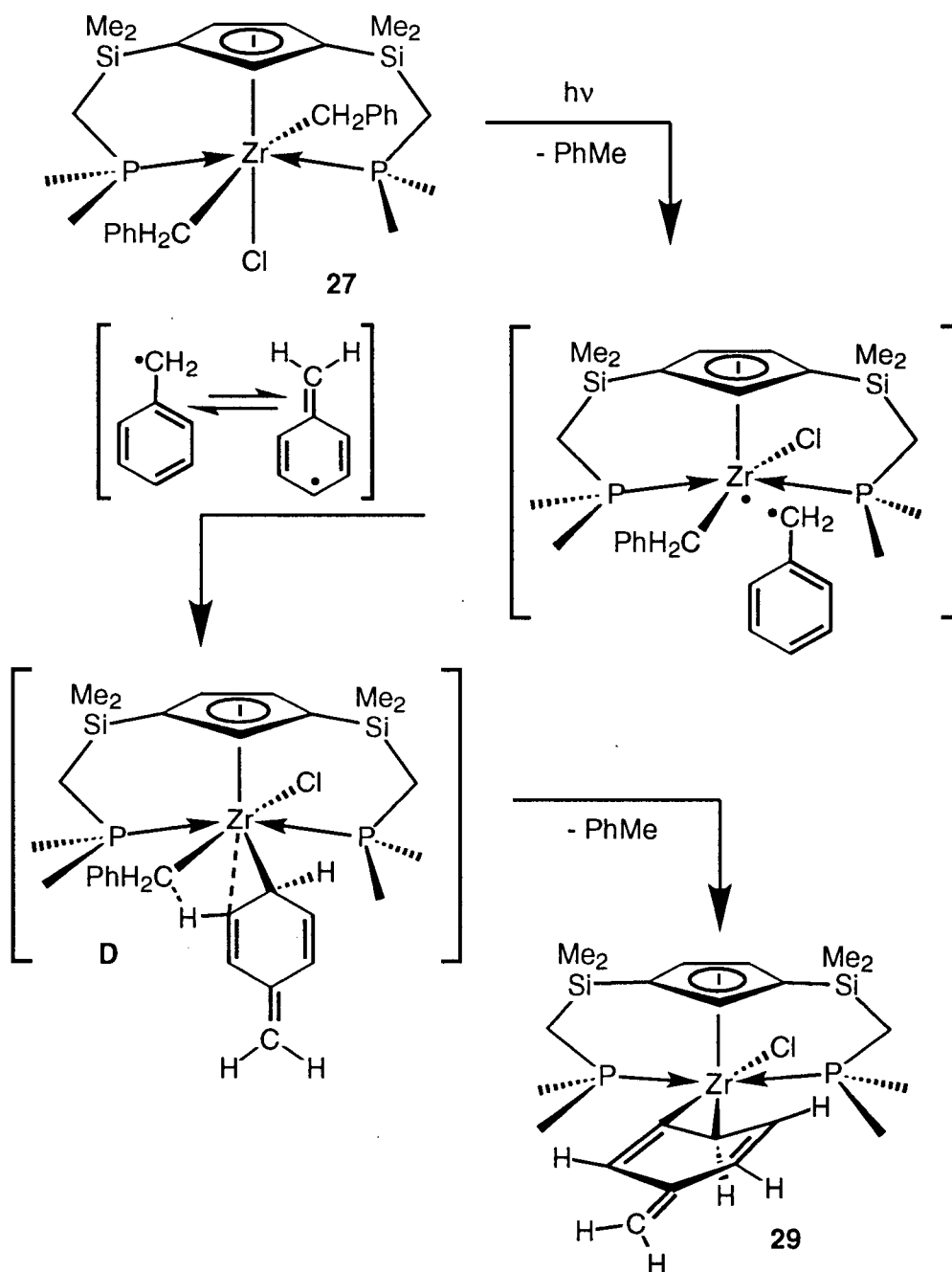
Scheme 4.2 Proposed mechanism for the photochemical decomposition of $^{Me}[P_2Cp]ZrCl(CH_2Ph)_2$ (**27**).

The photochemical product **29** is thermally sensitive and decomposes within hours under ambient conditions. A minor decomposition product is the Zr(III) chloride-bridged dimer {^{Me}[P$_2$Cp]ZrCl(μ-Cl)}$_2$ (**45**). The structure of this diamagnetic species will be discussed further in comparison to analogous Zr(III) derivatives in section 4.3.2, but the formation of this compound implies that a naked Zr(II) "(^{Me}[P$_2$Cp]ZrCl)" intermediate is generated in the decomposition process arising from loss of the organic ligand from **29**. Subsequent disproportionation of this intermediate could produce the observed Zr(III) chloride **45**. An organic compound, 4-benzyltoluene, identified by LC-MS and ^{1}H NMR spectroscopy, is also a byproduct in this decomposition, and is observed in small amounts from the thermal reaction that yields toluene **28**. This molecule can be broken down into a benzylic and a p-tolyl fragment, implying that its formation could arise from reductive elimination from intermediate **C** in Scheme 4.1, in competition with the production of **28**, or from an analogous coupling reaction of the benzyl ligands in the formation of **29**.
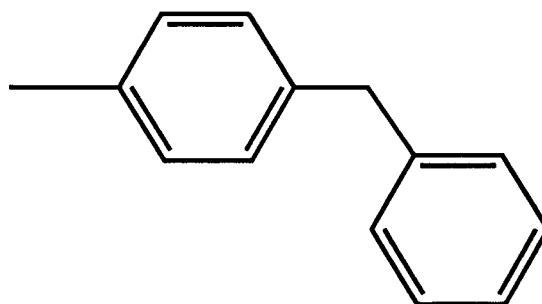
4-benzyltoluene

4.3.5 Preparation of ^{Me}[P$_2$Cp]Zr(CH$_2$Ph)$_3$

The tribenzyl complex ^{Me}[P$_2$Cp]Zr(CH$_2$Ph)$_3$ (**30**) can be prepared as a red crystalline solid from the reaction of trichloride **25** with 3 equivalents of KCH$_2$Ph in THF (equation 4.7).

$$^{Me}[P_2Cp]ZrCl_3 \xrightarrow[- 3\ KCl]{3\ KCH_2Ph} \ ^{Me}[P_2Cp]Zr(CH_2Ph)_3 \qquad (4.7)$$

$$\underset{\mathbf{25}}{} \qquad\qquad\qquad\qquad\qquad \underset{\mathbf{30}}{}$$
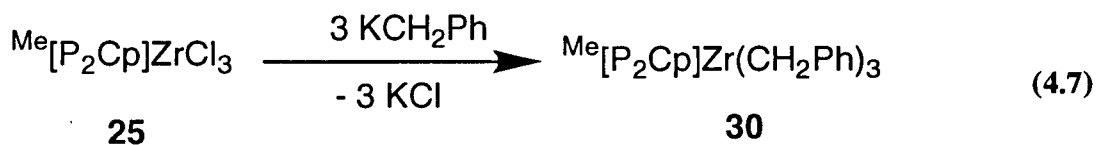
A crystal structure determination was obtained for tribenzyl **30**, and the molecular structure is shown in Figure 4.3, with selected bond lengths and bond angles listed in Table 4.4.
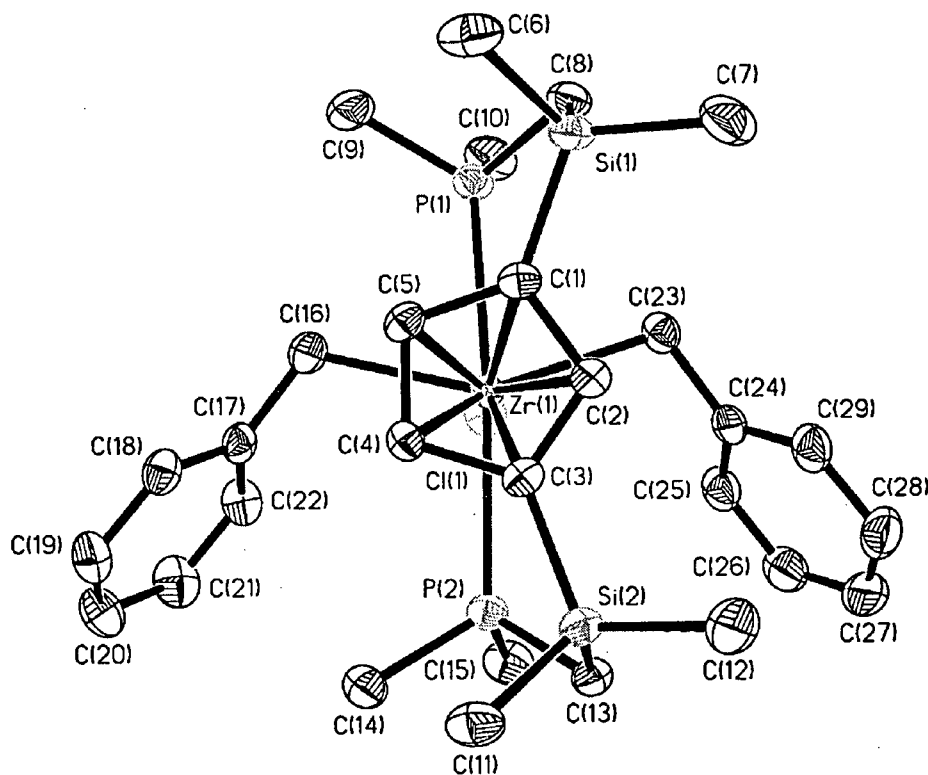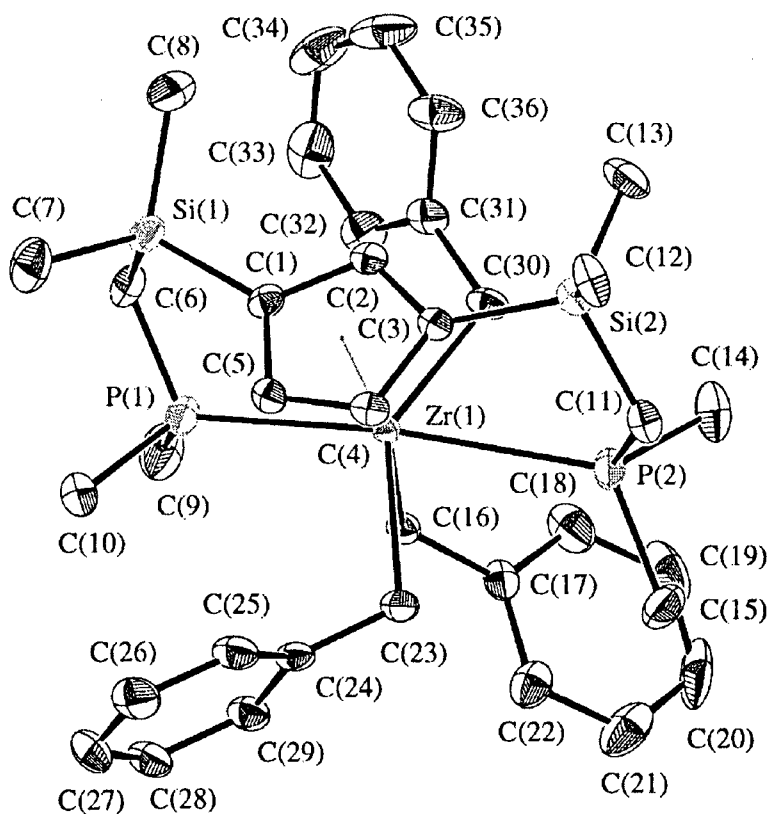
Figure 4.3 Molecular structure of $^{Me}[P_2Cp]Zr(CH_2Ph)_3$ (**30**); 33% probability thermal ellipsoids are shown. Hydrogen atoms are omitted for clarity.

Table 4.4   Selected Bond Lengths (Å) and Bond Angles (°) for $^{Me}[P_2Cp]Zr(CH_2Ph)_3$ (**30**).

Zr(1)-P(1)	2.9005(7)	P(1)-Zr(1)-P(2)	162.85(2)
Zr(1)-P(2)	2.9093(6)	P(1)-Zr(1)-C(16)	74.02(6)
Zr(1)-C(16)	2.416(3)	P(1)-Zr(1)-C(23)	106.80(6)
Zr(1)-C(23)	2.413(3)	P(1)-Zr(1)-C(30)	102.13(6)
Zr(1)-C(30)	2.391(3)	P(2)-Zr(1)-C(16)	89.15(6)
Zr(1)-Cp'	2.30	C(16)-Zr(1)-C(23)	80.93(9)
		C(23)-Zr(1)-C(30)	141.30(9)
		Zr(1)-C(23)-C(24)	111.6(2)

The structure shows that both phosphines are coordinated to the metal, in direct contrast to the solution structure of the $^{Pr}[P_2Cp]$ tribenzyl analogue **3**. The crowded quasi-octahedral arrangement of three bulky ligands in **30** evidently induces bond lengthening. The Zr-P bond distances (average 2.9 Å) are longer than in dibenzyl **27** and considerably longer (by 0.2 Å) than the corresponding Zr-P bond lengths in toluyne **28**. The Zr-Cp' bond distance of 2.30 Å is also approximately 0.07 Å longer than in comparatively uncrowded complexes with this ancillary ligand set. The saturated six-coordinate geometry results in undistorted η^1-coordination of all three benzyl ligands, as demonstrated by the normal Zr(1)-C(23)-C(24) bond angle of 111.6(2)°.

The ^1H and $^{31}P\{^1H\}$ NMR spectrum of **30** are consistent with the solid state structure. A broadened singlet at -23.8 ppm in the $^{31}P\{^1H\}$ NMR spectrum is indicative of two equivalent coordinated phosphines, while the downfield chemical shifts for the methylene (2.60 ppm) and ortho (7.50 ppm) protons of the benzyl groups are consistent with the h1-hapticity of these ligands observed in the solid state. The triplet for the methylene protons ($^3J_{PH}$ = 6 Hz) arises due to coupling to the bound phosphines. That all three inequivalent benzyl groups display one

averaged chemical environment indicates that these ligands undergo a similar exchange process as seen for dibenzyl **27**.

The distinct structural differences between the two tribenzyl complexes **3** and **30** attests to the ability of the small methyl substituents to permit the side-arm donors access to the metal within the same array of alkyl ligands. However, there must be an electronic component to the better donor ability of the ^{Me}[P$_2$Cp] ligand in addition to the obvious steric factors, since the coordination sphere in ^{Pr}[P$_2$Cp]ZrCl$_2$(CH$_3$) (**9**) must surely be less congested than that found in **30**, yet the former is still observed to undergo fluxional isomerization involving the side-arm donors. As mentioned previously, tribenzyl **3** is thermally unreactive, presumably because the pendant phosphines remain dangling and hence are unable to assist in a mechanism that may require phosphine complexation. However, preliminary studies indicate that the ^{Me}[P$_2$Cp] analogue **30** does in fact undergo a thermal reaction, in further support of the concept that the phosphines are an integral component in promoting this reactivity. As yet the product of this reaction has remained unidentified.
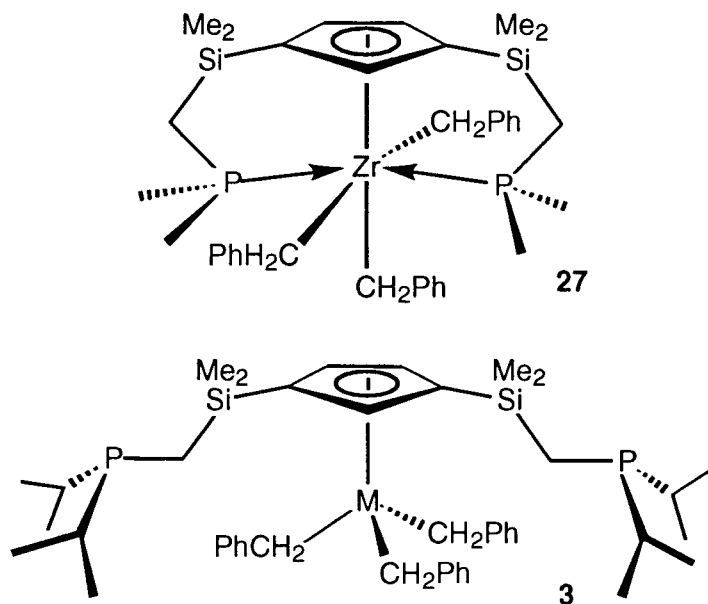
4.4 Synthesis and reactivity of the ethylene complexes $^R[P_2Cp]Zr(\eta^2\text{-}CH_2\text{=}CH_2)Br$ (R = Me, Pr^i)

In the previous chapter the isolation of ethylene complex **20** from the reaction of either alkylidene **16** or **18b** with excess ethylene was reported. An interest to study the reactivity of this complex, as a probe into the nature of the metal-alkene bonding in this formally Zr(II) species, prompted a more direct synthetic route from the starting chloride **1**. One advantage of this alternate preparation is the versatility to obtain the corresponding $^{Me}[P_2Cp]$ ethylene complex from **25**. Examples were noted in the previous sections, most notably with dibenzyl **27**, where the structure and reactivity of analogous complexes differed depending on the phosphine substituents. These ethylene derivatives thus provide an opportunity to compare further the effects of the two ligand systems on the chemical properties of analogous complexes.

4.4.1 Preparation of $^R[P_2Cp]Zr(\eta^2\text{-}CH_2\text{=}CH_2)Br$ (R = Pr^i, Me)

A toluene solution of **1** or **25** reacts with 2 equivalents of EtMgBr at -78 °C to give a bright yellow solution, which upon warming to room temperature generates the ethylene complex $^R[P_2Cp]Zr(\eta^2\text{-}CH_2\text{=}CH_2)Br$ (**31**: R = Pr^i, **32**: R = Me) in excellent yield, either as dark purple (**31**) or dark red (**32**) crystals (equation 4.8). The yellow precursor is presumed to be the diethyl species $^R[P_2Cp]ZrBr(CH_2CH_3)_2$, an intermediate which undergoes a β-H abstraction reaction with the elimination of ethane to form the final product. A quantitative halide exchange incorporates a bromide ligand in the final product, based on chemical analyses data and an X-ray structural determination for **32** (see below).

Me₂ Me₂
Si Si
R'''''P→Zr←P'''R
R Cl R
Cl
Cl

1 R = Pr^i
25 R = Me

2 EtMgBr

- MgCl₂
- MgBrCl

Me₂ Me₂
Si Si
R'''''P→Zr←P'''R
R CH₃CH₂ R
CH₂CH₃

(4.8)

Me₂ Me₂
Si Si
R'''''P→Zr←P'''R
R H₂C——CH₂ R

- CH₃CH₃

31 R = Pr^i
32 R = Me
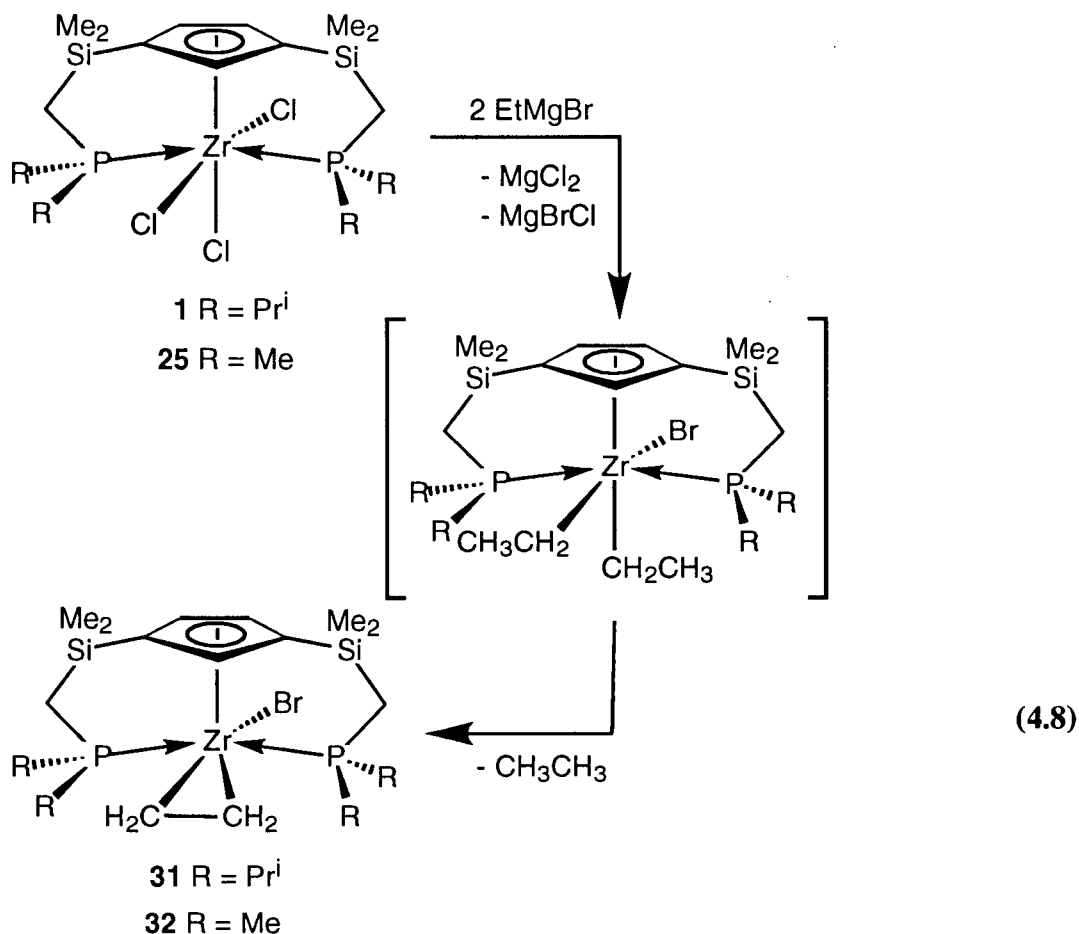
The ^{1}H and ^{31}P{^{1}H} NMR spectra of purple **31** are nearly identical to that of the red chloro derivative ^{Pr}[P₂Cp]Zr(η^2-CH₂=CH₂)Cl (**20**), showing two species in equilibrium in the same 9:1 ratio of syn (major) and anti (minor) isomers. One minor difference is evident in the chemical shifts of the respective methine protons of the ancillary ligand. In comparison, a single species is seen in solution for **32**, indicating that stronger phosphine coordination discourages an exchange process in this complex. The distinctive pattern of the Cp protons for **32** in the ^{1}H NMR spectrum with a triplet for the unique proton at 4.15 ppm and a doublet for the two equivalent protons at 6.02 ppm recalls a very similar pattern for the major isomers of **20** and **31**.

The molecular structure of the ^{Me}[P₂Cp] derivative **32**, determined by an X-ray crystal determination, is shown in Figure 4.4. Selected bond distances and bond angles are presented in

164

Table 4.5. The structure reveals the ethylene unit coordinated parallel to the Cp ring and oriented *syn* to the unique Cp carbon atom, precisely as found for **20**. As only one isomer is seen for **32** in solution it is assumed that it corresponds to this structure, from which it is inferred that the major isomers for **20** and **31** are also the *syn* isomer, based on the resemblances in the respective ^{1}H NMR spectra mentioned above. The C(16)-C(17) bond distance of 1.431(6) Å in **32** is similar to the corresponding value of 1.433(17) Å for **20**, suggesting that the degree of backbonding from the metal is not significantly altered upon substituting either the halide (Br for Cl) or the groups attached to the phosphines (methyl for isopropyl). However, the phosphines are bound considerably closer to the metal in **32**, with Zr-P bond distances averaging 2.72 Å in comparison to 2.86 Å for **20**.
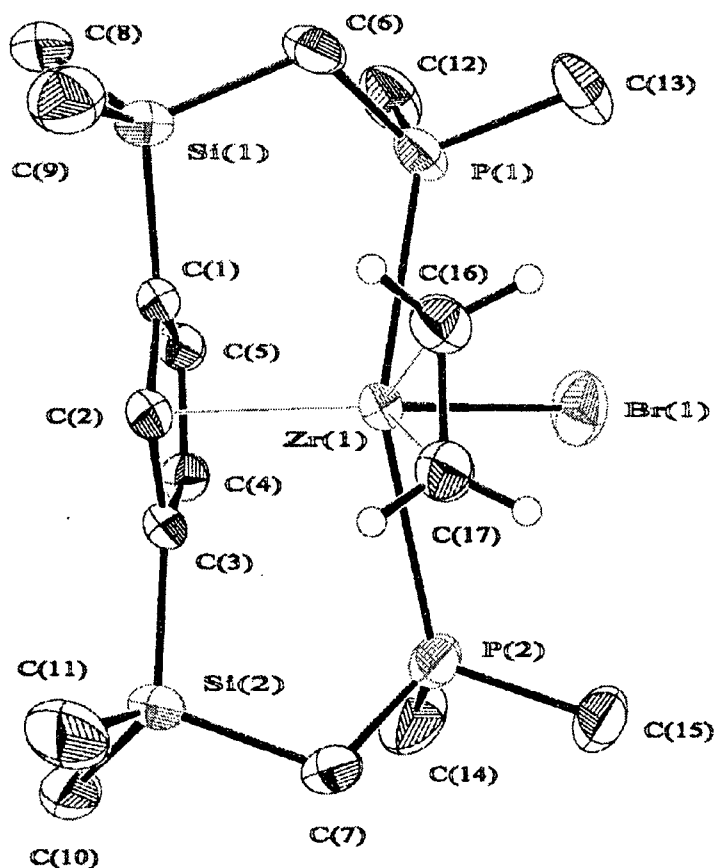
Table 4.5   Selected Bond Lengths (Å) and Bond Angles (°) for $^{Me}[P_2Cp]Zr(\eta^2\text{-}$
$CH_2{=}CH_2)Br$ **(2b)**.

Zr(1)-Br(1)	2.6744(6)	Br(1)-Zr(1)-P(1)	78.28(3)
Zr(1)-P(1)	2.730(1)	Br(1)-Zr(1)-P(2)	76.94(3)
Zr(1)-P(2)	2.703(1)	Br(1)-Zr(1)-C(16)	109.7(1)
Zr(1)-C(16)	2.293(5)	Br(1)-Zr(1)-C(17)	109.7(1)
Zr(1)-C(17)	2.312(5)	P(1)-Zr(1)-P(2)	155.17(4)
Zr(1)-Cp'	2.23	P(1)-Zr(1)-C(16)	75.6(1)
C(16)-C(17)	1.431(6)	P(1)-Zr(1)-C(17)	111.0(1)
		C(16)-Zr(1)-C(17)	36.2(2)

The formation of the ethylene complexes **31** and **32** directly from the respective starti
trichlorides offers a facile alternative to the multistep approach to **2c** *via* an alkylidene complex. Tl
general synthetic route has been employed elsewhere to obtain a number of early metal alke
complexes.[17,18] Unfortunately, this procedure could not be extended to other Zr alkene complexes w
this system. For example, propylene complexes could not be isolated by using Grignard reagents su
as Pr^nMgBr or Pr^iMgCl, nor was Bu^nLi helpful in obtaining a coordinated butene species. All of the
attempts resulted in complete decomposition of the reaction mixture, which recalls the instability of t
resulting propylene complex presumably generated from the metallacyclic intermediate in the reaction
either alkylidene **16** or **18b** with propylene. It is apparent from these results that the stability of alke
complexes with this ligand system is restricted to the ethylene derivatives.

4.4.2 Reaction of $^R[P_2Cp]Zr(\eta^2\text{-}CH_2=CH_2)Br$ with CO to give $^R[P_2Cp]Zr(CO)_2Br$ (R = Me, Pr^i)

A purple toluene solution of ethylene **31** reacts instantly under an atmosphere of CO to generate a dark greenish-orange solution that shows a single resonance in the $^{31}P\{^1H\}$ NMR spectrum at 29.1 ppm. In the ^1H NMR spectrum the only resonances observed are attributed to the ancillary ligand, and a sealed NMR tube reaction reveals a singlet at 5.25 ppm for the evolution of free ethylene. A similar result is obtained in the reaction with **32**. Therefore, it is apparent in both instances that the coordinated ethylene unit has been replaced by CO in a ligand substitution reaction to give a carbonyl complex (equation 4.9).

31 R = Pr^i

32 R = Me

(4.9)

33 R = Pr^i

34 R = Me

167
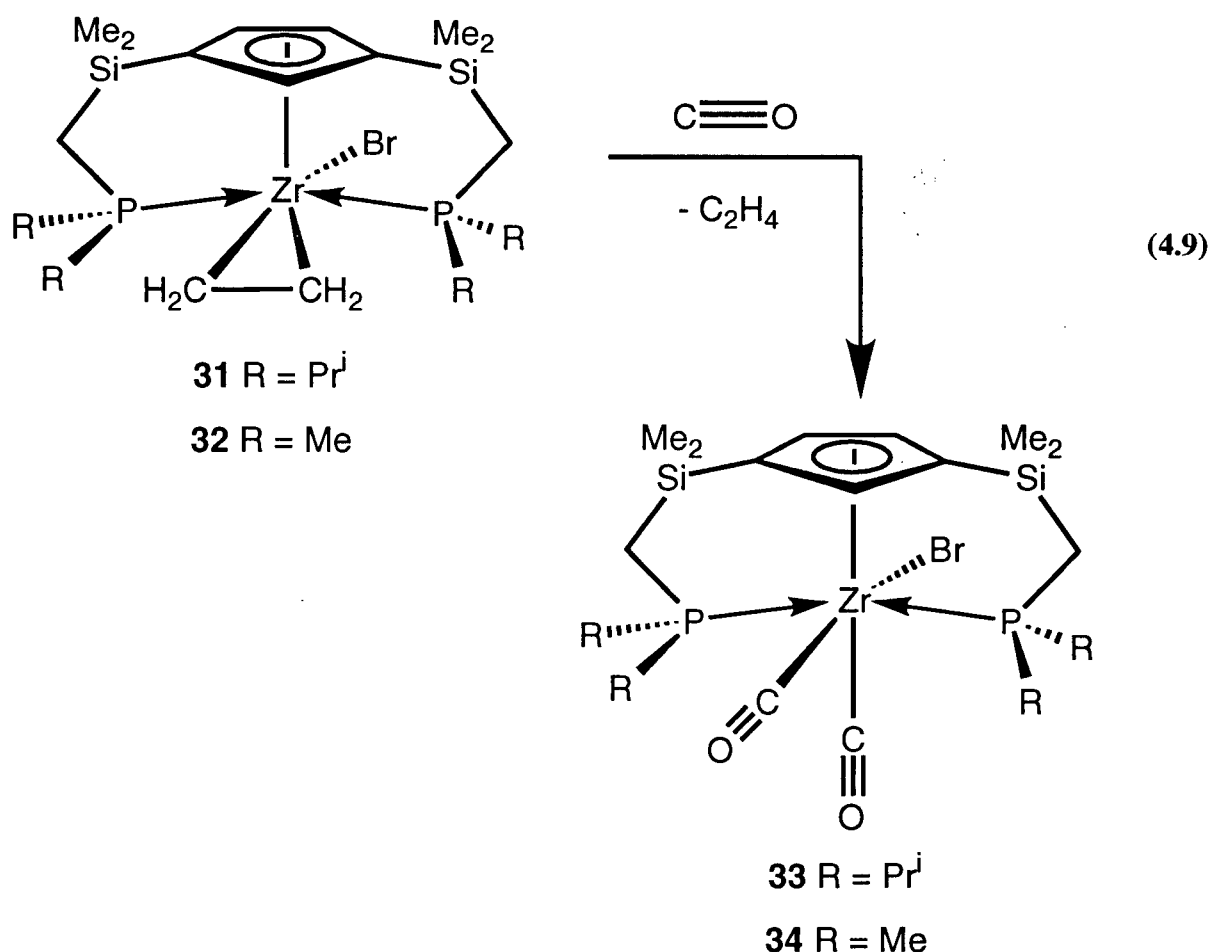
For the reaction of **31** with ^{13}CO the downfield region of the $^{13}C\{^1H\}$ NMR spectrum displays two carbonyl peaks at 241 and 249 ppm for **33** in addition to a third resonance at 184 ppm for excess free ^{13}CO, indicating that an 18-electron dicarbonyl species has been formed. In **34** the corresponding carbonyl resonances are located at 240 and 245 ppm, respectively. These complexes have a ligand arrangement that is similar to known derivatives such as $CpZr(CO)_2(dmpe)Cl.$[19] The presence of a carbonyl ligand is supported by absorptions in the IR spectra at 1890 and 1898 cm^{-1} for **33** and **34**, respectively, which shift to 1865 and 1855 cm^{-1} for the ^{13}C labeled isotopomers. The low ν_{CO} values of the coordinated carbonyl ligands in comparison to free CO (ν_{CO} = 2143 cm^{-1}) is due to strong back-bonding from the electron-rich Zr(II) centre to the π^* orbital of the CO ligand and is consistent with the stretching frequency in analogous Zr(II) carbonyls (i.e., $CpZr(CO)_2(dmpe)Cl$, ν_{CO} = 1940 cm^{-1}). Unfortunately, although both carbonyl complexes **33** and **34** are stable indefinitely in solution in the presence of excess CO, attempts to isolate these species in the absence of CO led to decomposition. This trait of instability outside of a protective CO atmosphere has been noted with other Zr carbonyl derivatives,[19] demonstrating the labile nature of these ligands with early metals.

An interesting feature of the ambient temperature $^{13}C\{^1H\}$ NMR spectrum of **33** is that the peak for free CO at 184 ppm is broadened, as is the carbonyl peak at 241 ppm. This curious observation suggests that this CO ligand is undergoing an exchange process with free CO in solution; the remaining ligand either is not involved in this process, or is at the slow exchange limit at this temperature, since the peak for this ligand at 249 ppm is quite sharp in comparison. This exchange process was monitored by variable temperature $^{13}C\{^1H\}$ NMR spectroscopy; the VT spectra, shown in Figure 4.5, demonstrate an increase in line broadening as the temperature is raised, in agreement with an increase in the exchange rate between free CO and the exchanging carbonyl ligand. The NMR spectra were simulated (DNMR-5) to obtain rate constants at each temperature, which were used in the resulting Eyring plot shown in Figure 4.6. The kinetic parameters $\Delta H^{\ddagger}$ = 9.2(5) kcal mol^{-1} and $\Delta S^{\ddagger}$ = -17(2) cal mol^{-1} K^{-1} were calculated from this

plot. The negative entropy term is unexpected, as ligand exchange from this saturated 18-electron species is anticipated to proceed in a dissociative mechanism that should produce a positive entropy term for a less ordered transition state. A concerted mechanism involving dissociation of a pendant phosphine may be a factor in this exchange. An associative process has also been suggested from a separate kinetic study into similar CO ligand exchange in other 18-electron Zr carbonyl species.[20,21]
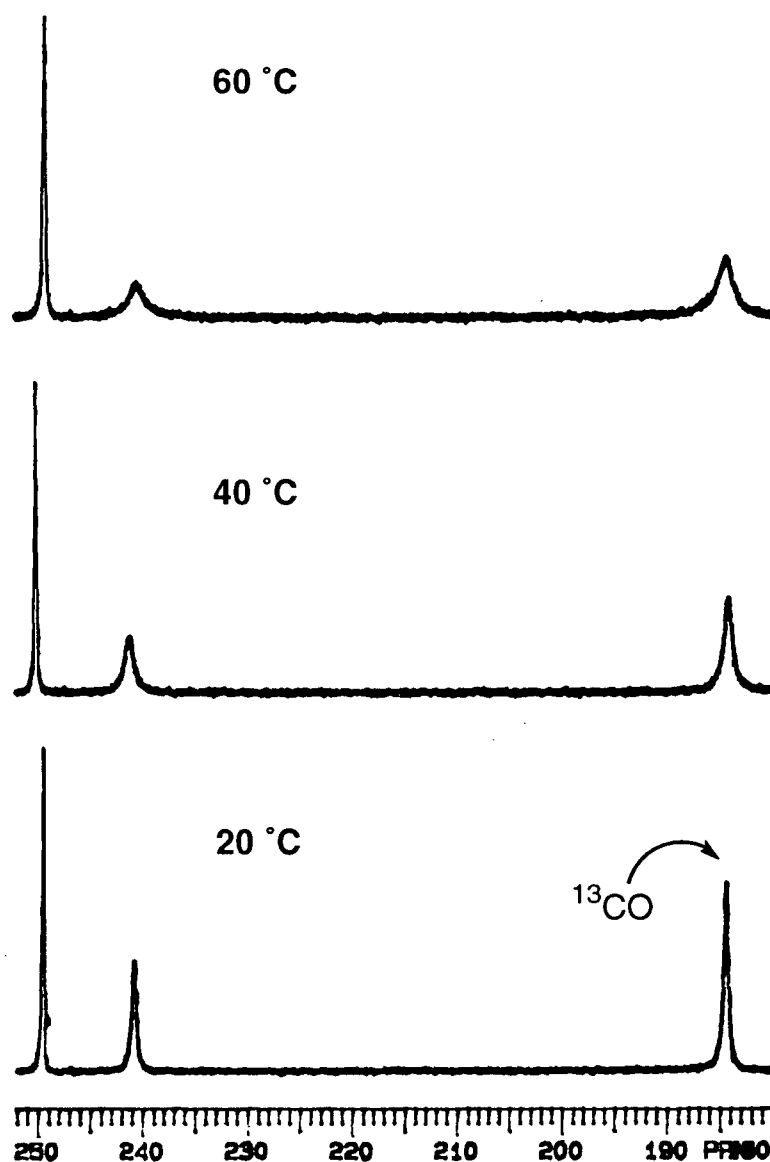
Figure 4.5   Variable temperature $^{13}C\{^1H\}$ NMR spectra of $^{Pr}[P_2Cp]Zr(CO)_2Br$ (**33**).
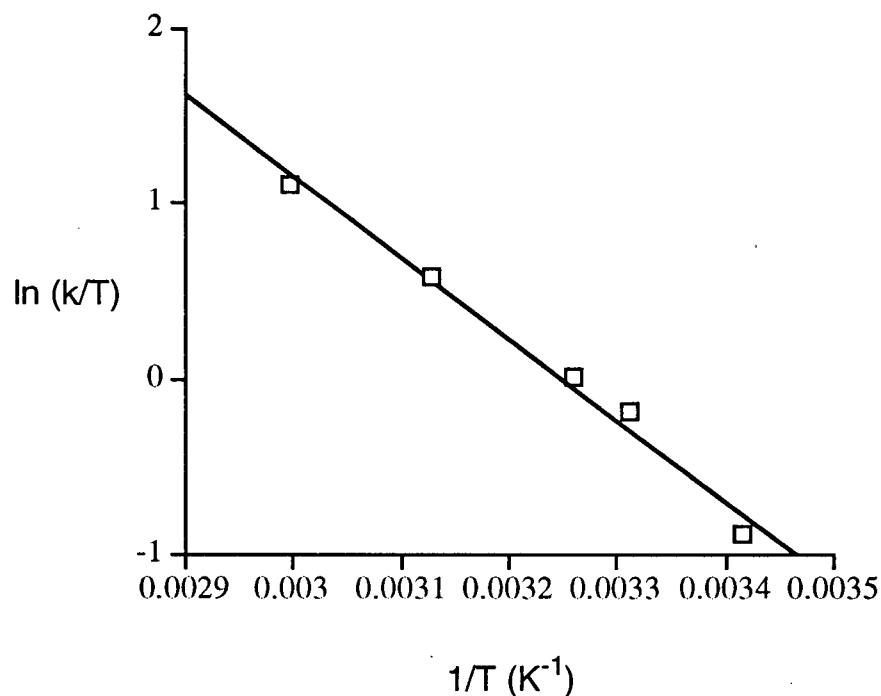
Figure 4.6   Eyring plot for the CO ligand exchange process in ^{Pr}[P$_2$Cp]Zr(CO)$_2$Br (**33**).

Ligand exchange is not uncommon for early metal carbonyl complexes. In Cp*Hf(CO)$_2$(dmpe)Cl)[21] both CO ligands are observed to rapidly and quantitatively exchange with excess ^{13}CO. One can speculate why only one carbonyl ligand in **33** undergoes this exchange. As mentioned in chapter 1 and seen for trichloride **1**, the ligand *trans* to the Cp group in a six-coordinate mono(cyclopentadienyl)complex is typically weakly bound, with a tendency for fluxional coordination in some instances. In **33** it is probable that one of the carbonyl ligands is located at this labile site trans to the Cp ring, while the other is trans to the bromide. There are two reasons why the former is more weakly bound in this geometry. First, the strong labilizing trans effect of the Cp donor contrasts with the weak trans effect of the electron withdrawing

bromide. Second, and as noted for ethylene **20**, backbonding from the metal in monocyclopentadienyl complexes is optimized by the $d_z{}^2$ and dxy orbitals (the z-axis passes through the Cp-centroid in this geometry), which are well suited to stabilize the carbonyl trans to the bromide but have a negligible effect on the other carbonyl ligand trans to the Cp group. Therefore, the combination of these factors may account for the observation that there is only one labile carbonyl ligand in **33** undergoing observable exchange with free CO.

The insertion reactions discussed in the previous chapter require dissociation of a labile phosphine to provide a vacant coordination site, and hence are relatively sluggish. In comparison to the slow insertion of CO into alkylidene **16** or **18b** to give ketene **21**, the immediate reaction of CO with ethylene **31** or **32** indicates an associative mechanism involving nucleophilic attack by a CO molecule without the need for prior phosphine dissociation. The ligand substitution reactions that produce these carbonyl derivatives also differ from the insertion chemistry outlined previously. The displacement of a coordinated ethylene unit by CO is a rare occurrence in early metal complexes.[22] The strong backbonding in Zr ethylene complexes should confer a degree of Zr(IV) metallacycle character in the metal-ethylene bonding; however, it is apparent that considerable Zr(II) character is still present in these ethylene derivatives.

4.4.3   Preparation of ^{Pr}[P$_2$Cp]Zr(η^2-PhCCPh)Br

Given the facile ligand substitution reaction observed for the ethylene derivatives **31** and **32** with CO, and the tendency for early metal alkene complexes to be substituted by alkynes, we were interested to test whether a bulky alkyne would give a similar result in these systems. In this context, none of the complexes described in the previous chapter were observed to react with internal alkynes. A toluene solution of ethylene **31** reacts with 1 equivalent of diphenylacetylene (PhCCPh) under ambient conditions to displace the ethylene ligand and generate the alkyne complex ^{Pr}[P$_2$Cp]Zr(η^2-PhCCPh)Br (**35**), which can be isolated as pale yellow crystals (equation

4.10). In contrast to the immediate displacement of ethylene by CO to give carbonyl **33**, the corresponding ligand substitution reaction of **31** with diphenylacetylene is slower, requiring 24 hours for completion. This observation is consistent with a slower rate for the bulky alkyne in comparison to the small linear CO molecule, and points to a probable requirement that a phosphine must dissociate to allow room for the incoming alkyne.

syn-**31**   *anti*-**31**

$- C_2H_4$ | $PhC \equiv CPh$

(4.10)

syn-**35**   *anti*-**35**
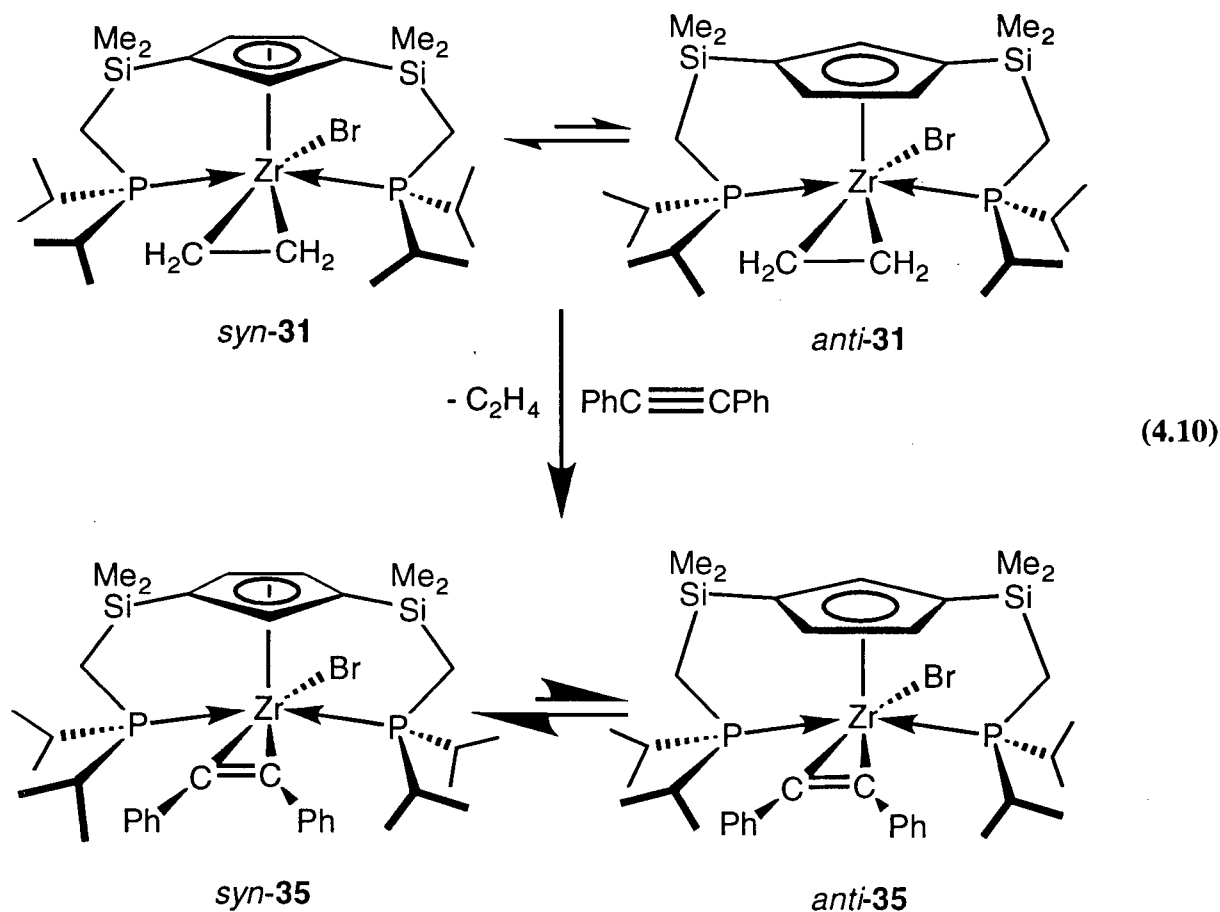
The molecular structure of alkyne **35**, shown in Figure 4.7, was determined by an X-ray crystal structure analysis. Selected bond lengths and bond angles are listed in Table 4.6.

172
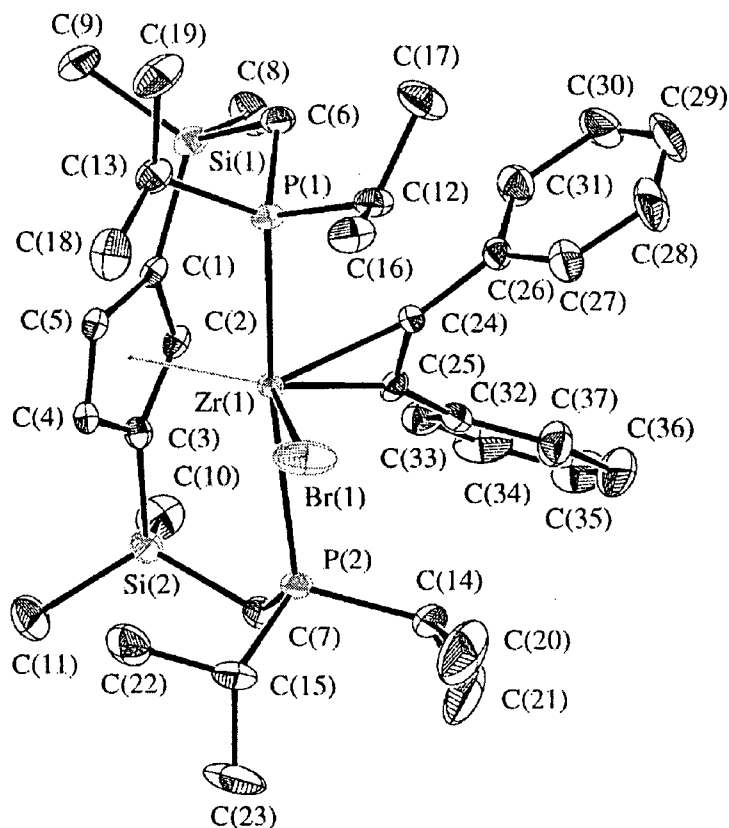
Figure 4.7 Molecular structure of $^{Pr}[P_2Cp]Zr(\eta^2\text{-PhCCPh})Br$ (**35**); 33% probability thermal ellipsoids are shown. Hydrogen atoms are omitted for clarity.

The solid state structure corresponds to the *syn* isomer, with the alkyne coordinated in a similar orientation parallel to the Cp ring as found in the structurally ethylene complexes **20** and **32**, and also as found in toluyne **27**. However, in **35** the alkyne unit is tilted from this parallel orientation by 9°. The short Zr(1)-C(24) and Zr(1)-C(25) bond lengths of 2.20 Å and 2.18 Å, respectively, are indicative of strong backbonding from the metal. This is also reflected in the C(25)-C(24)-C(26) bond angle of 127°, which illustrates the degree to which the phenyl rings are pulled back from the metal as a result of back-donation. Typical of metal alkyne complexes,[14] this gives a geometry of the coordinated alkyne resembling that of a metallacyclopropene (**E**), not unlike the

ortho-phenylene depiction for toluyne **28**. The double bond character is indicated by the C(24)-C(25) bond length of 1.32 Å.

$$
\begin{array}{c}
\mathbf{L_n} \\
\mathbf{M}
\end{array}
$$

Ph—C=C—Ph

E
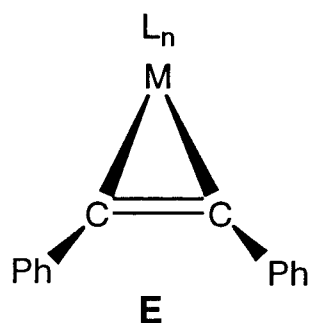
Table 4.6 Selected Bond Lengths (Å) and Bond Angles (°) for $^{Pr}[P_2Cp]Zr(\eta^2\text{-PhCCPh})Br$ (**35**).

Zr(1)-Br(1)	2.6771(5)	Br(1)-Zr(1)-P(1)	78.61(2)
Zr(1)-P(1)	2.8367(8)	Br(1)-Zr(1)-P(2)	76.35(2)
Zr(1)-P(2)	2.8129(8)	Br(1)-Zr(1)-C(24)	102.85(8)
Zr(1)-C(24)	2.197(3)	Br(1)-Zr(1)-C(25)	116.88(8)
Zr(1)-C(25)	2.182(2)	P(1)-Zr(1)-P(2)	154.87(4)
Zr(1)-Cp'	2.264	P(1)-Zr(1)-C(24)	77.57(7)
C(24)-C(25)	1.322(6)	Zr(1)-C(24)-C(26)	111.0(1)
C(24)-C(26)	1.471(4)	C(25)-C(24)-C(26)	126.8(2)

A comparison of the bonding in **35** with that of the ethylene complexes **20** and **32** shows in all cases that backbonding from the metal induces a lengthening of the C-C bond. However, the alkyne has a second π-orbital that can overlap with a metal d orbital of suitable symmetry such that this ligand can potentially be represented as a 4-electron donor. In **35** this interaction is in competition with one of the π-donor orbitals from the Cp ring, which diminishes the ability of the alkyne to donate electron density from its second π-bond. But the observation that alkyne **35** is unreactive in the presence of CO, in direct contrast to the rapid reaction seen for ethylene **31**,

174

suggests that the former complex is a fully saturated 18-electron species, implying that there is at least some component present to this π-bond from the alkyne to the metal centre.

In solution alkyne **35** exists as two isomers in a 3:2 ratio, based on the ^1H and $^{31}P\{^1H\}$ NMR spectra. There are two singlets in the $^{31}P\{^1H\}$ NMR spectrum for the major (8.53 ppm) and minor isomer (11.6 ppm), respectively, and a corresponding set of resonances in the ^1H NMR spectrum for each species. As with analogous examples encountered in the previous chapter, these species are likely the *syn* and *anti* stereoisomers. A ^1H NOEDIFF NMR experiment determined that the *anti* isomer is the major species in solution. Irradiation of the resonance assigned to the two equivalent protons in the Cp ring of the major isomer showed an enhancement of the signals for the ortho protons of the phenyl ring; no effect was detected when the resonance of the unique Cp proton was irradiated. The VT $^{31}P\{^1H\}$ NMR spectra show that these isomers interconvert, with increased line broadening evident in both peaks as the temperature is raised. Curiously, a change in the equilibrium ratio of these species was not detected from this study.

4.4.4 Preparation of asymmetric dinuclear hydrides {^{R}[P$_2$Cp]ZrBrH$_2$}$_2$ (R = Me, Pr^i)

The ethylene complexes **31** and **32** each react slowly under an atmosphere of H$_2$ to give dinuclear bridging hydride species of the general formula {^{R}[P$_2$Cp]ZrBrH$_2$}$_2$ (**36**: R = Pr^i, **37**: R = Me) (equation 4.11).

$$^R[P_2Cp]Zr(\eta^2\text{-}CH_2=CH_2)Br \xrightarrow[\text{- }CH_3CH_3]{H_2} \{^R[P_2Cp]ZrBrH_2\}_2 \quad (4.11)$$

31 R = Pr^i **36** R = Pr^i

32 R = Me   **37** R = Me

175
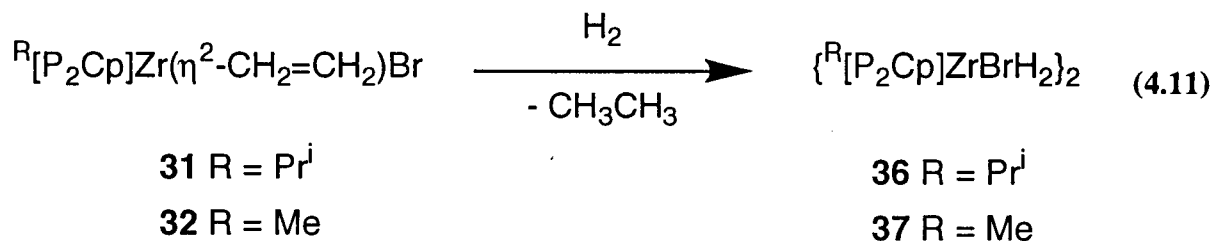
The ^{1}H and ^{31}P{^{1}H} NMR spectra indicate that both of these derivatives possess an asymmetric structure, and that this asymmetry is represented in a different manner for each. An X-ray crystal structure determination obtained for the ^{Me}[P₂Cp] derivative **37**, depicted in Figure 4.8, serves to evaluate the structural differences between the two complexes. Selected bond lengths and bond angles for **37** are listed in Table 4.8. A skeletal representation of the molecular structure shown below, with all the substituents removed from the silyl and phosphine groups, simplifies the important aspects of the asymmetric geometry.

P(4)

Si(4)

Si(1)

Si(2)

H(1)

Zr(2)   Zr(1)

H(2)   P(1)

Si(3)

Br(2)

P(2)   Br(1)

P(3)
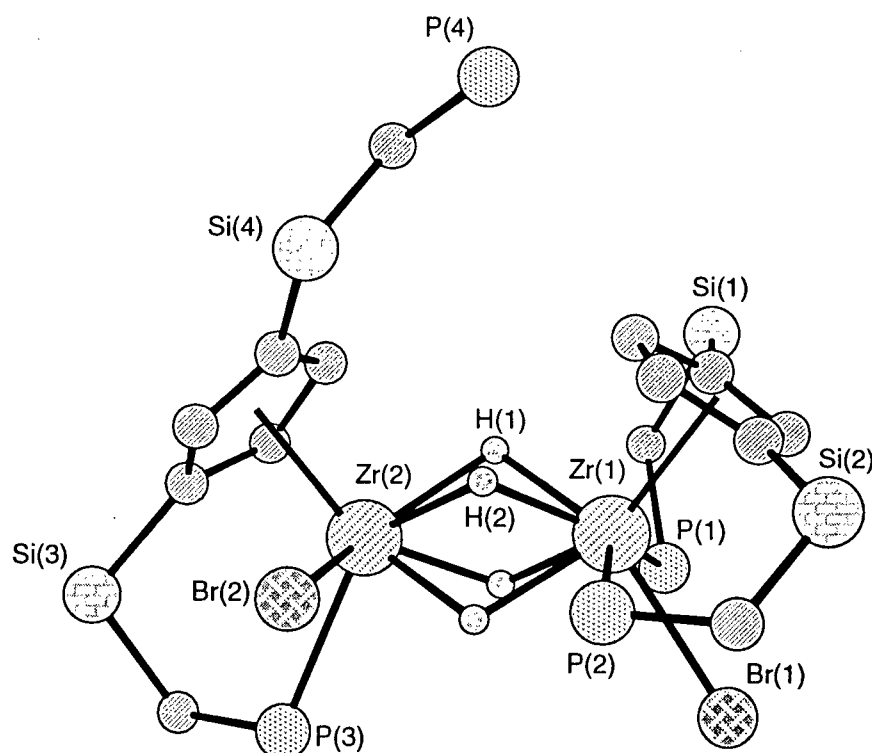
The structure above exhibits an asymmetric dinuclear framework bridged by four hydride ligands. Two of the bridging hydrides (H(1) and H(2)) were refined isotropically; the other two hydrides were placed in difference map or geometrically reasonable positions but were not refined. The two sides of this asymmetric structure can be assessed separately. The geometry

176

around Zr(1) approaches that of a normal piano-stool geometry. The two phosphine donors are coordinated *trans* to each other, while the bromide is located *syn* to both phosphines and *trans* to a general coordination site occupied by the bridging hydrides. In contrast, only one of the phosphines is coordinated to Zr(2), while the remaining side-arm is left dangling. A reduction in the number of ligands bound to Zr(2) is compensated for by a Zr-P bond distance that is 0.1 Å shorter than the corresponding Zr(1)-P bond lengths. A twist in the ancillary ligand of approximately 90 ° around the Zr(2)-Cp'(2) axis orients the dangling side-arm towards the other half of the molecule, and also gives rise to an eclipsed geometry between P(2) and Br(2), and between Br(1) and P(3).
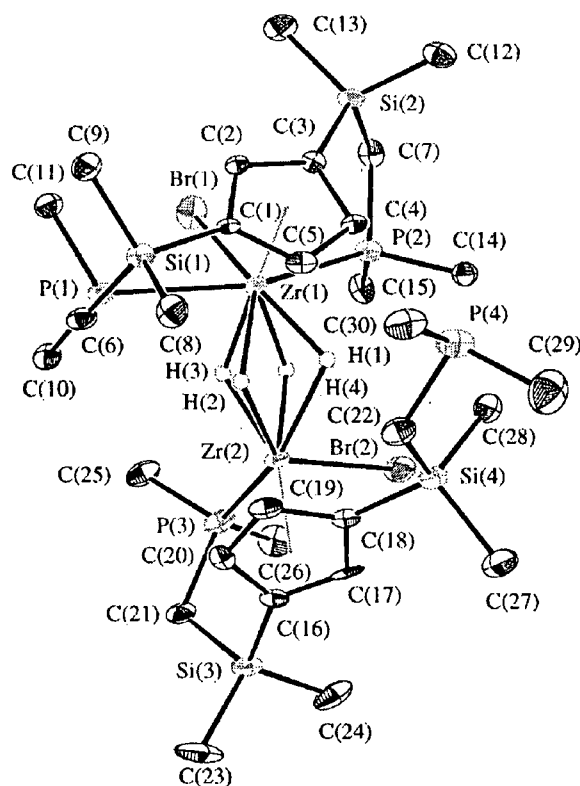
Figure 4.8   Molecular structure of {^{Me}[P$_2$Cp]ZrBr}$_2$(μ-H)$_4$ (**37**); 33% probability thermal ellipsoids are shown. Hydrogen atoms are omitted for clarity.

Table 4.7 Selected Bond Lengths (Å) and Bond Angles (°) for {^{Me}[P$_2$Cp]ZrBr}$_2$(μ-H)$_4$ (**37**).

Zr(1)···Zr(2)	3.1418(10)	Br(1)-Zr(1)-P(1)	74.43(5)
Zr(1)-Br(1)	2.7234(10)	Br(1)-Zr(1)-P(2)	74.41(5)
Zr(2)-Br(2)	2.7212(10)	P(1)-Zr(1)-P(2)	148.22(6)
Zr(1)-P(1)	2.8367(8)	Br(2)-Zr(2)-P(3)	79.84(5)
Zr(1)-P(2)	2.8129(8)	Br(1)-Zr(1)-Cp'(1)	112.7
Zr(2)-P(3)	2.711(2)	Br(2)-Zr(2)-Cp'(2)	105.5
Zr(1)-H(1)	1.86(5)	P(1)-Zr(1)-H(1)	127.2(15)
Zr(1)-H(2)	2.12(6)	P(1)-Zr(1)-H(2)	75.0(15)
Zr(2)-H(1)	2.03(5)	P(3)-Zr(2)-H(1)	136.5(15)
Zr(2)-H(2)	2.06(6)	P(3)-Zr(2)-H(2)	135.6(15)

The Zr···Zr contact of 3.142 is relatively short in comparison to some bridging hydride species, but similar to other analogues that also have phosphine coordination present. Bridging of the small hydrides brings the two Zr centres in close proximity to one another, which in turn induces significant steric interactions between the two ancillary ligands of each monomer. It is this steric pressure that forces one of the phosphines out of the coordination sphere.

The ^{31}P{^{1}H} NMR spectrum of **37** shows a singlet at -55 ppm for the dangling phosphine, another at -15 ppm for the lone phosphine coordinated to Zr(2), and an AB doublet of doublets ($^2J_{PP}$ = 58 Hz) at -15 ppm and -17 ppm for the two phosphines coordinated to the other metal centre. This spectrum is in agreement with the chemical environment of the phosphines in the solid state structure. The complicated ^{1}H NMR spectrum of **37** is also consistent with the C$_1$ symmetry shown in Figure 4.8, with separate resonances for each group in the ancillary ligands. For example, there are eight singlets for the silylmethyl groups, another eight peaks for the methyl substituents of the isopropyl groups, and six peaks in the Cp region. The hydride region

of the ^{1}H{^{31}P} NMR spectrum (Figure 4.9) shows two broad, equal intensity peaks at 3.74 ppm and 3.89 ppm that each integrate to two protons. These resonances are not observed when ethylene **32** is reacted with D$_2$. The narrower peak at 3.74 ppm is split into two resonances in the corresponding ^{1}H NMR spectrum ($^2J_{PH}$ = 80 Hz) (Figure 4.8).
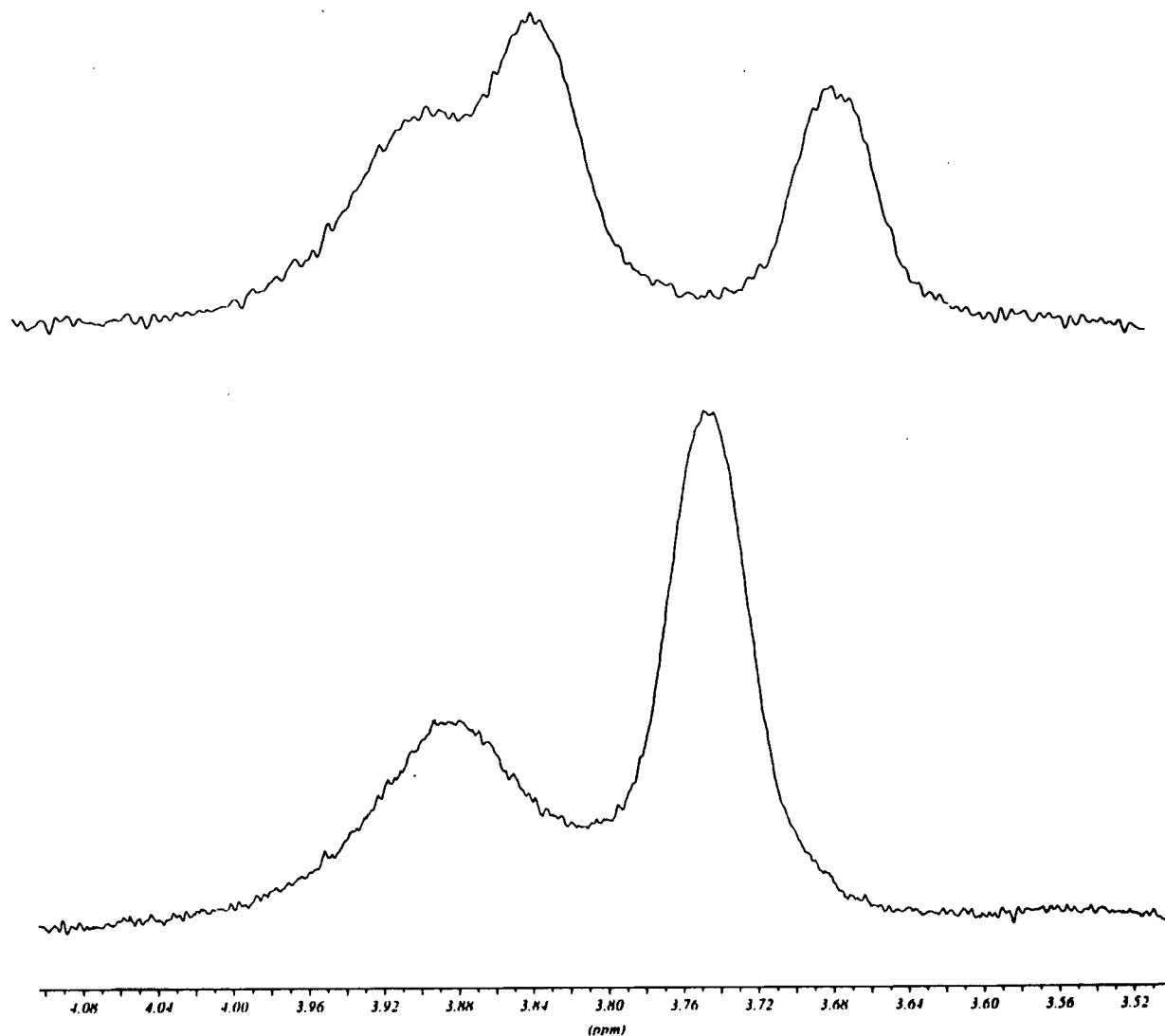
Figure 4.9   Hydride region of the ^{1}H NMR spectrum for {^{Me}[P$_2$Cp]ZrBr}$_2$(μ-H)$_4$ (**37**).

The bottom trace shows the corresponding ^{1}H{^{31}P} NMR spectrum.

179

These observations indicate that there are two averaged chemical environments for the hydrides, with an exchange process suggested by the broadened line widths. The chemical shifts are in the normal range for bridging ligands in Zr hydride complexes,[23] but the rather large $^2J_{PH}$ coupling for two of the hydrides is more suggestive of terminal ligands. The latter possibility is consistent with the vacant site on Zr(2) that is evident in the solid state structure, which could easily accommodate two terminal hydrides. As mentioned earlier, the positions of two of the metal hydrides were not refined. This arrangement could also account for the observed coupling of these protons to only one phosphorus nucleus. However, the chemical shift for a terminal hydride in a Zr complex is generally located further downfield in comparison to the resonances observed for **37**.

In contrast to crystalline **37**, the ^{Pr}[P$_2$Cp] derivative **36** was isolated as a hydrocarbon-soluble greenish oil. There are two singlets in the ^{31}P{^{1}H} NMR spectrum for **36**, at -5.6 ppm for an uncoordinated phosphine environment, and at 39.2 ppm for a bound phosphine. The ^{1}H NMR spectrum reveals the presence of two different ancillary ligand environments, each corresponding to C_s symmetry. For example, there are four silylmethyl resonances observed (two for each ligand), while the Cp region of the spectrum shows a separate doublet and triplet for each ligand. The remainder of the spectrum exhibits a similar duplication of peaks for two ancillary ligands. The hydride resonances are identified by those peaks that disappear in the ^{1}H NMR spectrum obtained from a sample of ethylene **31** that is treated with D$_2$. There is one broad hydride peak near 2.3 ppm, which integrates for three protons, that does not change appreciably in the ^{1}H{^{31}P} NMR spectrum. In contrast, a triplet at 5.23 ppm ($^2J_{PH}$ = 74 Hz) for one hydride in the ^{1}H NMR spectrum becomes a singlet in the corresponding ^{1}H{^{31}P} NMR spectrum.

36
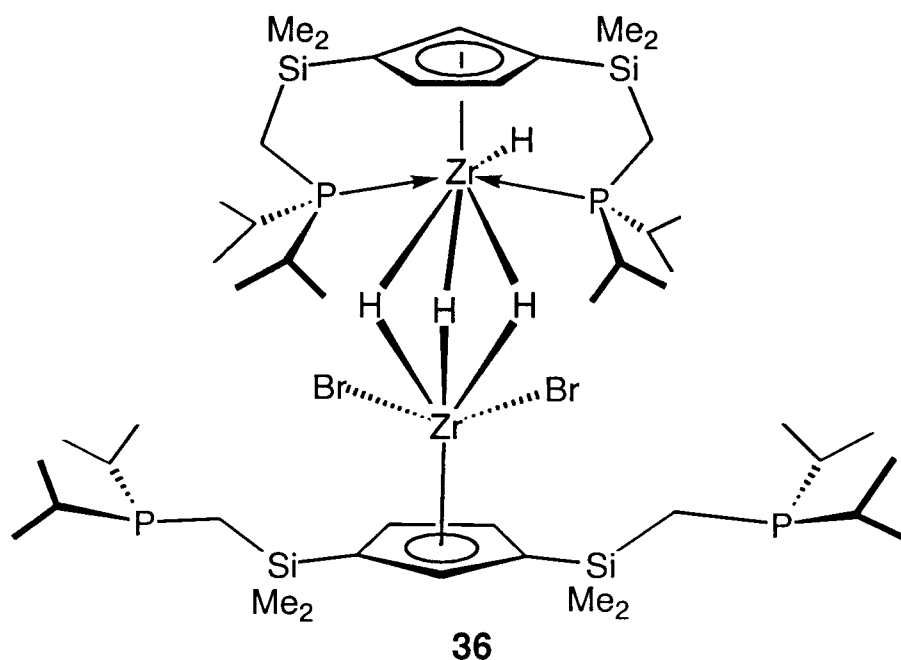
Based on the spectroscopic data the structure depicted above is proposed for **36**. This structure is consistent with two different ancillary ligand environments, each possessing C_s symmetry. The coordinated phosphines on one metal centre are equivalent, as are the two dangling phosphines on the other ligand, which overall give rise to two singlets in the $^{31}P\{^1H\}$ NMR spectrum as observed. The broad peak at 2.3 ppm is in an appropriate range for three bridging hydrides, while the downfield chemical shift and the large $^2J_{PH}$ value for the triplet at 5.23 ppm is consistent with a terminal hydride coupled to two equivalent phosphines. Unfortunately, an identifiable peak could not be detected in the solution IR spectrum of **36** for either an M-H or M-D bond stretch.

Although the asymmetric structures depicted above for hydrides **36** and **37** are unusual, there is precedent with other asymmetric dinuclear Group 4 hydride species,[24] including an analogous example, $Zr_2H_4(BH_4)_4(dmpe)_2$,[25] that contains a similar arrangement of one terminal and three bridging hydride ligands to that proposed for **36**. In comparing the structures of the two hydride complexes reported here, there is one less phosphine able to coordinate to the metal in the bulkier $^{Pr}[P_2Cp]$ derivative **36** than in **37**. This observation is consistent with the different

181

manner in which the two ancillary ligands adjust to the crowded geometry imposed by the bridging hydride structure.

4.4.5 Preparation of $^{Pr}[P_2Cp]Zr(\eta^2\text{-}CH_2=CH_2)R'$ (R' = Me, C_5H_5)

In contrast to the alkylidene and ketene complexes discussed in the previous chapter, which are resistant to alkylating agents, the bromide ligand in ethylene **31** can be substituted as shown below (equation 4.12) to yield new Zr ethylene derivatives.

$$^{Pr}[P_2Cp]Zr(\eta^2\text{-}CH_2=CH_2)Br \xrightarrow[\text{- MBr}]{\text{MR'}} {}^{Pr}[P_2Cp]Zr(\eta^2\text{-}CH_2=CH_2)R' \quad (4.12)$$

31

38 R' = Me

39 R' = C_5H_5
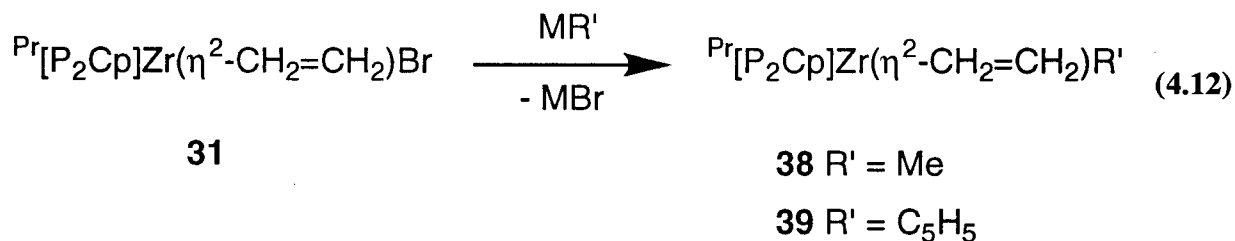
The characteristic spectroscopic feature of the methyl derivative **38** is the triplet ($^3J_{PH}$ = 10 Hz) at -0.67 ppm in the ^1H NMR spectrum for the methyl group attached to Zr. The distinctive Cp region of this spectrum is nearly identical to that of the major *syn* isomer of **31**, suggesting that the solution structure of **38** (only one species seen) is exclusively the *syn* isomer.

The Cp derivative **39** could be isolated as reddish-orange crystals. There are two equal intensity singlets in the $^{31}P\{^1H\}$ NMR spectrum for **39** at -5.3 and 42.3 ppm, corresponding to one coordinated and one dangling phosphine, respectively. The ^1H NMR spectrum shows a doublet ($^3J_{PH}$ = 2 Hz) at 5.20 ppm for the five protons of the C_5H_5 ring; the downfield chemical shift suggests that this ligand is coordinated in an η^5-mode, although rapid ring whizzing of an η^1-ligand could also account for the averaged chemical environment. As the ligand array in this complex is similar to that in the structurally characterized metallocene derivative $Cp_2Zr(\eta^2\text{-}CH_2=CH_2)(PMe_3)$,[26] it is reasonable to consider an analogous structure for **39** as shown below.
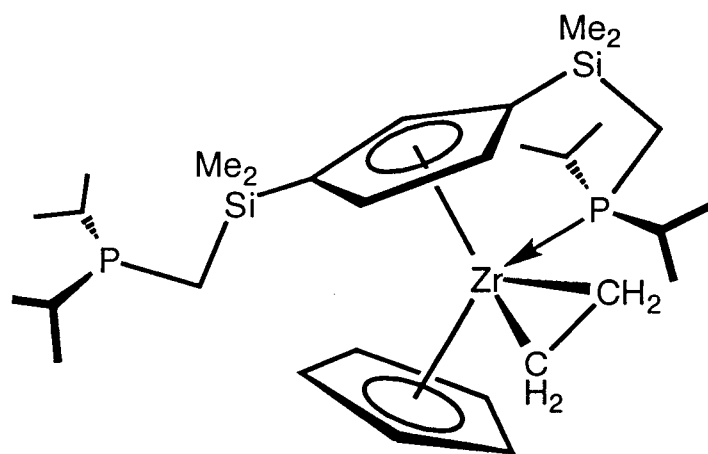
39

The asymmetric geometry renders all four ethylene protons inequivalent, thus generating a complicated second order splitting pattern in the ^{1}H NMR spectrum for each (with additional coupling to the coordinated phosphine). This asymmetry is also evident in three separate resonances for the Cp ring of the ancillary ligand. The presence of only one coordinated phosphine in **39** supports the view of the C_5H_5 ligand as η^5-bound; the steric and electronic saturation provided by this coordination mode yields an 18-electron species which would force one side arm to remain dangling, as observed. The ethylene unit and the coordinated phosphine thus can be considered to be occupying the metallocene wedge, with the other side-arm left out of the coordination sphere.

4.4.6   Reactivity of ^{Pr}[P$_2$Cp]Zr(η^2-CH$_2$=CH$_2$)(η^5-C$_5$H$_5$) with CO, H$_2$

The reactivity of the 18-electron ethylene complex **39** was briefly examined to compare with the results observed for the 16-electron ethylene analogue **31**. As opposed to **31**, which coordinates CO almost instantly, the reaction of **39** with CO is considerably slower, requiring more than two weeks for completion under the same reaction conditions (equation 4.13). This remarkable difference in reaction times can be traced to the electronic saturation in **39**, adding

further evidence that the C_5H_5 donor in this complex is η^5-coordinated. As a result, either a ligand in **39** must dissociate or alternatively the Cp ring must undergo η^5-η^3 ring slippage, prior to the coordination of a CO molecule. The similar lack of reactivity of alkyne **35** with CO presumably originates from the same electronic saturation of that species.

$$^{Pr}[P_2Cp]Zr(\eta^2\text{-}CH_2\text{=}CH_2)(\eta^5\text{-}C_5H_5) \xrightarrow[\text{- } C_2H_4]{C\equiv O} {}^{Pr}[P_2Cp]Zr(\eta^5\text{-}C_5H_5)(CO) \quad (4.13)$$

39 **40**
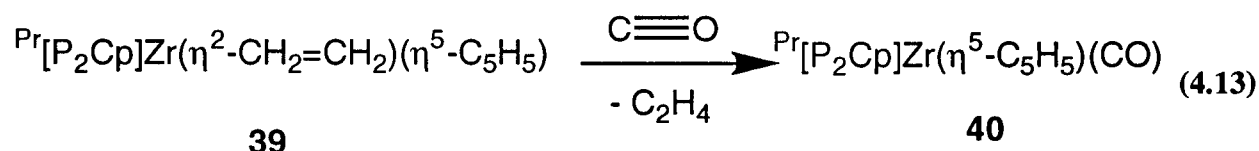
The eventual product from the above reaction is the carbonyl species $^{Pr}[P_2Cp]Zr(\eta^5\text{-}C_5H_5)(CO)$ (**40**), which is accompanied by the evolution of free ethylene as observed with the analogous reaction that forms carbonyl **33**. The $^{31}P\{^1H\}$ NMR spectrum of **40** is similar to that of the precursor **39**, with one singlet at 58.7 ppm and another at -4.8 ppm. The presence of the carbonyl ligand is indicated by a single downfield resonance at 308 ppm ($^2J_{PC} = 2$ Hz) in the reaction with ^{13}CO. In contrast to **33**, the line width of this carbonyl peak is very narrow, with no evidence for exchange with the peak for excess ^{13}CO at 184 ppm. This difference in the lability of the respective carbonyl ligands in **33** and **39** may originate from the presence of one less CO ligand in **39**, which is not in competition for backbonding and hence is less labile. As an analogue of the metallocene carbonyl species $Cp_2Zr(CO)(PMe_3)$,[27] the proposed structure of **40** is depicted as shown below.

40
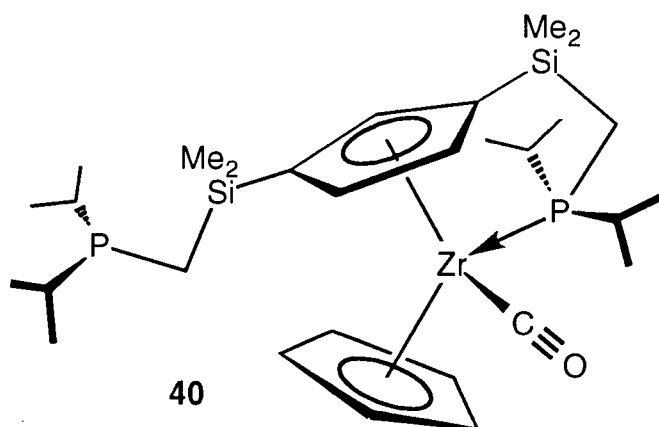
Exposure of a toluene solution of ethylene **39** to 4 atmospheres of H_2 over a period of one week yields very cleanly a new metal complex as a yellow oil that is proposed to be the hydride derivative $^{Pr}[P_2Cp]Zr(\eta^5\text{-}C_5H_5)H_2$ (**41**) (equation 4.14).

$$^{Pr}[P_2Cp]Zr(\eta^2\text{-}CH_2{=}CH_2)(\eta^5\text{-}C_5H_5) \xrightarrow[-\ CH_3CH_3]{H_2} {}^{Pr}[P_2Cp]Zr(\eta^5\text{-}C_5H_5)H_2 \qquad (4.14)$$

$$\mathbf{39} \qquad\qquad\qquad\qquad\qquad\qquad \mathbf{41}$$
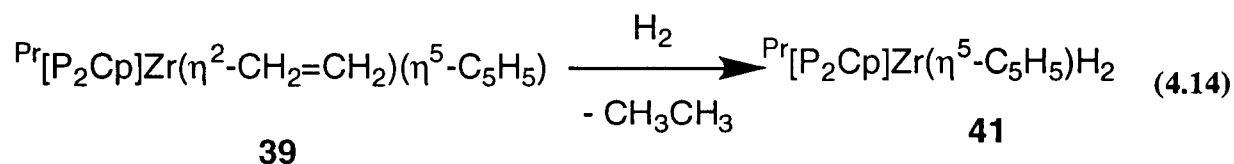
Unfortunately, the hydride resonances in **41** could not be located in the ^1H NMR spectrum between -10 and 20 ppm, although in a related hydride species, $(Cp^*CpZrH_2)_2$, the hydride resonances were similarly noted to be undetected. In the latter example this negative observation was ascribed to exchange processes involving the hydride ligands. The formulation of yellow **41** as a Zr(IV) hydride species is based on the absence of resonances in the ^1H NMR spectrum for either an intact ethylene ligand or an alkyl ligand resulting from an insertion reaction with H_2. The $^{31}P\{^1H\}$ NMR spectrum shows two new resonances for **41** at -5.6 and 43.9 ppm, indicating a structure that is similar to that of the precursor **39**. This complex is depicted here as a saturated, 18-electron metallocene analogue and hence a monomeric species, although examples of monomeric Zr and Hf hydrides are extremely scarce, as dimers are typically observed unless considerably bulky ligands are employed. Two notable examples are the metallocene derivative $Cp^*_2ZrH_2$[28] and the related anionic species $[Cp^*_2ZrH_3]^-$.[29] The 16-electron complex $Cp^*_2HfH_2$ does coordinate donor molecules at the central site of the equatorial wedge, but stable adducts have been restricted to using donors such as CO and PF_3.[30] In contrast, **41** may have an advantage in that the phosphine is an intramolecular donor already in place within the coordination sphere, to give a structure as proposed below.

185
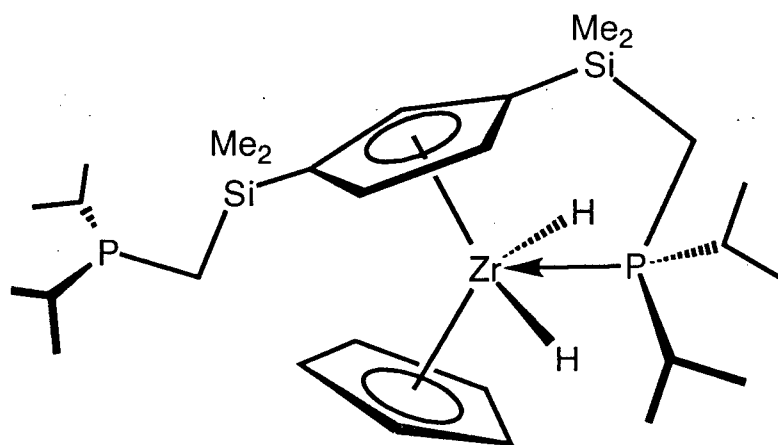
41

4.5 Future Work

In this chapter the steric and electronic effects of substituting methyl groups for isopropyl groups on the pendant phosphines were examined. This modification of the ancillary ligand resulted in a greater tendency for the less sterically hindered phosphines to coordinate, as illustrated by the structures of dibenzyl **27** and tribenzyl **30**. In **27** the improved phosphine binding eliminates the complicated equilibrium seen in the ^{Pr}[P$_2$Cp] analogue **14**, while the presence of two coordinated phosphines in **30** is in sharp contrast to the dangling side-arms evident in the other tribenzyl species **3**. The modified ligand can also affect the observed reactivity, as seen for the two dibenzyl complexes. The thermal reaction of one derivative leads to an alkylidene complex, while the other dibenzyl species yields a toluyne complex as a final product.

With the ethylene derivatives **31** and **32** the effects of the different ligands are more subtle. The structures of these complexes are evidently similar, and the observed reactivity with CO and H$_2$ yields similar products. However, although asymmetric dinuclear hydride species are

obtained in the latter reaction for each derivative, the different steric requirements of each ligand are manifested in a distinct structure for each hydride complex.

As mentioned in the introduction to this chapter, several aspects of the chemistry outlined here are preliminary results, which may be pursued further. For example, mechanistic information regarding the intramolecular thermal reaction that generates a toluyne complex **28** from dibenzyl **27** may be obtained from selective labeling studies. The thermal reactivity of analogous dialkyl species (i.e., the neosilyl or neopentyl derivatives) could also be compared to the results seen for the ^{Pr}[P$_2$Cp] analogues. In addition, the reactivity of several of the complexes described in this thesis has either not been tested or only briefly examined. Examples within this category include the hydride and carbonyl complexes.

Another direction for future work is outlined below in two alternate strategies to modify the steric or electronic properties of complexes coordinated by these hybrid ancillary ligands. The first is a modification of the cyclopentadienyl ring, while the second is an extension of P$_2$Cp chemistry with other metals.

4.5.1 Modification to a [P$_2$Cp'] ligand set

The strategy for a new ligand design, P$_2$Cp' (' denotes substitution at the Cp ring), is shown below in Scheme 4.3. The attachment of a bulky *tert*-butyl substituent to the Cp ring is anticipated to direct the two side-arms into adjacent 1,2 positions, in a manner similar to that observed in a related chiral metallocene-based ligand.[31] Otherwise, the synthetic steps shown below are analogous to those utilized in the preparation of the underivatized ancillary ligand outlined in Chapter 2.
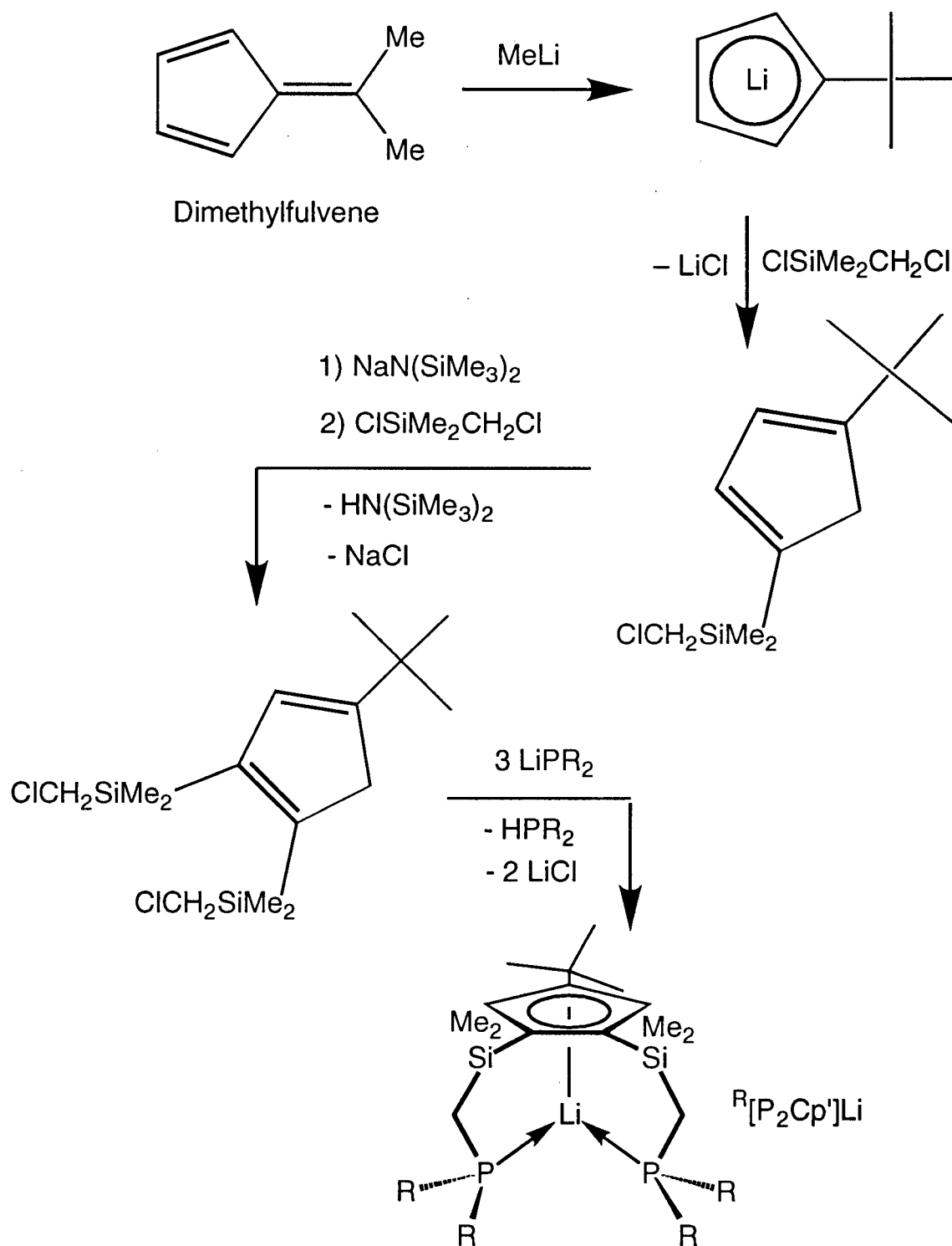
Scheme 4.3 Reaction scheme for the synthesis of the ancillary ligand $^R[P_2Cp']Li$.

The reactions leading up to the disubstituted side-arm precursor are very clean. However, initial attempts to obtain the lithiated salt of the ligand shown above have met with mixed results. The desired product is formed, but the yield is lowered by a complicating coupling reaction that generates R_2P-PR_2. This result is consistently observed in a variety of reaction conditions.

One surreptitious result has yielded a structurally characterized Zr(III) chloride complex, $^{Pr}[P_2Cp']ZrCl_2$, the structure of which is shown below in Figure 4.10. Selected bond lengths and bond angles are listed in Table 4.8.
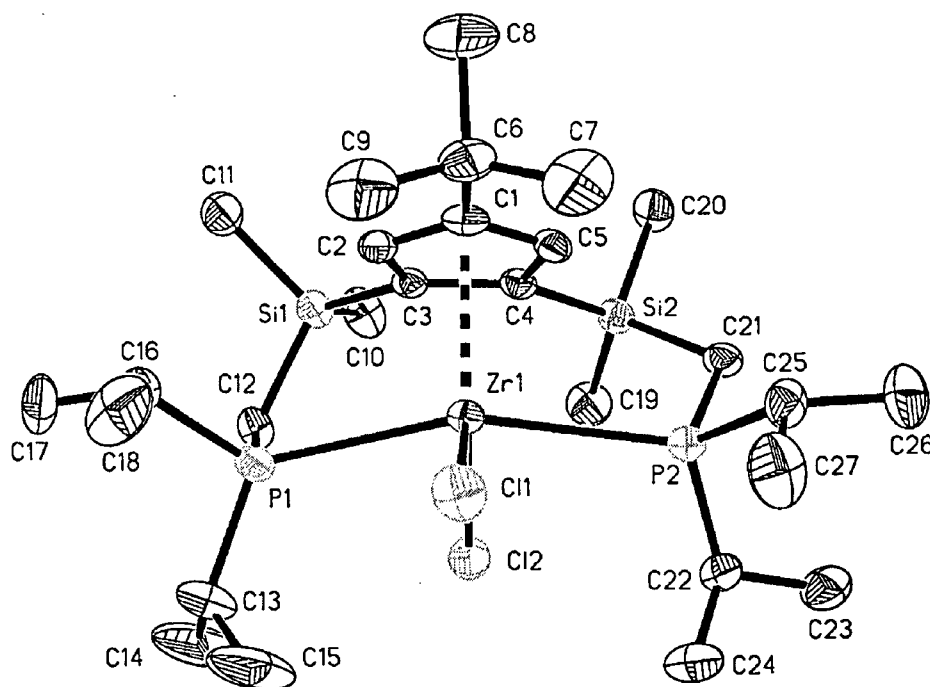
Figure 4.10 Molecular structure of $^{Pr}[P_2Cp']ZrCl_2$ (**42**); 33% probability thermal ellipsoids are shown. Hydrogen atoms are omitted for clarity.

Table 4.8   Selected Bond Lengths (Å) and Bond Angles (°) for $^{Pr}[P_2Cp']ZrCl_2$ (**32**).

Zr(1)-Cl(1)	2.4869(8)	Cl(1)-Zr(1)-Cl(2)	109.09(3)
Zr(1)-Cl(2)	2.5091(8)	Cl(1)-Zr(1)-P(1)	92.44(3)
Zr(1)-P(1)	2.8569(9)	Cl(1)-Zr(1)-P(2)	91.51(3)
Zr(1)-P(2)	2.8571(9)	P(1)-Zr(1)-P(2)	157.29(3)
Zr(1)-C(1)	2.622(3)	C(3)-Si(1)-C(12)	107.87(13)
Zr(1)-C(2)	2.502(3)	C(4)-Si(2)-C(21)	102.61(13)
Zr(1)-C(3)	2.406(3)	P(1)-C(12)-Si(1)	112.7(2)
Zr(1)-C(4)	2.390(3)	P(2)-C(21)-Si(2)	114.1(2)
Zr(1)-C(5)	2.500(3)		

An examination of the structure of this compound leads to a comparison with other Zr(III) derivatives as discussed below. The structure shown above for **42** depicts a monomeric Zr(III) species in a four-legged piano-stool geometry, with the phosphines located in mutually *trans* coordination sites. The steric impact of the bulky tert-butyl group is evident in the long Zr(1)-C(1) bond distance of 2.62 Å in comparison to the other Zr-Cp bond lengths. The monomeric structure is presumably due to the large isopropyl phosphine substituents preventing dimerization. A similar result is observed for the analogous $^{Pr}[P_2Cp]ZrCl_2$ derivative (**43**), an isolable intermediate in the preparation of the bridging dinitrogen complex $\{^{Pr}[P_2Cp]ZrCl\}_2(\mu$-$N_2)$ (**44**). As with the [P₂Cp'] derivative **42**, **43** is also a green paramagnetic species (an ESR triplet is observed due to coupling to two equivalent phosphines), which is consistent with a monomeric structure. Contrasting with these structures is that of the $^{Me}[P_2Cp]$ derivative (**45**), a minor product in the thermal decomposition of **29** as mentioned earlier. The solid state structure of **45** is depicted in Figure 4.11. Selected bond lengths and bond angles are given in Table 4.9. The structure of **45** reveals a chloride-bridged dimer as a result of a less crowded geometry afforded by the methyl groups on the phosphines. Each metal centre is also coordinated by a

terminal chloride ligand that is bound *trans* to the Cp donor. The diamagnetic behaviour of this

species in solution is consistent with the solid state structure.
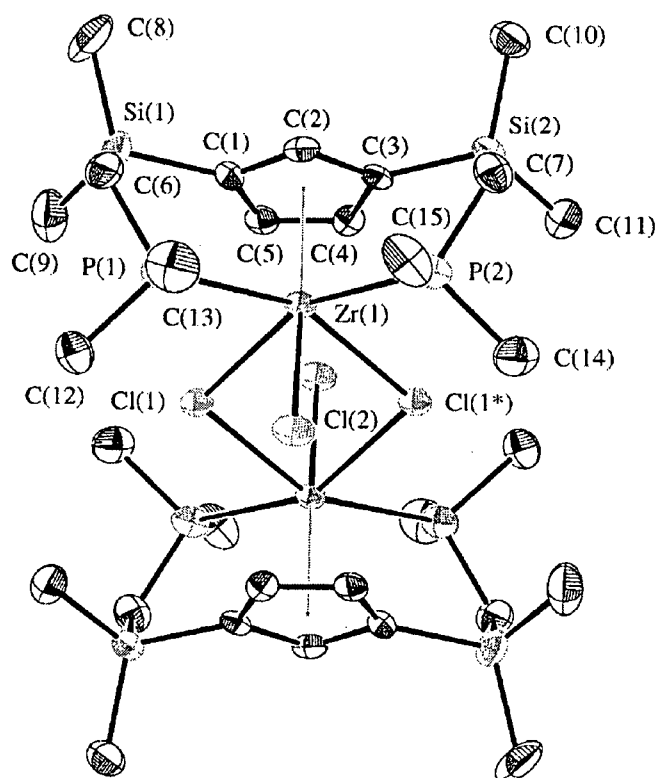
Figure 4.11   Molecular structure of {^{Me}[P$_2$Cp]ZrCl}$_2$(μ-Cl)$_2$ (**45**); 33% probability

thermal ellipsoids are shown. Hydrogen atoms are omitted for clarity.

Table 4.9   Selected Bond Lengths (Å) and Bond Angles (°) for {^{Me}[P$_2$Cp]ZrCl}$_2$(μ-Cl)$_2$

(45).

Zr(1)-Cl(1)	2.6712(15)	Cl(1)-Zr(1)-Cl(1*)	80.27(4)
Zr(1)-Cl(1*)	2.6673(14)	Cl(1)-Zr(1)-Cl(2)	82.75(5)
Zr(1)-Cl(2)	2.6014(15)	Cl(1)-Zr(1)-P(1)	84.92(5)
Zr(1)-P(1)	2.763(2)	Cl(1)-Zr(1)-P(2)	155.01(5)
Zr(1)-P(2)	2.750(2)	Cl(1)-Zr(1)-Cp	103.8
Zr(2)-Cl(1)	2.6492(14)	P(1)-Zr(1)-P(2)	96.48(5)
Zr(2)-Cl(1*)	2.6742(15)	Zr(1)-Cl(1)-Zr(2)	99.86(5)
Zr(2)-Cl(3)	2.6197(15)	Zr(1)-Cl(1*)-Zr(2)	99.32(5)
Zr(2)-P(3)	2.752(2)	Cl(1)-Zr(2)-Cl(1*)	80.54(4)
Zr(2)-P(4)	2.743(2)	P(3)-Zr(2)-P(4)	97.70(5)

4.5.2   P$_2$Cp complexes of Th(IV)

In considering other metals that might show interesting chemistry with the ancillary ligand utilized for Zr and Hf in this thesis, one appealing choice is Th(IV). This tetravalent actinide exhibits reactivity analogous to the heavier Group 4 analogues, including applications in metallocene-based catalysis.[32]   Another potential advantage is the large size (ionic radius = 0.90 Å compared to 0.75 Å for Zr(IV),[33] which provides ample room for the extended chelate size of this particular ligand. A suitable soluble precursor is the adduct ThBr$_4$(THF)$_4$, which reacts with one equivalent of ^{Pr}[P$_2$Cp]Li in toluene to give ^{Pr}[P$_2$Cp]ThBr$_3$ (**46**) in good yield as colourless crystals. The NMR spectroscopic features for this complex are very similar to the NMR spectrum seen for the Zr derivative **1**. Therefore, it is not unreasonable to assume that a similar six-coordinate geometry is present for **46**. Unfortunately, this complex exhibits poor solubility in organic solvents, and preliminary reactivity studies suggest a more inert behaviour in comparison to the chemistry that has been observed for Zr.

192

$$\text{ThBr}_4(\text{THF})_4 + {}^{Pr}[\text{P}_2\text{Cp}]\text{Li} \xrightarrow[\begin{array}{c}\text{- LiBr}\\\text{- 4 THF}\end{array}]{}$$

(4.15)

46
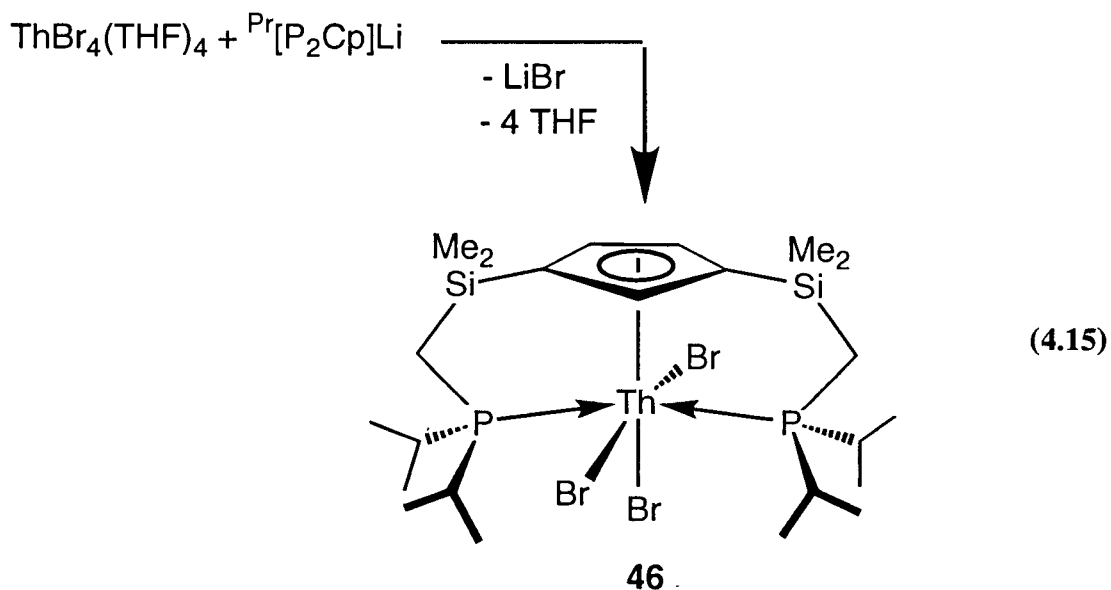
The large size and high electron count of this ancillary ligand restricts its use to metals with a large ionic radius and/or a low coordination number. For example, current work in laboratory is examining the chemistry of this ligand with Nb(III), Y(III) and Yb(II).

4.6   Concluding remarks

This thesis has investigated the structure, solution behaviour, and reactivity of a series of alkyl complexes of Zr and Hf coordinated by a cyclopentadienyldiphosphine ligand (P_2Cp). What emerges from this study is a common theme of subtle steric and electronic influences that becomes evident from the disparate solution dynamics of the two isostructural trichloride complexes to the appropriate balance of steric crowding and electronic stabilization that produces the alkylidene complexes.

4.7   Experimental Section

4.7.1   Procedures and Materials

Unless otherwise stated, general procedures were performed according to Section 2.7.1. ThBr$_4$(THF)$_4^{34}$ was synthesized according to literature preparations.

4.7.2   Syntheses

4.7.2.1 ^{Me}[P$_2$Cp]ZrCl$_3$ (25)

A solution of ^{Me}[P$_2$Cp]Li (3.56 g, 10.56 mmol) in 60 mL of toluene was added dropwise with stirring to a toluene slurry (60 mL) of ZrCl$_4$(THT)$_2$ (4.325 g, 10.56 mmol) at room temperature. The red colour of solution containing the lithiated ligand was discharged upon addition, and the slurry gradually turned yellow. The reaction mixture was left to stir for 48 h after which the solution was filtered, and the volume reduced to 30 mL and layered with hexanes. Pale yellow crystals were deposited from slow evaporation of this solution, and the procedure repeated by sequentially layering the mother liquor with hexanes. The isolated crystals were washed with cold hexanes and dried. Yield 4.73 g (85 %). ^{1}H NMR (20 °C, C$_6$D$_6$): δ 0.01 and 0.25 (s, 6H, Si(CH_3)$_2$), 0.60 and 0.72 (dt, 2H, $^2J_{HH}$ = 14Hz, $^2J_{PH}$ = 6Hz, SiCH_2P), 1.14 and 1.25 (t, 6H, $^2J_{PH}$ = 5Hz, P(CH_3)$_2$), 6.48 (d, 2H, $^4J_{HH}$ = 2Hz, Cp-H), 7.24 (t, 1H, $^4J_{HH}$ = 2Hz, Cp-H). ^{31}P{^{1}H} NMR (20 °C, C$_6$D$_6$): δ -21.0 (s). Anal. Calcd. for C$_{15}$H$_{31}$Cl$_3$P$_2$Si$_2$Zr: C, 34.18; H, 5.93. Found: C, 35.80; H, 5.98.

4.7.2.2 ^{Me}[P$_2$Cp]ZrCl$_2$(CH$_2$Ph) (26)

A solution of KCH$_2$Ph (74 mg, 0.57 mmol) in 20 mL of THF was added with stirring to a cooled (-78 °C) slurry of 25 (298 mg, 0.57 mmol) in 30 mL of THF. The dark red colour of the KCH$_2$Ph solution was discharged upon addition and the reaction mixture gradually turned

reddish after the addition was complete. The mixture was allowed to slowly warm to room temperature and left to stir for 12 h The solvent was then removed under vacuum and the red oily residue extracted with toluene and filtered. A bright red solid was obtained from a cold (-40 °C) toluene/hexanes mixture. Yield: (270 mg, 82 %). ^{1}H NMR (20 °C, C_6D_6): δ 0.01 and 0.28 (s, 6H, Si(CH_3)$_2$), 0.58 and 1.10 (dd, 2H, $^2J_{HH}$ = 7Hz, $^2J_{PH}$ = 8Hz, SiCH_2P), 0.93 and 1.51 (d, 6H, $^2J_{PH}$ = 5Hz, P(CH_3)$_2$), 3.27 (br t, 2H, $^2J_{PH}$ = 4Hz, CH$_2$Ph), 5.97 (d, 2H, $^4J_{HH}$ = 1Hz, Cp-H), 6.72 (t, 1H, $^4J_{HH}$ = 1Hz, Cp-H), 6.80 (t, 1H, $^3J_{HH}$ = 7Hz, p-C_6H_5), 7.09 (t, 2H, $^3J_{HH}$ = 7Hz, m-C_6H_5), 7.42 (d, 2H, $^3J_{HH}$ = 7Hz, o-C_6H_5). ^{31}P{^{1}H} NMR (20 °C, C_6D_6): δ -19.0 (s).

4.7.2.3 ^{Me}[P$_2$Cp]ZrCl(CH$_2$Ph)$_2$ (27)

A solution of KCH$_2$Ph (530 mg, 4.07 mmol) in 60 mL of THF was added with stirring to a cooled (-78 °C) slurry of **25** (1.070 g, 2.03 mmol) in 60 mL of THF. The dark red colour of the KCH$_2$Ph solution was discharged upon addition and the reaction mixture gradually changed from a cream coloured slurry to a cloudy brown solution. The mixture was allowed to slowly warm to room temperature and left to stir for 3 h, during which the colour turned more reddish. The solvent was then removed under vacuum and the red oily residue extracted with 30 mL of toluene and filtered. The filtrate was reduced to 10 mL, from which red crystals were obtained at -40 °C. A second crop of was obtained from the mother liquor, and the combined crystalline material was washed with cold hexanes. Yield: (820 mg, 60 %). ^{1}H NMR (20 °C, C_6D_6): δ 0.00 and 0.23 (s, 6H, Si(CH_3)$_2$), 0.19 and 0.84 (dd, 2H, $^2J_{HH}$ = 6Hz, $^2J_{PH}$ = 7Hz, SiCH_2P), 0.42 and 1.19 (d, 6H, $^2J_{PH}$ = 5Hz, P(CH_3)$_2$), 2.83 (br s, 4H, CH$_2$Ph), 6.35 (d, 2H, $^4J_{HH}$ = 1Hz, CpH), 6.78 (t, 2H, $^3J_{HH}$ = 7Hz, p-C_6H_5), 6.81 (t, 1H, $^4J_{HH}$ = 1Hz, Cp-H), 7.14 (t, 4H, $^3J_{HH}$ = 7Hz, m-C_6H_5), 7.66 (d, 4H, $^3J_{HH}$ = 7Hz, o-C_6H_5). ^{31}P{^{1}H} NMR (20 °C, C_6D_6): δ -18.5 (s). Anal. Calcd. for $C_{29}H_{45}ClP_2Si_2Zr$: C, 54.56; H, 7.10. Found: C, 54.90; H, 7.19.

4.7.2.4 ^{Me}[P$_2$Cp]Zr(η^2-C$_6$H$_3$Me)Cl (28)

A solution of **27** (520 mg, 0.81 mmol) in 20 of toluene was heated at 70 °C for 12 h. The bright red colour darkened slightly to a reddish brown. The solution was filtered and the volume reduced to 3 mL, from which pale yellow crystals were obtained at -40 °C. A second crop crystals was grown from the mother liquor, and the combined crystalline material was washed with cold hexanes. Yield: (263 mg, 59 %). ^{1}H NMR (20 °C, C$_6$D$_6$): δ -0.02 and 0.19 (s, 6H, Si(CH_3)$_2$), 0.90 and 1.01 (dd, 1H, $^2J_{HH}$ = 10Hz, $^2J_{PH}$ = 6Hz, SiCH_2P), 1.29 and 1.31 (d, 6H, $^2J_{PH}$ = 3Hz, P(CH_3)$_2$), 1.76 and 1.79 (dd, 1H, $^2J_{HH}$ = 6Hz, $^2J_{PH}$ = 5Hz, SiCH_2P), 2.43 (s, 3H, C$_6$H$_3$CH_3), 4.78 (t, 1H, $^4J_{HH}$ = 1Hz, Cp-H), 6.41 (d, 2H, $^4J_{HH}$ = 1Hz, CpH), 7.36 (d, 1H, $^3J_{HH}$ = 7Hz, C$_6$$H_3$), 7.82 (s, 1H, $^3J_{HH}$ = 7Hz, C$_6$$H_3$), 7.91 (d, 1H, $^3J_{HH}$ = 7Hz, C$_6$$H_3$). ^{31}P{^{1}H} NMR (20 °C, C$_6$D$_6$): δ -7.0 (s). Anal. Calcd. for C$_{22}$H$_{37}$ClP$_2$Si$_2$Zr: C, 48.37; H, 6.83. Found: C, 48.68; H, 6.75.

4.7.2.5 ^{Me}[P$_2$Cp]Zr(η^2-C$_6$H$_4$=CH$_2$)Cl (29)

A C$_6$D$_6$ NMR sample of **27** was immersed in a cooled bath (0 °C), and exposed to UV radiation ranging to 300 nm for a duration of 8 h. The bright red colour darkened slightly to a reddish brown. The 1H NMR spectrum obtained at intervals during this reaction showed the emergence of new resonances assigned to **29**. After 8 h the spectrum showed the persistence of residual **27**, and the emergence of additional peaks corresponding to the decomposition of **29**. Increasing the scale yielded a thermally sensitive reddish oil after workup in toluene. ^{1}H NMR (20 °C, C$_6$D$_6$): δ 0.21, 0.25, 0.30 and 0.42 (s, 3H, Si(CH_3)$_2$), 0.90 and 1.78 (dd, 2H, $^2J_{HH}$ = 8Hz, $^2J_{PH}$ = 7Hz, SiCH_2P), 0.72, 0.98, 1.12 and 1.21 (d, 3H, $^2J_{PH}$ = 5Hz, P(CH_3)$_2$), 2.78 (dd, 1H, $^3J_{HH}$ = 7Hz, $^4J_{HH}$ = 2Hz, H_A), 3.08 (dd, 1H, $^3J_{HH}$ = 7Hz, $^4J_{HH}$ = 1Hz, H_B), 3.17 (dd, 1H, $^4J_{HH}$ = 2Hz, $^4J_{PH}$ = 6Hz, H_C), 3.52 (m, 1H, $^3J_{HH}$ = 7Hz, $^4J_{HH}$ = 4Hz, $^4J_{PH}$= 7Hz, H_D), 5.04 (dd, 1H, $^3J_{HH}$ = 7Hz, $^4J_{HH}$ = 1Hz, H_E), 5.26, 5.59 and 6.47 (m, 1H, Cp-H), 5.99 (dd, 1H,$^3J_{HH}$ = 7Hz, $^4J_{HH}$ = 4Hz, H_F). ^{31}P{^{1}H} NMR (20 °C, C$_6$D$_6$): δ -13.8 and -13.9 (dd, $^2J_{PP}$ = 76Hz).

4.7.2.6 ^{Me}[P$_2$Cp]Zr(CH$_2$Ph)$_3$ (30)

A solution of KCH$_2$Ph (212 mg, 1.62 mmol) in 20 mL of THF was added with stirring to a cooled (-78 °C) slurry of **25** (266 mg, 0.54 mmol) in 30 mL of THF. The dark red colour of the KCH$_2$Ph solution was discharged upon addition and the reaction mixture gradually changed from a cream coloured slurry to a dark red solution. The mixture was allowed to slowly warm to room temperature and left to stir for 2 h. The solvent was then removed under vacuum and the red oily residue extracted with 20 mL of toluene and filtered. The filtrate was reduced to 3 mL and combined with hexamethyldisiloxane, from which red crystals were obtained at -40 °C. Yield: (820 mg, 75 %). ^{1}H NMR (20 °C, C$_6$D$_6$): δ 0.04 and 0.25 (s, 6H, Si(CH_3)$_2$), 0.11 and 0.39 (dd, 2H, $^2J_{HH}$ = 5Hz, $^2J_{PH}$ = 7Hz, SiCH_2P), 0.36 and 0.78 (t, 6H, $^2J_{PH}$ = 5Hz, P(CH_3)$_2$), 2.60 (t, 6H, $^2J_{PH}$ = 4Hz, CH_2Ph), 6.21 (d, 2H, $^4J_{HH}$ = 1Hz, Cp-H), 6.71 (t, 1H, $^4J_{HH}$ = 1Hz, Cp-H), 6.82 (t, 3H, $^3J_{HH}$ = 7Hz, p-C$_6$H$_5$), 7.01 (t, 6H, $^3J_{HH}$ = 7Hz, m-C$_6$H$_5$), 7.60 (d, 6H, $^3J_{HH}$ = 7Hz, o-C$_6$H$_5$). ^{31}P{^{1}H} NMR (20 °C, C$_6$D$_6$): δ -23.8 (s).

4.7.2.7 ^{Pr}[P$_2$Cp]Zr(η^2-CH$_2$=CH$_2$)Br (31)

A solution of 3.0 M EtMgBr (2.15 mL, 6.45 mmol) was diluted in 20 mL of toluene and added dropwise with stirring to a cooled (-78 °C) solution of **1** (2.06 g, 3.23 mmol) dissolved in 100 mL of toluene. The pale yellow colour of the solution turned to bright yellow upon addition. The mixture was stirred at -78°C for 1 hr and allowed to slowly warm to room temperature, whereupon the colour of the solution gradually changed to a dark reddish purple. The volatiles were then removed under vacuum and the residue extracted with pentane and filtered. Dark purple crystals of **31** were obtained from a cold (-40 °C) concentrated pentane solution. Yield 1.86 g (90 %). ^{1}H NMR (20 °C, C$_6$D$_6$): δ 0.21 and 0.23 (s, 6H, Si(CH_3)$_2$), 0.82 and 0.85 (d, 2H, $^2J_{PH}$ = 8Hz, SiCH_2P), 0.98 and 1.01 (m, 2H, $^3J_{PH}$ = 7Hz, CH_2=CH_2), 1.08, 1.15, 1.26 and 1.31 (dd, 6H, $^2J_{HH}$ = 7Hz, $^2J_{PH}$ = 7Hz, CH(CH_3)$_2$), 2.23 and 2.35 (sept, 2H, $^3J_{HH}$ = 7Hz,

CH(CH$_3$)$_2$), 4.37 (t, 1H, $^4J_{HH}$ = 1Hz, Cp-H), 6.31 (d, 2H, $^4J_{HH}$ = 2Hz, Cp-H). ^{31}P{^{1}H} NMR (20 °C, C$_6$D$_6$): δ 19.5 (s). Anal. Calcd. for C$_{25}$H$_{51}$BrP$_2$Si$_2$Zr: C, 46.85; H, 8.02. Found: C, 46.89; H, 8.06.

4.7.2.8 ^{Me}[P$_2$Cp]Zr(η^2-CH$_2$=CH$_2$)Br (32)

A solution of 3.0 M EtMgBr (1.50 mL, 4.50 mmol) was diluted in 20 mL of toluene and added dropwise with stirring to a cooled (-78 °C) solution of **25** (1.19 g, 2.26 mmol) dissolved in 60 mL of toluene. The reaction mixture was allowed to warm to room temperature and stirred for 3 h, during which a dark reddish brown colour was generated. The solvent was removed and the residue extracted with hexanes and filtered. Reducing this solution to 5 mL permitted the isolation of dark red crystals at -40 °C, which were washed with cold pentane and dried. Yield 0.93 g (79 %). ^{1}H NMR (20 °C, C$_6$D$_6$): δ 0.09 and 0.16 (s, 6H, Si(CH_3)$_2$), 0.84 and 1.15 (d, 2H, $^2J_{HH}$ = 12Hz, SiCH_2P), 0.88 and 1.33 (d, 2H, $^3J_{PH}$ = 9Hz, CH_2=CH_2), 1.24 and 1.27 (d, 6H, $^2J_{PH}$ = 7Hz, P(CH_3)$_2$), 4.15 (t, 1H, $^4J_{HH}$ = 1Hz, Cp-H), 6.02 (d, 2H, $^4J_{HH}$ = 1Hz, Cp-H). ^{31}P{^{1}H} NMR (20 °C, C$_6$D$_6$): δ 0.0 (s). Anal. Calcd. for C$_{17}$H$_{35}$BrP$_2$Si$_2$Zr: C, 38.62; H, 6.67. Found: C, 38.54; H, 6.74.

4.7.2.9 ^{Pr}[P$_2$Cp]Zr(CO)$_2$Br (33)

A benzene-d^6 solution of **31** was placed in a sealable NMR tube and affixed to a dual vacuum/nitrogen line. A small portion of solvent was removed under vacuum, and an atmosphere of carbon monoxide introduced at -78 °C. The colour of the solution instantly changed from dark purple to dark green. ^{1}H NMR spectroscopy revealed the evolution of free ethylene and the formation of one clean product with resonances associated solely with the ancillary ligand, while the ^{31}P{^{1}H} NMR spectrum showed a single new resonance. Repeating

the reaction in a sealed tube with the addition of ^{13}CO yielded diagnostic peaks for the carbonyl ligands in the ^{13}C NMR spectrum. Conducting the reaction on a larger scale in toluene generated the same colour change in solution as noted before upon addition of CO, although removal of the volatiles induced a subtle degradation of the green colour to this solution. A hydrocarbon-soluble, thermally labile dark orange-green oil was obtained after workup in hexanes. ^1H NMR (20 °C, C_6D_6): δ 0.12 and 0.28 (s, 6H, Si(CH_3)$_2$), 0.51 and 0.82 (dd, 2H, $^2J_{HH}$ = 15Hz, $^2J_{PH}$ = 9Hz, SiCH_2P), 0.97, 1.22, 1.29 and 1.32 (dd, 6H, $^3J_{HH}$ = 7Hz, $^3J_{PH}$ = 7Hz, CH(CH_3)$_2$), 1.95 and 2.48 (sept, 2H, $^3J_{HH}$ = 7Hz, CH(CH$_3$)$_2$), 5.16 (d, 2H, $^4J_{HH}$ = 1Hz, Cp-H), 5.19 (t, 1H, $^4J_{HH}$ = 1Hz, Cp-H). $^{31}P\{^1H\}$ NMR (20 °C, C_6D_6): δ 29.1 (s). $^{13}C\{^1H\}$ NMR (20 °C, C_6D_6): δ 241.1 (br s, Zr(CO)), 249.1 (s, Zr(CO)). IR (C_6D_6) v_{CO} 1890, 1865 (^{13}CO) cm^{-1}.

4.7.2.10 ^{Me}[P$_2$Cp]Zr(CO)$_2$Br (34)

The procedure followed was similar to that for **33**, reacting ethylene **32** in an atmosphere of CO. The colour of the solution gradually changed from dark red to a dull purplish red after the addition of CO. Once again, a scaled up version of this reaction permitted only the isolation of a thermally labile oil. ^1H NMR (20 °C, C_6D_6): δ 0.09 and 0.18 (s, 6H, Si(CH_3)$_2$), 0.57 and 1.03 (d, 2H, $^2J_{PH}$ = 7Hz, SiCH_2P), 1.41 and 1.50 (t, 6H, $^2J_{PH}$ = 5Hz, P(CH_3)$_2$), 4.82 (d, 2H, $^4J_{HH}$ = 1Hz, Cp-H), 5.08 (t, 1H, $^4J_{HH}$ = 1Hz, CpH). $^{31}P\{^1H\}$ NMR (20 °C, C_6D_6): δ -12.0 (s). $^{13}C\{^1H\}$ NMR (20 °C, C_6D_6): δ 240.5 and 245.1 (s, Zr(CO)). IR (C_6D_6) v_{CO} 1898, 1855 (^{13}CO) cm^{-1}.

4.7.2.11 ^{Pr}[P$_2$Cp]Zr(η^2-PhCCPh)Br (35)

A solution of diphenylacetylene (106 mg, 0.59 mmol) was diluted in 30 mL of toluene and added dropwise with stirring to a cooled (-78 °C) solution of **31** (410 mg, 0.59 mmol)

dissolved in 50 mL of toluene. The mixture was slowly warmed to room temperature and stirred for another 24 h The colour of the solution gradually changed from a deep purple to a dark brown. The volatiles were then removed under vacuum and the residue extracted with hexanes and filtered. Pale yellow crystals were obtained from slow evaporation of a concentrated hexamethyldisiloxane/hexanes mixture. The crystals were washed with two aliquots of cold hexamethyldisiloxane and dried. Yield 313 mg (67 %). Anal. Calcd. for $C_{37}H_{57}P_2Si_2Zr$: C, 56.18; H, 7.26. Found: C, 56.15; H, 7.31.

major isomer (60 %). ^1H NMR (20 °C, C_6D_6): δ 0.27 and 0.46 (s, 6H, Si(CH_3)$_2$), 0.84 and 1.28 (dd, 2H, $^2J_{HH}$ = 15Hz, $^2J_{PH}$ = 4Hz, SiCH_2P), 0.80, 0.98, 1.04 and 1.13 (dd, 6H, $^3J_{HH}$ = 7Hz, $^3J_{PH}$ = 7Hz, CH(CH_3)$_2$), 1.74 and 2.53 (sept, 2H, $^3J_{HH}$ = 7Hz, CH(CH$_3$)$_2$), 6.75 (d, 2H, $^4J_{HH}$ = 1Hz, Cp-H), 6.86 (t, 1H, $^4J_{HH}$ = 1Hz, Cp-H), 7.00 (t, 2H, p-C_6H_5), 7.24 (t, 4H, m-C_6H_5), 7.45 (d, 4H, o-C_6H_5). $^{31}P\{^1H\}$ NMR (20 °C, C_6D_6): δ 9.3 (s).

minor isomer (40 %). ^1H NMR (20 °C, C_6D_6): δ 0.21 and 0.33 (s, 6H, Si(CH_3)$_2$), 0.67and 1.14 (dd, 2H, $^2J_{HH}$ = 14Hz, $^2J_{PH}$ = 5Hz, SiCH_2P), 0.75, 1.19, 1.29 and 1.35 (dd, 6H, $^3J_{HH}$ = 7Hz, $^3J_{PH}$= 7Hz, CH(CH_3)$_2$), 2.10 and 2.15 (sept, 2H, $^3J_{HH}$ = 7Hz, CH(CH$_3$)$_2$), 6.46 (t, 1H, $^4J_{HH}$ = 1Hz, Cp-H), 6.80 (d, 2H, $^4J_{HH}$ = 1Hz, Cp-H), 6.94 (t, 2H, p-C_6H_5), 7.18 (t, 4H, m-C_6H_5), 7.35 (d, 4H, o-C_6H_5). $^{31}P\{^1H\}$ NMR (20 °C, C_6D_6): δ 6.9 (s).

4.7.2.12 {^{Pr}[P$_2$Cp]ZrBrH}(μ-H)$_3$[BrZr[P$_2$Cp]] (36)

A solution of **31** (1.390 g, 2.11 mmol) in 60 mL of toluene was placed in a 200 mL bomb and affixed to a dual vacuum/nitrogen line. The contents were frozen and the head space evacuated, and an atmosphere of hydrogen introduced at -196 °C. The bomb was sealed and the solution allowed to slowly warm to room temperature, resulting in a reaction vessel containing H_2 at a pressure of 4 atm. The colour of the solution slowly faded from dark purple to dark green. ^1H NMR (20 °C, C_6D_6): δ 0.01, 0.38, 0.51 and 0.62 (s, 6H, Si(CH_3)$_2$), 0.75 and 0.84 (m,

4H, SiCH_2P), 1.04 (m, 24H, CH(CH_3)$_2$), 1.18 and 1.37 (dd, 6H, $^3J_{HH}$ = 7Hz, $^3J_{PH}$ = 7Hz,

CH(CH_3)$_2$), 1.25 (dd, 12H, $^3J_{HH}$ = 7Hz, $^3J_{PH}$ = 7Hz, CH(CH_3)$_2$), 1.59 and 1.62 (sept, 2H, $^3J_{HH}$

= 7Hz, CH(CH$_3$)$_2$), 1.73 and 2.72 (m, 2H, CH(CH$_3$)$_2$), 2.30 (br, 3H, ZrH), 5.23 (t, 1H, $^2J_{PH}$ = 74

Hz, ZrH), 5.72 and 7.21 (t, 1H, $^4J_{HH}$ = 1Hz, Cp-H), 6.69 and 7.08 (d, 2H, $^4J_{HH}$ = 1Hz, Cp-H).

^{31}P{^{1}H} NMR (20 °C, C$_6$D$_6$): δ -5.6 (s, 2P), 39.2 (s, 2P).

4.7.2.13 {^{Me}[P$_2$Cp]ZrBr}$_2$(μ-H)$_4$ (37)

A solution of **32** (300 mg, 0.58 mmol) in 20 mL of toluene was placed in a 100 mL bomb and affixed to a dual vacuum/nitrogen line. The contents were frozen and the head space evacuated, and an atmosphere of hydrogen introduced at -196 °C. The bomb was sealed and the solution allowed to slowly warm to room temperature, resulting in a reaction vessel containing H$_2$ at a pressure of approximately 4 atm. The solution was left to stir for 24 h, during which the colour slowly faded from dark red to pale yellow. The solvent was removed and the residue extracted with hexanes. Colourless needles were obtained from a cold, concentrated hexamethyldisiloxane solution (-40 °C). Yield 170 mg (60 %). ^{1}H NMR (20 °C, C$_6$D$_6$): δ 0.18, 0.20, 0.21, 0.28, 0.33, 0.42, 0.81 and 0.86 (s, 3H, Si(CH_3)$_2$), 0.74, 0.79, 1.14 and 1.43 (d, 2H, $^2J_{pH}$ = 7Hz, SiCH_2P), 1.06, 1.17, 1.36, 1.39, 1.46, 1.63, 1.81 and 1.88 (d, 3H, $^2J_{PH}$ = 6Hz, P(CH_3)$_2$), 3.74 (br d, 2H, $^2J_{PH}$ = 80 Hz, ZrH), 3.89 (br, 2H, ZrH), 6.19, 6.35, 6.39, 6.42, 6.45 and 6.46 (br, 1H, Cp-H). ^{31}P{^{1}H} NMR (20 °C, C$_6$D$_6$): δ -54.9 (s), -17.6 and -14.7 (d, 1P, $^2J_{pp}$ = 58Hz), -13.0 (s).

4.7.2.14 ^{Pr}[P$_2$Cp]Zr(η^2-CH$_2$=CH$_2$)Me (38)

A solution of 1.4 M MeMgBr (0.75 mL, 1.05 mmol) was diluted in 10 mL of toluene and added dropwise with stirring to a cooled (-78 °C) solution of **31** (620 mg, 0.97 mmol) dissolved in 60 mL of toluene. The mixture was allowed to slowly warm to room temperature, during

which the colour of the solution gradually changed from a deep purple to a dark reddish orange. The reaction mixture was stirred for another 24 h, the volatiles then removed under vacuum and the residue extracted with hexanes and filtered. A pale pink, thermally sensitive solid was obtained by slow evaporation of the filtrate, washed with cold pentane and dried. Yield 425 mg (76 %). ^{1}H NMR (20 °C, C_6D_6): δ -0.67 (t, 3H, $^3J_{PH}$ = 10Hz, $ZrCH_3$), 0.24 and 0.26 (s, 6H, $Si(CH_3)_2$), 0.86 (m, 4H, $^2J_{PH}$ = 8Hz, $SiCH_2P$), 1.05 (m, 2H, $^3J_{PH}$ = 8Hz, $Zr(CH_2=CH_2)$), 1.10 (m, 24H, $CH(CH_3)_2$), 2.09 (sept, 4H, $^3J_{HH}$ = 7Hz, $CH(CH_3)_2$), 4.61 (t, 1H, $^4J_{HH}$ = 2Hz, Cp-*H*), 6.32 (d, 2H, $^4J_{HH}$ = 2Hz, Cp-*H*). $^{31}P\{^1H\}$ NMR (20 °C, C_6D_6): δ 20.1 (s).

4.7.2.15 $^{Pr}[P_2Cp]Zr(\eta^2\text{-}CH_2=CH_2)(\eta^5\text{-}C_5H_5)$ (39)

A solution of NaCp.DME (106 mg, 0.59 mmol) was diluted in 30 mL of toluene and added dropwise with stirring to a cooled (-78 °C) solution of **31** (410 mg, 0.59 mmol) dissolved in 50 mL of toluene. The mixture was stirred at -78 °C for 2 h, then allowed to slowly warm to room temperature and stirred for another 24 h The colour of the solution gradually changed from a deep purple to a orange-red. The volatiles were then removed under vacuum and the residue extracted with hexanes and filtered. Orange crystals were obtained from a cold (-40 °C) concentrated hexamethyldisiloxane/hexanes mixture. The crystals were washed with cold hexamethyldisiloxane and dried. Yield 310 mg (84 %). ^{1}H NMR (20 °C, C_6D_6): δ 0.08, 0.13, 0.52 and 0.58 (s, 3H, $Si(CH_3)_2$), 0.42, 0.75, and 0.85 (ddt, 1H, $^3J_{HH}$ = 10Hz(*cis* and *trans*), $^3J_{PH}$ = 6Hz, CH*H*=CH_2), 0.74 and 0.81 (dd, 2H, $^2J_{HH}$ = 15Hz, $^2J_{PH}$ = 4Hz, SiC*H*_2P), 0.94, 1.00, 1.02, 1.03, 1.04, 1.05, 1.05 and 1.13 (dd, 3H, $^3J_{HH}$ = 7Hz, $^3J_{PH}$ = 7Hz, CH(C*H*_3)_2), 1.59 and 1.60 (sept, 1H, $^3J_{HH}$ = 7Hz, C*H*(CH_3)_2), 1.74 (d of sept, 1H, $^3J_{HH}$ = 7Hz, $^2J_{PH}$ = 3Hz, C*H*(CH_3)_2), 1.98 (d of sept, 1H, $^3J_{HH}$ = 7Hz, $^2J_{PH}$ = 7Hz, C*H*(CH_3)_2), 5.21 (t, 1H, $^4J_{HH}$ = 2Hz, Cp-*H*), 5.35, (s, 5H, $^3J_{PH}$ = 1Hz, C_5H_5), 5.61 and 5.62 (dd, 1H, $^3J_{HH}$ = 6Hz, $^4J_{HH}$ = 2Hz, Cp-*H*). $^{31}P\{^1H\}$ NMR (20 °C, C_6D_6): δ -5.3 (s), 42.3 (s). Anal. Calcd. for $C_{30}H_{56}P_2Si_2Zr$: C, 57.55; H, 9.01. Found: C, 57.25; H, 9.15.

4.7.2.16 ^{Pr}[P$_2$Cp]Zr(η^5-C$_5$H$_5$)(CO) (40)

A benzene-d^6 solution of **39** was placed in a sealable NMR tube and affixed to a dual vacuum/nitrogen line. A small portion of solvent was removed under vacuum, and an atmosphere of carbon monoxide introduced at -78 °C. The contents within the sample were continually mixed under ambient temperature by a constant inversion of the sample by mechanical method. The reaction was monitored by ^{1}H and ^{31}P{^{1}H} NMR spectroscopy until the reaction was complete (approximately two weeks). There was no obvious colour change associated with this reaction. **40** was observed to be the major product (90 %) based on the NMR spectra. Repeating the procedure in a sealed tube with the addition of ^{13}CO yielded a strong diagnostic peak at 308 ppm for the carbonyl ligand in the ^{13}C NMR spectrum. Conducting the reaction on a larger scale in toluene generated a thermally sensitive hydrocarbon-soluble orange oil after workup that gradually decomposed at -40 °C. ^{1}H NMR (20 °C, C$_6$D$_6$): δ 0.13, 0.24, 0.35 and 0.47 (s, 3H, Si(CH_3)$_2$), 0.42 and 0.63 (dd, 1H, $^2J_{HH}$ = 11Hz, $^2J_{PH}$ = 9Hz, SiCH_2P), 0.69 (d, 2H, $^2J_{PH}$ = 7Hz, SiCH_2P), 0.75, 0.78, 0.90 and 0.91 (dd, 3H, $^3J_{HH}$ = 7Hz, $^3J_{pH}$ = 7Hz, CH(CH_3)$_2$), 1.05 (m, 12H, CH(CH_3)$_2$), 1.29 and 1.55 (sept, 1H, $^3J_{HH}$ = 7Hz, CH(CH$_3$)$_2$), 1.59 (sept, 2H, $^3J_{HH}$ = 7Hz, CH(CH$_3$)$_2$), 4.95 (s, 5H, $^3J_{PH}$ = 1Hz, C$_5H_5$), 5.08, 5.55 and 5.62 (dd, 1H, $^4J_{HH}$ = 1Hz, Cp-H). ^{31}P{^{1}H} NMR (20 °C, C$_6$D$_6$): δ -4.8 and 58.7 (s). ^{13}C{^{1}H} NMR (20 °C, C$_6$D$_6$): δ 308.0 (d, $^2J_{PC}$ = 3Hz, Zr(CO)).

4.7.2.17 ^{Pr}[P$_2$Cp]Zr(η^5-C$_5$H$_5$)H$_2$ (41)

A benzene-d^6 solution of **39** was placed in a sealable NMR tube and affixed to a dual vacuum/nitrogen line. The contents were frozen and the head space evacuated, and an atmosphere of hydrogen introduced at -196 °C. The NMR tube was sealed and the sample allowed to slowly warm to room temperature, resulting in a reaction vessel containing H$_2$ at a pressure of 4 atm. The orange colour of the sample slowly faded to a pale buff over the course of

four days until the reaction was complete as monitored by ^{1}H and ^{31}P{^{1}H} NMR spectroscopy. A new complex was obtained quantitatively (> 99 %) based on the NMR spectra. Conducting the reaction on a larger scale in toluene generated a yellow hydrocarbon-soluble oil after workup. ^{1}H NMR (20 °C, C$_6$D$_6$): δ 0.16, 0.40, 0.43 and 0.55 (s, 3H, Si(CH_3)$_2$), 0.69 and 0.85 (dd, 1H, $^2J_{HH}$ = 10Hz, $^2J_{PH}$ = 12Hz, SiCH_2P), 0.74 and 0.75 (dd, 1H, $^2J_{HH}$ = 2Hz, $^2J_{PH}$ = 2Hz, SiCH_2P), 0.93, 0.98, 1.01, 1.02, 1.03, 1.04, 1.06, and 1.17 (dd, 3H, $^3J_{HH}$ = 7Hz, $^3J_{PH}$ = 7Hz, CH(CH_3)$_2$), 1.30 (sept, 2H, $^3J_{HH}$ = 7Hz, CH(CH$_3$)$_2$), 1.35 and 1.56 (d of sept, 1H, $^3J_{HH}$ = 7Hz, $^2J_{PH}$ = 2Hz, CH(CH$_3$)$_2$), 5.21, 6.42 and 6.46 (dd, 1H, $^4J_{HH}$ = 1Hz, Cp-H), 5.52 (s, 5H, $^3J_{PH}$ = 1Hz, C$_5$$H_5$). ^{31}P{^{1}H} NMR (20 °C, C$_6$D$_6$): δ -5.6 (s), 43.9 (s).

4.7.2.18   Ligand synthesis: ^{Pr}[P$_2$Cp']Li

C$_5$H$_4$SiMe$_2$CH$_2$Cl-3-CMe$_3$

A 500 mL 3-necked round-bottomed flask was equipped with a magnetic stir bar, a 100 mL dropping funnel, a rubber septum cap, and a ground glass stopper. The flask was charged with dimethylfulvene (12.0 mL, 99.6 mmol) and diethyl ether (150 mL) under a nitrogen purge, and the contents cooled in an ice bath (0 °C). A solution of 1.4 M MeLi (70.0 mL, 98.0 mmol) was added dropwise from the dropping funnel over a period of 20 min, during which the orange colour of the dimethylfulvene solution turned to a pale yellow slurry. The reaction mixture was left to stir at 0 °C for 90 min. This mixture was then added dropwise via cannula to a 1 L 3-necked round-bottomed flask charged with ClSiMe$_2$CH$_2$Cl (13.5 mL, 102 mmol) and THF (250 mL), cooled at -78 °C. The reaction mixture became viscous and pale yellowish-green in colour during the course of the addition. The solution was slowly warmed to room temperature and stirred for 12 h. The solvent was then removed in vacuo and 100 mL water added to the flask, and extracted with four aliquots (25 mL) of diethyl ether. The ether layer was dried over MgSO$_4$ and filtered, and the solvent subsequently removed to give a clear yellow oil. Vacuum

distillation yielded a clear yellow liquid (bp 74-78 °C, 10^{-2} Torr) consisting mainly of the 1,3-isomer (> 85 % by ^{1}H NMR spectroscopy). Yield: (15.88 g, d = 0.97 g mol^{-1}, 73 %). ^{1}H NMR (20 °C, C_6D_6): δ -0.02 (s, 6H, Si(CH_3)$_2$), 1.09 (s, 9H, C(CH_3)$_3$), 2.68 (s, 2H, SiCH_2Cl), 3.40 (br s, 1H, Cp-HSi(CH$_3$)$_2$), 6.02, 6.41 and 6.64 (br s, 1H, Cp-H).

C_5H_3-1,1-SiMe$_2$CH$_2$Cl$_2$-3-CMe$_3$

A 250 mL 3-necked round-bottomed flask was equipped with a magnetic stir bar, a 100 mL dropping funnel, a rubber septum cap, and a ground glass stopper. The flask was charged with C_5H_4SiMe$_2$CH$_2$Cl-3-CMe$_3$ (5.2 mL, 21.8 mmol) and THF (60 mL) under a nitrogen purge, and the contents cooled in an ice bath (0 °C). A solution of NaN(SiMe$_3$)$_2$ (4.00 g, 21.8 mmol) in 50 mL of THF was added dropwise from the dropping funnel over a period of 25 min, during which the yellow solution became slightly viscous. The reaction mixture was left to stir at 0 °C for 30 min, after which the solution became darker (orange) and more viscous. This mixture was then added dropwise via cannula to a 500 mL 3-necked round-bottomed flask charged with ClSiMe$_2$CH$_2$Cl (3.0 mL, 23 mmol) and THF (600 mL), cooled at -78 °C. The reaction mixture turned ochre-yellow and translucent in appearance during the course of the addition. The solution was slowly warmed to room temperature and stirred for 2 h, after which the colour was a paler yellow. The solvent was then removed in vacuo and 80 mL water added to the flask, and extracted with four aliquots (25 mL) of diethyl ether. The ether layer was dried over MgSO$_4$ and filtered, and the solvent subsequently removed to give a clear yellow oil. Vacuum distillation yielded a viscous yellow oil (bp 118-121 °C, 10^{-2} Torr) consisting solely of the 1,1-side-arm disubstituted species. Yield: (4.30 g, 60 %). ^{1}H NMR (20 °C, C_6D_6): δ 0.02 and 0.03 (s, 6H, Si(CH_3)$_2$), 1.04 (s, 9H, C(CH_3)$_3$), 2.36 (s, 4H, SiCH_2Cl), 5.98 (dd, 1H, $^4J_{HH}$ = 4Hz, $^4J_{HH}$ = 3Hz, Cp-H), 6.35 (dd, 1H, $^4J_{HH}$ = 4Hz, $^4J_{HH}$ = 8Hz, Cp-H), 6.63 (dd, 1H, $^3J_{HH}$ = 3Hz, $^4J_{HH}$ = 8Hz, Cp-H).

^{Pr}[P$_2$Cp']Li

A mixed solvent solution of 34 (2.05 g, 6.15 mmol) in 60 mL of THF and 10 mL of toluene was added dropwise with stirring to a heated (50 °C) solution of LiPPri2 (2.25 g, 18.3 mmol) dissolved in 90 mL of THF. Upon addition of the last drops of 34 the bright yellow phosphide solution dimmed rapidly to give a pale greyish-yellow colour. The reaction mixture was immediately removed from the oil bath and allowed to cool to room temperature. The solvent was removed under vacuum and the viscous gray residue extracted with hexanes and filtered. A small yield of colourless crystals was obtained form a cold (-40 °C), concentrated hexanes solution. X-ray diffraction data revealed that this compound consisted of a 1:1 mixture of ^{P}r[P$_2$Cp']Li with one of the phosphines bridged to a unit of (η^5-C$_5$H$_2$-1,2-SiMe$_2$CH$_2$CH$_2$SiMe$_2$-3-CMe$_3$). Yield 1.40 g (54 %). ^{1}H NMR (20 °C, C$_6$D$_6$): δ 0.33, 0.46, 0.53 and 0.67 (s, 6H, Si(CH_3)$_2$), 0.72 and 0.78 (dd, 2H, $^2J_{HH}$ = 14Hz, $^2J_{PH}$ = 5Hz, SiCH_2P), 0.93, 0.95, 0.96 and 1.01 (dd, 6H, $^3J_{HH}$ = 8Hz, $^3J_{PH}$ = 7Hz, CH(CH_3)$_2$), 1.06 (m, 4H, SiCH_2CH_2Si), 1.14 (t, 4H, $^3J_{HH}$ = 7Hz, THF), 1.46 and 1.46 (s, 9H, C(CH3)3), 1.53 and 1.67 (sept, 2H, CH(CH3)2), 3.12 (t, $^3J_{HH}$ = 7Hz, THF), 6.47 and 6.50 (s, 1H, Cp-H). ^{31}P{^{1}H} NMR (20 °C, C$_6$D$_6$): δ 0.0 (q, $^1J_{PLi}$ = 33Hz). ^{7}Li{^{1}H} NMR (20 °C, C$_6$D$_6$): δ -11.7 (br s), -10.9 (t, $^1J_{PLi}$ = 33Hz). Anal. Calcd. for C$_{46}$H$_{90}$Li$_2$OP$_2$Si$_4$: C, 65.20; H, 10.70. Found: C, 64.80; H, 10.20.

4.7.2.19   Isolation of ^{Pr}[P$_2$Cp']ZrCl$_2$ (42)

This product was obtained inminute quantities as dark green crystals, with poor solubility in organic solvents, in n unsuccesful attempt to alkylate the trichloride derivative [P$_2$Cp']ZrCl$_3$. Anal. Calcd. for C$_{27}$H$_{55}$Cl$_2$P$_2$Si$_2$Zr: C, 49.14; H, 8.40. Found: C, 48.93; H, 8.47.

4.7.2.20 Stepwise reduction to ^{Pr}[P$_2$Cp]ZrCl$_2$ (43) and {^{Pr}[P$_2$Cp]ZrCl}$_2$(μ-N$_2$) (44)

An intimate mixture of **1** (640 mg, 1.00 mmol) and KC$_8$ (474 mg, 3.50 mmol) was placed in a 200 mL bomb and 50 mL of toluene added. The mixture immediately turned to a dark blue slurry. The mixture was stirred at room temperature for 3 days, at which time the colour of the solution was dark green. Two possibilities follow at this stage. Isolation of the intermediate Zr(II) species could be obtained by filtration, followed by reducing the volume of the solvent to 3 mL. Dark green crystals of [P$_2$Cp]ZrCl$_2$ were obtained at -40 °C from toluene. Anal. Calcd. for C$_{23}$H$_{47}$Cl$_2$P$_2$Si$_2$Zr: C, 45.75; H, 7.84. Found: C, 45.41; H, 7.83. ESR (toluene): g = 1.96; a(^{31}P) = 18.00G, 2P.

If the above reduction is conducted with heating at 40 °C for one week the solution gradually turns brown. Filtration of the graphite, followed by removal of the solvent, yields a red oil that is soluble in hexanes. Dark reddish crystals were obtained from cold hexanes (-40 °C). Yield 425 mg (76 %). Anal. Calcd. for C$_{46}$H$_{94}$Cl$_2$N$_2$P$_4$Si$_4$Zr$_2$: C, 47.43 H, 8.13 N, 2.40. Found: C, 48.03; H, 8.40 N, 2.20. ^{1}H NMR (20 °C, C$_6$D$_6$): δ 0.28, 0.29, 0.32 and 0.35 (s, 6H, Si(CH_3)$_2$), 0.80 (m, 8H, SiCH_2P), 1.19 (m, 48H, CH(CH_3)$_2$), 2.38 and 2.41 (sept, 4H, $^3J_{HH}$ = 7Hz, CH(CH$_3$)$_2$), 6.30 and 6.52 (d, 2H, $^4J_{HH}$ = 2Hz, Cp-H), 6.73 and 7.00 (t, 1H, $^4J_{HH}$ = 2Hz, Cp-H). ^{31}P{^{1}H} NMR (20 °C, C$_6$D$_6$): δ 16.4 (s).

4.7.2.21 {^{Me}[P$_2$Cp]ZrCl}$_2$(μ-Cl)$_2$ (45)

This compound was isolated as dark red crystals as a minor product (< 5 %) from the thermal decomposition of the photolysis product **29**. ^{1}H NMR (20 °C, C$_6$D$_6$): δ 0.12, 0.19, 0.30 and 0.42 (s, 6H, Si(CH_3)$_2$), 0.8, 1.22, 1.39 and 1.41 (d, 2H, $^2J_{PH}$ = 6Hz, SiCH_2P), 6.15 and 6.26 (d, 2H, $^4J_{HH}$ = 1Hz, CpH), 6.23 and 6.40 (t, 2H, $^4J_{HH}$ = 1Hz, CpH). ^{31}P{^{1}H} NMR (20 °C, C$_6$D$_6$): δ -18.0 and -17.4 (dd, 2H, $^4J_{PP}$ = 3Hz).

4.7.2.22 ^{Pr}[P$_2$Cp]ThBr$_3$ (46)

A solution of ^{Pr}[P$_2$Cp]Li (1.12 g, 2.50 mmol) in 30 mL of toluene was added dropwise with stirring to ThBr$_4$(THF)$_4$ (2.10 g, 2.50 mmol) dissolved in 30 mL of toluene at room temperature. The solution gradually became turbid during the course of the addition but remained colourless. The reaction mixture was left to stir for 48 h after which the solution was filtered, and the volume reduced to 3 mL. Colourless crystals were deposited from slow evaporation of this concentrated solution. The isolated crystals were washed with cold hexanes and dried. Yield 1.67 g (73 %). ^{1}H NMR (20 °C, C$_6$D$_6$): δ 0.18 and 0.56 (s, 6H, Si(CH_3)$_2$), 1.05 (dd, 4H, $^2J_{HH}$ = 6Hz, $^2J_{PH}$ = 7Hz, SiCH_2P), 1.34 (m, 24H, CH(CH_3)$_2$), 2.08 and 2.37 (sept, 2H, $^3J_{HH}$ = 7Hz, CH(CH$_3$)$_2$), 6.97 (d, 2H, $^4J_{HH}$ = 1Hz, Cp-H), 7.68 (t, 1H, $^4J_{HH}$ = 1Hz, Cp-H). ^{31}P NMR (20 °C, C$_6$D$_6$): δ 33.2 (s). Anal. Calcd. for C$_{23}$H$_{47}$Br$_3$P$_2$Si$_2$Th: C, 30.24; H, 5.19. Found: C, 29.68; H, 5.14.

4.8 References

(1)   Davies, G. R.; Jarvis, J. A. J.; Kilbourn, B. T.; Pioli, A. J. P. *Chem.Commun.* **1971**, 677.

(2)   Jordan, R. F.; LaPointe, R. E.; Baenziger, N.; Hinch, G. D. *Organometallics* **1990**, *9*, 1539.

(3)   Buchwald, S. L.; Watson, B. T.; Huffman, J. C. *J. Am. Chem. Soc.* **1986**, *108*, 7411.

(4)   Rosa, P.; Floch, P. L.; Ricard, L.; Mathey, F. *J. Am. Chem. Soc.* **1997**, *119*, 9417.

(5)   Dupuis, L.; Pirio, N.; Meunnier, P.; Igau, A.; Donnadieu, B.; Majoral, J.-P. *Angew. Chem., Int. Ed. Engl.* **1997**, *36*, 987.

(6)   Broene, R. D.; Buchwald, S. L. *Science* **1993**, *261*, 1696.

(7)   Erker, G. *J. Organomet. Chem.* **1977**, *134*, 189.

(8)   Buchwald, S. L.; Nielson, R. B. *Chem. Rev.* **1988**, *88*, 1047.

(9)   Coles, M. P.; Gibson, V. C.; Clegg, W.; Elsegood, M. R. J.; Porrelli, P. A. *J. Chem. Soc., Chem. Commun.* **1996**, 1963.

(10)   Lockwood, M. A.; Clark, J. R.; Parkin, B. C.; Rothwell, I. P. *J. Chem. Soc., Chem. Commun.* **1996**, 1973.

(11)   Tran, E.; Legzdins, P. **1997**.

(12)   Heijden, H.; Hessen, B. *J. Chem. Soc., Chem. Commun.* **1995**, 145.

(13)   Bulls, A. R.; Schaefer, W. P.; Serfas, M.; Bercaw, J. E. *Organometallics* **1987**, *6*, 1219.

(14)   Crabtree, R. H. *The Organometallic Chemistry of the Transition Metals*; Wiley: New York, 1994;

(15)   Zucchini, U.; Albizzata, E.; Gianni, U. *J. Organomet. Chem.* **1971**, *26*, 357.

(16)   Ryabov, A. D. *Chem Rev* **1990**, *90*, 403.

(17)   Takahashi, T.; Murakami, M.; Kunishige, M.; Saburi, M.; Uchida, Y.; Kozawa, K.; Uchida, T.; Swanson, D. R.; Negishi, E. *Chem.Lett.* **1989**, 761.

(18)   Binger, P.; Muller, P.; Benn, R.; Rufinska, A.; Gabor, B.; Kruger, C.; Betz, P. *Chem. Ber.* **1989**, *122*, 1035.

(19)   Wielstra, Y.; Gambarotta, S.; Roedelof, J. B. *Organometallics* **1988**, *7*, 2177.

(20)   Palmer, G. T.; Basolo, F.; Kool, L. B.; Rausch, M. D. *J. Am. Chem. Soc.* **1986,** *108,* 4417.

(21)   Stein, B. K.; Frerichs, S. R.; Ellis, J. E. *Organometallics* **1987,** *6,* 2017.

(22)   Poole, A. D.; Gibson, V. C.; Clegg, W. *J. Chem. Soc., Chem. Commun.* **1992,** 237.

(23)   Siemeling, U.; Gibson, V. C. *J. Organomet. Chem.* **1992,** *426,* C25.

(24)   Booij, M.; Blenkers, J.; Sinnema, J. C. M.; Meetsma, A.; Bolhuis, F. v.; Teuben, J. H. *Organometallics* **1988,** *7,* 1029.

(25)   Gozum, J. E.; Wilson, S. R.; Girolami, G. S. *J. Am. Chem. Soc.* **1992,** *114,* 9483.

(26)   Alt, H. G.; Denner, C. E.; Thewalt, U.; Rausch, M. D. *J. Organomet. Chem.* **1988,** *356,* C83.

(27)   Demerseman, B.; Bouquet, G.; Bigorne, M. *J. Organomet. Chem.* **1977,** *132,* 223.

(28)   Manriquez, J. M.; McAlister, D. R.; Sanner, R. D.; Bercaw, J. E. *J. Am. Chem. Soc.* **1978,** *100,* 2716.

(29)   Etkin, N.; Hoskin, A. J.; Stephan, D. W. *J. Am. Chem. Soc.* **1997,** *119,* 11420.

(30)   Roddick, D. M.; Fryzuk, M. D.; Seidler, P. F.; Hillhouse, G. L.; Bercaw, J. E. *Organometallics* **1985,** *4,* 97.

(31)   Mitchell, J. P.; Hajela, S.; Brookhart, S. K.; Hardcastle, K. I.; Henling, L. M.; Bercaw, J. E. *J. Am. Chem. Soc.* **1996,** *118,* 1045.

(32)   He, M.-Y.; Xiong, G.; Toscano, P.; Burwell, R. L.; Marks, T. J. *J. Am. Chem. Soc.* **1985,** *107,* 641.

210

(33)   Cotton, F. A.; Wilkinson, G. *Advanced Inorganic Chemistry*; 5th ed.; Wiley: New York, 1988;

(34)   Clark, D. L.; Frankom, T. M.; Miller, M. M.; Watkin, J. G. *Inorg. Chem.* **1992,** *31*, 1628.

Appendix One: X-ray Crystal Structure Data

Table A1.1   Crystallographic data.[a, b]

Compound	2 ^{Pr}[P$_2$Cp]HfCl$_3$	13 ^{Pr}[P$_2$Cp]ZrCl$_2$ (η^2-C(O)CH$_2$Ph)	17 ^{Pr}[P$_2$Cp]Hf=CH Ph(Cl)	18b ^{Pr}[P$_2$Cp]Zr=CH SiMe$_3$(Cl)
Empirical Formula	C$_{23}$H$_{47}$Cl$_3$HfP$_2$Si$_2$	C$_{31}$H$_{54}$Cl$_2$OP$_2$Si$_2$Zr	C$_{33.50}$H$_{57}$ClHfP$_2$Si$_2$	C$_{27}$H$_{57}$ClZrP$_2$Si$_3$
fw	726.57	723.01	791.88	654.62
Color, habit	yellow, block	yellow, plate	yellow, irregular	yellow, block
Crystal system	monoclinic	monoclinic	triclinic	monoclinic
Space group	$P2_1/n$	$P2_1/c$	$P\overline{1}$	$P2_1/n$
a, Å	17.0071(1)	15.248(6)	11.7554(11)	12.982(5)
b, Å	11.7419(2)	16.192(5))	12.488(2)	16.679(6)
c, Å	17.1842(1)	15.524(2))	13.9584(10)	16.710(5)
α, deg	90	90	98.3839(7)	-
β, deg	116.509(1)	100.007(2)	95.0101(9)	98.99
γ, deg	90	90	111.100(3)	-
V, Å^3	3070.82(6)	3774(2)	1869.5(3)	3573.7(22)
Z	4	4	2	4
ρ_{calc}, g/cm^3	1.572	1.272	1.407	1.22
$F(000)$	1464	1520.00	810.00	1392
Radiation	Mo	Mo	Mo	Mo
μ, cm^{-1}	3.851	6.02	30.26	5.1
Crystal size, mm	0.32 × 0.18 × 0.12	0.15 × 0.40 × 0.45	0.45 × 0.35 × 0.15	0.30 × 0.40 × 0.50
Transmission factors	0.775-1.000	0.7066-1.0226	0.92-1.00	0.823 to 0.999
Scan type	ω-2θ	ω-2θ	ω-2θ	ω-2θ
Scan range, ω°	1.00+0.35 tan θ	-	1.00+0.35 tan θ	-

Scan speed, °min^{-1}	4.2 (1 rescan)	-	16 (up to 8 scans)	-
$2\theta_{max}$, deg	45	63.8	60.1	45
Crystal. decay, %	-	-		-
Total reflections	15681	31051	15781	4817
Unique reflections	5391	7757	8376	4640
R_{merge}	0.0260	0.0933	0.043	0.040
Number w/ $I \geq 3\sigma(I)$	1832	2529	6427	-
Variables	334	352	374	334
R	0.064	0.219	0.069	0.056
R_w	0.037	0.168	0.072	0.055
gof	1.87	0.733	1.82	3.16
Max Δ/σ (final cycle)	0.004	0.0002	0.0006	-
Residual density e/Å^3	--1.052 to 0.588	-2.88 to 2.67	-2.97 to 2.47	-0.610 to 0.880

Compound	**20** ^{Pr}[P2Cp]Zr (η^2-CH$_2$=CH$_2$)Cl	**21a** ^{Pr}[P2Cp]Zr C(O)=CHPh(Cl)	**23b** ^{Pr}[P2Cp]ZrCH$_2$ CH$_2$C(O)=CH SiMe$_3$(Cl)	**27** ^{Me}[P2Cp]ZrCl (CH$_2$Ph)$_2$
Formula	C$_{25}$H$_{51}$ClZrP$_2$Si$_2$	C$_{31}$H$_{53}$ClOP$_2$Si$_2$Zr	C$_{30}$H$_{61}$ClOP$_2$Si$_3$Zr	C$_{29}$H$_{45}$ClP$_2$Si$_2$Zr
fw	596.47	686.55	710.69	638.44
Color, habit	red, block	orange, irregular	yellow, prism	red-brown, block
Crystal system	triclinic	monoclinic	monoclinic	triclinic
Space group	$P\bar{1}$	$P2_1/c$	$P2_1/c$	$P\bar{1}$
a, Å	115.432(3)	8.666(1)	12.6352(12)	11.6130(2)
b, Å	20.483(3)	24.244(1))	16.520(2)	12.0201(1)
c, Å	20.995(7)	17.543(1)	18.5436(4)	12.9477(2)
α, deg	76.50(3)	90	90	75.805(1)
β, deg	83.12(7)	100.936(8)	92.4321(4)	70.011(1)

213

γ, deg	88.52(4)	90	90	75.118(1)
V, Å³	6407(3)	3618.9(6)	3867.1(4)	1616.66(4)
Z	8	4	4	2
ρ_{calc}, g/cm³	1.24	1.26	1.221	1.312
$F(000)$	2528	1448	1512.00	668
Radiation	Mo	Mo	Mo	Mo
μ, cm⁻¹	6.0	5.53	5.49	6.12
Crystal size, mm	0.30 × 0.40 × 0.45	0.25 × 0.30 × 0.45	0.20 × 0.45 × 0.45	0.40 × 0.30 × 0.25
Transmission factors	0.903-1.00	0.956-1.000	0.5744-1.0291	0.844-1.000
Scan type	ω-2θ	ω	ω-2θ	ω-2θ
Scan range, $\omega°$	1.05+0.35 tan θ	0.79+0.35 tan θ	1.56+0.35 tan θ	1.25+0.20 tan θ
Scan speed, °min⁻¹	16 (up to 8 scans)	16 (up to 9 scans)	3-30 (up to 8 scans)	16 (up to 9 scans)
$2\theta_{max}$, deg	40.0	60	60	-
Crystal. decay, %	-	1.95	-	-
Total reflections	11928	11425	36109	5433
Unique reflections	11917	10783	9656	5433
R_{merge}	0.023	0.034	0.046	
Number w/ $I \geq 3\sigma(I)$	7589	5598	5373	
Variables	396	344	343	369
R	0.055	0.034	0.064	
R_w	0.060	0.031	0.045	
gof	3.71	1.49	1.83	1.021
Max Δ/σ (final cycle)	0.02	0.003	0.007	-
Residual density e/Å³	-0.550 to 0.640	-0.35 to 0.31	-2.19 to 1.77	-0.383 to 0.333
Compound	**28** Me[P₂Cp]Zr (η^2-C₆H₃Me)Cl	**30** Me[P₂Cp]Zr (CH₂Ph)₃	**32** Me[P₂Cp]Zr (η^2-CH₂=CH₂)Br	**35** Pr[P₂Cp]Zr (η^2-PhCCPh)Br

Formula	$C_{29}H_{47}ClP_2Si_2Zr$	$C_{36}H_{52}P_2Si_2Zr$	$C_{17}H_{35}CBrP_2Si_2Zr$	$C_{37}H_{57}BrP_2Si_2Zr$
fw	640.46	1256.07	528.71	791.10
Color, habit	-	red, irregular	red-brown, prism	yellow, plate
Crystal system	monoclinic	monoclinic	monoclinic	monoclinic
Space group	$P2_1/n$	$P2_1/c$	$P2_1/c$	$P2_1/a$
a, Å	15.1458(8)	8.9145(5)	12.352(1)	18.8932(11)
b, Å	9.9410(5)	35.292(2)	15.333(1)	23.2223(14)
c, Å	23.252(1)	20.6605(3)	13.567(1)	20.5753(2)
α, deg	90	90	90	-
β, deg	105.135(1)0)	93.3670(3)	108.352(6)	118.1110(2)
γ, deg	90	90	90	-
V, Å^3	3379.5(3)	6488.9(4)	2438.7(3)	7962.4(5)
Z	4	4	4	8
ρ_{calc}, g/cm^3	1.259	1.286	1.440	1.320
$F(000)$	1344	2640.00	1080.00	3296.00
Radiation	Mo	Mo	Mo	Mo
μ, cm^{-1}	5.86	4.88	78.93	14.47
Crystal size, mm	$0.10 \times 0.10 \times 0.10$	$0.15 \times 0.35 \times 0.45$	$0.20 \times 0.30 \times 0.45$	$0.30 \times 0.30 \times 0.10$
Transmission factors	0.95-1.00	0.8201-0.9972	0.736 - 1.000	0.6288 - 1.0000
Scan type	ω-2θ	ω-2θ	ω-2θ	ω-2θ
Scan range, $\omega°$	1.10+0.35 tan θ	1.15+0.35 tan θ	1.00+0.20 tan θ	1.37+0.20 tan θ
Scan speed, °min^{-1}	32 (up to 8 scans)	16 (up to 8 rescans)	16 (up to 9 scans)	16 (up to 8 scans)
2θ_{max}, deg	55	60.2	155	60.1
Crystal. decay, %	-1.66	-	-	-
Total reflections	19827	61655	5395	74849
Unique reflections	7924	16262	5163	20481

R_{merge}	0.027		0.0777	0.044
Number w/ $I \geq 3\sigma(I)$	3617	10192	3408	11170
Variables	366	722	225	775
R	0.038		0.031	0.035
R_w	0.039	0.040	0.033	0.030
gof	1.95	1.17	1.78	1.26
Max Δ/σ (final cycle)	0.01	0.04	0.0004	0.002
Residual density e/Å^3	-0.687 to 0.471	-4.38 to 6.03	-0.49 to 0.42	-1.99 to 1.64

Compound	37 $\{^{Me}[P_2Cp]ZrBr\}_2$ (μ-H)$_4$	43 $^{Pr}[P_2Cp']ZrCl_2$	44 $\{^{Me}[P_2Cp]ZrCl\}_2$ (μ-Cl)$_2$
Formula	$C_{30}H_{66}Br_2P_4Si_4Zr_2$	$C_{27}H_{55}Cl_2P_2Si_2Zr$	$C_{33.50}H_{66}Clr_4P_2Si_4Zr_2$
fw	1005.34	659.95	1029.38
Color, habit	colorless, needle	dark green, block	red, prism
Crystal system	monoclinic	monoclinic	monoclinic
Space group	$P2_1/c$	$P2_1/c$	$P2_1/c$
a, Å	13.576(2)	16.2492(3)	12.7313(7)
b, Å	10.3435(7)	11.2733(2)	35.0096(5)
c, Å	32.0759(10)	19.1230(3)	22.0768(13)
α, deg	90	90	90
β, deg	92.2027(9)	96.478	90.1059(4)
γ, deg	90	90	90
V, Å^3	4500.9(5)	3480.63(10)	9840.0(6)
Z	4	4	8
ρ_{calc}, g/cm^3	1.483	1.259	1.390
$F(000)$	2048.00	1396	4248.00
Radiation	Mo	Mo	Mo

216

μ, cm^{-1}	25.12	6.45	8.90
Crystal size, mm	$0.04 \times 0.08 \times 0.50$	$0.30 \times 0.18 \times 0.16$	$0.15 \times 0.25 \times 0.30$
Transmission factors	0.5022 - 1.0005	0.838 - 1.000	0.8270-1.0100
Scan type	ω-2θ	ω-2θ	ω-2θ
Scan range, $\omega°$	-	-	0.94+0.20 tan θ
Scan speed, $°$min^{-1}	-	-	16 (up to 9 scans)
$2\theta_{max}$, deg	60	-	56.7
Crystal. decay, %	-	-	-
Total reflections	41794	17147	74078
Unique reflections	10785	6049	20251
R_{merge}		-	-
Number w/ $I \geq 3\sigma(I)$	4787	4824	11200
Variables	387	377	837
R	0.063	0.0735	0.133
R_w	0.061	0.01274	0.150
gof	1.92	1.021	2.59
Max Δ/σ (final cycle)	-	-	0.09
Residual density e/Å^3	-0.53 to 1.51	-0.327 to 0.332	-1.71 to 2.82

[a] Complex **2, 13, 21a, 23b, 32**: Temperature 294 K, Rigaku AFC6S diffractometer, Mo K_α (λ = 0.71069 Å) radiation; by Dr. S. J. Rettig at UBC. Complex **17, 30, 35, 37, 44**: Temperature 294 K, Rigaku AFC6S diffractometer, Cu K_α (λ = 1.54178 Å) radiation; by Dr. S. J. Rettig at UBC. Complex **18b, 20**: Temperature 294 K, Nonius CAD-4 diffractometer, Mo K_α (λ = 0.70930 Å) radiation; by Dr. M. J. Zaworotko at Dalhousie Univ. Complex **27, 43**: Temperature 173 K, Siemens SMART Platform CCD diffractometer, Mo K_α (λ = 0.71073 Å) radiation; by Dr. V. G. Young at Univ. of Minnesota. Complex **28**: Temperature 294 K, Siemens SMART Platform CCD diffractometer, Mo K_α (λ = 0.71073 Å) radiation; by Dr. G. P. Yap at Univ. of Windsor.

[b] For Rigaku structures, function minimized $\Sigma w(|F_0|-|F_c|)^2$ where $w = 4F_0^2/\sigma^2(F_0^2)$, $R = \Sigma||F_0|-|F_c||/\Sigma|F_0|$, $R_w = (\Sigma w(|F_0|-|F_c|)^2/\Sigma w|F_0|^2)^{1/2}$, and gof = $[\Sigma w(|F_0|-|F_c|)^2/(m-n)]^{1/2}$ (where m = number of observations, n = number of variables). Values given for R, R_w, and gof are based on those reflections with $I \geq 3\sigma(I)$. For Siemens structures, function minimized $\Sigma w(|F_0|-|F_c|)^2$ where $w^{-1} = \sigma^2(F_0) + 0.0010F_0^2$, $R = \Sigma|F_0-|F_c||/\Sigma|F_0|$, $R_w = \Sigma|(w^{1/2}(F_0-$

$F_c)|/\Sigma(w)^{1/2}F_o|$, and gof = $[\Sigma w(|F_o|-|F_c|)^2/(m-n)]^{1/2}$. Values given for R, R_w and gof are based on those reflections with $I \geq 4\sigma(I)$.

Table A1.2 Fractional Atomic Coordinates and U_{eq} ($\text{Å}^2 \text{x} 10^3$) for

$^{Pr}[P_2Cp]HfCl_3$ (**2**).

atom	x	y	z	Ueq
Hf(1)	0.54890	0.94400	0.81040	15(1)
Cl(1)	0.61660	0.80960	0.74540	26(1)
Cl(2)	0.42990	0.95370	0.65710	25(1)
Cl(3)	0.44030	1.06710	0.82960	27(1)
P(1)	0.44770	0.75140	0.80600	17(1)
C(1)	0.38250	0.77400	0.86790	24(1)
C(2)	0.29730	0.83710	0.81350	33(1)
C(3)	0.36600	0.66800	0.91100	36(1)
C(4)	0.37030	0.69340	0.69790	25(1)
C(5)	0.31260	0.59320	0.70040	34(1)
C(6)	0.41900	0.65770	0.64520	34(1)
C(7)	0.52480	0.63730	0.86170	21(1)
Si(1)	0.62160	0.68480	0.96480	22(1)
C(8)	0.60240	0.66720	1.06260	37(1)
C(9)	0.71860	0.60210	0.97420	41(1)
C(10)	0.70220	0.88980	0.92930	20(1)
C(11)	0.63980	0.84090	0.95320	19(1)
C(12)	0.59840	0.93510	0.97270	20(1)
C(13)	0.63400	1.03710	0.95920	20(1)
C(14)	0.69880	1.01160	0.93120	20(1)

Si(2)	0.77270	1.11370	0.91070	20(1)
C(15)	0.88620	1.05430	0.95150	32(1)
C(16)	0.77810	1.25050	0.96780	30(1)
C(17)	0.72410	1.12780	0.78920	23(1)
P(2)	0.60430	1.12270	0.73850	19(1)
C(18)	0.56760	1.26150	0.76400	26(1)
C(19)	0.46990	1.28220	0.70440	38(1)
C(20)	0.62290	1.36790	0.76740	38(1)
C(21)	0.56980	1.12020	0.61990	25(1)
C(22)	0.59650	1.22690	0.58540	38(1)
C(23)	0.60320	1.01310	0.59300	33(1)

Table A1.3 Fractional Atomic Coordinates and B_{eq} ($Å^2$) for
$^{Pr}[P_2Cp]ZrCl_2(\eta^2$-C(O)CH$_2$Ph) (**13**).

atom	x	y	z	B_{eq}
Zr(1)	0.21456	0.19237	0.19888	3.03
Cl(1)	0.2076	0.0538	0.1327	3.71
Cl(2)	0.2610	0.1425	0.3503	3.96
P(1)	0.0355	0.3384	0.2351	2.76
P(2)	0.5281	0.2603	-0.0117	4.37
Si(1)	0.1676	0.4066	0.1044	3.43
Si(2)	0.4370	0.1415	0.1082	3.61
O(1)	0.0908	0.2216	0.1334	2.8
C(1)	0.2541	0.3279	0.1398	3.0
C(2)	0.2912	0.2651	0.0911	3.0
C(3)	0.3610	0.2207	0.1450	2.9

219

C(4)	0.3705	0.2562	0.2304	2.9
C(5)	0.3071	0.3211	0.2274	3.2
C(6)	0.1030	0.4187	0.1986	2.9
C(7)	0.5393	0.1986	0.0896	4.0
C(8)	0.0977	0.3781	-0.0030	4.2
C(9)	0.2260	0.5083	0.0965	4.4
C(10)	0.0362	0.3631	0.3490	3.5
C(11)	0.1288	0.3413	0.4075	4.1
C(12)	-0.0392	0.3269	0.3938	4.3
C(13)	-0.0789	0.3515	0.1802	2.8
C(14)	-0.0964	0.3244	0.0853	3.8
C(15)	-0.1165	0.4378	0.1895	4.2
C(16)	0.3822	0.0930	0.0023	3.6
C(17)	0.4673	0.0649	0.1973	5.4
C(18)	0.63315	0.2290	-0.0539	3.8
C(19)	0.6199	0.1430	-0.0912	5.2
C(20)	0.6545	0.2902	-0.1238	6.4
C(21)	0.5543	0.3653	0.0308	5.4
C(22)	0.6390	0.3763	0.0953	7.0
C(23)	0.4749	0.4022	0.0667	5.9
C(24)	0.0797	0.2380	0.2244	3.6
C(25)	0.0325	0.1658	0.2612	2.8
C(26)	-0.0554	0.1360	0.2089	3.2
C(27)	-0.0572	0.0947	0.1300	3.2
C(28)	-0.1382	0.0673	0.0830	4.3
C(29)	-0.2176	0.0811	0.1160	4.1
C(30)	-0.2143	0.1188	0.1911	4.5

| C(31) | -0.1351 | 0.1459 | 0.2412 | 3.4 |

Table A1.4   Fractional Atomic Coordinates and B_{eq} ($Å^2$) for ^{Pr}[P$_2$Cp]Hf=CHPh(Cl) (**17**).

atom	x	y	z	B_{eq}
Hf(1)	0.41538	0.22299	0.270757	1.34
Cl(1)	0.55695	0.12692	0.32591	2.50
P(1)	0.65229	0.39149	0.27821	1.88
P(2)	0.25280	0.00248	0.29033	1.59
Si(1)	0.49836	0.54651	0.26367	1.68
Si(2)	0.06801	0.12857	0.27850	1.72
C(1)	0.3922	04179	0.3064	1.60
C(2)	0.2761	0.3390	0.2575	1.48
C(3)	0.2200	0.2532	0.3138	1.53
C(4)	0.3064	0.2822	0.4020	1.49
C(5)	0.4091	0.3812	0.3973	1.58
C(6)	0.6551	0.5417	0.2921	2.16
C(7)	0.0991	-0.0021	0.3097	1.91
C(8)	0.4947	0.6834	0.3351	2.55
C(9)	0.4497	0.5386	0.1321	2.35
C(10)	-0.04105	0.1569	0.3576	3.05
C(11)	0.0097	0.1134	0.1462	2.46
C(12)	0.7309	0.3763	0.1698	2.80
C(13)	0.7434	0.2601	0.1506	3.55
C(14)	0.6652	0.3971	0.0771	2.63
C(15)	0.7735	0.4046	0.3790	2.88

C(16)	0.7307	0.4165	0.4785	2.88
C(17)	0.8973	0.5030	0.3798	6.4
C(18)	0.21770	-0.1200	0.1844	2.22
C(19)	0.3346	-0.1369	0.1598	3.04
C(20)	0.1472	-0.1016	0.0943	2.46
C(21)	0.3006	-0.0575	0.3939	2.38
C(22)	0.3335	0.0312	0.4907	3.23
C(23)	0.2081	-0.1769	0.4048	3.43
C(24)	0.3796	0.1868	.01248	1.74
C(25)	0.3381	0.1762	0.0193	1.60
C(26)	0.3707	0.1078	-0.0558	2.11
C(27)	0.3309	0.0981	-0.1532	2.71
C(28)	0.2575	0.1561	-0.1813	2.40
C(29)	0.2225	0.2227	-0.1117	2.26
C(30)	0.2634	0.2336	-0.0124	1.89
C(31)	0.0784	0.4768	0.1238	8.0
C(32)	0.0363	0.5226	0.0708	7.1
C(33)	-0.0105	0.5853	0.0694	7.4
C(34)	0.0584	0.4202	0.0208	7.5
C(35)	0.139	0.543	0.2076	8.3

Table A1.5   Fractional Atomic Coordinates and B_{iso} (Å^2) for
$^{Pr}[P_2Cp]Zr=CHSiMe_3(Cl)$ (**18b**).

atom	x	y	z	B_{iso}
Zr(1)	.77343	.31361	.01264	2.99

222

Cl(1)	.61477	.37854	-.06587	5.68
P(1)	.63425	.32524	.1273	4.05
P(2)	.83602	.33571	-.14002	3.91
Si(1)	.84008	.2985	.24829	4.67
Si(2)	1.04766	.2873	-.04109	4.09
Si(3)	.7844	.085	-.00407	5.95
CP1	.8899	.323	.1515	3.6
CP2	.8848	.402	.1167	3.4
CP3	.9342	.3999	.0477	3.4
CP4	.9725	.3201	.0388	3.3
CP5	.9461	.2768	.1034	3.8
C(1)	.7028	.3192	.2313	7.0
C(2)	.8754	.1958	.2791	9.3
C(3)	.9079	.3648	.3324	10.3
C(4)	1.1143	.1899	-.013	6.0
C(5)	1.1495	.3615	-.0548	6.0
C(6)	.9529	.276	-.1373	4.7
C(7)	.5575	.4191	.1263	7.0
C(8)	.6243	.4914	.1222	7.1
C(9)	.49	.4258	.1915	9.9
C(10)	.5292	.25	.1215	8.1
C(11)	.5868	.1657	.1397	13.3
C(12)	.4619	.2429	.0479	17.1
C(13)	.8859	.4386	-.1595	5.0
C(14)	.8072	.5042	-.1461	6.5
C(15)	.9245	.4503	-.2404	7.4
C(16)	.7572	.3038	-.2358	7.4

C(17)	.7156	.2204	-.2312	10.7
C(18)	.6693	.3597	-.2642	9.4
C(19)	.7595	.1941	-.0032	4.2
C(20)	.6621	.0274	-.0219	8.4
C(21)	.8623	.0492	.0901	10.1
C(22)	.8618	.0524	-.0847	8.5

Table A1.6 Fractional Atomic Coordinates and B_{eq} ($Å^2$) for
$^{Pr}[P_2Cp]Zr(\eta^2\text{-}CH_2\text{=}CH_2)Cl$ **(20)**.

atom	x	y	z	B_{iso}
Zr	.86636	.26553	.28801	3.40
Cl	.85694	.26009	.40883	5.44
P1	.91701	.12938	.33997	4.02
P2	.78304	.38902	.29842	4.17
Si1	.917	.12195	.19602	4.95
Si2	.7864	.40293	.14769	4.50
CP1	.8566	.2013	.1979	3.9
CP2	.8749	.2681	.1628	3.5
CP3	.8063	.3111	.1777	3.6
CP4	.7431	.2694	.2218	3.6
CP5	.7723	.2038	.2341	3.5
C1	.8994	.0753	.2848	4.2
C2	1.034	.1367	.1626	6.3
C3	.8663	.0751	.1443	6.3

C4	.8863	.4504	.1081	5.8
C5	.7031	.4151	.0879	6.4
C6	.7313	.4269	.2249	4.6
C7	.8534	.0885	.4200	5.1
C8	.8752	.0138	.4493	6.0
C9	.7544	.0989	.4132	5.1
C10	1.036	.1151	.3537	4.8
C11	1.0754	.0446	.3541	5.9
C12	1.0539	.1418	.4152	5.2
C13	.8524	.4587	.3105	8.7
C14	.8656	.5176	.2701	16.9
C15	.8894	.4394	.3762	7.6
C16	.6886	.3808	.3676	6.0
C17	.6307	.4455	.3632	9.7
C18	.6350	.3190	.3710	6.6
C19	1.0174	.2713	.2630	4.4
C20	.9835	.3383	.2486	4.1

Table A1.7   Fractional Atomic Coordinates and B_{eq} (Å^2) for
$^{Pr}[P_2Cp]ZrC(O)=CHPh(Cl)$ **(21a)**.

atom	x	y	z	B_{eq}
Zr(1)	.49748	.879344	.24186	2.212
Cl(1)	.26683	.91947	.28863	3.81
P(1)	.6855	.91379	.38361	2.63
P(2)	.27696	.81154	.14252	2.72
Si(1)	.70857	1.02012	.28962	3.51

Si(2)	.25922	.9149	.0413	3.22
O(1)	.6383	.81142	.25361	2.73
C(1)	.6265	.97033	.2110	2.67
C(2)	.7021	.92597	.1782	2.83
C(3)	.593	.90196	.11807	2.75
C(4)	.4463	.92938	.11054	2.82
C(5)	.4702	.97229	.16799	2.80
C(6)	.6792	.98916	.38507	3.18
C(7)	.9185	1.03352	.2861	3.34
C(8)	.5948	1.08518	.2743	6.6
C(9)	.0939	.94666	.0759	5.64
C(10)	.2738	.93882	-.0581	4.26
C(11)	.2377	.83775	.04211	4.93
C(12)	.6327	.89021	.47677	3.61
C(13)	.4621	.90084	.4765	3.46
C(14)	.7347	.91335	.5503	4.27
C(15)	.8948	.89533	.38838	3.40
C(16)	1.0185	.93066	.4405	5.7
C(17)	.9228	.8342	.4081	4.87
C(18)	.0850	.80967	.1740	5.32
C(19)	-.0628	.79701	.1146	6.2
C(20)	.0959	.7736	.2456	6.7
C(21)	.3416	.73903	.1328	6.4
C(22)	.4945	.73736	.1021	4.61
C(23)	.2166	.70271	.0832	5.27
C(24)	.5354	.8007	.30274	2.81
C(25)	.5353	.75526	.34689	3.13

C(26)	.6373	.70661	.35237	3.13
C(27)	.6266	.66575	.4075	4.73
C(28)	.7165	.61876	.4133	6.3
C(29)	.8226	.61095	.3658	6.0
C(30)	.8354	.65052	.3107	5.31
C(31)	.7444	.69627	.3037	4.22

Table A1.8 Fractional Atomic Coordinates and B_{eq} (Å^2) for $^{Pr}[P_2Cp]ZrCH_2CH_2C(O)=CHSiMe_3(Cl)$ (**23b**).

atom	x	y	z	B_{eq}
Zr(1)	.15920	.01898	.28411	2.550
Cl(1)	.08992	-.11699	.24182	3.93
P(1)	.35087	-.07855	.31755	3.89
P(2)	-.06068	.06954	.28351	2.93
Si(1)	.37138	-.05512	.15225	4.47
Si(2)	-.01419	.1417	.13575	3.31
Si(3)	.28006	.26496	.44148	4.26
O(1)	.2074	.10509	.35682	2.80
C(1)	.2728	.0238	.1706	3.26
C(2)	.1668	.0286	.1429	3.18
C(3)	.1176	.1018	.1648	2.90
C(4)	.1986	.1435	.2067	3.04
C(5)	.2899	.0974	.2100	3.41
C(6)	.4400	-.0744	.2424	7.5
C(7)	-.0869	.1538	.2216	3.22

227

C(8)	.3080	-.1447	.1117	12.1
C(9)	.4755	-.0127	.0974	11.2
C(10)	-.0796	.0718	.0699	5.64
C(11)	.0002	.2423	.0940	25.32
C(12)	.3238	-.1852	.3399	5.98
C(13)	.3990	-.2488	.3096	9.7
C(14)	.3140	-.1968	.4220	9.9
C(15)	.4455	-.0413	.3933	6.38
C(16)	.4660	.0457	.3887	7.7
C(17)	.5491	-.0912	.4000	9.3
C(18)	-.1502	-.0137	.2510	3.99
C(19)	-.1620	-.0770	.3097	5.61
C(20)	-.2572	.0111	.2162	5.57
C(21)	-.1125	.1057	.3701	4.04
C(22)	-.0506	.1805	.3944	5.48
C(23)	-.2302	.1221	.3706	5.81
C(24)	.1160	-.0305	.3969	3.34
C(25)	.1668	.0212	.4566	4.38
C(26)	.2051	.1026	.4297	2.93
C(27)	.2335	.1656	.4706	3.28
C(28)	.1685	.3282	.4061	11.5
C(29)	.3763	.2609	.3704	8.2
C(30)	.3433	.3167	.5210	10.2

Table A1.9   Fractional Atomic Coordinates and U_{eq} ($Å^2 \times 10^3$) for

Me[P$_2$Cp]ZrCl(CH$_2$Ph)$_2$ (**27**)

atom	x	y	z	U_{eq}
Zr(1)	.3668	.3038	.3265	18(1)
Cl(1)	.2081	.491	.3593	31(1)
C(1)	.5855	.1795	.2448	22(1)
C(2)	.5006	.1460	.2064	21(1)
C(3)	.4128	.0898	.2966	21(1)
C(4)	.4426	.0899	.3948	20(1)
C(5)	.5486	.1426	.3626	22(1)
Si(1)	.7232	.2485	.1537	26(1)
C(6)	.8567	.1811	.2125	42(1)
C(7)	.7648	.2209	.0080	42(1)
C(8)	.6762	.4111	.1522	28(1)
P(1)	.5497	.4380	.2797	26(1)
C(9)	.6421	.4127	.3767	37(1)
C(10)	.4954	.5958	.2656	41(1)
Si(1)	.2958	.0158	.2828	23(1)
C(11)	.2797	-.1191	.3912	34(1)
C(12)	.3520	-.0290	.1427	42(1)
C(13)	.1451	.1268	.3008	26(1)
P(2)	.1362	.2204	.3964	24(1)
C(14)	.1009	.1233	.5322	32(1)
C(15)	-.0125	.3232	.4085	37(1)
C(16)	.3785	.3280	.5015	28(1)
C(17)	.2844	.2783	.6008	26(1)
C(18)	.3158	.1695	.6654	28(1)
C(19)	.2302	.1228	.7609	34(1)

atom	x	y	z	U_eq
C(20)	.1085	.1846	.7951	38(1)
C(21)	.0746	.2913	.7334	40(1)
C(22)	.1598	.3382	.6379	32(1)
C(23)	.3977	.4037	.1368	27(1)
C(24)	.3041	.3758	.0967	27(1)
C(25)	.1773	.4307	.1280	34(1)
C(26)	.0914	.4084	.0863	43(1)
C(27)	.1278	.3317	.0124	47(1)
C(28)	.2522	.2753	-.0197	42(1)
C(29)	.3375	.2972	.0222	34(1)

Table A1.10 Fractional Atomic Coordinates (x10^4) and U_{eq} (Å^2x10^3) for

^{Me}[P$_2$Cp]Zr(η^2-C$_6$H$_3$Me)Cl (**28**).

atom	x	y	z	U_{eq}
Zr	19600	8543	1344	38(1)
Cl	19555	11012	1059	68(1)
P(1)	21369	9053	1357	48(1)
P(2)	17863	9262	1333	58(1)
Si(1)	21360	6142	964	55(1)
Si(2)	17535	6257	1106	62(1)
C(1)	21978	10197	1939	70(1)
C(2)	21641	9807	702	75(1)
C(3)	22008	7487	1475	55(1)
C(4)	21677	6144	239	87(1)
C(5)	21574	4457	1328	94(1)
C(6)	20117	6551	817	43(1)

C(7)	19484	6043	1114	44(1)
C(8)	18606	6599	874	45(1)
C(9)	18696	7446	395	45(1)
C(10)	19606	7419	364	44(1)
C(11)	16589	5911	426	115(2)
C(12)	17736	4785	1614	116(2)
C(13)	17257	7787	1502	67(1)
C(14)	17092	9942	650	91(1)
C(15)	17764	10544	1873	82(1)
C(16)	19226	7901	2789	55(1)
C(17)	19487	8073	2256	45(1)
C(18)	20388	8004	2257	44(1)
C(19)	21064	7757	2791	55(1)
C(20)	20806	7628	3313	60(1)
C(21)	19890	7702	3317	58(1)
C(22)	19687	7583	3917	74(2)

Table A1.11 Fractional Atomic Coordinates and B_{eq} ($Å^2$) for

^{Me}[P$_2$Cp]Zr(CH$_2$Ph)$_3$ (**30**).

atom	x	y	z	B_{eq}
Zr(1)	0.25509	0.68132	0.567653	1.134
Zr(2)	0.21393	0.520815	0.178298	1.454
P(1)	0.12261	0.73646	0.65136	1.94
P(2)	0.30709	0.61363	0.4918	1.87
P(3)	0.37504	0.45597	0.22494	1.54
Si(1)	0.28697	0.79351	0.57253	1.92

Si(2)	0.50372	0.6685	0.41585	1.74
Si(3)	0.1376	0.41534	0.13735	1.99
C(1)	0.3741	0.74717	0.55086	1.59
C(2)	0.3671	0.7299	0.48881	1.53
C(3)	0.4644	0.69828	0.48762	1.43
C(4)	0.5353	0.69611	0.55151	1.58
C(5)	0.4797	0.72508	0.58951	1.58
C(6)	0.109	0.78271	0.61287	2.11
C(7)	0.4235	0.81952	0.6283	3.17
C(8)	0.2417	0.82111	0.4974	3.35
C(9)	-0.0607	0.72981	0.6853	3.33
C(10)	0.2362	0.74706	0.7252	2.96
C(11)	0.4745	0.61901	0.4475	2.08
C(12)	0.6996	0.6719	0.3921	2.58
C(13)	0.3800	0.6813	0.3447	2.76
C(14)	0.1695	0.5976	0.4291	3.11
C(15)	0.3473	0.56701	0.5318	3.27
C(16)	0.0504	0.64912	0.61611	1.52
C(17)	0.0041	0.60964	0.60217	1.88
C(18)	-0.1104	0.60151	0.5545	3.36
C(19)	-0.151	0.56468	0.5381	4.71
C(20)	-0.0811	0.53427	0.5692	4.64
C(21)	0.0278	0.54132	0.6186	3.71
C(22)	0.0688	0.57807	0.63478	2.47
C(23)	0.3987	0.63807	0.63731	1.68
C(24)	0.4323	0.65438	0.70232	1.69
C(25)	0.5672	0.67371	0.71882	2.20

C(26)	0.5969	0.68992	0.7792	2.79
C(27)	0.4935	0.68711	0.82709	2.90
C(28)	0.3621	0.66706	0.81283	2.36
C(29)	0.3318	0.65128	0.75235	2.02
C(30)	0.0836	0.68211	0.47424	1.83
C(31)	-0.0036	0.7175	0.46208	1.97
C(32)	-0.1193	0.72853	0.5012	2.49
C(33)	-0.204	0.76112	0.4884	3.38
C(34)	-0.1746	0.78359	0.4367	4.05
C(35)	-0.0631	0.77342	0.3963	3.85
C(36)	0.0211	0.74095	0.40874	2.84
C(37)	0.0543	0.46359	0.14651	1.80
C(38)	-0.0098	0.4794	0.20201	2.18
C(39)	-0.0688	0.51528	0.1861	3.10
C(40)	-0.0425	0.52259	0.1211	3.17
C(41)	0.0313	0.49106	0.09645	2.51
C(42)	0.3402	0.41824	0.16522	1.81
C(43)	0.1158	0.40257	0.05	3.49
C(44)	0.0355	0.38106	0.1871	3.60
C(45)	0.5791	0.45691	0.23816	2.32
C(46)	0.3166	0.43389	0.29932	2.15
C(47)	0.1981	0.58515	0.15047	2.04
C(48)	0.0832	0.61069	0.1757	1.94
C(49)	-0.0506	0.61914	0.1398	2.91
C(50)	-0.1598	0.64174	0.164	3.87
C(51)	-0.1415	0.65752	0.2244	4.13
C(52)	-0.0102	0.65055	0.2607	3.55

C(53)	0.1012	0.62765	0.23669	2.67
C(54)	0.4096	0.51303	0.11004	2.41
C(55)	0.4119	0.53971	0.05448	2.22
C(56)	0.4964	0.57279	0.0578	3.38
C(57)	0.4897	0.59878	0.0063	4.74
C(58)	0.3962	0.59139	-0.0483	5.21
C(59)	0.3162	0.55877	-0.0527	4.55
C(60)	0.3241	0.53319	-0.0029	3.20
C(61)	0.2413	0.53501	0.28729	2.00
C(62)	0.4002	0.54068	0.31038	2.00
C(63)	0.4952	0.56533	0.27872	2.61
C(64)	0.6454	0.56943	0.2984	3.38
C(65)	0.7074	0.54905	0.3508	3.64
C(66)	0.6154	0.52505	0.3833	3.04
C(67)	0.4658	0.52098	0.36405	2.44

Table A1.12   Fractional Atomic Coordinates and B_{eq} (Å^2) for

$^{Me}[P_2Cp']Zr(\eta^2\text{-CH}_2\text{=CH}_2)Br$ (**32**).

atom	x	y	z	B_{eq}
Zr(1)	.25164	.1281	.33516	3.362
Br(1)	.35572	-.00551	.27573	6.50
P(1)	.46524	.1938	.36653	4.30
P(1)	.0879	.00401	.2835	5.31
Si(1)	.34727	.36592	.38574	4.35
Si(2)	-.07305	.15529	.279	5.54

234

C(1)	.2259	.2931	.3168	3.50
C(2)	.1351	.2626	.3499	3.63
C(3)	.0606	.2089	.2743	3.87
C(4)	.1077	.2053	.1904	4.01
C(5)	.2071	.2558	.2164	3.75
C(6)	.4805	.298	.4352	4.9
C(7)	-.038	.0381	.315	6.7
C(8)	.367	.4493	.2928	5.7
C(9)	.3152	.4193	.4967	6.4
C(10)	-.1843	.1623	.1492	7.7
C(11)	-.1225	.2094	.3788	8.6
C(12)	.514	.2197	.2556	6.2
C(13)	.5851	.1292	.4456	6.4
C(14)	.0328	-.0275	.1472	8.5
C(15)	.1217	-.102	.3459	7.2
C(16)	.3246	.1459	.5116	4.4
C(17)	.2225	.0953	.4913	4.6

Table A1.13   Fractional Atomic Coordinates and B_{eq} (Å^2) for

$^{Pr}[P_2Cp]Zr(\eta^2\text{-PhCCPh})Br$ (**35**).

atom	x	y	z	B_{eq}
Zr(1)	.28571	.309908	.058288	1.044
Br(1)	.445	.29557	.13184	3.388
P(1)	.33788	.42261	.11315	1.34
P(2)	.30709	.19366	.03323	1.50

235

Si(1)	.15584	.43208	.05443	1.52
Si(2)	.14133	.17982	.03065	1.74
C(1)	.1764	.35487	.07848	1.36
C(2)	.1398	.30666	.03161	1.32
C(3)	.1715	.25376	.06818	1.58
C(4)	.2277	.26965	.14178	1.49
C(5)	.2312	.32884	.1484	1.44
C(6)	.2482	.46571	.05758	1.61
C(7)	.2086	.15821	-.00931	1.83
C(8)	.0691	.43701	-.04002	2.42
C(9)	.1292	.46833	.1204	2.52
C(10)	.0358	.17975	-.0444	2.97
C(11)	.146	.1306	.1041	3.18
C(12)	.4198	.45139	.09624	1.98
C(13)	.3586	.44453	.2078	1.93
C(14)	.344	.18637	-.0368	2.34
C(15)	.3763	.14716	.1105	2.28
C(16)	.5038	.44505	.1628	2.50
C(17)	.4073	.5133	.0661	3.12
C(18)	.4199	.4052	.26873	2.85
C(19)	.378	.50796	.2281	3.29
C(20)	.4342	.1847	-.0034	5.50
C(21)	.307	.1376	-.0922	5.14
C(22)	.3718	.15892	.1824	3.01
C(23)	.3688	.08307	.094	4.35
C(24)	.2684	.35673	-.04091	1.30
C(25)	.2298	.30713	-.06174	1.38

C(26)	.2724	.40192	-.08918	1.57
C(27)	.3437	.41371	-.0898	2.43
C(28)	.3478	.4532	-.1384	3.42
C(29)	.2804	.4829	-.1864	3.62
C(30)	.2097	.47259	-.1872	3.28
C(31)	.2045	.43248	-.13904	2.44
C(32)	.1841	.28379	-.13729	1.68
C(33)	.1045	.26789	-.1661	2.20
C(34)	.0613	.24793	-.2384	3.23
C(35)	.0982	.243	-.2821	3.71
C(36)	.1779	.2585	-.2551	3.82
C(37)	.2204	.27953	-.1828	2.71

Table A1.14 Fractional Atomic Coordinates and B_{iso} ($\text{Å}^2 \times 10^3$) for

$\{^{Me}[P_2Cp]ZrBr\}_2(\mu\text{-H})_4$. (**37**).

atom	x	y	z	B_{iso}
Zr (1)	.11172	.33924	.36729	1.628
Zr(2)	.3355	.28637	.35236	1.96
Br(1)	-.03218	.2136	.32178	3.57
Br(2)	.36614	.43295	.28361	3.59
P(1)	.08343	.1071	.40832	2.19
P(2)	.07645	.4888	.29694	2.13
P(3)	.3709	.0982	.29605	2.78
P(4)	.3128	.7492	.47929	3.96
Si(1)	.0942	.2744	.48542	2.28

Si(2)	-.1015	.5719	.34791	2.22
Si(3)	.5788	.1235	.33423	2.89
Si(4)	.4391	.5995	.41284	2.69
C(1)	.0677	.3905	.4422	1.24
C(2)	-.0200	.4076	.4168	1.8
C(3)	-.0105	.5129	.3876	1.7
C(4)	.0886	.5621	.3963	1.7
C(5)	.1337	.4866	.4293	2.1
C(6)	.1367	.1203	.4612	2.7
C(7)	-.0520	.5360	.2947	2.6
C(8)	.1922	.3398	.5205	3.6
C(9)	-.0185	.2509	.5145	3.5
C(10)	.1325	-.0402	.3867	3.0
C(11)	-.0442	.0622	.4168	2.9
C(12)	-.1173	.7483	.3548	3.3
C(13)	-.2179	.4874	.3556	3.6
C(14)	.1413	.6419	.2920	2.6
C(15)	.0981	.4151	.2472	2.8
C(16)	.5155	.2380	.3703	2.3
C(17)	.5088	.3730	.3682	2.6
C(18)	.4527	.4236	.3994	2.2
C(19)	.4209	.3158	.4239	2.6
C(20)	.4591	.2016	.4057	2.2
C(21)	.4807	.0071	.3141	2.9
C(22)	.3931	.6114	.4677	3.3
C(23)	.6788	.0313	.3626	6.1
C(24)	.6334	.2197	.2913	4.5

C(25)	.2756	-.0268	.2897	3.8
C(26)	.3962	.1351	.2413	4.0
C(27)	.5648	.6725	.4113	4.5
C(28)	.3574	.6889	.3752	3.2
C(29)	.4034	.8786	.4818	6.1
C(30)	.2988	.7256	.5355	4.5
H	.2310	.4240	.3600	1.0
H	.2450	.3060	.4020	2.9
H	.2073	.2321	.3565	2.1
H	.2100	.3100	.3200	2.1

Table A1.15 Fractional Atomic Coordinates and U_{eq} (Å^2 x 10^3) for

$^{Pr}[P_2Cp]ZrCl_2$ (**43**)

atom	x	y	z	U_{eq}
Zr(1)	0.2554	0.9313	0.7911	21(1)
Cl(1)	0.3597	0.893	0.7081	39(1)
Cl(2)	0.1302	0.8049	0.757	36(1)
C(1)	0.346	1.0882	0.866	26(1)
C(2)	0.3292	0.9906	0.9078	25(1)
C(3)	0.2414	0.9791	0.9118	22(1)
C(4)	0.2018	1.0726	0.8674	23(1)
C(5)	0.2687	1.1366	0.8404	25(1)
C(6)	0.4311	1.1392	0.8561	38(1)
C(7)	0.4295	1.2078	0.7871	59(1)
C(8)	0.4545	1.2248	0.9181	60(1)

239

C(9)	0.4971	1.0413	0.8582	57(1)
Si(1)	0.2055	0.8614	0.9705	27(1)
C(10)	0.0982	0.8866	0.9931	44(1)
C(11)	0.2775	0.8614	1.0539	43(1)
C(12)	0.2117	0.714	0.9245	29(1)
P(1)	0.2911	0.7121	0.8632	27(1)
C(13)	0.2777	0.5681	0.8142	48(1)
C(14)	0.2045	0.4978	0.8256	95(1)
C(15)	0.2997	0.5762	0.7421	90(1)
C(16)	0.3891	0.6861	0.9219	34(1)
C(17)	0.3876	0.58	0.9727	60(1)
C(18)	0.4628	0.681	0.8794	65(1)
Si(2)	0.0942	1.1275	0.8384	25(1)
C(19)	0.0058	1.0214	0.8334	40(1)
C(20)	0.0698	1.2534	0.8964	37(1)
C(21)	0.1038	1.1866	0.7473	27(1)
P(2)	0.1675	1.093	0.6948	23(1)
C(22)	0.0899	1.0185	0.631	29(1)
C(23)	0.0239	1.0929	0.5888	46(1)
C(24)	0.1316	0.9343	0.5829	44(1)
C(25)	0.2254	1.2059	0.6476	33(1)
C(26)	0.1737	1.3067	0.6106	49(1)
C(27)	0.2829	1.1523	0.5984	56(1)

Table A1.16 Fractional Atomic Coordinates and B_{eq} ($\ddot{A}^2$) for

$\{^{Pr}[P_2Cp]ZrCl\}_2(\mu\text{-}Cl)_2$ **(44)**.

240

atom	x	y	z	B_{eq}
Zr(3)	0.63287	0.29429	0.45373	1.488
Zr(4)	0.41796	0.21022	0.42391	1.402
Cl(5)	0.48835	0.25379	0.51331	1.73
Cl(6)	0.56025	0.25125	0.36318	1.79
Cl(7)	0.47163	0.33645	0.42583	2.38
Cl(8)	0.58100	0.16805	0.45183	2.13
P(5)	0.60932	0.34647	0.54611	2.36
P(6)	0.70260	0.34567	0.36770	2.21
P(7)	0.35398	0.16101	0.51380	2.18
P(8)	0.44236	0.15714	0.33363	2.43
Si(5)	0.75679	0.29219	0.61088	2.51
Si(6)	0.87867	0.28915	0.35572	2.08
Si(7)	0.16786	0.21408	0.52016	2.24
Si(8)	0.29442	0.21011	0.26617	2.23
C(31)	0.76898	0.27776	0.53107	1.90
C(32)	0.81758	0.29803	0.48311	2.04
C(33)	0.81730	0.27521	0.42835	1.80
C(34)	0.76595	0.24052	0.44417	1.78
C(35)	0.73821	0.24107	0.50418	2.06
C(36)	0.71014	0.34332	0.60489	3.22
C(37)	0.84131	0.34128	0.34921	2.25
C(38)	0.88793	0.29074	0.64893	3.76
C(39)	0.66130	0.26132	0.65181	2.90
C(40)	1.02348	0.28258	0.35903	3.40
C(41)	0.82396	0.26054	0.29250	2.91

C(43)	0.48848	0.33967	0.58958	3.64
C(44)	0.68626	0.39733	0.37855	3.75
C(45)	0.63807	0.33931	0.29552	3.65
C(46)	0.23026	0.22789	0.44806	1.50
C(47)	0.23399	0.20518	0.39380	1.79
C(48)	0.28301	0.22612	0.34575	1.90
C(49)	0.31215	0.26237	0.37168	1.89
C(50)	0.27962	0.26303	0.43182	1.82
C(51)	0.21535	0.16414	0.53233	2.70
C(52)	0.34442	0.15965	0.27338	2.76
C(53)	0.02110	0.21445	0.51492	4.17
C(54)	0.20914	0.24696	0.58105	3.95
C(55)	0.16089	0.20914	0.23051	3.27
C(56)	0.38585	0.24139	0.22298	2.77
C(57)	0.41951	0.17108	0.58564	3.27
C(58)	0.37376	0.10980	0.50695	3.78
C(59)	0.56511	0.16284	0.29093	4.16
C(60)	0.44728	0.10636	0.35057	3.89